Thin Films and Nanostructures: Cavity Polaritons

Alexey Kavokin
Guillaume Malpuech

Elsevier

Thin Films and Nanostructures

Cavity Polaritons

Volume 32

Thin Films and Nanostructures

Cavity Polaritons

Alexey Kavokin

Guillaume Malpuech

LASMEA CNRS
Blaise Pascal University
Clermont-Ferrand II
63177 Aubere, France

VOLUME 32

2003

ELSEVIER

Amsterdam Boston Heidelberg London New York Oxford Paris
San Diego San Francisco Singapore Sydney Tokyo

ELSEVIER B.V.
Sara Burgerhartstraat 25
P.O. Box 211, 1000 AE
Amsterdam, The Netherlands

ELSEVIER Inc.
525 B Street, Suite 1900
San Diego, CA 92101-4495
USA

ELSEVIER Ltd
The Boulevard, Langford Lane
Kidlington, Oxford OX5 1GB
UK

ELSEVIER Ltd
84 Theobalds Road
London WC1X 8RR
UK

First edition 2003

ISBN: 0-12-533032-4

♾ The paper used in this publication meets the requirements of ANSI/NISO Z39.48-1992 (Permanence of Paper).
Printed in The Netherlands.

Contents

Authors of this book vii
Preface ix

Introduction 1
Frequently Asked Questions 13

Part I. Linear Properties of Microcavities

Chapter 1. Dispersion of Cavity Polaritons

1.1. Reflection and Transmission of Light by Quantum Wells Containing Excitons 29
1.2. Reflectivity of Bragg Mirrors 36
1.3. Dispersion of Exciton–Polaritons in Microcavities Containing Single Quantum Wells . 40
References 45

Chapter 2. Examples of Microcavity Systems

2.1. Multiple Quantum Wells in a Cavity 47
2.2. Coupled Microcavities 53
2.3. Bulk Microcavities 58
2.4. Regular Gratings of Quantum Wires and Quantum Dots in a Microcavity 70
2.5. Magnetic Field Effect. Kerr and Faraday Rotation 77
References 84

Chapter 3. Disorder Effect on Cavity Polaritons

3.1. Reflection and Elastic Scattering of Light by Localised Excitons 88
3.2. Motional Narrowing of Cavity Polaritons 95
3.3. Photoluminescence and Resonant Rayleigh Scattering from Microcavities (Linear Regime) 101
3.4. Time-Resolved Reflection of Light from Quantum Wells and Microcavities 107
References 113

Part II. Non-Linear Properties of Microcavities

Chapter 4. Photoluminescence of Strongly Coupled Microcavities

4.1. Qualitative Features 120
4.2. Semi-Classical Treatment of the Relaxation Kinetics of Cavity Polaritons 124
4.3. Relaxation Kinetics of Cavity Polariton 133
4.4. Conclusions 143
References 144

Chapter 5. Resonant Excitation Case and Parametric Amplification

5.1. Experimental Aspects 148
5.2. Theoretical Approach: Semi-Classical Model 164
5.3. Theoretical Approach: Quantum Model 166
References 179

Chapter 6. Toward Polariton Bose Condensation and Polariton Lasers

6.1. Eighty Years of Research on BEC 185
6.2. Thermodynamic Properties of Cavity Polariton Systems 190
6.3. Relaxation Kinetics of Cavity Polaritons: Towards Polariton Lasing 198
6.4. Spin Dynamics of Exciton–Polaritons in Microcavities 211
6.5. Conclusive Remarks 220
References 221

Appendix. Transfer Matrix Method for a Light Wave Propagating in a Planar Structure

A. Basis of Tangential Components of Electric and Magnetic Fields 225
B. Basis of Amplitudes of Light Waves Propagating Towards $z = +\infty$ and $z = -\infty$ 228
C. Photonic Bands of 1D Periodic Structures 230
Reference 231

Subject Index 233

Authors of this book

Alexey Kavokin, born in St-Petersburg, 1970, graduated from the St-Petersburg State Polytechnical University in 1991, PhD at the A.F. Ioffe Physico-Technical institute, 1993. In 1992–1998 researcher at Ioffe institute, research contracts in Montpellier, Regensburg, Pavia, Rome. Since 1998 professor at the Blaise Pascal university, Clermont-Ferrand, France.

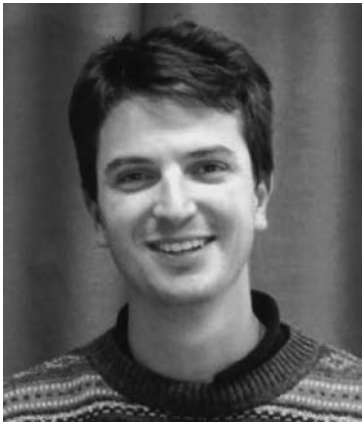

Guillaume Malpuech, born in Clermont-Ferrand, 1974, graduated from Ecole Central de Lyon in 1998, PhD at the Blaise Pascal university, Clermont-Ferrand, France, postdoc in universities of Rome and Southampton, 2001–2002. Since 2002 researcher at the CNRS, Blaise Pascal university, Clermont-Ferrand, France.

This page intentionally left blank

Preface

To Nikita Kavokin and Anne Tournadre

The decade from 1992 to 2002 in semiconductor optics can be called the "decade of microcavities". A few hundred, if not thousands, of papers dedicated to the physics of light–matter interaction in microcavities have appeared. Nevertheless, microcavities remain one of the most intriguing semiconductor systems, and are extremely rich in new fundamental effects. These include the strong coupling of photons and excitons, the optical coupling of macroscopically separated quantum wells, giant Faraday rotation, as well as the motional narrowing and stimulated scattering of exciton–polaritons, their weak localisation and Bose condensation. Many laboratories across the world are currently working on the growth of the microcavity samples of increasingly high quality. All kinds of optical spectroscopy techniques are being applied to study the properties of exciton–polaritons in microcavities, and the phenomena observed are still puzzling the theorists involved in these studies.

The authors of the present book were charmed by the physics of microcavities in its early years. We have enjoyed the collaboration of well-known experts in this field, including Profs. Ivchenko, Andreani, Skolnick, Baumberg and Gibbs. We do not pretend to write the story of microcavities from beginning to end, for the simple reason that the story is not yet finished. We try to give an overview of the first decade of the "microcavity boom" and to address those experimental findings and theoretical results that seem to us the most interesting.

While we were writing this book, the monograph on microcavity polaritons treated within the quantum electrodynamics written by Yamamoto, Tassone, and Cao has appeared, also many review papers or separate chapters devoted to such cavities have been published in other books. We believe that our present book is oriented for more general audience than the above-mentioned texts. As we hope, it will allow the non-specialist to find quickly all the basic information on this subject. We describe a variety of optical phenomena observed in microcavities in the framework of a uniform semiclassical formalism, contrary to many reviews published previously.

Our point of view on the theory of cavity polaritons can be briefly formulated as follows. We suppose that the most natural and simple way to interpret linear optical effects (all effects connected with polaritons are optical effects) is to use classical optics. We shall avoid in this book the unnecessary use of quantum mechanics, and will consider the interaction of light with excitons in terms of Maxwell's equations for a system with a non-local dielectric response function.

We are convinced that the language of classical optics is the most suitable for a description of coherent optical spectra (reflection, transmission and resonant elastic scattering spectra), and can be successfully applied to interpret a number of non-linear effects in cavities. We only use the alternative formalism of quantum electrodynamics in the second part of the book, when talking about Bose condensation of exciton–polaritons and perspectives of polariton laser realisation.

We have divided the book into two parts that address linear and non-linear optical effects, respectively. Historically, studies of microcavities began with reflectivity measurements that revealed the strong coupling between the exciton resonance and the confined cavity mode (Weisbuch, 1992). This is why we begin with a careful calculation of light reflection by the basic elements of a microcavity, namely Bragg mirrors and quantum wells. We introduce exciton–polaritons in quantum wells following the works of Andreani, Bassani and Ivchenko (1990–1992). Using the transfer matrix formalism we show how to obtain the dispersion equations for exciton–polaritons in microcavities. Within the same formalism we then consider some important particular cases: coupled microcavities, microcavities containing quantum wires or quantum dots, and the effects of a magnetic field on cavity polaritons. Special attention is paid to the effect of potential disorder. This is an issue that has inspired a number of controversial theories. We discuss these theories and present in detail our own model based on solution of Maxwell's equations in a system containing a set of localised exciton states distributed in energy.

In the "non-linear" part of the book, we address first the simplest non-linear experiment: photoluminescence under strong optical pumping. The strong-to-weak coupling threshold due to screening of excitons is also discussed. We then focus on the most recent experimental data on the dynamics of energy relaxation of exciton–polaritons in microcavities. Observation of the stimulated scattering of exciton–polaritons by Baumberg et al. (2000) has opened a new field that currently attracts a huge number of experimental groups and theorists. The bosonic behavior of polaritons observed in the experiments of Baumberg and collaborators has inspired much speculation on the possibility of realisation of a new generation of optoelectronic devices, namely polariton lasers, which do not require a population inversion. We shall carefully describe all the main mechanisms of polariton relaxation in cavities: scattering with acoustic and optical phonons, polariton–polariton scattering and polariton–electron scattering. The famous "bottleneck" problem essential for the realisation of polariton lasers will also be addressed. Finally, we give a simple theory of polariton Bose condensation in a finite two-dimensional system and discuss the possibility of realisation of a polariton laser.

We have limited our scope to only microcavities in the strong coupling regime; for all effects connected with vertical cavity surface emitting lasers (VCSELs) or vertical cavity light emitting diodes (VCLEDs) the reader is advised to search elsewhere.

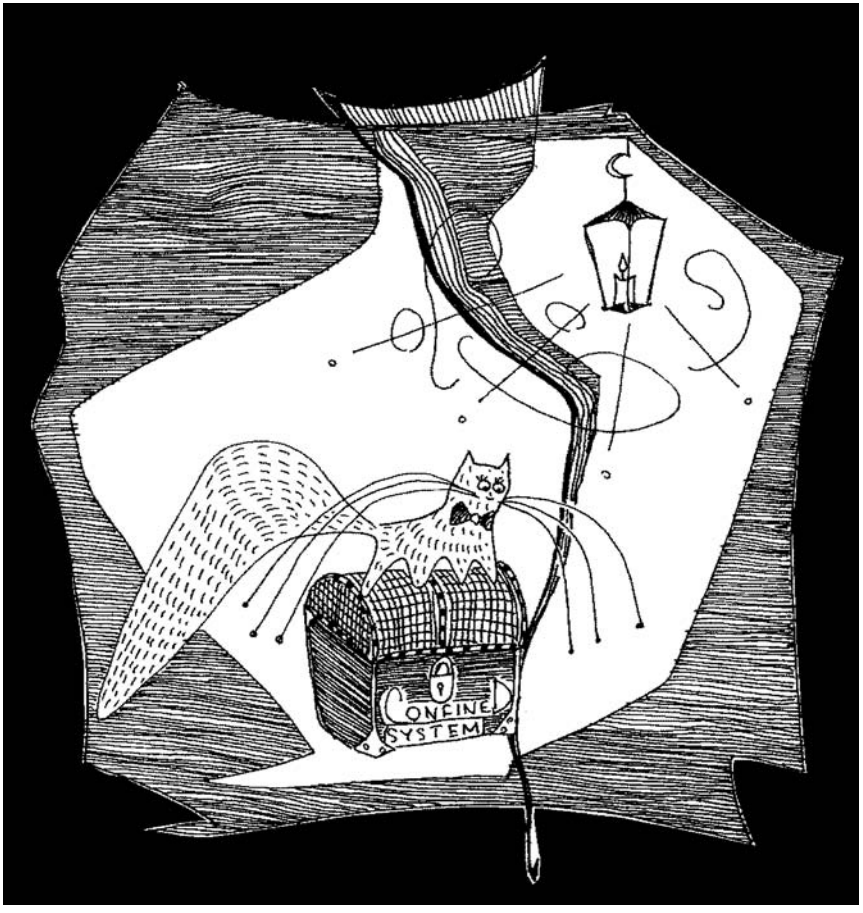

Light–matter coupling in microcavities with quantum boxes.

While our book presents a theory of cavity polaritons, each chapter also refers to the experimental data. We describe real microcavity samples and include a number of figures showing the most essential experimental curves. However, we do not describe in detail the experimental techniques. The book is oriented to the general reader, including undergraduate students who have already passed a course in solid-state physics, postgraduate students, and researchers working in solid-state physics. No special knowledge of mathematics is required from the reader. The two main formalisms we use, the Green's function formalism and the transfer matrix formalism, will be described to the extent needed for understanding of the analytical development in the text. The transfer matrix formalism will

be given in detail in the Appendix. The bibliography contains the most essential textbooks in the area of semiconductor optics, as well as an extensive list of articles on the physics of microcavities that have appeared in the last decade. Note also that we shall only use the cgs system of units.

This book would not have been possible without the help, encouragement and advice of Vladimir Moiseevich Agranovich, who proposed that we should start work on a textbook on microcavities at the end of 2001. It is our pleasure to thank all the people who have worked with us in this area. We would like to mention here, in particular, Masha Vladimirova, Eugenius Ivchenko, Mikhail Kaliteevski, Claudio Andreani, Giovanna Panzarini, Maurice Skolnick, Jeremy Baumberg, Fabrice Laussy, Yury Rubo, Kirill Kavokin, Bernard Gil, Wolfgang Langbein and Aldo Di Carlo. None of the authors of this book is a native English speaker. The reader will probably find a lot of stylistic if not orthographic errors. We are extremely grateful to D. Parfitt and F. Laussy who have corrected a huge number of such errors in the manuscript, and we deeply apologize for remaining language imperfections. We wish the reader a pleasant encounter with microcavities. We would greatly appreciate any feedback in the form of criticisms, remarks or suggestions.

ALEXEY KAVOKIN AND GUILLAUME MALPUECH
7 May 2003

Introduction

A typical microcavity structure is shown schematically in Figure 1. It consists of a planar Fabry–Perot cavity sandwiched between two so-called *Bragg mirrors*, and containing an embedded quantum well (QW), or possibly a thin layer of bulk semiconductor, multiple QWs, quantum wires or quantum dots. A Bragg mirror is a periodic structure composed of two semiconductor or dielectric materials with different refractive indices. The thicknesses of the layers are chosen so that the light reflected by all the interfaces interferes negatively within a spectral range further referred to as a *stop-band*. In high-quality structures the reflectivity of Bragg mirrors within the stop-band exceeds 99%. Their spectral width can be up to 100 meV. The thickness of the cavity layer is usually one to three wavelengths of light at the centre of the stop-band. A so-called *cavity mode*, i.e., a light mode confined in the cavity, has a finesse dependent on the reflectivity of the mirrors. It can be as high as 1500–2000 in the best samples. In quantum microcavities the parameters of the Bragg mirrors and cavity are chosen so as to have a resonance between the cavity mode frequency and the *exciton* transition in a quantum structure embedded into the cavity. We remind the reader that excitons are Coulomb-correlated electron–hole pairs characterised by discrete transition frequencies. Effects originating from coupling of the exciton resonance and the cavity mode are referred to as *exciton–polariton* effects, where an *exciton–polariton* is a half-light

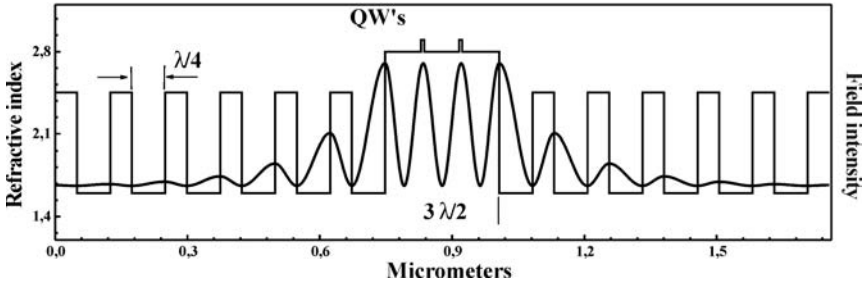

Fig. 1. A typical microcavity structure. The central cavity layer having a thickness equal to an integer number of half-wave-lengths of light at the exciton resonance frequency is sandwiched between two Bragg mirrors. A quantum well (several quantum wells) should be embedded in the antinodes of the cavity mode electric field in order to provide the strongest coupling to light.

half-matter crystal excitation, a quasi-particle combining the properties of excitons and photons.

Exciton–polaritons, predicted theoretically by Hopfield [1] and Agranovich [2] in the end of 1950s, have been extensively studied in bulk semiconductor materials [3,4], thin films [5,6], quantum wells [7,8], and quantum wires and dots [9,10]. They can be interpreted as virtual exciton–photon pairs that propagate in the crystal because of a chain of processes of virtual absorption and emission of photons by excitons. It is essential to note that the polariton states are true eigenstates of the system, so that once the polaritons are present there are no more pure excitons or photons. Although the original theory of exciton–polaritons was written using the second quantisation technique, it was quickly understood that a so-called semiclassical approach is formally equivalent to the quantum description for any linear optical problem. Within the semiclassical approach, which will be mostly used in this book, the Maxwell equations are resolved for light propagating within a dielectric medium characterised by frequency-dependent, and eventually wave-vector-dependent, complex polarisation induced by excitons. Dispersion of exciton–polaritons in this case is nothing but dispersion of light modified due to the presence of the exciton resonance. The semiclassical technique is highly suitable for calculation of coherent optical spectra (reflection, transmission and elastic scattering), while it hardly describes the energy relaxation and dephasing of exciton–polaritons.

Exciton–polaritons in microcavities have very particular properties resulting from the reduced dimensionality of the system with respect to semiconductor structures with no optical confinement. In particular, the strength of exciton–light coupling is greatly enhanced in microcavities, which results in the so-called *strong-coupling* regime manifested by *anticrossing* of the exciton–polariton modes, observed for the first time by Claude Weisbuch et al. [11] in 1992. Figure 2 shows a series of reflection spectra of a microcavity sample studied by Weisbuch [11]. The sample chosen for this experiment was spatially inhomogeneous in its plane, thus giving experimentalists an opportunity to tune the cavity mode to the exciton resonance by changing the light-spot position on the surface of the sample. They found a point of exact resonance between the light mode and the exciton resonance, where the reflection spectrum exhibited two distinct dips corresponding to two exciton–polariton eigenmodes of the microcavity. These eigenmodes appeared to be split at the anticrossing point that defines the strong-coupling regime. Splitting between modes at this point is widely referred to as *vacuum-field Rabi splitting* or simply *Rabi splitting*, although the term ‘Rabi splitting’ was originally used in atomic physics to describe a different effect. Note that in the opposite case of the weak-coupling regime, there is no splitting between polariton eigenmodes at the crossing point. The weak-coupling regime is realised, in particular, in vertical-cavity surface emitting lasers (VCSELs) and vertical cavity light emitting diodes (VCLEDs).

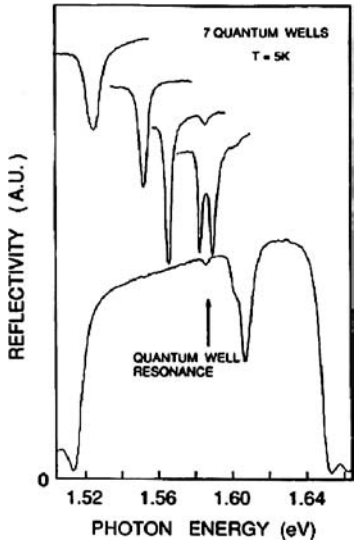

Fig. 2. Experimental reflectivities of a GaAs-based microcavity sample taken from Ref. [11]. The spectra have been taken from different positions on the sample grown so that layer thicknesses were gradually changing from its center to its boards. Thus, scanning the sample, experimentalists were able to change the *detuning* between the exciton and cavity mode resonances. As a result, an *anticrossing* of two modes has been documented.

In the course of this book we shall only discuss phenomena that are characteristic of the strong-coupling regime. Among these phenomena one should mention first the particular dependence of the polariton eigenfrequencies on the in-plane wave-vector of the incident light. This dependence, which will subsequently be referred to as *in-plane dispersion* of cavity polaritons, has been measured experimentally using angle-resolved reflection by Houdré et al. [12]. It has been shown that the shape of polariton dispersion curves is strongly dependent on the *detuning* between the bare cavity mode $\omega_c(k)$ and the bare exciton mode $\omega_0(k)$ at zero in-plane wave-vector $k = 0$. The detuning is given by $\omega_c(0) - \omega_0(0)$. Figure 3 shows three typical dispersion curves of cavity polaritons calculated for positive, zero and negative detunings. One can see that at small k the dispersion of exciton–polaritons in the cavity is essentially parabolic, and can be characterised by some effective mass, while this mass varies dramatically as a function of detuning. The possibility of tuning the polariton effective mass over a wide range is an important peculiarity of microcavities.

Between 1992 and 2002 a variety of microcavity structures have been studied. The observed Rabi splittings have reached about 45 meV in the best inorganic cavities and are an order of magnitude larger in organic cavities [13]. An external magnetic field has been shown to increase the polariton splitting [14]. Microcav-

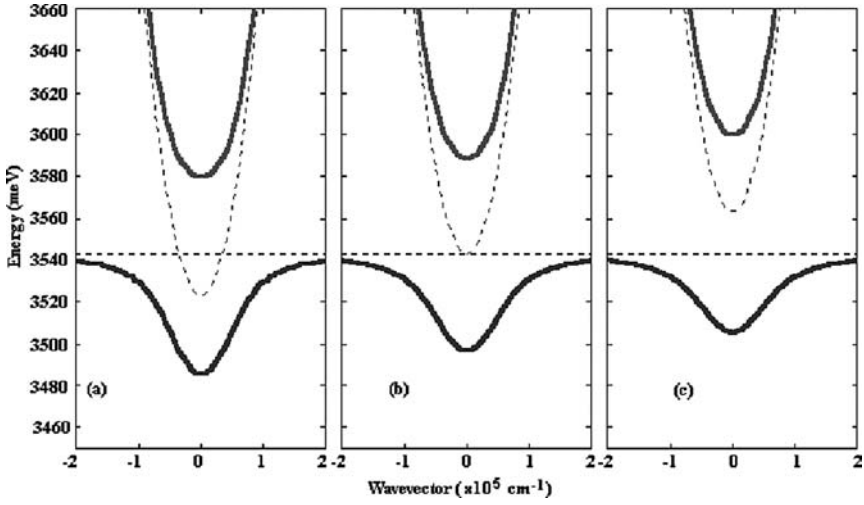

Fig. 3. In-plane dispersion of two exciton–polariton modes in a typical GaAs-based microcavity calculated for different detunings between exciton and photon modes: $\delta = 10$ meV (a), $\delta = 0$ (b), and $\delta = -10$ meV (c). Dashed lines show the energies of uncoupled exciton and photon modes.

ities containing layers of bulk semiconductor, multiple QWs, and quantum wires and dots, as well as coupled microcavities, pillar microcavities and photonic cavities, have been studied. Some of these structures, offering new optical effects, are addressed in this book. Conventional microcavities with embedded QWs have shown the greatest number of interesting phenomena. At the end of the 1990s, the scientific community enthusiastically discussed the so-called *motional narrowing* effect [15], initially associated with the observed narrowing of polariton spectral resonances in the vicinity of the anticrossing point. Further profound studies of the *disorder* scattering of cavity polaritons [16] helped to understand the dynamics of these unusual quasi-particles. We address the scattering of polaritons at the end of the first part of this book ("linear effects").

Before starting the "linear part" of the book, we advice the reader to look through Frequently Asked Questions section that addresses on a qualitative level without any equations some important issues concerning the cavity polaritons.

Chapter 1 of the "linear part" addresses the linear optical properties of the basic elements composing a microcavity, namely, quantum wells (QWs) containing exciton resonances and Bragg mirrors. We apply so-called "non-local dielectric response model" [7–9] to describe the interaction of light with excitons in QWs. Using the transfer matrix technique described in detail in Appendices A–C to this book we calculate reflection coefficients of the Bragg mirrors. Within the same technique we find the eigen-energies of exciton–polaritons in microcavities, trace

their in-plane dispersion curves, and analyze weak and strong exciton–light coupling regimes.

Chapter 2 gives an overview of linear optical properties of four different kinds of microcavity systems: namely, microcavities containing multiple QWs, bulk semiconductor microcavities, coupled microcavities with QWs, and cavities containing gratings of quantum wires. We investigate the eigen-energies and in-plane dispersion of exciton–polaritons in all these cases. We also address in this chapter the magnetic field effect on the polariton states, including very peculiar polarization properties of microcavities subjected to the magnetic field.

Chapter 3 is devoted to the problem of in-plane potential disorder in microcavities. We consider the resonant scattering of light by individual localized excitons and by ensembles of localized excitons that allows us to describe within the same formalism reflection, transmission and resonant Rayleigh scattering experiments. We analyze as well the time-resolved optical response of the microcavities in the dynamics of photoluminescence from the cavities in the linear regime. This chapter concludes the "linear" part of the book.

The second part of this book presents an overview of the non-linear optical properties of semiconductor microcavities, which have been studied systematically since the second half of 1990s, still remaining a very young research field. We try, as much as possible, to give here an instantaneous picture of the state of the art in this rapidly evolving area.

The first experimental studies of microcavities in the non-linear regime [17–19] were mainly focused on the transition between strong-coupling and weak-coupling regimes. The challenge was at that time to understand whether the strong-coupling collapse was associated with the exciton oscillator strength loss or carrier-induced exciton broadening. A related effect, associated with the possibility of saturating the excitonic absorption, is the AC Stark splitting reported in 1998 by F. Quochi et al. [20]. To briefly summarise, the general trend that followed the discovery of the strong-coupling regime was to understand the extent to which it resists an excitation density or temperature increase.

This early stage was followed by two breakthroughs, the first one conceptual and the second one experimental, but both associated with the bosonic nature of polaritons. Imamoglu [21] was the first, in 1996, to propose the use of the bosonic character of cavity polaritons to build up an exciton–polariton condensate that would emit coherent laser light spontaneously. The build-up of a ground-state coherent population can be interpreted as a phase transition towards a Bose condensed state or as a "polariton lasing" effect resulting from bosonic stimulated scattering. The criterion for Bose condensation in a macroscopic ground-state density in the thermodynamic limit is:

$$\lim \frac{N_0(R)}{R^2} \underset{R\to\infty}{\longrightarrow} n_0,$$

where N_0 is the ground-state population, n_0 is a finite, positive, real number, and R is the system size. On the other hand, bosonic stimulated scattering is not necessarily an equilibrium property and the criterion is less restrictive:

$$N_0(R) \gg 1.$$

Both BEC and stimulated scattering effects are based on the same physics, namely on the tendency of bosons to accumulate in the same (ground) quantum state. Actually, stimulated scattering represents a dynamical aspect of Bose condensation.

"Polariton lasers" exploit both of these effects. Formation of the condensate within the polariton lifetime is only possible because of the rapidity of stimulated scattering. Once condensed, polaritons emit coherent monochromatic light. Here and in what follows, by "emission of light by polaritons" we mean escape of light from the cavity by its tunneling across the Bragg mirrors. As the light emission by a polariton quasi-condensate is spontaneous there is no population inversion condition required in polariton lasers, absorption of light does not play any role, and ideally there is no threshold for lasing. Concerning this latter point, the argument is that it is sufficient to have two polaritons in the ground state for creating a condensate and then collecting two coherent photons. Imamoglu's idea was to create an equilibrium polariton distribution by external optical pumping. Relaxation of this (non-thermal) distribution via its interaction with acoustic phonons was assumed to be able to provide an efficient polariton accumulation in their ground state. However, a number of peculiarities of cavity polaritons, especially their unusual dispersion shape, was not taken into account in the proposed model, which therefore omitted most of the physics of real microcavities. This conceptual proposal of a polariton laser has inspired many researchers to work on the realisation of this new quantum device. This work is in progress at the moment of writing.

The research efforts to realise polariton lasers can be briefly summarised as follows. A few months after Imamoglu's prediction, the Yamamoto group [22] published an experimental paper claiming the observation of polariton lasing. However, what they actually observed was rather "normal laser emission", as they recognised a few months later. It was then demonstrated theoretically, by Tassone [23], that acoustic phonons cannot provide an efficient polariton relaxation towards the ground state because of the steep central part of the polariton dispersion "*bottleneck region*", where its slope exceeds the sound velocity. Nevertheless, a quadratic dependence of emission on the non-resonant pumping power has been observed experimentally in II–VI [24] and III–V [25] microcavities. This was a proof that other relaxation mechanisms allow a part of the polaritons to cross the bottleneck region. The principal of these additional mechanisms is the exciton–exciton scattering [26]. F. Boeuf et al., and others [27] have reported an exponentially growing emission intensity versus pumping in-

tensity, and have claimed that bosonic stimulation of relaxation to the ground state takes place in their experiments. However, neither the ground-state occupation factor nor the coherence of the emitted light have been checked in these works, and it seems to us that no clear evidence of polariton lasing has been given.

The second breakthrough came from an experiment performed under resonant excitation by Savvidis and Baumberg [28]. They macroscopically populated the inflection point of the lower polariton branch (wave-vector k_0) by a 1 ps pump pulse. A weak probe pulse sent at a normal angle to the sample within a short delay was used to seed the polariton ground state. This stimulated a simultaneous scattering of one k_0 polariton to the ground state and another to the state $2k_0$. This process conserves energy and wave-vector, and has provided an amplification of the probe reflection by a factor of 70. Similar results have been obtained under *cw* excitation by Stevenson and Skolnick in GaAs-based cavities [29], and by Saba et al. in CdTe-based structures [30]. In this latter case, stimulated scattering to the ground state was seen up to 200 K. Strong dressing of the dispersion relation due to the interaction between coherently populated states has also been observed [31], and successfully interpreted by Ciuti [31] by a generalisation of the Bogoliubov [32] approach. These experimental results have clearly demonstrated the bosonic behaviour of cavity polaritons up to quite high pumping intensities and temperatures. The occurrence of "spontaneous symmetry breaking", namely of a bosonic phase transition [33] in the Stevenson et al. experiment [29] is under debate [34]. A complex spin dynamics, which is a signature of strong bosonic effects, has also been observed under resonant excitation by Lagoudakis et al. [35], and recently under non-resonant excitation by Martín et al. [36]. These last results are not yet fully understood [37], but reveal the possibilities associated with this new research area. Finally, in the end of 2002, an increase of coherence of light emitted from a ground polariton state in a GaAs-based microcavity containing 12 QWs versus non-resonant pumping intensity has been reported [38]. If confirmed, this discovery could represent a step towards the achievement of a quasi-Bose condensation effect in solid state systems. Readers interested in theoretical aspects of this problem will enjoy reading of the "Semiconductor Cavity Quantum Electrodynamics" by Yamamoto, Tassone, and Cao [39].

Since the Savvidis and Baumberg experiment, both in theory and experiment, the regimes of resonant excitation and non-resonant excitation are clearly distinguished. The most important milestone on the path towards experimental realisation of polariton lasers would be evidence for spontaneously appearing polariton coherence in non-resonantly pumped microcavities. The build-up of a ground-state coherent population can be interpreted as a phase transition toward a Bose condensed state or as a "polariton lasing" effect resulting from bosonic stimulated scattering.

Chapter 4 presents PL experiments performed during the decade 1992–2002, and where polariton stimulated scattering has not been observed. The differences between cavity polariton PL and QW exciton PL are pointed out. The weak-strong coupling transition is discussed. The appearance of a kinetic blocking in the polariton relaxation, also called the bottleneck effect, is described and discussed. Tools allowing for a theoretical description of cavity PL are introduced. We present the mechanisms of scattering of polaritons in semiconductor microcavities. The matrix elements of the different processes are obtained analytically in the Born approximation and in the framework of the Fermi golden rule. The model describing the kinetic relaxation of particles with use of the semi-classical Boltzmann equation is presented. Numerical applications are also presented and the relative efficiency of the various processes is discussed.

Chapter 5 presents and reviews experimental and theoretical results on microcavity emission at resonant excitation. We focus on the experimental configuration at which the stimulated scattering was observed due to formation of a dynamical condensate of polaritons. Pump-probe and *cw* experiments are described as well. Dressing of the polariton dispersion because of inter-condensate interaction is also discussed. The semi-classical and the quantum theories of these effects are presented and their results analysed.

Chapter 6 is entitled: "Toward Polariton Bose Condensation, and Polariton Lasers". The thermodynamic equilibrium of bosons and the critical conditions for their condensation are described. The theoretical polariton phase diagram of a wide class of microcavity systems is presented. We show that the critical temperature for polariton Bose condensation can in some cases be higher than the room temperature. We present a review of experimental and theoretical efforts devoted to the comprehension of the relaxation kinetics of quantum well excitons and cavity polaritons. The model describes the kinetic relaxation of particles using the semi-classical Boltzmann equation. The solutions allowing the removal of this kinetic blocking and the achievement of the polariton Bose condensation are presented. A quantum kinetic theory, describing relaxation of cavity polaritons and the formation of a quasi-condensate in non-resonantly pumped finite-size microcavities is presented. Finally, polariton spin relaxation dynamics in microcavities is addressed.

We estimate the potential of microcavities for both basic studies and applications to be very high. Much work remains to be done in order to understand the quantum kinetics of exciton–polaritons and their spin-relaxation mechanisms. Intriguing consequences of the Bose condensation of polaritons, such as the optical Josephson effect, to give an example, are awaiting further investigation. Our knowledge of microcavity polaritons is far from complete, and its further advancement is certainly in the hands of the readers of this book.

References

1. J. J. Hopfield, Theory of the contribution of excitons to the complex dielectric constant of crystals, *Phys. Rev.* 112, 1555 (1958).
2. V. M. Agranovich, *Zh. Eksper. Teoret. Fiz.* 37, 1555 (1959).
3. V. M. Agranovich, V. L. Ginzburg, "Spatial Dispersion in Crystal Optics and the Theory of Excitons". Interscience Publ., London, 1966.
4. E. L. Ivchenko, Spatial dispersion effects in exciton resonance region, in "Excitons" (E. I. Rashba and M. D. Sturge, Eds.). Elsevier, North-Holland, 1982.
5. D. Frölich, A. Kulik, B. Uebbing, A. Mysyrowicz, V. Langer, H. Stolz, W. von der Osten, Coherent propagation and quantum beats of quadrupole polaritons in Cu_2O, *Phys. Rev. Lett.* 67, 2343 (1991).
6. G. Panzarini, L. C. Andreani, Bulk polariton beatings and two-dimensional radiative decay: Analysis of time-resolved transmission through a dispersive film, *Solid State Comm.* 102, 505 (1997).
7. L. C. Andreani, F. Tassone, F. Bassani, Radiative lifetime of free excitons in quantum wells, *Solid State Comm.* 77, 641 (1991).
8. E. L. Ivchenko, Excitonic polaritons in periodic quantum well structures, *Sov. Phys. Solid State* 33, 1344 (1991).
9. E. L. Ivchenko, A. V. Kavokin, Light reflection from quantum well, quantum wire and quantum dot structures, *Sov. Phys. Solid State* 34, 1815 (1992).
10. A. D'Andrea, R. Del Sole, Excitons in semiconductor confined systems, *Solid State Comm.* 74, 1121 (1990).
11. C. Weisbuch, M. Nishioka, A. Ishikawa, Y. Arakawa, Observation of coupled exciton–photon mode splitting in a semiconductor quantum microcavity, *Phys. Rev. Lett.* 69, 3314 (1992).
12. R. Houdré, C. Weisbuch, R. P. Stanley, U. Oesterle, P. Pellandini, M. Ilegems, Measurement of cavity-polariton dispersion curve from angle-resolved photoluminescence experiments, *Phys. Rev. Lett.* 73, 2043 (1994).
13. D. G. Lidzey, D. D. C. Bradley, M. S. Skolnick, T. Virgili, S. Walker, D. M. Whittaker, Strong exciton–photon coupling in an organic semiconductor microcavity, *Nature* 395, 53 (1998); D. G. Lidzey, A. M. Fox, M. D. Rahn, M. S. Skolnick, V. M. Agranovich, S. Walker, Experimental study of light emission from strongly coupled organic semiconductor microcavities following nonresonant laser excitation, *Phys. Rev. B* 65, 195312 (2002).
14. J. D. Berger, O. Lyngnes, H. M. Gibbs, G. Khitrova, T. R. Nelson, E. K. Lindmark, A. V. Kavokin, M. A. Kaliteevski, V. V. Zapasskii, Magnetic field enhancement of the exciton–polariton splitting in a semiconductor quantum well microcavity, *Phys. Rev. B* 54, 1975 (1996).
15. D. M. Whittaker, What determines inhomogeneous linewidths in semiconductor microcavities?, *Phys. Rev. Lett.* 80, 4791 (1998).
16. W. Langbein, J. M. Hvam, Elastic scattering dynamics of cavity polaritons: Evidence for time-energy uncertainty and polariton localization, *Phys. Rev. Lett.* 48, 47401 (2002).
17. R. Houdré, J. L. Gibernon, P. Pellandrini, R. P. Stanley, U. Oesterle, C. Weisbuch, J. O'Gorman, B. Roycroft, M. Ilegems, Saturation of the strong coupling regime in a semiconductor microcavity: free carrier bleaching of cavity polaritons, *Phys. Rev. B* 52, 7810 (1995).
18. F. Jahnke, M. Kira, S. W. Koch, G. Khitrova, E. K. Lindmark, T. R. Nelson, Jr., D. V. Wick, J. D. Berger, O. Lyngnes, H. M. Gibbs, Excitonic nonlinearities of semiconductor microcavities in the nonperturbative regime, *Phys. Rev. Lett.* 77, 5257 (1996).
19. For a review see, for example, G. Khitrova, H. M. Gibbs, F. Jahnke, M. Kira, S. W. Koch, Nonlinear optics of normal-mode-coupling semiconductor microcavities, *Rev. Mod. Phys.* 71, 1591 (1999) and ref. therein.

20. F. Quochi, C. Bongiovanni, A. Mura, J. L. Staehli, B. Deveaud, R. P. Stanley, U. Oesterle, R. Houdré, Strongly driven microcavities: from the polariton doublet to an AC Stark triplet, *Phys. Rev. Lett.* 80, 4733 (1998).

21. A. Imamoglu, J. R. Ram, Nonequilibrium condensates and lasers without inversion: Exciton–polariton lasers, *Phys. Lett. A* 214, 193 (1996); A. Imamoglu, J. R. Ram, S. Pau, Y. Yamamoto, Nonequilibrium condensates and lasers without inversion: Exciton–polariton lasers, *Phys. Rev. A* 53, 4250 (1996).

22. S. Pau, H. Cao, J. Jacobson, G. Bjork, Y. Yamamoto, A. Imamoglu, Observation of a laser-like transition in a microcavity exciton polariton system, *Phys. Rev. A* 54 (3), R1789 (1996).

23. F. Tassone, C. Piermarocchi, V. Savona, A. Q. P. Schwendimann, Bottleneck effects in the relaxation and photoluminescence of microcavity polaritons, *Phys. Rev. B* 56, 7554 (1997).

24. L. S. Dang, D. Heger, R. André, F. Boeuf, R. Romestain, Stimulation of polariton photoluminescence in semiconductor microcavity, *Phys. Rev. Lett.* 81, 3920 (1998).

25. P. Senellart, J. Bloch, Nonlinear emission of microcavity polaritons in the low density regime, *Phys. Rev. Lett.* 82, 1233 (1999); P. Senellart, J. Bloch, B. Sermage, J. Y. Marzin, Microcavity polariton depopulation as evidence for stimulated scattering, *Phys. Rev. B* 62, R16 263 (2000).

26. F. Tassone, Y. Yamamoto, Exciton–exciton scattering dynamics in a semiconductor microcavity and stimulated scattering into polaritons, *Phys. Rev. B* 59, 10 830 (1999).

27. F. Boeuf, R. André, R. Romestain, Le Si Dang, E. Péronne, J. F. Lampin, D. Hulin, A. Alexandrou, Evidence of polariton stimulation in semiconductor microcavities, *Phys. Rev. B* 62, R2279 (2000); A. Alexandrou, G. Bianchi, E. Péronne, B. Hallé, F. Boeuf, R. André, R. Romestain, Le Si Dang, Stimulated scattering and its dynamics in semiconductor microcavities at 80 K under nonresonant excitation conditions, *Phys. Rev. B* 64, 233318 (2001); R. Huang, Y. Yamamoto, R. André, J. Bleuse, M. Muller, H. Ulmer-Tuffigo, Exciton–polariton lasing and amplification based on exciton–exciton scattering in CdTe microcavity quantum wells, *Phys. Rev. B* 65, 165314 (2002).

28. P. G. Savvidis, J. J. Baumberg, R. M. Stevenson, M. S. Skolnick, D. M. Whittaker, J. S. Roberts, Angle resonant stimulated polariton amplifier, *Phys. Rev. Lett.* 84, 1547 (2000).

29. R. M. Stevenson, V. N. Astratov, M. S. Skolnick, D. M. Whittaker, M. Emam-Ismail, A. I. Tartakovskii, P. G. Savvidis, J. J. Baumberg, J. S. Roberts, Continuous wave observation of massive polariton redistribution by stimulated scattering in semiconductor microcavities, *Phys. Rev. Lett.* 85, 3680 (2000).

30. M. Saba, C. Ciuti, J. Bloch, V. Thierry-Mieg, R. André, Le Si Dang, S. Kundermann, A. Mura, G. Bongiovanni, J. L. Staehli, B. Deveaud, High temperature ultrafast polariton amplification in semiconductor microcavities, *Nature* 414, 731 (2001).

31. P. G. Savvidis, C. Ciuti, J. J. Baumberg, D. M. Whittaker, M. S. Skolnick, J. S. Roberts, Off-branch polaritons and multiple scattering in semiconductor microcavities, *Phys. Rev. B* 63, 041303 (R) (2001).

32. N. N. Bogoliubov, *J. Phys. USSR* 11, 23 (1947); N. N. Bogoliubov, "Quantum Statistics, Lectures on Quantum Statistics, Vol. 1". Gordon and Breach Science Publisher, New York, 1970; V. A. Zagrebnov, J. B. Bru, The Bogoliubov model of weakly imperfect Bose gas, *Phys. Rep.* 350, (2001) and ref. therein.

33. A. Griffin, D. W. Snoke, S. Stringari, Eds., "Bose Einstein Condensation". Cambridge University Press, 1995.

34. D. Snoke, Spontaneous Bose coherence of excitons and polaritons, *Science* 298, 1368 (2002).

35. P. G. Lagoudakis, P. G. Savvidis, J. J. Baumberg, D. M. Whittaker, P. R. Eastham, M. S. Skolnick, J. S. Roberts, Stimulated spin dynamics of polaritons in semiconductor microcavities, *Phys. Rev. B* 65, 161310 (2002).

36. M. D. Martín, G. Aichmayr, L. Viña, R. André, Polarization control of the nonlinear emission of semiconductor microcavities, *Phys. Rev. Lett.* 89, 077402 (2002).

37. A. Kavokin, G. Malpuech, P. G. Lagoudakis, J. J. Baumberg, K. Kavokin, Polarization rotation in resonant emission of semiconductor microcavities, *Phys. Stat. Sol. (a)* 195, 579 (2003); A. Kavokin, G. Malpuech, P. G. Lagoudakis, J. J. Baumberg, Polarization rotation in parametric scattering of polaritons in semiconductor microcavities, *Phys. Rev. B* 67, 195321 (2003).

38. H. Deng, G. Weihs, C. Santori, J. Bloch, Y. Yamamoto, Condensation of semiconductor microcavity exciton polaritons, *Science* 298, 199 (2002).

39. Y. Yamamoto, F. Tassone, H. Cao, "Semiconductor Cavity Quantum Electrodynamics". Springer, Berlin, 2000.

This page intentionally left blank

Frequently Asked Questions

We advise the readers to look through this chapter as it will help them to understand some essential aspects of the physics of microcavities. It addresses a few simple but important 'Frequently Asked Questions', and is oriented in particular towards those who do not like heavy mathematics in books on physics. We fully understand and respect their point of view, and apologise that in the rest of the book we shall nevertheless use long equations. This chapter contains no formulas and its role is to give a simple qualitative image of most of the effects discussed later in the book.

What is the difference between a microcavity and a wave-guide?

Both in wave-guides and in microcavities light modes can be confined. The difference is that optical confinement in wave-guides is due to the effect of full reflectivity that requires necessarily oblique incidence of light, while in microcavities the confinement is provided by highly-reflecting mirrors and does not require the oblique incidence. That is why the wave-vector of light in the plane of a wave-guide cannot be equal to zero for a confined mode, while a photon mode of a microcavity can have a zero in-plane wave-vector. This difference allows one to observe the eigenstates of a microcavity in direct optical experiments, such as reflection or transmission.

What is the difference between a microcavity and a VCSEL?

There is no difference. Vertical cavity surface emitting lasers (VCSELs) are based on microcavities. On the other hand, there is a difference between the *strong coupling regime* in which most specific microcavity effects are observed and the *weak coupling regime* in which VCSELs operate. In the strong coupling regime, if the frequency of the optical mode of the cavity is tuned to the exciton resonance frequency, exciton–light coupling results in the splitting of the eigenstates of the system (called *exciton–polariton modes*). This splitting ranges from a few meV to a few tens of meV in existing microcavity samples, and is usually (not very correctly!) referred to as *vacuum-field Rabi splitting*. In VCSELs at resonance, however, the cavity photon and exciton states remain degenerate, while the exciton radiative lifetime typically becomes shorter due to its coupling to the cavity mode. This effect is exploited in lasers as it accelerates the stimulated emission of light by electron–hole pairs.

What is the difference between dielectric and metallic mirrors?

Reflection of light by metallic mirrors is due to absorption of light in a metal. The refractive index of an absorbing media has an imaginary part. If it strongly exceeds the real part of the refractive index, the reflection coefficient of the metal is close to unity, and losses of light due to absorption are small. On the other hand, due to absorption metallic mirrors are not completely transparent. Therefore, one cannot excite an exciton–polariton in a microcavity through a metallic mirror. That is why the back mirrors of microcavities can be made metallic while the front mirrors should be dielectric (or semiconductor). In metallic mirrors, the electric field of the reflected light wave has a node at the surface of the mirror. In dielectric mirrors (*Bragg mirrors*), a high reflectivity is achieved because of the positive interference of light reflected by different interfaces between dielectric layers with different refractive indices. In order to obtain the strongest interference, the thicknesses of these layers are chosen to be equal to a quarter of the wavelength of light in the corresponding material at some frequency referred to as the *Bragg frequency*. Usually, there is no absorption in Bragg mirrors as the absorption edge of the materials that compose the mirror is higher in energy. Its reflectivity is dependent on the number of pairs of quarter-wave layers and on the contrast between the refractive indices of the two materials that make up the mirror. The reflection spectrum of a Bragg mirror exhibits a plateau of very high reflectivity centred on the *Bragg frequency*. This plateau is referred to as a *stop-band*. This stop-band represents a one-dimensional photonic band-gap. In an infinite ideal Bragg-mirror there are no allowed photonic states within the stop-band. Real mirrors are slightly transparent, even in the stop-band spectral range. This transparency is because of tunnelling of light across the mirror, and it allows one to excite exciton–polaritons resonantly in microcavities. Note also that an electric field of light may have either a node or antinode on the surface of the Bragg mirror. If the refractive index of the first dielectric layer of the mirror from the surface side exceeds the index of the second layer (which is usually the case in semiconductor microcavities), the field has an antinode on the surface, and vice versa. A Bragg mirror also reflects light at oblique incidence while the stop band shifts towards higher frequencies, in this case with respect to the normal incidence case.

What is the difference between Frenkel and Wannier–Mott excitons?

The difference is of a quantitative nature. Frenkel and Wannier–Mott excitons represent different theoretical models for the same object: a neutrally-charged crystal excitation called an exciton. Frenkel excitons originate from excited molecular states coupled by a crystal potential. The interaction of an electron and a hole within this state is stronger than the intermolecular coupling, so that the crystal potential can be considered as a perturbation with respect to the Coulomb interac-

tion within the exciton. This is why Frenkel excitons are not attached to the crystal bands, but themselves form excitonic bands in a molecular crystal. They have a typical binding energy of a few hundreds of meV and a typical Bohr radius of a few angstroms. Frenkel excitons dominate the optical properties of organic materials. They have a huge oscillator strength but a very small size, which makes them unsuitable for Bose condensation. In contrast, Frenkel exciton–polaritons are spatially extended and can Bose condense. In existing organic microcavities the coupling constant between a Frenkel exciton and an optical mode is an order of magnitude larger than in inorganic cavities, which makes organic cavities excellent candidates for realisation of polariton lasers. A huge structural and potential disorder, however, induces a rapid decoherence of polaritons in organic cavities, thus preventing Bose condensation. Excitons in organic materials are addressed in detail in another book of this series (Vol. 31, V. Agranovich and F. Bassani).

Wannier–Mott excitons are formed in inorganic semiconductor crystals where the interatomic coupling dominates over the Coulomb interaction of electrons and holes. As a result, for this kind of excitons the Coulomb attraction can be considered as a perturbation. Wannier–Mott excitons form a discrete, hydrogen-atom-like energy spectrum near the band-edge of a semiconductor. Their binding energy ranges from a few meV to a few tens of meV, depending on a material. In general, the binding energy is larger in wide-band-gap semiconductors than in narrow-band-gap ones. In a number of semiconductor materials, excitons dissociate at room temperature, which is one of the main difficulties for realisation of optical devices using excitons. The Bohr radii of Wannier–Mott excitons vary from a few tens to hundreds of angstroms. The dipole–dipole interaction between these excitons is strong enough to allow for their Bose condensation under certain conditions.

Why do excitons in quantum wells reflect light?

This is because an exciton has a dipole moment. This dipole moment contributes to the dielectric polarisation of a quantum well (QW), and changes it at the exciton resonance frequency. This variation of dielectric polarisation reflects light, but on the other hand, this variation is induced by light itself. A polariton effect consists of a coherent chain of absorption–emission processes of a photon by an exciton. Due to this effect, an exciton resonance has a radiative broadening (a few tens of microvolts in typical QWs), and an exciton has a radiative lifetime (about 10 ps for a free exciton in typical QWs). Note that an individual localised exciton state scatters light rather than reflects it. Due to the positive interference of light waves scattered by different localised excitons in the reflection or transmission directions, the intensities of light waves reflected or transmitted by QWs are about six orders of magnitude higher than the average intensity of scattered light in typical QW structures.

Why do excitons couple more strongly to light in microcavities than in other structures?

A semiclassical image that allows us to understand the enhancement of light–matter coupling in microcavities is as follows. Imagine a photon that propagates in a cavity. Once it arrives at the border of the cavity, it is reflected by a Bragg mirror (it can also escape from the cavity by tunnelling through the mirror, but the probability of this is relatively small). If it is reflected, it crosses the cavity and eventually interacts with an exciton located in a QW. If it is not absorbed in a QW, it arrives at the opposite Bragg mirror and is reflected once again. In high-quality cavities, photons make about one hundred round trips on average before penetrating outside. Thus, the probability for them to interact with an exciton is a hundred times higher than in conventional QW structures with no mirrors. The average number of round trips is dependent on the *quality factor* of the cavity, which is dependent on the reflectivity of its mirrors. The higher the reflectivity, the higher the quality factor and the average number of round trips. The strong coupling regime holds if photons make enough round trips to be absorbed and re-emitted many times by QWs excitons before to leave the cavity.

What are "dark" and "bright" polaritons?

The *darkness* or *brightness* of a given polariton state is proportional to its radiative decay rate. The criterion is the relation of this rate to the decay rate Γ_0 of a free exciton in a single QW (typically about 10 ps). In multiple QW structures the number of polariton modes is equal to the number of QWs. Some of these modes have a faster radiative decay than Γ_0, whereas others have slower radiative decay. In the particular case of a *Bragg-arranged* multiple QW structure with a period equal to half the wavelength of light at the exciton resonance frequency, there is only one very bright (*superradiant*) mode with a decay rate of $N\Gamma_0$, where N is the number of QWs. All other modes have a radiative decay rate equal to zero, and thus they are extremely dark. In microcavities, dark polaritons can be formed in particular by excitons located in QWs placed at the nodes of the photon mode of the cavity. They are optically decoupled from other polaritons. These dark states can be populated by some scattering processes and represent a kind of trap for polaritons. Excitons having their in plane wave vector larger than the wave vector of light in the media are also uncoupled to the light. They represent another kind of dark states. Excitonic transitions optically forbidden because of the spin selection rules are also referred to as dark.

What is the difference between the dispersion of exciton–polaritons in bulk crystals, QWs and microcavities?

In the first two cases, at zero wave-vector the energy of an exciton–polariton is zero, while in the case of a microcavity it is non-zero and depends on the thickness of the cavity. This is because of the confinement of the photonic mode

in the cavity, which provides it with a fixed normal-to-plane component of the wave-vector that is inversely proportional to the thickness of the cavity. Due to this component, dispersion of a bare photonic mode in a cavity becomes quasi-parabolic at low wave-vectors, and can be described by an effective mass that is typically four to five orders of magnitude lower than the excitonic mass. In the *strong coupling regime*, interaction of an exciton with this confined photon mode results in anticrossing of the dispersion curves, so that two branches of *exciton–polariton* dispersion appear, the so-called lower polariton branch and upper polariton branch. The shape of these branches is essentially dependent on two parameters: the *vacuum-field Rabi splitting* (i.e., the splitting between two polariton eigenstates at the anticrossing point) and *detuning* between the exciton resonance and the bare photon mode frequency at zero in-plane wave-vector k. The detuning is negative if at $k = 0$ the light mode lies lower than the exciton state, and positive in the opposite case. In cases of negative or zero detuning, the lower polariton branch is composed of a "photon-like" part (at low k, below the anticrossing point), and an "exciton-like" part (at larger k, above the anticrossing point).

What is the strong-to-weak coupling threshold?

Consider an exciton and a photon mode in a microcavity as two coupled harmonic oscillators. Assume that they have the same frequency. For a system of two oscillators there are two possibilities: either they continue to oscillate with the same frequency, or the system starts with two new eigenfrequencies split by a value proportional to the coupling strength between the two oscillators. The first regime is called the "weak-coupling" regime, and the second is called the "strong-coupling regime". If there is no attenuation in the system it is always in the strong-coupling regime. Attenuation means the appearance of non-zero imaginary parts of the eigenfrequencies of the two oscillators. In the case of a microcavity, these imaginary parts are given by broadenings of the exciton and photon resonances due to acoustic phonons and the finite transmittivity of the mirrors, respectively. Once the geometrical average of the two imaginary parts exceeds the coupling constant, the system passes to the weak-coupling regime. In this regime, at resonance, the real parts of the two eigenfrequencies coincide, while the imaginary parts are split. To move from strong to weak coupling in microcavities one should suppress the interaction between an exciton and a cavity mode. This can be done via exciton screening by an electron–hole plasma created by optical pumping. On the other hand, by applying a magnetic field to the system one can achieve an increase of the exciton oscillator strength and pass to the strong-coupling regime. Exciton broadening can be varied by varying the temperature: the higher the temperature the broader the exciton lines. This is why, in existing semiconductor microcavities, strong coupling is usually lost at room temperature.

What is vacuum-field Rabi splitting?

This term has come to microcavity physics from atomic physics. In atomic cavities, it means the splitting of an atomic energy level due to coupling of the cavity photon mode with an interatomic transition. "Vacuum-field" indicates that the linear optical regime is assumed, which means the interaction of a single photon with a single atom in the case of atomic cavities. In semiconductor microcavities, this term is frequently used instead of exciton–polariton splitting, although the correctness of its use has been questioned by different experts in the field. The appearance of Rabi splitting is a signature of the strong-coupling regime in microcavities. It can be detected by anticrossing of exciton and cavity-photon resonances in reflection spectra taken at different incidence angles. It should be noted, however, that two dips in reflection can be seen even in the weak-coupling regime, if the exciton inhomogeneous broadening exceeds the cavity mode width. Thus, the dip positions in reflection spectra do not coincide, in general, with the eigenmodes of a microcavity. Typical values of the Rabi splitting are from a few meV in GaAs-based microcavities with a single QW or in bulk microcavities, to more than 100 meV in organic cavities with Frenkel excitons. The record in non-organic microcavities is currently about 45 meV, while splittings up to 100 meV are expected theoretically in wide-band-gap microcavities based on GaN or ZnO.

What is the role of detuning between an exciton and a cavity mode?

Detuning is the difference between the energies of uncoupled exciton and photon modes at $q = 0$, where q is the in-plane wave-vector. The detuning is negative if the photon mode frequency is below the exciton resonance, zero if it coincides with the exciton resonance, and positive if it is above it. Detuning can take any value depending on the width of the cavity and the energy of the exciton resonance. It has a strong influence on the shape of the two branches of the exciton–polariton dispersion. At negative detunings, the lower polariton branch is composed of a "photon-like" part (from $q = 0$ to q that corresponds to the anticrossing point) and an "exciton-like" part (above anticrossing). A "photon-like" dispersion is characterised by an extremely light effective mass (about $10^{-4}m_0$), while an "exciton-like" part follows the dispersion curve of an uncoupled exciton (with an effective mass of about m_0). At positive detunings the lower polariton dispersion is essentially exciton-like, while at small q the effective mass becomes lighter due to the mixing of exciton and photon modes. The detuning strongly affects relaxation of exciton polaritons along dispersion branches, as will be discussed below.

What are the specifics of bulk microcavities?

Although the conventional image of a microcavity implies a QW (or a few QWs) at the antinodes of the confined light mode, microcavities containing no

QWs are not strongly different, and a bulk exciton coupled to a light mode exhibits very similar properties to a QW exciton. The differences come from *exciton centre of mass quantisation* in the cavity layer. Bulk exciton–polaritons in thin semiconductor films are quantised because excitons are not able to move outside the films. Theoretically, it implies the appearance of additional boundary conditions imposed on the solutions of Maxwell's equations for light waves propagating in semiconductors. The resulting solutions are discrete exciton–polariton states, whose spacing in energy is governed by an exciton translational mass. These bulk polariton modes all interact with a photon mode of a microcavity, while the strength of this interaction is dependent on the overlap integral between the electric field of a given bulk polariton eigenstate and a cavity mode. In some cases this integral can be zero for parity reasons, so that bulk polaritons remain uncoupled to the cavity mode. Note that this image is valid only if excitons are able to cross the cavity layer freely. If, due to a potential disorder, excitons are localised within the cavity, they are coupled to light in the same manner as excitonic states in quantum dots (see below).

What one should expect from microcavities containing gratings of quantum wires?

Diffraction. A grating of quantum wires can diffract light at the exciton resonance frequency. This leads to the appearance of additional cavity modes coupled via the grating. Exciton–polariton states having large in-plane wave-vectors can be excited in this way. This has a practical importance for realisation of lasers with a distributed positive feedback. Dispersion of exciton–polaritons may become quite complicated in this case, exhibiting numerous crossings and anticrossings. Moreover, in the presence of quantum wires a microcavity loses its in-plane isotropy and its optical properties become strongly polarisation-dependent. Light polarised parallel to the wires is not reflected in the same way as light polarised perpendicularly to the wires. In practice, realisation of high-quality microcavities containing regular gratings of quantum wires is not easy. The huge inhomogeneous broadening of excitons in quantum wires prevents strong coupling. In general, excitonic states in realistic quantum wires are dot-like, i.e., excitons are not able to move along the wire axes freely because of a strong potential disorder.

What are the optical properties of quantum dots in microcavities?

An exciton in a single quantum dot (QD) has essentially a fermionic nature. Actually, if the electron and hole are strongly confined in a dot, one cannot excite more than two excitons (with opposite spins) at each energy corresponding to a transition between electron and hole quantum confined states. This makes a microcavity with an embedded single QD a very peculiar quantum object, similar to an atomic cavity. To achieve a strong coupling in this structure, light con-

finement should also be strengthened with respect to a conventional microcavity. Three-dimensional confinement of light is possible in spherical microcavities or in photonic crystals containing cavities. Such a cavity must have strongly nonlinear optical properties. In particular, if no exciton is present in the cavity, its transmission spectrum will exhibit two splitted peaks, but once the only allowed exciton state is created only one transmission peak is observed. On the other hand, a planar microcavity containing an ensemble of QDs has similar optical properties to a cavity with an embedded QW. Actually, if the energies of exciton resonances in two different QDs are different by less than the cavity mode width, both excitons get optically coupled by a photon mode of the cavity if it passes through their energies. If many QD excitons are coupled with each other by light they form exciton–polariton modes, and one may see the polariton splitting (Rabi splitting) in this regime. Otherwise, the weak coupling regime holds in the cavity.

How an external magnetic field influences cavity polaritons?

A magnetic field has no influence on photonic states. On the other hand, it strongly affects excitons. Three kinds of effect can be selected: Landau quantisation of the exciton state, which leads to a blue shift of the exciton transition and its splitting into a "Landau fan" (i.e., a series of equidistant lines split by the cyclotron frequency), Zeeman splitting (spin-splitting) of excitonic levels, and modification of the exciton binding energy and oscillator strength (usually an increase with increasing magnetic field). As excitons are coupled to light in microcavities, all these effects modify the optical properties of the cavity. In a strong quantising magnetic field, a single exciton cavity mode anticrossing can be replaced by a series of anticrossings of the cavity mode with different exciton states from the "Landau fan". An increase of the exciton oscillator strength leads to an increase of polariton splitting that is proportional to the square root of the oscillator strength. Exciton Zeeman splitting results in a modification of the polarisation of light passing through the cavity. In particular, in the case of linear polarisation, the polarisation plane experiences a rotation each time the light passes through the QW. As the average number of round trips of light waves within the cavity mode can be up to 100, this results a giant Faraday rotation of the polarisation plane of light. A magnetic field also affects the spin relaxation of exciton–polaritons and formation of polariton condensates.

What is the motional narrowing effect?

This is a quantum effect that consists in the narrowing of a distribution function of a quantum particle propagating in a disordered medium due to averaging of the disorder potential on the size of the wave-function of a particle. In other words, quantum particles that are never localised at a given point of the space, but always occupy some non-zero volume, have a potential energy that is the average

of the potential within this volume. This is why, in a random fluctuation potential, the energy distribution function of a quantum particle is always narrower than the potential distribution function. Motional narrowing of exciton–polaritons was evoked after an experimental finding that the sum of the broadenings of two exciton–polariton modes measured in reflection spectra of microcavities is not a constant, but has a minimum near the anticrossing of two polariton modes. The initial interpretation was that exciton–polaritons with a lighter effective mass than excitons average a disorder fluctuation potential more effectively, which results in the motional narrowing of cavity eigenmodes. A more detailed consideration has shown that the motional narrowing effect has a negligibly small effect on reflection spectra of microcavities, although it can influence the Rayleigh scattering and photoluminescence spectra. Later, a manifestation of motional narrowing of exciton–polaritons was found in time-resolved reflection spectra of multiple QWs.

Weak localisation of exciton–polaritons: is it possible?

Yes, at certain energies and for a certain shape and amplitude of the disorder potential. Weak localisation implies interference of polaritons scattered many times by potential fluctuations with themselves. It is possible if the in-plane wavelength of a polariton is smaller than the typical distance between scatters, if the scattering has an elastic character and is efficient enough to strongly change a polariton trajectory, and if the kinetic energy of a polariton exceeds the depth of fluctuation potential wells in its path. Experimentally, weak localisation of exciton–polaritons can be observed in resonant backscattering of light from a microcavity. It is easy to see that the backscattering is enhanced by weak localisation: imagine a polariton that passes through quantum states $A, B, C, \ldots,$ and finally returns to A. It is clear that with the same probability it can take the same route backwards, i.e., A, ..., C, B, A. At the final point (A), polaritons which reach this point from both directions will have the same phase and will positively interfere. This is why backscattering of light from a cavity should exceed scattering in all other directions (although it will still be much weaker than reflection or transmission).

Photoluminescence from microcavities: what does it look like?

In the weak-coupling regime, the effect of the cavity reduces to filtering of the excitonic emission. In the strong-coupling regime, photoluminescence from both upper and lower polariton modes can be observed. It is a remarkable peculiarity of microcavities that exciton–polaritons in these structures dominate the photoluminescence spectra. In most semiconductor structures with no optical confinement, the photoluminescence is completely incoherent and is mostly governed by localised exciton states weakly coupled to light. The temporary dynamics of microcavity photoluminescence is strongly dependent on the exciton–polariton energy relaxation rate, which in turn depends on the shape of dispersion

curves, temperature, exciton parameters, etc. In most cases exciton–polaritons have no time to relax down to their ground state, and emit light mostly from the states with $q \neq 0$, i.e., at oblique angles. This is a manifestation of the so-called *bottleneck effect* (see below). If polaritons relax quickly enough they may Bose condense in the ground state. In this case the photoluminescence line becomes extremely narrow and intense, which is a signature of *polariton lasing* (see below).

What is the bottleneck effect in polariton relaxation?

Polariton relaxation along the lower dispersion branch is rapid in the exciton-like part due to scattering with acoustic phonons, but then becomes much slower in the vicinity of the anticrossing point due to the so-called *bottleneck effect*, i.e., a sharp decrease of the polariton density of states. The main obstacle for polariton relaxation in this region comes from the lack of acoustic phonons that are able to scatter with polaritons of very light effective mass. Note that any scattering act must conserve the energy and the wave-vector. The bottleneck effect prevents polaritons from relaxation down to their ground state at $q = 0$, which represents a major problem for realisation of *polariton lasers*.

The bottleneck effect formally exists also for bulk or QW exciton–polaritons. Actually, their dispersion curves also necessarily have a photon-like part and an exciton-like part. The "detuning" in this case is always negative, since at $q = 0$ the photon energy is zero in the 3D case. It is much harder to achieve a strong exciton–light coupling in bulk crystals or in QWs, because the strength of the exciton–light coupling is orders of magnitude weaker than in microcavities in this case. Moreover, relaxation of exciton–polaritons along their dispersion curves has practically no physical sense, because of an extremely rapid *dephasing* of exciton–polaritons, i.e., transformation of a coherent free exciton–polariton state occupying the entire the structure to a more or less localised exciton state weakly coupled to light. Thus, photoluminescence spectra of bulk semiconductors or QWs have no polaritonic features and are dominated by localised excitons in most cases. Polaritons only influence the reflection, transmission and resonant Rayleigh scattering spectra of these structures. On the contrary, in microcavities, photoluminescence spectra are governed by coherent polariton states, so that the anticrossing behaviour of polariton branches can be observed experimentally by measuring the photoluminescence as well as by measuring reflection or transmission.

What is the role of stimulated scattering of exciton–polaritons?

Exciton polaritons, being bosons, are subject to stimulated scattering. Its probability is proportional to the occupation number of the final state to which the polaritons are scattered. Clearly, if the final state is macroscopically populated, i.e., represents a Bose condensate, scattering to such a state is strongly ampli-

fied and becomes extremely rapid. Experimental evidence of stimulated scattering of exciton–polaritons has been obtained in a pump-probe optical experiment. A pump pulse was used to illuminate the structure at the *magic angle* (see below), while the probe pulse was sent at normal incidence in order to populate the ground polariton state. A resonant scattering of polaritons from the state excited by the pump pulse was greatly amplified upon arrival of the probe pulse, which proved experimentally that exciton–polaritons are "good" bosons, and that their scattering can be stimulated by the final state occupation. Stimulated scattering is necessary for *polariton lasing* (see below).

What is the magic angle?

A point q_M at the lower polariton dispersion branch, from which a resonant polariton–polariton scattering can be organised to the states with $q = 0$ and $q = 2q_M$, corresponds to the so-called *magic angle* of incidence. Both energy and wave-vector are conserved in the course of this process. Note that there is only one such angle whose value is dependent on the shape of the lower dispersion branch, and therefore on the detuning. Excitation at the magic angle allows one to populate quasi-directly the polariton ground state, thus transferring the coherence of the exciting laser pulse to light emitted by the cavity normally to its surface. In typical GaAs-based cavities the magic angle varies between 15 and 20 degrees at detunings close to zero.

What is parametric amplification of exciton–polaritons?

The classical parametric amplifier has been described in the last century by Faraday and lord Rayleigh. Parametric amplification is the resonant scattering of two waves (photons, polaritons, ...) of frequency ω_0 into two waves of frequency $\omega_0 + \omega_1$ and $\omega_0 - \omega_1$ which are called signal and idler, respectively. In terms of classical optics this is a non-linear process governed by a χ_3 susceptibility parameter. If a non-linear media generating the parametric amplification is placed in a resonator, the corresponding device can be referred to as a parametric oscillator. In microcavities such a parametric amplification process is extremely efficient if one pumps at the magic angle (see neighbouring questions). In this case, the scattering of two pumped polaritons into a ground state (signal) and an excited state (idler) is resonant (conserves both energy and wave vector). The non-linear driving force of the scattering is the Coulomb interaction between polaritons. The parametric amplification can be stimulated by a probe pulse which seeds the ground state, injecting a polariton population larger than one (see question on stimulated scattering). The process can also be strong enough to be self-stimulated. In any case the transfer of the pumped polaritons into the signal is extremely efficient. A polariton parametric amplifier is intrinsically a parametric oscillator since the signal and idler states are polariton eigenmodes.

What is the difference between Bose condensation of excitons and exciton–polaritons?

In bulk crystals or QWs Bose condensation of exciton–polaritons is forbidden since the lowest energy state of the lower polariton branch has zero energy in this case. Moreover, energy relaxation of exciton–polaritons quickly leads to their decoherence in bulk crystals or QWs. Free excitons occupying the entire space scatter to localised exciton states. At low excitonic concentration these states weakly overlap, which makes their interaction and eventual formation of condensates problematic. On the contrary, exciton–polaritons in microcavities in the strong-coupling regime keep their coherence, while relaxing in energy towards their ground state with a non-zero energy. They do not scatter into localised states. At $k = 0$ exciton polaritons are still free quasi-particles with very light effective mass (typically four orders of magnitude lighter than excitons uncoupled to light). Because of this light mass, the critical temperature for Bose condensation of exciton–polaritons is extremely high, and reaches 300 K for certain wide-band-gap semiconductors.

What is the difference between a polariton laser and a conventional laser?

A conventional laser implies a stimulated emission of radiation. Light amplification in lasers takes place if a condition of *population inversion* is fulfilled, i.e., the population of an excited state of the medium must exceed the population of the ground state. Only in this case does the stimulated emission of light exceed absorption. To achieve a condition of population inversion the pumping of a conventional laser must exceed some threshold value. In a polariton laser the emission of light has a spontaneous character. However, the emitted light has all the key properties of the laser light, i.e., it is monochromatic, unidirectional and coherent. This is achieved because the light is emitted by a macroscopic population of exciton–polaritons accumulated in the lowest energy state of their spectrum due to stimulated scattering. Note that no inversion of population is needed in a polariton laser. This is because there is no absorption in a polariton laser at the frequency of the emitted light. Actually, absorption is intrinsically taken into account when, instead of excitons and photons, exciton–polaritons are introduced as the only quasi-particles existing inside the cavity. Photons formally exist only outside the cavity. Emission of photons by a polariton laser is a tunnelling effect: light passes through a mirror from inside the cavity (where it is incorporated in an exciton–polariton condensate) to outside the cavity (where it becomes conventional light composed of free photons). Thus, polariton lasers have no threshold linked to the population inversion. Amplification of light in polariton lasers is governed by the ratio between the lifetime of exciton polaritons and their relaxation time towards the condensate. Note that this relaxation has a stimulated character in polariton lasers, which is why it can be quite rapid.

What is the Kosterlitz–Thouless phase transition?

This is a transition towards a super-fluid phase in two-dimensional bosonic systems. It has been described for the first time by J.M. Kosterlitz and D.J. Thouless in 1973. In infinite two-dimensional systems the Bose-condensation is impossible while a superfluid can be formed. A superfluid is a collective bosonic state, in which the particles can move throughout the space along a phase-coherent, dissipation-less path. Superfluidity implies that statistically, two points in space are connected by a phase-coherent path, even if the whole space is not covered by a phase-coherent wave-function. In ideal infinite microcavities, the exciton–polaritons may undergo the Kosterlitz–Thouless transition and form a superfluid if a critical condition linking the concentration of polaritons with temperature is fulfilled. Even at temperatures higher than the critical one, formation of finite-size droplets of the condensate is possible. In realistic microcavity structures characterized by some lateral potential disorder, two scenario can be discussed: either the fusion of spatially separated droplets or fusion of vortices in the condensate wave-function at the critical temperature. Taking into account finite lateral sizes of realistic microcavity samples and the finite size of the optical beam exciting the condensate, true Bose-condensation in a finite size system may happen before the Kosterlitz–Thouless transition, that remains though an important but hardly achievable theoretical limit in microcavities.

What are the quantum properties of light emitted by a polariton laser?

A condensate can be formed by a small number of exciton–polaritons, so that an emission mode of a polariton laser can have a small number of photons. Thus, a polariton laser can operate in a regime of a quantum source of light. The phase and coherence of light emitted by a condensate of polaritons should be the same as the phase and coherence of the condensate itself. The properties of the condensate depend mostly on the way in which it was created. Here, different regimes can be envisaged. If polaritons are created by a non-resonant excitation they relax with random phases. The phase of the condensate can take any arbitrary value in this case, although once it is established, the condensate keeps its phase. Otherwise, a quantum state of the condensate can be prepared by putting a limited number of exciton–polaritons in the ground state prior to its non-resonant excitation. These initially introduced polaritons play the role of seeds, around which the condensate will be formed, keeping their phase. Thus, the phase of the seed can be kept by a polariton laser during a macroscopically long time, since its phase relaxation is orders of magnitude slower than the relaxation and recombination rates of individual exciton–polaritons. In this regime a polariton laser serves as a quantum memory device. An effect of spontaneous symmetry breaking in the polariton statistical distribution at the ground state can be considered as a criterion of Bose-condensation. Polariton lasing itself does not necessarily imply the

symmetry breaking: emitted light may have a thermal (randomly phased) distribution. An emission line narrowing is not necessarily a signature of polariton Bose condensation because of particle self-interaction V. In a condensate, an increase of the particle number N_0 results in a line narrowing $\sim\Gamma_0/N_0$ where Γ_0 is the low density line width. However, a particle number increase also results in a broadening $\sim V N_0$. Therefore, the line narrows with N_0 up to N_0 verifies $V N_0 = \Gamma_0/N_0$. Further increase of N_0 results in the broadening of the line. A symmetry breaking may take place in this region.

Part I

Linear Properties of Microcavities

This page intentionally left blank

Chapter 1

Dispersion of Cavity Polaritons

1.1. Reflection and Transmission of Light by Quantum Wells Containing Excitons 29
1.1.1. Normal Incidence Case 29
1.1.2. Oblique Incidence Case 34
1.2. Reflectivity of Bragg Mirrors 36
1.2.1. Normal Incidence Case 36
1.2.2. Oblique Incidence Case 39
1.3. Dispersion of Exciton–Polaritons in Microcavities Containing Single Quantum Wells . . 40
1.3.1. Oblique Incidence Case 44
References 45

In Chapter 1, the optical response of two basic elements of a conventional microcavity, namely a QW and a Bragg mirror, will be analysed. Then, the simple transfer-matrix procedure will yield the equation for the eigenfrequencies of the cavity polaritons (dispersion equation). The effect of light polarisation on the polariton dispersion will be addressed in the last paragraph.

1.1. Reflection and Transmission of Light by Quantum Wells Containing Excitons

Here we derive the amplitude reflection and transmission coefficients for light incident on a quantum well in the vicinity of the exciton resonance frequency.

1.1.1. Normal Incidence Case

Let us consider a light wave propagating in a dielectric medium homogeneous in the plane of the wave (xy-plane), but possibly inhomogeneous in the propagation direction (z-direction). The electric $\vec{E}$ and magnetic $\vec{B}$ fields of the wave are given by Maxwell's equations:

$$\begin{aligned} \operatorname{curl} \vec{E} &= -\frac{1}{c}\frac{\partial \vec{B}}{\partial t}; \\ \operatorname{div} \vec{B} &= 0; \\ \operatorname{curl} \vec{B} &= \frac{1}{c}\frac{\partial \vec{D}}{\partial t}; \\ \operatorname{div} \vec{D} &= 0; \end{aligned} \tag{1.1.1}$$

where $\vec{D} = \vec{E} + 4\pi\vec{P}$, and $\vec{P}$ is the dielectric polarisation vector. Consider a QW parallel to the plane *xy* and characterised by an exciton resonance frequency ω_0. The displacement field near this frequency can be written as:

$$\vec{D} = \varepsilon_B \vec{E} + 4\pi \vec{P}_{\text{exc}}, \tag{1.1.2}$$

where $\vec{P}_{\text{exc}}$ is the excitonic contribution to the dielectric polarisation and ε_B is the background dielectric constant, which is assumed to be the same in the QW and surrounding barriers for simplicity. Eqs. (1.1.1) and (1.1.2) yield:

$$-\frac{\partial^2 \vec{E}}{\partial z^2} = k_0^2\big(\varepsilon_B \vec{E} + 4\pi \vec{P}_{\text{exc}}(z)\big), \tag{1.1.3}$$

where $k_0 = \omega_0/c$ is the wave-vector of light in a vacuum.

In the *local* model:

$$4\pi P_{\text{exc}}(z) = \chi(z)E(z), \tag{1.1.4}$$

where $\chi(z)$ is the *local* dielectric susceptibility. This model is the simplest and can be successfully applied for a description of *cw* experiments in QWs. However, it fails to describe correctly the dynamics of exciton–polaritons in quantum structures, and thus for the purposes of this book it is not suitable. The reader can find a detailed description of the local model applied both to QWs and superlattices in the book by Ivchenko and Pikus [1].

In the rest of this paragraph we will follow so-called *non-local dielectric response theory*, developed by Andreani, Tassone, Bassani, and Ivchenko in the end of 1980s to describe the optical response of excitons in QWs [2,3]. It takes into account the fact that if an exciton is born at the point z' of the crystal, the dielectric polarisation is changed at all points z within the exciton wave-function. This effect is conveniently described in the framework of the theory of *spatial dispersion* in optical media, where the exciton wave-function plays the role of a *correlation function*. This theory is based on the assumption that the exciton-induced dielectric polarisation can be written in the form:

$$4\pi P_{\text{exc}}(z) = \int_{-\infty}^{\infty} \chi(z, z')E(z')\,dz', \tag{1.1.5}$$

where

$$\chi(z, z') = \tilde{\chi}(\omega)\Phi(z)\Phi(z'), \tag{1.1.6}$$

with

$$\tilde{\chi}(\omega) = \frac{Q}{\omega_0 - \omega - i\gamma}, \quad Q = \varepsilon_B \omega_{LT} \pi a_B^3.$$

Here, $\Phi(z)$ is the exciton wave-function taken with equal electron and hole coordinates (thus, z is the coordinate of both the electron and hole), ω is the frequency

of the incident light, γ is the *homogeneous* broadening of the exciton resonance caused by acoustic phonons, and ω_{LT} and a_B are two intrinsic excitonic parameters called the *longitudinal-transverse* splitting and *Bohr radius.* Physically, the exciton Bohr radius is analogous to the hydrogen atom Bohr radius, in that it is proportional to the average distance between the electron and hole for the ground exciton state. The value of a_B in GaAs is 150 Å, whereas in wide-band semiconductors it is 2–4 times less. The parameter ω_{LT} is a measure of the exciton–light coupling strength in bulk semiconductors. For the ground exciton state in GaAs, $\hbar\omega_{LT} = 0.08$ meV, while in wide-band-gap materials (GaN, ZnO) it is an order of magnitude larger.

Eq. (1.1.6) is based on a micromodel described in detail by Haug and Koch [4].

Once the polarisation (1.1.5) is introduced, Eq. (1.1.3) becomes an integro-differential equation and can be solved exactly by using of the Green's function method. Within this method the solution of Eq. (1.1.3) is represented in the form

$$E(z) = E_0 \exp(ikz) + k_0^2 \int dz'\, 4\pi\, P_{\text{exc}}(z') G(z - z'), \tag{1.1.7}$$

where E_0 is the amplitude of the incident light, and the Green's function G satisfies the equation

$$\left(\frac{\partial^2}{\partial z^2} + k^2\right) G(z) = -\delta(z), \quad k = \sqrt{\varepsilon_B}\, k_0. \tag{1.1.8}$$

Bearing in mind that $\int_{-\infty}^{\infty} dz\, f(z')\delta(z - z') = f(z)$, one can easily check that G is given by

$$G(z) = \frac{i \exp(ik|z|)}{2k}. \tag{1.1.9}$$

Eq. (1.1.7) can be solved with respect to $E(z)$ as it is contained both in the left-hand side and right-hand side (in the polarisation P). In order to do it, let us multiply both parts by $\Phi(z)$ and integrate over z. This procedure yields:

$$\int dz\, E\Phi(z) = E_0 \int dz\, \Phi(z) \exp(ikz) + k_0^2 \tilde{\chi} \iint dz\, dz'\, \Phi(z)\Phi(z') G(z - z') \int dz''\, E\Phi(z''), \tag{1.1.10}$$

which means that

$$\int dz\, E\Phi(z) = \frac{E_0 \int dz\, \Phi(z) \exp(ikz)}{1 - k_0^2 \tilde{\chi} \iint dz\, dz'\, \Phi(z')\Phi(z) G(z - z')}. \tag{1.1.11}$$

We now return to Eq. (1.1.7) and substitute Eq. (1.1.11) into its right-hand side:

$$E = E_0 \exp(ikz) + k_0^2 \tilde{\chi} \int dz'\, \Phi(z') G(z - z') \int dz''\, E(z'') \Phi(z'')$$

$$= E_0 \left[e^{ikz} + \frac{k_0^2 \tilde{\chi} \int dz'\, \Phi(z') G(z - z') \int e^{ikz''} \Phi(z'')\, dz''}{1 - k_0^2 \tilde{\chi} \iint dz\, dz'\, G(z - z') \Phi(z) \Phi(z')} \right]. \quad (1.1.12)$$

Using Eq. (1.1.9) we finally obtain

$$E(z) = E_0 e^{ikz} + \frac{\frac{ik_0}{2\sqrt{\varepsilon_B}} Q E_0 \int \Phi(z'') e^{ikz''}\, dz'' \int \Phi(z') e^{ik|z - z'|}\, dz'}{\omega_0 - \omega - i\gamma - Q \frac{ik_0}{2\sqrt{\varepsilon_B}} \iint dz'\, dz''\, e^{ik|z' - z''|} \Phi(z') \Phi(z'')}. \quad (1.1.13)$$

The amplitude reflection (r) and transmission (t) coefficients of the QW can then be obtained as:

$$r \equiv \left. \frac{E(z) - E_0(z) e^{ikz}}{E_0(z) e^{ikz}} \right|_{z \to -\infty}, \qquad t \equiv \left. \frac{E(z)}{E_0 e^{ikz}} \right|_{z \to \infty}. \quad (1.1.14)$$

If we consider a ground exciton state, $\Phi(z)$ is an even function, and the integrals on the right-hand side of Eq. (1.1.13) can be easily simplified.

In the case $z \to +\infty$:

$$\int dz'\, \Phi(z') G(z - z')$$

$$= \frac{i}{2k} \int dz'\, \Phi(z') e^{ik(z - z')} = \frac{i e^{ikz}}{2k} \int dz'\, \cos(kz') \Phi(z');$$

and in the case $z \to -\infty$:

$$\int dz'\, \Phi(z') G(z - z')$$

$$= \frac{i}{2k} \int dz'\, \Phi(z') e^{ik(z' - z)} = \frac{i e^{-ikz}}{2k} \int dz'\, \cos(kz') \Phi(z'),$$

$$\int dz \int dz'\, G(z - z') \Phi(z) \Phi(z')$$

$$= \frac{i}{2k} \left[\int dz\, \Phi(z) \cos(kz) \right]^2 - \frac{1}{2k} \iint dz\, dz'\, \Phi(z) \Phi(z') \sin k|z - z'|.$$

This allows us to obtain the reflection and transmission coefficients of the QW in a simple and elegant form:

$$r(\omega) = \frac{i\Gamma_0}{\tilde{\omega}_0 - \omega - i(\Gamma_0 + \gamma)}, \quad (1.1.15)$$

$$t(\omega) = 1 + r(\omega), \tag{1.1.16}$$

where

$$\Gamma_0 = \frac{Qk_0}{2\sqrt{\varepsilon_B}}\left[\int \Phi(z)\cos kz\, dz\right]^2 \tag{1.1.17}$$

is an important characteristic further referred to as the *exciton radiative broadening*, and

$$\widetilde{\omega}_0 = \omega_0 + \frac{Qk_0}{2\sqrt{\varepsilon_B}}\int\int dz\, dz'\, \Phi(z)\Phi(z')\sin k|z - z'| \tag{1.1.18}$$

is the renormalisation of the exciton resonance frequency due to the polariton effect.

The radiative broadening Γ_0 is connected with the exciton *radiative lifetime* τ by the relation (for more details see Section 3.4):

$$\tau = \frac{1}{2\Gamma_0}. \tag{1.1.19}$$

A finite exciton radiative lifetime is a peculiarity of confined electronic systems. In an infinite bulk crystal, an exciton–polariton can freely propagate in any direction and its lifetime is limited only by non-radiative processes such as scattering with acoustic phonons. On the contrary, in a QW the exciton–polariton can disappear by giving its energy to a photon emitted perpendicular to the QW plane direction. The polariton effect (sometimes referred to as the *retardation effect*) consists, in this case, in the possibility for the emitted photon to be reabsorbed once again by the same exciton. The chain of virtual emission–absorption processes leads to a finite value of τ, and is also responsible for the renormalisation of the exciton frequency (1.1.18). This renormalisation does not exceed a few μeV in realistic QWs, although it becomes more important in quantum dots. Short radiative lifetimes of exciton–polaritons in 2D and 1D systems have been predicted in 1960s by Agranovich and Dubovskii [5]. The radiative lifetime τ is about 10 ps in typical GaAs-based QWs. Although it is extremely hard to observe free excitons in the photoluminescence governed mainly by excitons localised at imperfections of a QW, a lifetime τ of 12 ps for a free exciton has been measured experimentally by Deveaud et al. [6] in a record-quality 100 Å-thick GaAs/AlGaAs QW. The renormalisation of the exciton energy due to the polariton effect described by $\hbar(\widetilde{\omega}_0 - \omega_0)$ is quite small in typical QWs (a few μeV). It does not play an essential role in microcavities, and we shall neglect it hereafter. Note, however, that in quantum dots (QDs) this renormalisation causes a peculiar fine-structure of excitonic transitions, as has been observed in near-field experiments [7] and described theoretically [8] in the mid 1990s. For a review on radiative properties of excitons in confined systems we address the reader to a paper by Weisbuch et al. [9].

1.1.2. OBLIQUE INCIDENCE CASE

If light is incident on a QW at an oblique angle, Eq. (1.1.3) takes a more complex form. Here we examine reflection and transmission of linearly polarised light for TE-polarisation (the electric field of the light wave in the QW plane, also called s-polarisation) and TM-polarisation (the magnetic field of the light wave in the QW plane, also called p-polarisation). Any light wave with a different polarization can be represented as a linear combination of s- and p-polarised waves. In the rest of this section we follow Ref. [10].

In s-polarisation an additional term appears in Maxwell's equations for light incident on a QW (1.1.3):

$$\left(-\frac{\partial^2}{\partial z^2}+q^2\right)\vec{E}=k_0^2\big(\varepsilon_B\vec{E}+4\pi\vec{P}_{\rm exc}(z)\big), \tag{1.1.20}$$

where q is the in-plane component of the wave-vector of light. The transformations (1.1.4)–(1.1.17) all remain valid if ε_B is substituted by $\varepsilon_B(k_z^2/k_0^2)$, where

$$k_z^2\equiv k_0^2\varepsilon_B-q^2=k\cos\varphi, \tag{1.1.21}$$

and φ is the incidence angle.

Thus, in s-polarisation, the reflection and transmission coefficients are given by:

$$r^s(\omega)=\frac{i\widetilde{\Gamma}_0}{\widetilde{\omega}_0-\omega-i(\widetilde{\Gamma}_0+\gamma)},\qquad t^s(\omega)=1+r^s(\omega), \tag{1.1.22}$$

where $\widetilde{\Gamma}_0=\Gamma_0/\cos\varphi$.

In p-polarisation, Maxwell's equations (1.1.3) take a more complex form. Assuming that the electric field vector lies in the xz-plane, its components are given by:

$$\frac{\partial^2 E_x}{\partial z^2}+k_z^2E_x=-\frac{iq}{\varepsilon_B}4\pi\frac{\partial P_{{\rm exc},z}}{\partial z}-\frac{4\pi}{\varepsilon_B}k_z^2P_{{\rm exc},x}, \tag{1.1.23}$$

$$k_z^2E_z=ik_x\frac{\partial E_x}{\partial z}-4\pi k_0^2P_{{\rm exc},z}. \tag{1.1.24}$$

Here

$$4\pi k_0^2P_{{\rm exc},x\ (z)}=Q\Phi(z)\int dz'\,\Phi(z')E_{x\ (z)}(z'). \tag{1.1.25}$$

Using the Green's function

$$G(x,z-z')=\frac{i}{2k_z}\exp\big[i\big(k_z|z-z'|+k_xx\big)\big], \tag{1.1.26}$$

one can express the projections of the electric field as follows:

$$E_x(z) = E_x^0 e^{ik_z z} + \frac{k_z^2}{k^2} Q\Lambda_x \int dz'\, \Phi(z') G(x, z - z') + \frac{ik_x}{k^2} Q\Lambda_z \int dz'\, \Phi(z') \frac{\partial}{\partial z} G(x, z - z'), \tag{1.1.27}$$

$$E_z(z) = E_z^0 e^{ik_z z} + \frac{ik_x}{k^2} Q\Lambda_x \int dz'\, \Phi(z') \frac{\partial}{\partial z} G(x, z - z') + \frac{Q\Lambda_z}{\varepsilon_B} \int dz'\, \Phi(z') \left[\frac{1}{k_0^2} - \frac{\varepsilon_B}{k_z^2} \right] \frac{\partial^2}{\partial z^2} G(x, z - z') - \frac{k_0^2}{k_z^2} 4\pi P_{\mathrm{exc},z}, \tag{1.1.28}$$

where

$$\Lambda_{x\ (z)} = \int \Phi(z') E_{x\ (z)}(z')\, dz'. \tag{1.1.29}$$

The system of integro-differential equations (1.1.27), (1.1.28) can be resolved in the same manner as Eq. (1.1.7). Namely, multiplying Eqs. (1.1.27), (1.1.28) by $\Phi(z)$ and integrating over z one can obtain explicitly the coefficients $\Lambda_{x\ (z)}$. Then, assuming that $\Phi(z)$ is an even function, one can simplify most of the integrals and finally obtain the reflection and transmission coefficients in the following form:

$$r^p = p_0 - p_1, \qquad t^p = 1 + p_0 + p_1, \tag{1.1.30}$$

where

$$p_0 = \frac{i\overline{\Gamma}_x \cos\varphi}{\widetilde{\omega}_0 - \omega - i(\overline{\Gamma}_x \cos\varphi + \gamma)}, \tag{1.1.31}$$

$$p_1 = \frac{i\overline{\Gamma}_x (\cos^{-1}\varphi - \cos\varphi)}{\widetilde{\omega}_0 + \Delta\omega - \omega - i[\overline{\Gamma}_z (\cos^{-1}\varphi - \cos\varphi) + \gamma]}, \tag{1.1.32}$$

with

$$\overline{\Gamma}_x = \Gamma_0 \cos\varphi, \qquad \overline{\Gamma}_z = \Gamma_0 \frac{\sin^2\varphi}{\cos\varphi}, \tag{1.1.33}$$

$$\Delta\omega \approx \omega_{LT} \pi a_B^3 \int \Phi^2(z)\, dz. \tag{1.1.34}$$

The parameter $\overline{\Gamma}_{x,z}$ is proportional to the oscillator strength for excitons polarised parallel and normal to the interface, and $\Delta\omega_0$ is the splitting between these states. As follows from the interband selection rules, $\overline{\Gamma}_z = 0$ for e1-hh1 excitons,

whereas for the e1-lh1 state both $\overline{\Gamma}_z$ and $\overline{\Gamma}_x$ are non-zero: $\overline{\Gamma}_z \approx 4\overline{\Gamma}_x$ (here e, hh and lh denote the terms electron, heavy hole and light hole, respectively). Therefore, two poles separated by an angle-dependent value of $\Delta\omega_0$ are present in the expression for the p-polarised reflection or transmission coefficient near the light-hole exciton resonance. The allowance for the second pole is important for sufficiently large values of φ. More details on dispersion of exciton–polaritons in QWs can be found in Ref. [11].

1.2. Reflectivity of Bragg Mirrors

1.2.1. NORMAL INCIDENCE CASE

A Bragg mirror is a periodic structure composed of pairs of layers of dielectric or semiconductor materials characterised by different refractive indices (say n_a and n_b). The thicknesses of the layers (a and b, respectively) are chosen so that

$$n_a a = n_b b \equiv \bar{\lambda}/4. \tag{1.2.1}$$

Condition (1.2.1) is usually called the *Bragg interference condition*. The wavelength of light $\bar{\lambda}$ marks the centre of the *stop-band* of the mirror, i.e., the band of the wavelengths for which the reflectivity of the mirror is close to unity. In the following we assume $n_a < n_b$. We shall describe the optical properties of the mirror within its stop-band using the transfer matrix approach.

At normal incidence, the transfer matrices across the layers that compose the mirror are:

$$\widehat{T}_a = \begin{bmatrix} \cos k_a a & \frac{i}{n_a}\sin k_a a \\ i n_a \sin k_a a & \cos k_a a \end{bmatrix}, \qquad \widehat{T}_b = \begin{bmatrix} \cos k_b b & \frac{i}{n_b}\sin k_b b \\ i n_b \sin k_b b & \cos k_b b \end{bmatrix}, \tag{1.2.2}$$

where $k_a = (\omega/c)n_a$, $k_b = (\omega/c)n_b$. The transfer matrix $\widehat{T}$ across the period of the mirror is their product:

$$\widehat{T} = \widehat{T}_b \widehat{T}_a. \tag{1.2.3}$$

An infinite Bragg mirror represent the simplest one-dimensional photonic crystal. Its band structure is given by the equation

$$\cos Q(a+b) = (T_{11} + T_{22})/2, \tag{1.2.4}$$

where T_{ij} are the matrix elements of $\widehat{T}$ and Q is the effective wave-vector of light in a mirror. Eq. (1.2.4) is derived in Appendix C. Its solutions with real Q form allowed photonic bands, while solutions with complex Q having a non-zero imaginary part form *photonic gaps* or *stop-bands*.

At the central frequency of the stop-band, given by

$$\overline{\omega} = \frac{2\pi c}{\bar{\lambda}}, \tag{1.2.5}$$

the matrix $\widehat{T}$ becomes:

$$\widehat{T} = \begin{bmatrix} -\dfrac{n_a}{n_b} & 0 \\ 0 & -\dfrac{n_b}{n_a} \end{bmatrix}. \tag{1.2.6}$$

Its eigenvalues are:

$$\exp\big[i\,Q(a+b)\big] = -\frac{n_a}{n_b}, \qquad \exp\big[-i\,Q(a+b)\big] = -\frac{n_b}{n_a}. \tag{1.2.7}$$

The reflection coefficient of a semi-infinite Bragg mirror at $\omega = \overline{\omega}$ can be found from the condition:

$$\widehat{T}\begin{bmatrix} 1+r \\ n_0(1-r) \end{bmatrix} = -\frac{n_a}{n_b}\begin{bmatrix} 1+r \\ n_0(1-r) \end{bmatrix}, \tag{1.2.8}$$

which readily yields $r = 1$.

In the vicinity of $\overline{\omega}$ one can derive a simple and useful expression for the reflection coefficient, leaving in the matrix $\widehat{T}$ only terms linear in

$$x \equiv (\omega - \overline{\omega})\frac{\bar{\lambda}}{4c}. \tag{1.2.9}$$

The matrix is written in this approximation as:

$$\widehat{T} = -\begin{bmatrix} \dfrac{n_A}{n_B} & i\left(\dfrac{1}{n_A} + \dfrac{1}{n_B}\right)x \\ i(n_A + n_B)x & \dfrac{n_B}{n_A} \end{bmatrix}. \tag{1.2.10}$$

Eq. (1.2.8) yields in this case

$$r = \frac{n_0\left(\frac{n_A}{n_B} - \frac{n_B}{n_A}\right) - i(n_A + n_B)x}{n_0\left(\frac{n_A}{n_B} - \frac{n_B}{n_A}\right) + i(n_A + n_B)x} = \exp\left(i\frac{n_A n_B \bar{\lambda}}{2n_0(n_B - n_A)c}(\omega - \overline{\omega})\right). \tag{1.2.11}$$

The coefficient

$$L_{\mathrm{DBR}} \equiv \frac{n_A n_B \bar{\lambda}}{2(n_B - n_A)} \tag{1.2.12}$$

is frequently called the *effective length* of a Bragg mirror. Note that it has nothing in common with the penetration length $\tilde{L}$ of the light field into the mirror at $\omega = \overline{\omega}$. $\tilde{L}$ can be easily obtained from the eigenvalues of the matrix (1.2.6):

$$\tilde{L} = \frac{a+b}{\ln\frac{n_B}{n_A}}. \tag{1.2.13}$$

Figure 1.1 shows the profile of an electric field of a light wave propagating in a Bragg mirror at the centre of the stop-band. The decay of the field is dependent

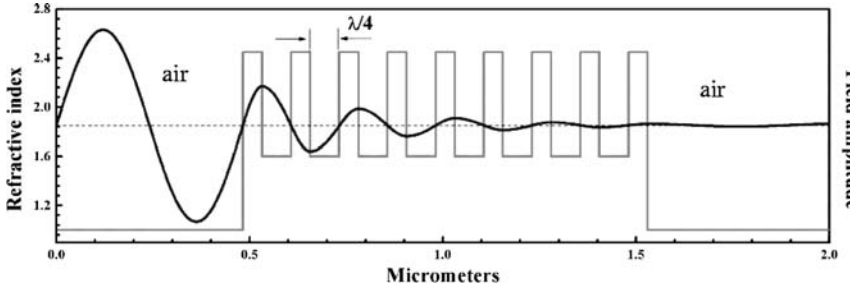

Fig. 1.1. An electric field profile of a light-wave incident normally on in a Bragg mirror at the center of its stop-band.

on the contrast between the refractive indices n_A and n_B: the higher the contrast the faster the decay.

For a finite-size mirror, the reflection coefficient within the stop-band is different from unity due to the tunnelling of light across the mirror. It can be found from the matrix equation:

$$\widehat{T}^N \begin{bmatrix} 1+\bar{r} \\ n_0(1-\bar{r}) \end{bmatrix} = \begin{bmatrix} \bar{t} \\ n_f \bar{t} \end{bmatrix}, \tag{1.2.14}$$

where $\bar{r}$ and $\bar{t}$ are the amplitude reflection and transmission coefficients of the mirror, N is the number of periods in the mirror, and n_f is the refractive index behind the mirror. At the centre of the stop-band:

$$\bar{r} = \frac{\left(\frac{n_B}{n_A}\right)^{2N} - \frac{n_f}{n_0}}{\left(\frac{n_B}{n_A}\right)^{2N} + \frac{n_f}{n_0}}, \qquad \bar{t} = \frac{2\left(-\frac{n_B}{n_A}\right)^{N}}{\left(\frac{n_B}{n_A}\right)^{2N} + \frac{n_f}{n_0}}. \tag{1.2.15}$$

As follows from these formulas, the higher the contrast between n_A and n_B the better the reflectivity of the mirror. In many cases we shall approximate the reflection coefficient of the mirror in the vicinity of $\overline{\omega}$ by

$$r_B = \bar{r} e^{i\alpha(\omega - \overline{\omega})}. \tag{1.2.16}$$

Note that, strictly speaking, this approximation is valid only if light propagates normal to the surface of the mirror. Oblique incidence of light on a Bragg mirror will be considered later in this section.

A further important characteristic of a Bragg mirror is the width of its stop-band, and this can be found from Eq. (1.2.4). The boundaries of the first stop-band are given by the condition:

$$(T_{11} + T_{22})/2 = -1. \tag{1.2.17}$$

Keeping only terms up to the second order in x one can transform this equation to yield:

$$-1 = x^2 - \frac{1}{2}\left(\frac{n_A}{n_B} + \frac{n_B}{n_A}\right)\left(1 - x^2\right). \tag{1.2.18}$$

The splitting between its two solutions is proportional to the stop-band width (in frequency):

$$\Delta = \frac{8c}{\bar{\lambda}} \frac{n_B - n_A}{n_B + n_A}. \tag{1.2.19}$$

The stop-band width increases with an increase in the contrast between the two refractive indices. Note that Eq. (1.2.20) is valid only if $\Delta \ll \overline{\omega}$, i.e.,

$$\frac{n_B - n_A}{n_B + n_A} \ll \frac{\pi}{4}, \tag{1.2.20}$$

which is usually the case in realistic structures. Otherwise, one should resolve Eq. (1.2.17) numerically.

1.2.2. OBLIQUE INCIDENCE CASE

Under oblique incidence the optical thickness of layers composing a Bragg mirror changes. The phase gained by light crossing a layer of thickness a at an angle φ_A is given by

$$\theta = \frac{\omega}{c} n_A a \cos\varphi_A, \tag{1.2.21}$$

where n_A is the refractive index of this layer. It is evident that the frequency which fulfills the Bragg interference condition $\theta = \pi/2$ is higher for oblique angles than for a normal angle. This is why, at oblique angles, stop-bands of any Bragg mirror shift towards higher frequencies. Bearing in mind also that at oblique angles the condition (1.2.21) is satisfied at different frequencies for layers with different refractive indices, one can conveniently define the centre of the stop-band as a frequency $\overline{\omega}$, for which the phase of the reflection coefficient of the mirror is zero. The transfer matrices (1.2.2) are modified in the case of oblique incidence and are different for s- and p-polarisations, as described in Appendix A. Condition (1.2.8) still holds at oblique incidence. It allows one to obtain the reflection coefficient of the Bragg mirror in the form

$$\begin{aligned} r_{s,p} &= \bar{r}_{s,p} \exp\left(i\alpha_{s,p}(\omega - \overline{\omega}_{s,p})\right) \\ &= \bar{r}_{s,p} \exp\left(i \frac{n_c}{c} L_{\mathrm{DBR}}^{s,p} \cos\varphi_0 (\omega - \overline{\omega}_{s,p})\right), \end{aligned} \tag{1.2.22}$$

where for s-polarisation:

$$\bar{r}_s = \left[1 - 4\frac{n_f}{n_0}\frac{\cos\varphi_f}{\cos\varphi_0}\left(\frac{n_A\cos\varphi_A}{n_B\cos\varphi_B}\right)^{2N}\right]^{1/2}, \tag{1.2.23}$$

$$\overline{\omega}_s = \frac{\pi c}{2(a+b)}\frac{n_A\cos\varphi_A + n_B\cos\varphi_B}{n_A n_B\cos\varphi_A\cos\varphi_B}, \tag{1.2.24}$$

$$L^s_{\mathrm{DBR}} = \frac{2n_A^2 n_B^2(a+b)\cos^2\varphi_A\cos^2\varphi_B}{n_0^2(n_B^2 - n_A^2)\cos^2\varphi_0}, \tag{1.2.25}$$

where φ_0 is the incidence angle, $\varphi_{A,B}$ are the propagation angles in layers with refractive indices n_A, n_B, respectively, and φ_f is the propagation angle in the material behind the mirror which has a refractive index n_f. They are linked by the Snell–Descartes law:

$$n_0\sin\varphi_0 = n_A\sin\varphi_A = n_B\sin\varphi_B = n_f\sin\varphi_f. \tag{1.2.26}$$

In p-polarisation:

$$\bar{r}_p = \left[1 - 4\frac{n_f}{n_0}\frac{\cos\varphi_0}{\cos\varphi_f}\left(\frac{n_A\cos\varphi_B}{n_B\cos\varphi_A}\right)^{2N}\right]^{1/2}, \tag{1.2.27}$$

$$\overline{\omega}_p = \frac{\pi c}{2}\frac{(n_A\cos\varphi_B + n_B\cos\varphi_A)}{n_A n_B(a\cos^2\varphi_A + b\cos^2\varphi_B)}, \tag{1.2.28}$$

$$L^p_{\mathrm{DBR}} = \frac{2n_A^2 n_B^2(a\cos^2\varphi_A + b\cos^2\varphi_B)}{n_0^2(n_B^2\cos^2\varphi_A - n_A^2\cos^2\varphi_B)}. \tag{1.2.29}$$

One can see that $\overline{\omega}_p$ increases faster than $\overline{\omega}_s$ with an increase in the incidence angle. L_{DBR} increases with the angle in p-polarisation and decreases in s-polarisation. Finally, $\bar{r}$ increases with angle in s-polarisation and decreases in p-polarisation if $n_0 = n_f$. All these dependencies are rather weak and can be neglected in most of cases. They become important in experiments that reveal the fine-structure of exciton–polariton resonances in microcavities.

1.3. Dispersion of Exciton–Polaritons in Microcavities Containing Single Quantum Wells

Consider a symmetric microcavity with a single QW embedded in the centre. In the basis of amplitudes of light waves propagating in positive and negative

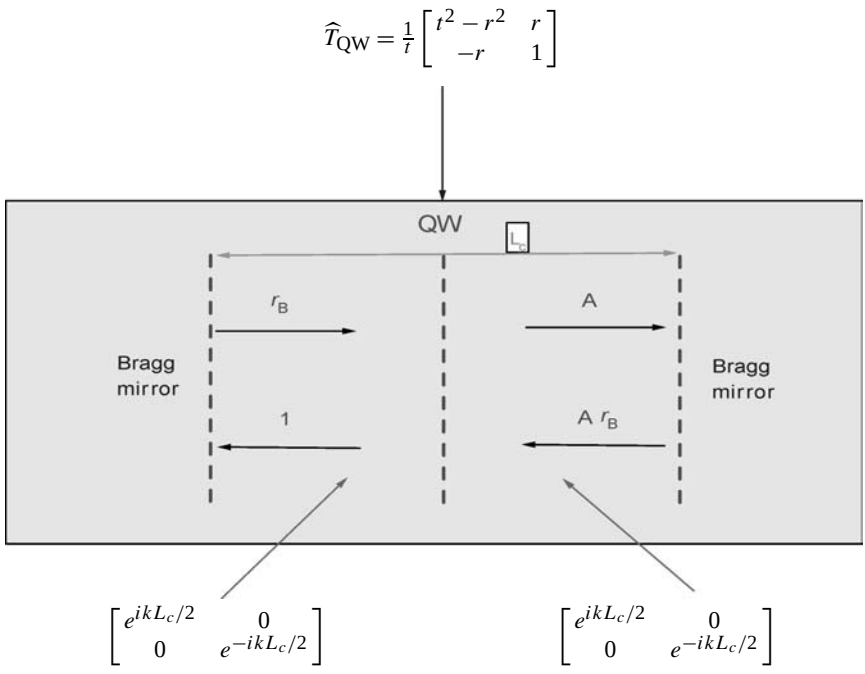

Fig. 1.2. A scheme illustrating how to construct a transfer matrix across the cavity layer containing an embedded quantum well. The transfer matrix $\widehat{T}_c$ links amplitudes of electromagnetic waves propagating in positive and negative directions at the boundaries of the cavity with left and right Bragg mirrors.

directions along the z-axis, the transfer matrix across the QW has the form

$$\widehat{T}_{\rm QW} = \frac{1}{t}\begin{bmatrix} t^2 - r^2 & r \\ -r & 1 \end{bmatrix}, \tag{1.3.1}$$

where r and t are the angle- and polarisation-dependent amplitude reflection and transmission coefficients of the QW derived in Section 1.1.

The transfer matrix across the cavity from one Bragg mirror to the other is the product:

$$\widehat{T}_c = \begin{bmatrix} e^{ikL_c/2} & 0 \\ 0 & e^{-ikL_c/2} \end{bmatrix} \frac{1}{t} \begin{bmatrix} t^2 - r^2 & r \\ -r & 1 \end{bmatrix} \begin{bmatrix} e^{ikL_c/2} & 0 \\ 0 & e^{-ikL_c/2} \end{bmatrix}, \tag{1.3.2}$$

where L_c is the cavity width, as illustrated in Figure 1.2. The elements of this matrix are:

$$T^c_{11} = \frac{t^2 - r^2}{t} e^{ikL_c}, \quad T^c_{12} = \frac{r}{t}, \quad T^c_{21} = -\frac{r}{t}, \quad T^c_{22} = \frac{1}{t} e^{-ikL_c}. \tag{1.3.3}$$

To find the eigenfrequencies of the exciton–polariton modes of the microcavity, one should search for non-trivial solutions of Maxwell's equations under the requirement of no light incident on the cavity from outside. This yields

$$\widehat{T}_c \begin{bmatrix} r_B \\ 1 \end{bmatrix} = A \begin{bmatrix} 1 \\ r_B \end{bmatrix}, \tag{1.3.4}$$

where r_B is the angle-dependent reflection coefficient of the Bragg mirrors for light incident from inside the cavity, introduced in Section 1.2. Excluding the coefficient A from Eq. (1.3.4), we obtain the following equation for polariton eigenmodes:

$$\frac{T_{21}^c r_B + T_{22}^c}{T_{12}^c + T_{11}^c r_B} = r_B. \tag{1.3.5}$$

This is already a dispersion equation because the coefficients of the transfer matrix and r_B are dependent on the in-plane wave-vector of light and frequency. Substituting into Eq. (1.3.5) the coefficients (1.3.3), one can represent the dispersion equation in the following form:

$$\left[r_B(2r+1)e^{ikL_c} - 1\right]\left[r_B e^{ikL_c} + 1\right] = 0. \tag{1.3.6}$$

Here we have used the relation $t - r = 1$. Solutions of Eq. (1.3.6), coming from zeros of the second bracket on the left-hand side, coincide with pure *odd* optical modes of the cavity. These modes have a node at the centre of the cavity where the QW is situated. Therefore, they are not coupled with the ground exciton state having an *even* wave-function. The first bracket on the left-hand side of Eq. (1.3.6) contains the reflection coefficient of the QW, which is dependent on excitonic parameters. The zeros of this bracket describe the eigenstates of exciton–polaritons resulting from coupling of *even* optical modes with the exciton ground state. From now on we shall consider only these states, neglecting excited exciton states that may be coupled to odd cavity modes.

For the even modes and normal incidence, if we take

$$r_B = \bar{r}\exp\bigl(i\alpha(\omega-\omega_c)\bigr) \approx \bar{r}\left(1 + iL_{\mathrm{DBR}}\frac{n_c}{c}(\omega-\omega_c)\right), \tag{1.3.7}$$

where $\bar{r}$ is close to 1 (see Section 1.2), and assume $e^{ikL_c} \approx 1 + i((\omega-\omega_c)/c)n_c L_c$, we obtain, using the explicit form for the reflection coefficient r (1.1.15):

$$\begin{aligned}&\bar{r}\left(1 + iL_{\mathrm{DBR}}\frac{n_c}{c}(\omega-\omega_c)\right)\bigl(\omega_0 - \omega - i(\gamma-\Gamma_0)\bigr)\left(1 + i\frac{\omega-\omega_c}{c}n_c L_c\right)\\ &\quad = \omega_0 - \omega - i(\gamma+\Gamma_0),\end{aligned}$$

which finally yields, after trivial transformations:

$$(\widetilde{\omega}_0 - \omega - i\gamma)(\omega_c - \omega - i\gamma_c) = V^2, \tag{1.3.8}$$

where

$$\gamma_c = \frac{1-\bar{r}}{\bar{r}\frac{n_c}{c}(L_{\mathrm{DBR}}+L_c)}, \qquad V^2 = \frac{1+\bar{r}}{\bar{r}}\frac{\Gamma_0 c}{n_c(L_{\mathrm{DBR}}+L_c)}. \tag{1.3.9}$$

Here, quadratic terms in $(\omega_c - \omega)$ are omitted. In all further calculations we shall assume $\widetilde{\omega}_0 = \omega_0$ for simplicity. Eq. (1.3.8) is an equation for eigenstates of a system of two coupled harmonic oscillators, namely, the exciton resonance and the cavity mode. Note, that in this form Eq. (1.3.8) was published for the first time by Savona et al. [12], while its general form (1.3.5) has been obtained in [13]. The solutions of Eq. (1.3.8) are

$$\omega_{1,2} = \frac{\omega_0+\omega_c}{2} - \frac{i}{2}(\gamma+\gamma_c) \pm \sqrt{\left(\frac{\omega_0-\omega_c}{2}\right)^2 + V^2 - \gamma\gamma_c + \frac{i}{2}(\omega_0-\omega_c)(\gamma_c-\gamma)}. \tag{1.3.10}$$

The parameter V has the sense of the strength of coupling between the cavity photon mode and the exciton resonance. If $\omega_0 = \omega_c$, the splitting of the two solutions is given by $2\sqrt{V^2-\gamma\gamma_c}$. If

$$V > \sqrt{\gamma\gamma_c}, \tag{1.3.11}$$

an anticrossing takes place between exciton and photon modes, which is characteristic for the *strong-coupling regime*. In this regime, two distinct exciton–polariton branches manifest themselves as two optical resonances in the reflection or transmission spectra. The splitting between these two resonances is referred to as *vacuum-field Rabi splitting*. It reaches 4–15 meV in existing GaAs-based microcavities, up to 30 meV in CdTe-based microcavities, and is expected to be as large as 50 meV in future GaN cavities. The advantage of GaN is that A and B excitons in this semiconductor have a record oscillator strength, which exceeds by an order of magnitude the oscillator strength in GaAs [14].

If

$$V < \sqrt{\gamma\gamma_c}, \tag{1.3.12}$$

the weak-coupling regime holds, which is characterised by crossing of the exciton and photon modes and an increase of the exciton decay rate at the resonance point. This regime is typically used in vertical cavity surface emitting lasers (VCSELs). Note that all the above theory neglects the effect of disorder on the exciton resonance. Taking into account the inevitable inhomogeneous broadening of the exciton resonance and Rayleigh scattering of exciton–polaritons, one should also modify the criterion (1.3.11) for weak-to-strong coupling threshold (more details on this point are given in Section 3.2).

1.3.1. OBLIQUE INCIDENCE CASE

Eq. (1.3.8) is only applicable in the normal incidence case. Thus, in order to calculate the dispersion relations of exciton–polaritons in microcavities, one should use Eq. (1.3.5), where the angle-dependent reflection coefficients of the QW (Eqs. (1.1.22) and (1.1.30)) and Bragg mirrors (see Eqs. (1.2.17) and (1.2.27)) are substituted. On the other hand, in most cases it is sufficient just to take into account the in-plane wave-vector dependence of the resonance frequencies ω_c and ω_0 in order to obtain a reasonable approximation to the true dispersion curves:

$$\hbar\omega_c = \frac{\hbar^2 q^2}{2m_{\rm ph}}, \qquad \hbar\omega_0 = \frac{\hbar^2 q^2}{2M_{\rm exc}}, \tag{1.3.13}$$

where $M_{\rm exc}$ is the sum of the electron and hole effective masses in the QW plane, and $m_{\rm ph}$ is the photonic effective mass, which can be estimated as follows. In an ideal λ-microcavity, the normal-to-plane component of the wave-vector of the eigenmode is given by $k_z = 2\pi/L_c$. The energy of the mode is

$$\hbar\omega_c = \hbar\frac{c}{n_c}\sqrt{q^2 + k_z^2} \approx \hbar\frac{c}{n_c}k_z\left(1 + \frac{q^2}{2k_z^2}\right) \equiv \frac{hc}{n_c L_c} + \frac{\hbar^2 q^2}{2m_{\rm ph}}, \tag{1.3.14}$$

and thus $m_{\rm ph} = hn_c/cL_c$. This mass is extremely light in comparison with the exciton mass, and usually amounts 10^{-5}–$10^{-4}m_0$, where m_0 is the free exciton mass. Note also that the in-plane wave-vector q is related to the angle of incidence of light illuminating the structure, φ, by the relation:

$$q = \frac{\omega}{c}\sin\varphi. \tag{1.3.15}$$

By measuring the angle dependence of the resonances in the reflection or transmission spectra of microcavities, one can restore the true dispersion curves of exciton–polaritons.

The coupling constant V is renormalised in the case of oblique incidence and it becomes polarisation-dependent. In s-polarisation, $\Gamma_0^s = \Gamma_0/\cos\varphi_c$, where φ_c is the propagation angle within the cavity. In p-polarisation, $\Gamma_0^p = \Gamma_0\cos\varphi_c$. The effective length of the Bragg mirrors, $L_{\rm DBR}$, is also angle- and polarisation-dependent: it decreases with angle in s-polarisation but increases in p-polarisation. Also, the coefficient $\bar{r}$ slightly depends on the angle (see Eqs. (1.2.23)–(1.2.29)). All these factors make the coupling constant increase with angle in s-polarisation, while in p-polarisation the opposite tendency occurs. This is why, in p-polarisation at some critical angle the strong coupling regime can be lost. Note also that in p- and s-polarisations the eigenfrequencies of pure cavity modes $\omega_c^{\rm TE,TM}$ are slightly split, so that

$$\omega_c^p > \omega_c^s. \tag{1.3.16}$$

A detailed calculation of these quantities can be found in a review paper [15].

The appearance in p polarisation of an additional Z-polariton resonance for light-hole excitons (see Eq. (1.1.30)) induces an additional feature in the optical spectra of microcavities at oblique angles. Usually, this resonance is much weaker than the L- and T-polariton resonances in a cavity [13], and does not exhibit a strong coupling to light. The exciton longitudinal-transverse splitting becomes essential at large in-plane wave-vectors, and has an impact on the spin-relaxation of exciton–polaritons.

References

1. E. L. Ivchenko, G. E. Pikus, "Superlattices and Other Heterostructures: Symmetry and Optical Properties". Springer, Berlin, 1995.
2. L. C. Andreani, F. Tassone, F. Bassani, Radiative lifetime of free excitons in quantum wells, *Solid State Commun.* 77, 641 (1991).
3. E. L. Ivchenko, Excitonic polaritons in periodic quantum well structures, *Sov. Phys. Solid State* 33, 1344 (1991).
4. H. Haug, S. W. Koch, "Quantum Theory of the Optical and Electronic Properties of Semiconductors", p. 3. World Scientific, Singapore, 1994.
5. V. M. Agranovich, O. A. Dubovskii, *JETP Lett.* 3, 233 (1966).
6. B. Deveaud, F. Clérot, N. Roy, K. Satzke, B. Sermage, D. S. Katzer, Enhanced radiative recombination of free excitons in GaAs quantum wells, *Phys. Rev. Lett.* 67, 2355 (1991).
7. D. Gammon, E. S. Snow, B. V. Shanebrook, D. S. Katzer, D. Park, Fine structure splitting in the optical spectra of single GaAs quantum dots, *Phys. Rev. Lett.* 76, 3005 (1996).
8. S. V. Goupalov, E. L. Ivchenko, A. V. Kavokin, Fine structure of localized exciton levels in quantum wells, *J. Experiment. Theoret. Phys.* 86, 388 (1998).
9. C. Weisbuch, H. Benisty, R. Houdré, Overview of fundamentals and applications of electrons, excitons, and photons in confined structures, *J. of Luminescence* 85, 271 (2000).
10. E. L. Ivchenko, A. V. Kavokin, Light reflection from quantum well, quantum wire, and quantum dot structures, *Sov. Phys. Solid State* 34, 1815 (1992).
11. F. Tassone, F. Bassani, L. C. Andreani, Quantum well reflectivity and exciton–polariton dispersion, *Phys. Rev. B* 45, 6023 (1992).
12. V. Savona, L. C. Andreani, P. Schwendimann, A. Quattropani, Quantum well excitons in semiconductor microcavities: Unified treatment of weak and strong coupling regimes, *Solid State Commun.* 93, 733 (1995).
13. A. V. Kavokin, M. A. Kaliteevski, Excitonic light reflection and absorption in semiconductor microcavities at oblique incidence, *Solid State Commun.* 95, 859 (1995).
14. A. V. Kavokin, B. Gil, GaN microcavities: Giant Rabi splitting and optical anisotropy, *Appl. Phys. Lett.* 72, 2880 (1998).
15. G. Panzarini, L. C. Andreani, A. Armitage, D. Baxter, M. S. Skolnick, V. N. Astratov, J. S. Roberts, A. V. Kavokin, M. R. Vladimirova, M. A. Kaliteevski, Cavity-polariton dispersion and polarization splitting in single and coupled semiconductor microcavities, *Phys. Solid State* 41, 1223 (1999).

This page intentionally left blank

Chapter 2
Examples of Microcavity Systems

2.1. Multiple Quantum Wells in a Cavity 47
2.2. Coupled Microcavities 53
2.2.1. Empty Coupled Cavities 53
2.2.2. Coupled Cavities with Quantum Wells 55
2.3. Bulk Microcavities 58
2.3.1. Spatial Dispersion of Exciton–Polaritons 58
2.3.2. Transfer Matrix Across a Resonant Layer 60
2.3.3. 2D Photon Coupling with Bulk Excitons in Microcavities 63
2.4. Regular Gratings of Quantum Wires and Quantum Dots in a Microcavity 70
2.4.1. Regular Grating of Quantum Wires 70
2.4.2. Rectangular Grating of Quantum Dots 72
2.4.3. Cavity Mode Interaction with a Periodic Grating of Wires or Dots 74
2.5. Magnetic Field Effect. Kerr and Faraday Rotation 77
2.5.1. Landau Quantisation and Renormalisation of Rabi Splitting 78
2.5.2. Faraday Rotation 81
References 84

In this chapter we consider particular microcavity systems that represent a substantial interest from our point of view. Namely, we address microcavities containing multiple quantum wells (MQWs), coupled microcavities with QWs, bulk microcavities where the optical mode is coupled to a bulk exciton resonance, and microcavities with embedded grating of quantum wires. A magnetic field effect on cavity polaritons is also addressed in this chapter. We will show that a rich variety of polaritonic spectra can be achieved by combining different types of exciton states with quasi-two-dimensional photonic modes in microcavities. Only linear optical effects will be addressed.

2.1. Multiple Quantum Wells in a Cavity

N identical quantum wells interacting with light give rise to $N + 1$ exciton–polariton eigenstates. Some of these states have an enhanced oscillator strength with respect to an exciton in a single QW, and are usually referred to as *bright* or *superradiant* states. Others, with a reduced oscillator strength, are referred to as *dark states*.

Before discussing a cavity mode coupling with multiple QWs, let us study the properties of exciton–polaritons in a periodic structure of N identical QWs. We

shall follow Ref. [1]. The period of the structure is d, and the background refractive index n is assumed to be the same in the wells and barriers. We shall only consider propagation of light in the direction normal to the QW planes.

We use the transfer matrix approach and the basis of amplitudes of plane waves propagating in positive and negative directions. As is shown in Appendix B (Eq. (B.10)), the transfer matrix across a QW can be written in the form

$$T_{\mathrm{QW}} = \frac{1}{t}\begin{bmatrix} t^2 - r^2 & r \\ -r & 1 \end{bmatrix}, \tag{2.1.1}$$

where r and t are, respectively, the amplitude reflection and transmission coefficients of the QW (see Section 1.2):

$$r = \frac{i\Gamma_0}{\omega_0 - \omega - i(\gamma + \Gamma_0)}, \qquad t = 1 + r. \tag{2.1.2}$$

The transfer matrix across the period of the structure T_d is given by

$$T_d = T_{\mathrm{QW}}\begin{bmatrix} e^{ikd} & 0 \\ 0 & e^{-ikd} \end{bmatrix}. \tag{2.1.3}$$

Here $k = (\omega/c)n$. The eigenvalues of this matrix can be represented in the form (see Appendix C (Eq. (C.3))):

$$\lambda_{\pm} = e^{\pm iQd}, \tag{2.1.4}$$

and the eigenvectors in the form

$$\widehat{C}_{\pm} = \begin{bmatrix} 1 \\ a_{\pm} \end{bmatrix}, \tag{2.1.5}$$

where $a_{\pm} = r/(e^{-ikd} - t\lambda_{\pm})$. The quantity Q has the meaning of the wave-vector of light at frequency ω in an infinite periodic structure, and satisfies the dispersion equation (see Appendix C, Eq. (C.7)):

$$\cos Qd = G(\omega), \qquad G(\omega) = \cos kd - \sin kd\frac{\Gamma_0}{\omega_0 - \omega - i\gamma}. \tag{2.1.6}$$

For a structure containing a finite number N of quantum wells, the spectrum of eigenfrequencies is found from the homogeneous boundary conditions, which signify the absence of an external wave impinging on the structure from the left or right, and which are equivalent to the relation

$$a_+ e^{iNQd} = a_- e^{-iNQd}. \tag{2.1.7}$$

After substituting the explicit expressions for coefficients $a_{\pm}$ into this relation and performing some additional transformations, we obtain a transcendental equation

for finding the N complex eigenfrequencies of the system

$$te^{ikd} = \frac{U_{N-1}(G(\omega))}{U_{N-2}(G(\omega))}, \tag{2.1.8}$$

where

$$U_\nu(x) \equiv \left(1 - x^2\right)^{-1/2} \sin\left[(\nu + 1) \arccos x\right] \tag{2.1.9}$$

are Chebyshev polynomials of the second kind of degree ν (see, for example, Ref. [2]), and the argument $G(\omega)$ is the same as in Eq. (2.1.6).

The amplitude reflection and transmission coefficients for a system of N QWs sandwiched between infinite homogeneous barriers can be expressed in terms of $a_\pm$ and Q in the following manner:

$$r_N = \frac{a_+ a_- (1 - e^{2iNQd})}{a_+ a_- e^{2iNQd}}, \qquad t_N = \frac{(a_- - a_+) e^{iNQd}}{a_- - a_+ e^{2iNQd}}. \tag{2.1.10}$$

The reflection and transmission coefficients are defined in planes shifted by $d/2$ to the left from the centre of the extreme left-hand well and by $d/2$ to the right from the centre of the extreme right-hand well, respectively. Note that the transfer matrix between these two planes can be written in the simple form

$$T_N = \frac{1}{t_N} \begin{bmatrix} t_N^2 - r_N^2 & r_N \\ -r_N & 1 \end{bmatrix}. \tag{2.1.11}$$

If the multiple QW structure is embedded in a microcavity, one can obtain eigenfrequencies of polariton modes in exactly the same way as in Section 1.3, where instead of the matrix (1.3.1) one should use the matrix (2.1.11). Note, however, that in the case of multiple QWs, $t_N \neq 1 + r_N$ in general. Using Eq. (1.3.5) we derive the resulting equation for the eigenfrequencies as:

$$\left[(t_N + r_N) r_B e^{ik_z L_c} - 1\right]\left[(t_N - r_N) r_B e^{ik_z L_c} + 1\right] = 0. \tag{2.1.12}$$

Here, as well as in Eq. (1.3.6), the zeros of the first bracket yield even exciton–polariton modes, while the zeros of the second bracket yield odd modes.

Eq. (2.1.12) is not easy to analyse because of the complex form of r_N and t_N. It can be reduced to the problem of $N + 1$ coupled oscillators if the same assumptions as in Section 1.3 are made:

$$\det \| A_{jj'} - \omega \delta_{jj'} \| = 0, \tag{2.1.13}$$

with the matrix elements

$$\begin{aligned} A_{lm} &= (\omega_0 - i\gamma)\delta_{lm} - i\Gamma_0 e^{ikd|l-m|}, \\ A_{N+1\,l} &= A_{l\,N+1} = V \cos k(z_l - z_c), \\ A_{N+1\,N+1} &= \omega_c - i\gamma_c \end{aligned} \tag{2.1.14}$$

where ω_c, γ_c, V_c are the same as in Section 1.3, z_c is the coordinate of the antinode of the cavity field, and z_l is the coordinate of lth QW, $l, m = 1, 2, \ldots, N$.

Since the trace of any square matrix is equal to the sum of its eigenvalues, the following constraint can be imposed on this sum:

$$\sum_{j=1}^{N+1} \omega_j = N\omega_0 + \omega_c - iN(\gamma + \Gamma_0) - i\gamma_c. \tag{2.1.15}$$

According to Gerschgorin's circle theorem [3], the eigenvalues of a complex square matrix $A_{jj'}$ lie in a closed region of the complex plane $z = z' + iz''$ formed by the circles

$$|z - A_{jj}| \leqslant \sum_{j \neq j'} |A_{jj'}|. \tag{2.1.16}$$

In our case, this means that all solutions are grouped around $(\omega_0 - i(\gamma + \Gamma_0))$ and $(\omega_c - i\gamma_c)$ within circles of radii $R_1 = (N-1)\Gamma_0 + V$ and $R_2 = V\sum_l |\cos k(z_l - z_c)|$, respectively, while N solutions are located within the first circle and only one within the second circle. These circles necessarily overlap in the strong-coupling regime at the anticrossing point, while in the weak-coupling regime, if the coupling constant is small with respect to the *difference* of broadenings of the exciton and cavity resonances, they do not overlap.

Figure 2.1(a) shows the distribution in the complex plane of exciton–polariton eigenfrequencies for a system of 10 GaAs/AlGaAs QWs with a period of 20 nm. For comparison, an eigenfrequency of a single QW exciton–polariton is shown ($\omega_{\mathrm{SQW}} = \omega_0 - i(\gamma + \Gamma_0)$). The imaginary parts of all eigenfrequencies are negative, which reflects the fact that there are no sources of light in the structure and light can only be re-emitted while absorbed. If we compare the absolute values of the imaginary parts of the eigenmodes, we see that most of them are less than $\Gamma_0 + \gamma$. These are *dark modes*. A few others, with an absolute value of the imaginary part exceeding $\Gamma_0 + \gamma$, are *bright modes*.

The radiative lifetime of the jth polariton eigenstate is given by

$$\tau_j = -\tfrac{1}{2}\big(\mathrm{Im}(\omega_j) + \gamma\big)^{-1}. \tag{2.1.17}$$

It exceeds $\tau_0 = 1/2\Gamma_0$ for the dark states and is less than τ_0 for the bright states. The bright states are also called superradiant because the emission rate of light from them is enhanced with respect to a single QW. Note that in a typical 20 nm-thick GaAs/AlGaAs QW $\tau_0 \approx 10$ ps.

Figure 2.1(b) shows the eigenfrequencies of the same multiple QW structure embedded in the centre of a microcavity with a central layer width of $3\lambda/2$, where λ is the wavelength of light at frequency ω_0. One can see that the distribution of eigenmodes is changed dramatically due to the coupling with the photon mode of the cavity. The bright modes are more strongly affected by the cavity mode and

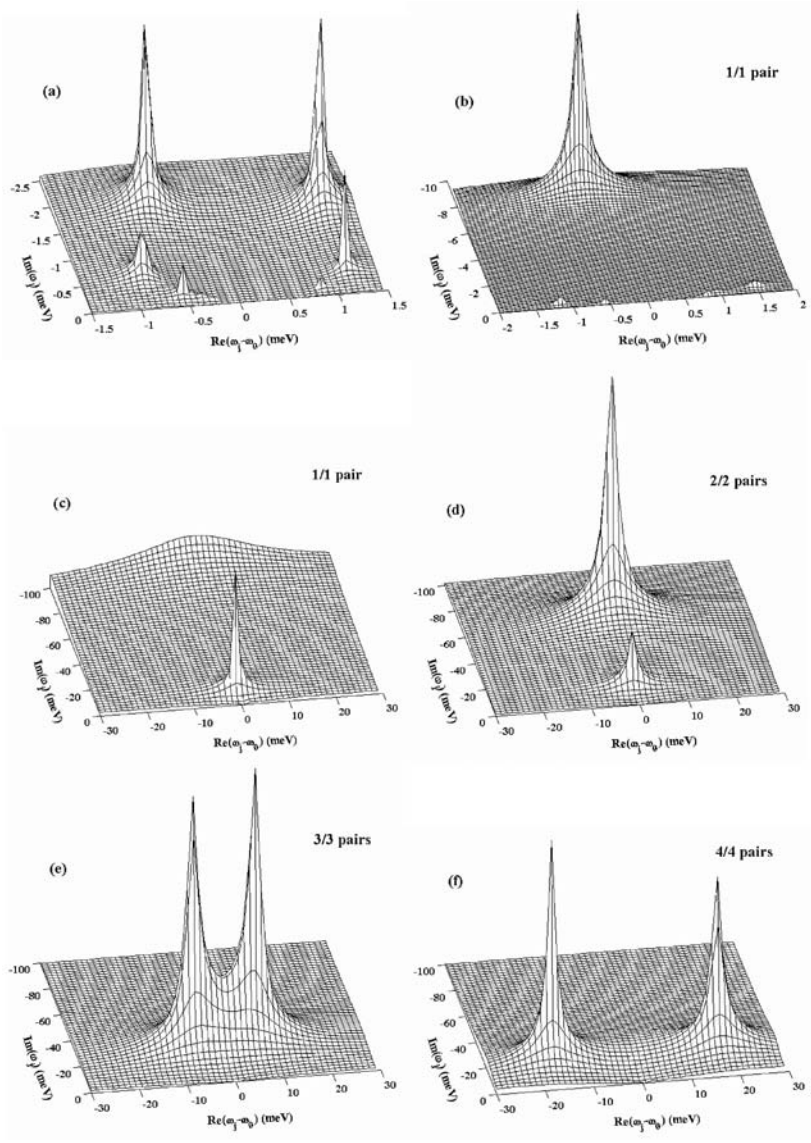

Fig. 2.1. Complex eigen-frequencies of exciton–polaritons in a periodical structure of 10 identical QWs surrounded by an infinite homogeneous media (a) or embedded in a microcavity having an optical mode frequency equal to the exciton resonance frequency in QWs (b)–(f). The number of pairs of quarter-wave layers in microcavities is changing from 1 to 4 (graphs (b)–(f)) in order to see the weak-strong coupling threshold. The exciton energy is $\hbar\omega_0 = 3.543$ eV, its radiative damping rate is $\hbar\Gamma_0 = 400$ μeV, exciton non-radiative broadening $\gamma = 0.1$ meV. All parameters in this calculation correspond to GaN-based structures.

are in the strong coupling regime, while the dark modes remain in their places and are only weakly coupled to the cavity.

The interesting case of so-called Bragg-arranged QWs was first analysed by Ivchenko in the mid 1990s [4]. In Bragg-arranged QWs

$$kd = \pi \tag{2.1.18}$$

at the frequency ω_0. Under this condition, Eq. (2.1.8) has $N-1$ identical solutions:

$$\omega_j = \omega_0 - i\gamma, \quad j = 1, 2, \ldots, N-1. \tag{2.1.19}$$

These are absolutely dark (we would say, *black*) states that have an infinite radiative lifetime. There is only one superradiant state in this system with the eigenfrequency

$$\omega_N = \omega_0 - i(\gamma + N\Gamma_0). \tag{2.1.20}$$

This state emits light N times faster than a single QW exciton.

The reflection and transmission coefficients of Bragg-arranged QWs have a simple form

$$r_N = \frac{iN\Gamma_0}{\omega_0 - \omega - i(\gamma + N\Gamma_0)}, \qquad t_N = 1 + r_N. \tag{2.1.21}$$

Bragg QWs are particularly interesting for microcavity physics. While strongly coupled to the cavity photon state, the superradiant mode of a Bragg arranged structure of multiple QWs yields a polariton (Rabi) splitting $\sqrt{N}$ larger than a single QW exciton–polariton (see Eq. (1.3.9)). The QWs must be placed at the antinodes of the electric field of the cavity mode in order to allow for the strongest coupling. In this case all the cosine functions in Eq. (2.1.14) can be replaced by 1.

Indeed, by increasing the number of QWs embedded in the microcavity, one can increase the polariton splitting. The limitation to this increase comes from the fact that in very large microcavities, the splitting between confined photon modes becomes small compared to the polariton splitting. In this case, the polariton spectrum becomes extremely complicated, and a huge number of resonances appear in the spectra, so that a simple two-coupled oscillator model no longer works.

Another way to achieve increased Rabi splittings is to embed short-period structures of a few QWs at all antinodes of a rather large ($5\lambda/2$ or $7\lambda/2$) microcavity. The idea is to keep the distance between each QW and the antinode small with respect to the wavelength of light, in order to keep $\cos k(z_j - z_c) \approx 1$ for all QWs. In this case, the Rabi splitting is still proportional to the square root of the number of QWs embedded in the cavity, as in the case of Bragg-arranged wells. This method allows one to obtain a larger Rabi splitting for the same thickness of the cavity. Note, however, that the distance between neighbouring QWs should be large enough to avoid electronic coupling between wells and formation

of superlattice minibands, instead of the discrete single QW exciton levels. Excitons in minibands lose a part of their oscillator strength, so that the Rabi splitting decreases in microcavities with embedded superlattices.

Finally, we recall that the above analysis is performed assuming ideal QW structures with single free-exciton resonances with the same resonance frequencies in all wells. In reality, an inhomogeneous broadening of exciton states makes the picture more complicated. While the image of superradiant and dark polariton states still holds, radiative decay of polaritons will also become strongly dependent on the inhomogeneous line-width of the exciton resonance. The associated *motional narrowing* effect and *resonant Rayleigh scattering* of light by a potential disorder in QWs are discussed in Chapter 3.

2.2. Coupled Microcavities

Coupled microcavities represent an excellent model system to study optical coupling between excitonic states separated by macroscopic distances. Figure 2.2 shows schematically the refractive index profile in a structure containing two coupled microcavities with embedded QWs, studied experimentally by Armitage et al. [5]. Two cavities are separated by a common symmetric Bragg mirror containing $N_c - 1/2$ pairs of quarter-wave layers. In order to analyse the optical properties of such a system, let us consider first two coupled empty cavities, and then introduce the coupling with excitons.

2.2.1. EMPTY COUPLED CAVITIES

The central mirror breaks the degeneracy of the isolated cavity modes. The coupled modes may be classified as symmetric (S) and antisymmetric (A). Since the central mirror is assumed to be symmetric, the equation for the eigenfrequencies

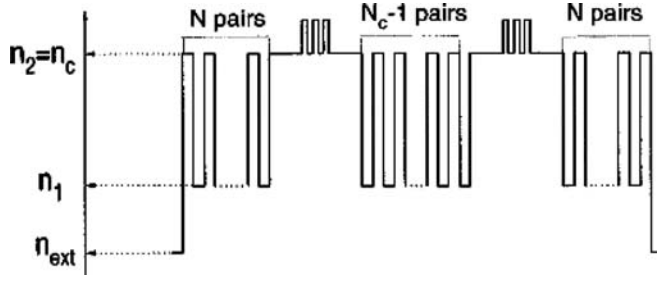

Fig. 2.2. Refractive index profile in a coupled-microcavity structure with embedded QWs studied in Ref. [5]. Bragg mirrors are made of GaAs/AlAs, cavity layers of GaAs, and QWs of InGaAs.

of the entire system has the same form as for a MQW structure embedded in the cavity (see Section 2.1):

$$\left[(t_c + r_c)r_B e^{ik_z L_c} - 1\right]\left[(t_c - r_c)r_B e^{ik_z L_c} + 1\right] = 0, \tag{2.2.1}$$

where $k_z = (\omega/c)n_c \cos\varphi_c$, with n_c, φ_c being the refractive index and propagation angle of light in the cavity material. The reflection and transmission coefficients of the central mirror satisfy

$$r_c/t_c = -r_c^*/t_c^*. \tag{2.2.2}$$

This follows from the specific form of the transfer matrix across any symmetric layer (see Appendix B, Eq. (B.11)). In addition, as there is no absorption in the central Bragg mirror

$$R_c \equiv |r_c|^2 = 1 - |t_c|^2. \tag{2.2.3}$$

From Eqs. (2.2.2), (2.2.3) one can easily obtain

$$t_c = \pm i r_c \sqrt{(1 - R_c)/R_c}, \tag{2.2.4}$$

where the $\pm$ sign corresponds to an even or odd N_c. Substituting Eq. (2.2.4) in (2.2.1), we obtain

$$r r_c e^{2ik_z L_c} = \frac{1}{1 \pm i\sqrt{(1 - R_c)/R_c}}. \tag{2.2.5}$$

For $R_c \to 1$ the two cavities are decoupled, and thus the secular equation for each is

$$r r_c e^{2ik_z L_c} = 1. \tag{2.2.6}$$

If the complex eigenfrequency in each individual cavity is

$$\omega = \omega_m - i\gamma_m, \tag{2.2.7}$$

the eigenfrequencies of a coupled microcavity system can be expressed as

$$\omega = \omega_m - i\gamma_m + \frac{ic \ln(1 \pm i\sqrt{(1 - R_c)/R_c})}{2n_c L_c \cos\varphi_c}. \tag{2.2.8}$$

The imaginary part of the logarithm yields the optical splitting between S and A modes, while the real part gives a correction to the single cavity linewidth. Writing

$$\omega = \omega_m \pm V_{\text{opt}} - i\tilde{\gamma}_m, \tag{2.2.9}$$

we obtain

$$V_{\text{opt}} = \frac{c}{2n_c L_c \cos\varphi_c} \arcsin\sqrt{1 - R_c} \tag{2.2.10}$$

for the coupling constant between the two cavities, and

$$\tilde{\gamma}_m = \frac{c}{4n_c L_c \cos\varphi_c}(-\ln R_c) \overset{R_c\to 1}{\approx} \frac{c(1-R_c)}{4n_c L_c \cos\varphi_c} \tag{2.2.11}$$

for the half-width.

For even N_c the symmetric mode lies at higher energy, while for odd N_c the reverse is true (we are now considering the specific case $n_A < n_B$, where $n_{A(B)}$ is the refractive index of the first (second) from outside quarter-wave layer of the central mirror; otherwise the identification of S and A modes is interchanged). The angular dependence of R_c for the two polarisations (see Section 1.2) is such that the coupling V_{opt} increases with angle for p-polarisation and decreases for s-polarisation.

When the two cavities have different lengths, it is no longer possible to speak of a symmetric and an asymmetric mode: the thicker (thinner) cavity has a larger weight in the low- (high-)energy mode. Figure 2.3 displays the calculated normal incidence reflectivity of two coupled GaAs microcavities with AlAs/GaAs mirrors. The thicknesses of two cavities are either taken the same, or different (dotted, dashed, and solid lines). Figure 2.3(a) (real refractive index, no absorption) demonstrates that the cavity mismatch alone yields reflectivity dips that are much less pronounced if the structure is unbalanced while the spectrum remains symmetric even at very strong mismatch. Also, an important point is that reflection spectra taken from both sides of a non-absorbing structure are the same, which is a consequence of the time-reversal invariance.

In Figure 2.3(b) optical absorption is introduced by assuming that the refractive index of GaAs layers has an imaginary part $\kappa = 0.005$. In this figure, the cavity mismatch is taken to be much smaller, thus the dip positions are almost unchanged: however, a small cavity unbalancing does produce a sizeable peak broadening and asymmetry when combined with a finite imaginary part of the refractive index. Moreover, the reflectivity spectra change when the order of cavities is changed: when the top cavity is thinner (dashed line) the dip at higher energy is stronger than the dip at lower energy, while when the top cavity is thicker (solid line) the lower dip is stronger. Thus only the combined effects of cavity mismatch and absorption give rise to differing intensities of the reflectivity dips, since in the presence of absorption it is the top (outer) cavity which gives the largest contribution to the reflectivity spectrum.

2.2.2. COUPLED CAVITIES WITH QUANTUM WELLS

Let us consider now two identical microcavities of length $L_c = \lambda$, each containing a QW at the antinode of the electric field (see Figure 2.2). The two-fold degenerate lowest exciton state in two identical and electronically uncoupled QWs has the

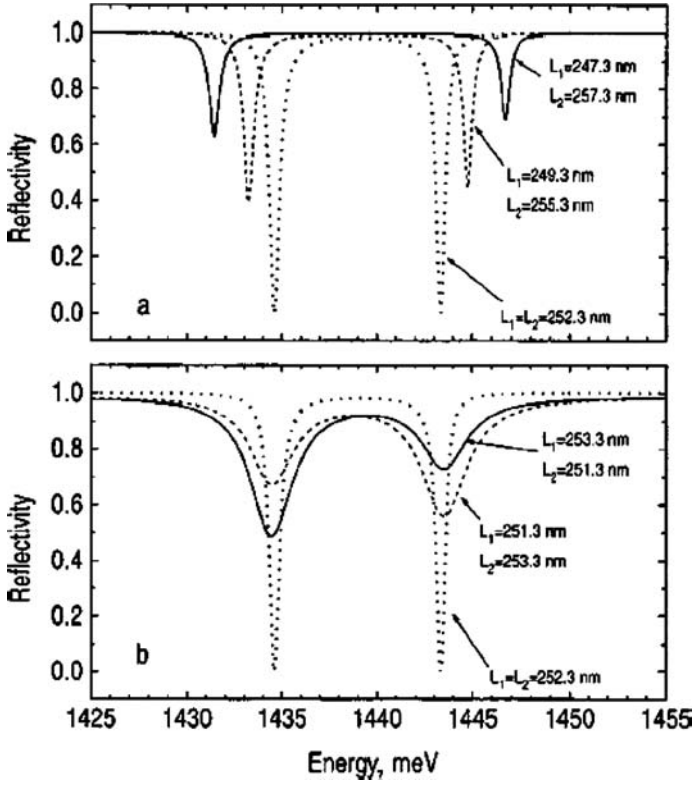

Fig. 2.3. Calculated normal incidence reflectivities of two coupled empty GaAs microcavities. (a) Each layer of the structure is described by a real refractive index. (b) The GaAs layers are described by complex refractive indices with imaginary parts $\kappa = 0.005$.

symmetric and antisymmetric eigenfunctions

$$|S\rangle = \big(|QW1\rangle + |QW2\rangle\big)\big/\sqrt{2}, \tag{2.2.12}$$

$$|A\rangle = \big(|QW1\rangle - |QW2\rangle\big)\big/\sqrt{2}, \tag{2.2.13}$$

where $|QW1\rangle$ and $|QW2\rangle$ are the single exciton wave-functions in the two QWs. Evidently, $|S\rangle$ state can be only coupled to the symmetric photon mode of the coupled cavities, and $|A\rangle$ state can be only coupled to the antisymmetric photon mode. Thus the dispersion equations in two coupled microcavities can be written as two independent equations for symmetric and antisymmetric modes:

$$(\omega_0 - \omega - i\gamma)(\omega_m - \omega + V_{\text{opt}} - i\tilde{\gamma}_m) = V^2, \tag{2.2.14}$$

$$(\omega_0 - \omega - i\gamma)(\omega_m - \omega - V_{\text{opt}} - i\tilde{\gamma}_m) = V^2, \tag{2.2.15}$$

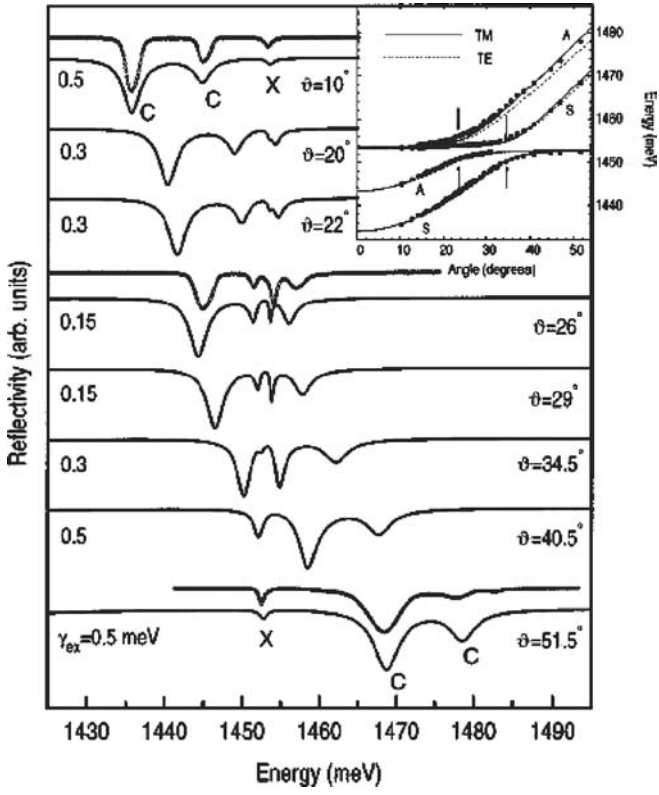

Fig. 2.4. Calculated oblique incidence reflectivity spectra (solid lines) for two coupled GaAs cavities each containing three $In_{0.06}Ga_{0.94}As$ QWs. A few selected experimental curves are also plotted (open points). Inset: dispersion of cavity polaritons. Arrows indicate separate anticrossings for *S* and *A* modes.

where ω_0 and γ are the exciton resonance frequency and broadening, V is the coupling constant between an exciton state and a cavity mode, which is approximately given by Eq. (1.3.9) if the reflectivities of the central mirror is the same as reflectivities of two other mirrors.

Figure 2.4 shows a series of reflection spectra taken from a coupled-microcavity structure with embedded QWs at different incidence angles (Ref. [5]). The inset shows positions of the dips in measured reflection spectra as a function of the incidence angle in comparison with calculated curves for *s* (TE) and *p* (TM) polarizations. One can see two pairs of modes each showing an anticrossing behaviour. They correspond to symmetric and antisymmetric polariton modes. Anticrossings are observed at different angles because of the energy splitting between *S* and *A* photonic modes of coupled cavities. *S* and *A* anticrossings are completely in-

dependent in this structure. No perturbation is observed when A mode crosses S mode or vice-versa. A remarkable fact is that in the range of angles from 20° to 40°, i.e., between two anticrossings, four distinct dips are clearly resolved in the spectra. This means that the degeneracy of excitonic states in two QWs is lifted due to exciton coupling with the cavity modes. Note that two QWs in this structure are separated by more than 1 μm, which means that the optical coupling in coupled microcavities is effective over the macroscopic distances. This is not surprising, since the coherence of electro-magnetic waves is maintained on much larger scales than the coherence of electronic wave-functions, in general. Exciton–polaritons have an advantage of being crystal excitations coherent over macroscopic distances due to their photonic components.

If two microcavities are not identical, decoupling of symmetric and antisymmetric modes is no more possible. A four-oscillator model yields the following equation for eigen-modes:

$$\det\begin{bmatrix} \omega_1-\omega-i\gamma_1 & V_{\rm opt} & V & 0 \\ V_{\rm opt} & \omega_2-\omega-i\gamma_2 & 0 & V \\ V & 0 & \omega_0-\omega-i\gamma & 0 \\ 0 & V & 0 & \omega_0-\omega-i\gamma \end{bmatrix}, \quad (2.2.16)$$

where $\omega_{1,2}$, $\gamma_{1,2}$ are frequencies and broadenings of the cavity mode in two microcavities.

Clearly, coupled microcavities allow for large-scale engineering of the exciton–polariton bands, that can be used potentially for applications in polariton lasers or optical memory elements described in the last chapters of this book.

2.3. Bulk Microcavities

2.3.1. SPATIAL DISPERSION OF EXCITON–POLARITONS

The appearance of additional light modes in crystals at the exciton resonance frequency was theoretically predicted by Pekar in 1957 [6]. This effect, resulting from the so-called *spatial dispersion* of exciton–polaritons, was later confirmed experimentally [7,8]. The spatial dispersion effect on the polariton spectra has attracted considerable attention, and is particularly important in microcavities, where the light mode is tuned to the bulk exciton resonance in the cavity material.

In crystal optics, *spatial dispersion* means dependence of the tensor of the dielectric susceptibility of a crystal on the wave-vector of light. Consider a layer of a cubic semiconductor crystal with a distinct excitonic transition at the frequency ω_0. Taking into account a finite translational mass of the exciton, the dielectric

constant of the crystal is replaced by [9]:

$$\varepsilon(\omega, k) = \varepsilon_B + \frac{4\pi\alpha_0\omega_0^2}{\omega_0^2 - \omega^2 + \frac{\hbar k^2}{M}\omega_0 - 2i\omega\gamma}, \tag{2.3.1}$$

where ε_B is the background dielectric constant, ω is the frequency of light, k is its wave-vector in the media, γ is the non-radiative broadening, M is the exciton effective mass, $\alpha_0 = 2D^2/\hbar\omega_0$, and D is the matrix element of the interband transition in a semiconductor. Substitution of Eq. (2.3.1) into the wave equation

$$-\Delta\vec{E} = k_0^2\varepsilon(\omega, k)\vec{E} \tag{2.3.2}$$

yields two kinds of solution. The first describes propagation of *transverse* waves, i.e., modes with zero electric field projection on the wave-vector direction, and is given by

$$\frac{k^2}{k_0^2} = \varepsilon(\omega, k). \tag{2.3.3}$$

The second kind of solution is related to *longitudinal* waves with an electric field vector parallel to the wave-vector:

$$0 = \varepsilon(\omega, k). \tag{2.3.4}$$

As follows from Eqs. (2.3.3) and (2.3.4), at a given frequency there are three independent light modes propagating in a given direction, including two transverse and one longitudinal mode. TE-polarised light excites only transverse modes, while TM-polarised waves with an electric field component normal to the plane direction excite all types of mode.

Figure 2.5 shows the dispersion of transverse (solid) and longitudinal (dashed) polariton modes in a layer of GaAs. The following parameters were taken for this calculation: $\hbar\omega_0 = 1.515$ eV $\hbar\omega_{LT} = 2\pi\alpha_0\omega_0 = 0.08$ meV, $\hbar\gamma = 0.1$ meV, $M = 0.5m_0$, $\varepsilon_B = 12$, layer thickness $d = 114.8$ nm. The vertical dotted lines show the wave-vector values that satisfy the quantisation condition $kd = j\pi$, $j = 1, 2, 3, \ldots$. The intersection points of the dispersion curves with the dotted lines give eigenstates of transverse and longitudinal exciton–polaritons in the layer. These states manifest themselves in reflection or transmission spectra of thin layers of semiconductors, as has been demonstrated experimentally by Kiselev et al. [7]. In order to see the longitudinal modes, the reflection at oblique angle in TM-polarisation should be measured. This kind of experiment allows one to obtain detailed information about the translational exciton mass and eventual non-parabolicity of the exciton band, as well as to extract the exciton longitudinal-transverse splitting ω_{LT}. If the homogeneous broadening $\hbar\Gamma = 0$ and $M = \infty$, ω_{LT} is exactly the difference between the frequencies ω_T given by the condition

$$\varepsilon(\omega_T, k) = \infty, \tag{2.3.5}$$

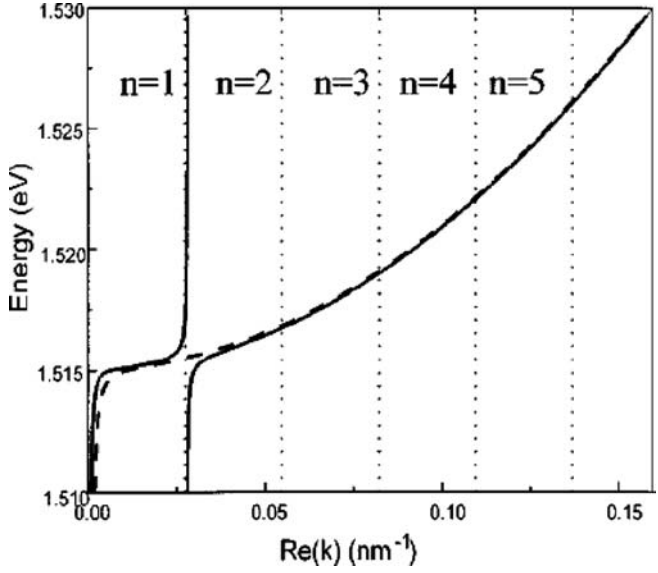

Fig. 2.5. Dispersion of transverse (solid) and longitudinal (dashed) polariton modes in a layer of GaAs. Chosen excitonic parameters are given in the text. The layer thickness $d = 114.8$ nm. Vertical dotted lines show the wave-vector values that verify a quantisation condition $kd = j\pi$, $j = 1, 2, 3, \ldots$.

and ω_L given by

$$\varepsilon(\omega_L, k) = 0. \tag{2.3.6}$$

It is easy to see that at ω_T only the transverse waves can propagate, while at ω_L the only propagating light mode is longitudinal. This is why ω_{LT} is called the longitudinal-transverse splitting. This splitting is a direct measure of the coupling strength between the exciton and light, and is proportional to the *exciton oscillator strength* f:

$$f = \frac{\sqrt{\varepsilon_B}}{\pi} \frac{m_0 c}{e^2} \omega_{LT}. \tag{2.3.7}$$

2.3.2. TRANSFER MATRIX ACROSS A RESONANT LAYER

In order to calculate the optical spectra of semiconductor films containing exciton resonances we shall apply the generalised transfer matrix method (see Appendix B). In order to write down the transfer matrix taking into account spatial dispersion of exciton–polaritons, one should describe propagation of four waves with amplitudes $E_1^{\pm}$, $E_2^{\pm}$ at the beginning and the end of the layer, respectively, where "+" denotes a wave propagating in the positive direction and "−" denotes

a wave propagating in the negative direction. The usual Maxwell boundary conditions are not sufficient in this case. Some additional boundary conditions must be imposed. The simplest additional boundary conditions have been proposed by Pekar:

$$P|_{z=\pm d/2} = 0, \tag{2.3.8}$$

where P is the exciton-induced dielectric polarisation, and $z = \pm d/2$ correspond to the boundaries of the resonant field under study. The conditions (2.3.8) are exact for a molecular crystal and Frenkel excitons [10]. For Wannier–Mott excitons in semiconductors they can be considered as a good approximation in the most part of cases. In a number of works the concept of a so-called "dead-layer" is used, assuming that the exciton centre of mass cannot approach the interface closer than some critical length of the order of the exciton Bohr radius. In general, Neumann-type conditions on the polarisation and its derivative may be formulated. Here, we use the Pekar conditions (2.3.8) as they are the simplest and give reasonably good agreement with experiment, as has been demonstrated many times. We shall neglect the "dead-layer" effect.

For s-polarised light, the matrix Q connecting $E_1^{\pm}$ and $E_2^{\pm}$, so that

$$\begin{bmatrix} E_2^+ \\ E_2^- \end{bmatrix} = Q \begin{bmatrix} E_1^+ \\ E_1^- \end{bmatrix}, \tag{2.3.9}$$

can be written as

$$\begin{aligned} Q &= -\frac{\varepsilon_1}{\varepsilon_2} \begin{bmatrix} \lambda_2^+ & \lambda_2 \\ \lambda_2 & \lambda_2^+ \end{bmatrix}^{-1} \begin{bmatrix} \lambda_1^+ & \lambda_1 \\ \lambda_1 & \lambda_1^+ \end{bmatrix}, \quad \varepsilon_j = \frac{k_j^2}{k_0^2} - \varepsilon_B, \\ \lambda_j &= \exp\left(ik_j \frac{d}{2}\right), \qquad \lambda_j^+ = \exp\left(-ik_j \frac{d}{2}\right), \\ k_j &= n_j k_0 \cos\varphi_{\hat{1}}, \quad n_j = \sqrt{\varepsilon_j}, \ j = 1, 2, \end{aligned} \tag{2.3.10}$$

where φ_j is the propagation angle of the jth wave in the resonant layer ($j = 1, 2$). It can be found from:

$$\begin{aligned} \cos\varphi_i &= \frac{u_i + iv_i}{a_i + ia_i b_i}, \\ 2u_i^2 &= \left[a_i^2\left(1 - b_i^2\right) - n_0^2 \sin^2\varphi_0\right] + \sqrt{\left(a_i^2(1 - b_i^2) - n_0^2 \sin^2\varphi_0\right)^2 4a_i^4 b_i^2}, \\ 2v_i^2 &= -\left[a_i^2\left(1 - b_i^2\right) - n_0^2 \sin^2\varphi_0\right] + \sqrt{\left(a_i^2(1 - b_i^2) - n_0^2 \sin^2\varphi_0\right)^2 4a_i^4 b_i^2}, \end{aligned} \tag{2.3.11}$$

where a_i, b_i are the components of the effective refractive index, $n_i \equiv a_i(1 + ib_i)$, and φ_0 and n_0 are the incidence angle and refractive index outside the resonant

layer, respectively. We leave it to the reader to check that the matrix (2.3.10) is compatible with the Pekar and Maxwell boundary conditions.

For p-polarised light, six complex amplitudes need to be connected by the boundary conditions, taking into account two transverse and one longitudinal polariton modes. Projecting the Pekar condition (2.3.8) onto the z-axis (normal to the film) and x-axis (in the incidence plane, $x \perp z$), we obtain:

$$\widehat{M}_{1z}\begin{pmatrix} E_1^+ \\ E_1^- \end{pmatrix} + \widehat{M}_{2z}\begin{pmatrix} E_2^+ \\ E_2^- \end{pmatrix} + \widehat{S}_z\begin{pmatrix} E_L^+ \\ E_L^- \end{pmatrix} = 0, \tag{2.3.12}$$

$$\widehat{M}_{1x}\begin{pmatrix} E_1^+ \\ E_1^- \end{pmatrix} + \widehat{M}_{2x}\begin{pmatrix} E_2^+ \\ E_2^- \end{pmatrix} + \widehat{S}_x\begin{pmatrix} E_L^+ \\ E_L^- \end{pmatrix} = 0, \tag{2.3.13}$$

where

$$\widehat{M}_{jz} = \varepsilon_j \sin\varphi_j \begin{bmatrix} \lambda_j^+ & \lambda_j \\ \lambda_j & \lambda_j^+ \end{bmatrix}, \qquad \widehat{M}_{jx} = \varepsilon_j \cos\varphi_j \begin{bmatrix} \lambda_j & \lambda_j^+ \\ \lambda_j^+ & \lambda_j \end{bmatrix}, \quad j = 1, 2;$$

$$\widehat{S}_z = \varepsilon_L \cos\varphi_L \begin{bmatrix} \lambda_L^+ & \lambda_L \\ \lambda_L & \lambda_L^+ \end{bmatrix}, \qquad \widehat{S}_x = -\varepsilon_L \sin\varphi_L \begin{bmatrix} \lambda_L^+ & \lambda_L \\ \lambda_L & \lambda_L^+ \end{bmatrix}, \tag{2.3.14}$$

and

$$\varepsilon_j = \frac{k_j^2}{k_0^2} - \varepsilon_b, \quad \lambda_j = \exp\left(ik_j\frac{d}{2}\right), \quad \lambda_j^+ = \exp\left(-ik_j\frac{d}{2}\right),$$

$$k_j = n_j k_0 \cos\varphi_{\hat{1}}, \quad n_j = \sqrt{\varepsilon_j}, \quad j = 1, 2;$$

$$\varepsilon_L = \frac{k_L^2}{k_0^2} - \varepsilon_b, \quad \lambda_L = \exp\left(ik_L\frac{d}{2}\right), \quad \lambda_L^+ = \exp\left(-ik_L\frac{d}{2}\right),$$

$$k_L = n_L k_0 \cos\varphi_L n_L = \sqrt{\varepsilon_L},$$

where $\varphi_{\hat{1}}$ and φ_L are propagation angles of the jth and Lth mode in the resonant layer, respectively, given by Eq. (2.3.11).

Using Eqs. (2.3.9), (2.3.10) for s-polarised light and Eqs. (2.3.12), (2.3.13) for p-polarised light, one can express *all* the complex amplitudes via $E_1^{\pm}$. The transfer matrix $\widehat{T}$ across the resonant film, i.e., the matrix that connects the in-plane components of the electric and magnetic fields at the boundaries, can be written for s-polarised light as:

$$\widehat{T}_s = \left\{\begin{bmatrix} \lambda_1^+ & \lambda_1 \\ n_1\lambda_1^+ & -n_1\lambda_1 \end{bmatrix} + \begin{bmatrix} \lambda_2^+ & \lambda_2 \\ n_2\lambda_2^+ & -n_2\lambda_2 \end{bmatrix}\widehat{Q}\right\} \times \left\{\begin{bmatrix} \lambda_1 & \lambda_1^+ \\ n_1\lambda_1 & -n_1\lambda_1^+ \end{bmatrix} + \begin{bmatrix} \lambda_2 & \lambda_2^+ \\ n_2\lambda_2 & -n_2\lambda_2^+ \end{bmatrix}\widehat{Q}\right\}^{-1}, \tag{2.3.15}$$

and for p-polarised light as:

$$\widehat{T}_p = \widehat{W}^{(1)}\big(\widehat{W}^{(2)}\big)^{-1}, \tag{2.3.16}$$

where

$$\begin{aligned}
&\widehat{W}^{(\alpha)} = \widehat{P}_1^{(\alpha)} + \widehat{P}_2^{(\alpha)}\widehat{U} + \widehat{Z}^{(\alpha)}\big(\widehat{Q}_1^z + \widehat{Q}_2^z\widehat{U}\big), \quad \alpha = 1,2;\\
&\widehat{P}_j^{(1)} = \begin{bmatrix} \lambda_j^+\cos\varphi_j & \lambda_j\cos\varphi_j \\ n_j\lambda_j^+ & -n_j\lambda_j \end{bmatrix}, \quad \widehat{P}_j^{(2)} = \begin{bmatrix} \lambda_j\cos\varphi_j & \lambda_j^+\cos\varphi_j \\ n_j\lambda_j & -n_j\lambda_j^+ \end{bmatrix},\\
&\quad j = 1,2;\\
&\widehat{Z}^{(1)} = \begin{bmatrix} \lambda_L^+\sin\varphi_L & \lambda_L\sin\varphi_L \\ -n_L\lambda_L^+ & n_L\lambda_L \end{bmatrix}, \quad \widehat{Z}^{(2)} = \begin{bmatrix} \lambda_L\sin\varphi_L & \lambda_L^+\sin\varphi_L \\ -n_L\lambda_L & n_L\lambda_L^+ \end{bmatrix};\\
&\widehat{U} = \big[\hat{I} - \widehat{Q}_2^x\widehat{Q}_2^z\big]^{-1}\big[\widehat{Q}_1^x + \widehat{Q}_2^x\widehat{Q}_1^z\big];
\end{aligned} \tag{2.3.17}$$

$\hat{I}$ is the identity matrix, and

$$\begin{aligned}
\widehat{Q}_1^z &= -\widehat{S}_z^{-1}\widehat{M}_{1z}, \qquad \widehat{Q}_2^z = -\widehat{S}_z^{-1}\widehat{M}_{2z},\\
\widehat{Q}_1^x &= -\widehat{M}_{2x}^{-1}\widehat{M}_{1x}, \qquad \widehat{Q}_2^x = -\widehat{M}_{2x}^{-1}\widehat{S}_x.
\end{aligned}$$

In the normal incidence case the matrices $\widetilde{T}_s$ and $\widetilde{T}_p$ coincide. In the form used here, these two matrices were obtained in [11], while the corresponding transfer matrix for the normal incidence case was proposed earlier, in [12]. Generally speaking, introduction of these heavy matrices is of no use in the case of a single resonant layer, where it would be better to write directly the reflection or transmission coefficients. On the other hand, for complicated multilayer structures such as microcavities, the transfer matrix method is almost the only compact and efficient way to solve Maxwell's equations.

2.3.3. 2D PHOTON COUPLING WITH BULK EXCITONS IN MICROCAVITIES

Here we shall describe the optical properties of microcavities containing bulk exciton resonances with the use of the transfer matrix technique, and taking into account the spatial dispersion of excitons. The transfer matrix across the entire microcavity structure is given by the product of transfer matrices across all the layers. As we have already discussed in Section 1.2, for a non-resonant layer of thickness a with a refractive index n, at normal incidence the transfer matrix has the form:

$$\widehat{T}_a = \begin{bmatrix} \cos nk_0a & \frac{i}{n}\sin nk_0a \\ in\sin nk_0a & \cos nk_0a \end{bmatrix}. \tag{2.3.18}$$

In the case of oblique incidence of s-polarised light, one should substitute in Eq. (2.3.18):

$$n \to n \cos\varphi, \tag{2.3.19}$$

where φ is the light propagation angle in the layer. For p-polarised light, the same replacement should be made in the arguments of the trigonometrical functions in Eq. (2.3.18), while in the coefficients one should substitute:

$$n \to \frac{n}{\cos\varphi}, \tag{2.3.20}$$

where $\cos\varphi$ is given in general by Eq. (2.3.11), while for a non-absorbing medium it can be simply found from the law of Snell–Descartes.

The reflection coefficient from the microcavity can be found from the elements of the transfer matrix across the entire structure, $T[i, j]$ (see Appendix A). For s-polarised light:

$$R_s = \left| \frac{n_0 \cos\varphi_0 (T[1,1] + T[1,2] n_f \cos\varphi_f) - (T[2,1] + T[2,2] n_f \cos\varphi_f)}{n_0 \cos\varphi_0 (T[1,1] + T[1,2] n_f \cos\varphi_f) - (T[2,1] + T[2,2] n_f \cos\varphi_f)} \right|^2, \tag{2.3.21}$$

and for p-polarised light:

$$R_p = \left| \frac{n_0 (T[1,1] \cos\varphi_f + T[1,2] n_f) - \cos\varphi_0 (T[2,1] \cos\varphi_f + T[2,2] n_f)}{n_0 (T[1,1] \cos\varphi_f + T[1,2] n_f) - \cos\varphi_0 (T[2,1] \cos\varphi_f + T[2,2] n_f)} \right|^2, \tag{2.3.22}$$

where φ_0 and φ_f, n_0 and n_f are the propagation angles and the refractive indices of light in the media before and after the cavity, respectively.

The complex frequencies for which the reflection coefficient is infinite are eigenfrequencies of the exciton–polariton modes in the cavity. They can be found equally as the complex poles of the transmission coefficient or as the frequencies for which Maxwell's equations have non-trivial solutions with no light incident from outside on the structure. All these conditions yield the same equation for the polariton eigenmodes of s-polarised light:

$$\frac{T[2,1] + T[2,2] n_f \cos\varphi_f}{T[1,1] + T[1,2] n_f \cos\varphi_f} + n_0 \cos\varphi_0 = 0, \tag{2.3.23}$$

and for p-polarised light:

$$\frac{T[2,1] \cos\varphi_f + T[2,2] n_f}{T[1,1] \cos\varphi_f + T[1,2] n_f} + \frac{n_0}{\cos\varphi_0} = 0. \tag{2.3.24}$$

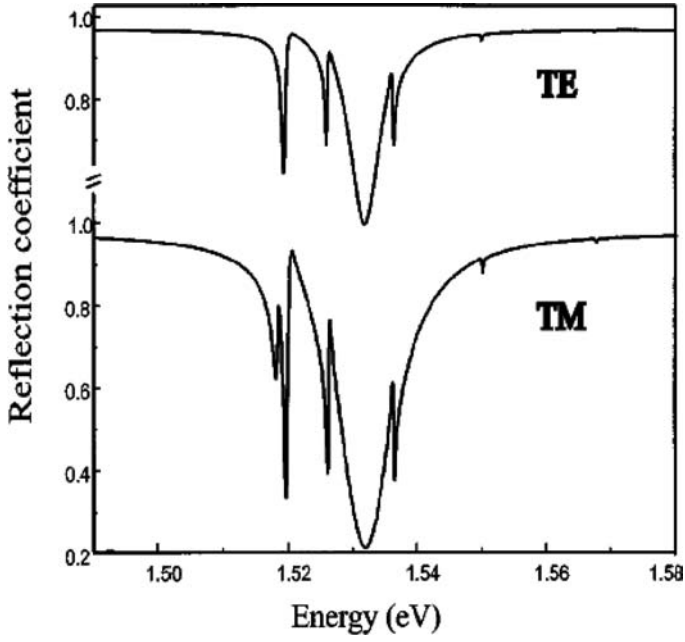

Fig. 2.6. Calculated reflection spectra of light from a bulk microcavity structure in s- and p-polarisations at the incidence angle of 55°. All the parameters of the structure are given in the text.

The last two equations can be resolved numerically to yield the exciton–polariton dispersion curves in semiconductor microcavities containing bulk exciton resonances.

Consider a model $\lambda/2$-microcavity with a GaAs central layer, characterised by a refractive index $n_c = 3.64$ and exciton energy $\hbar\omega_0 = 1.515$ eV. The chosen thickness of the cavity layer, $d = 114.8$ nm, is equal to half the wavelength of light λ in the cavity material at the exciton resonance frequency. Each mirror is composed of ten pairs of $\lambda/4$ layers of $Al_{0.35}Ga_{0.65}As$ and $Al_{0.10}Ga_{0.90}As$ with refractive indices 2.98 and 3.515, respectively. We assume a semi-infinite substrate with refractive index $n_f = 3.64$. Light is incident from a vacuum ($n_0 = 1$).

Figure 2.6 shows the reflection spectra of light in s- and p-polarisations at an incidence angle of 55°. In both cases, on the background of the stop-band one can see a number of dips due to the exciton–polariton resonances that originate from the cavity photon mode interacting with the bulk exciton confined within the cavity layer. In order to analyse the contributions of different exciton states to the spectra it is essential to consider the overlap integrals of the exciton wave-function with the profile of the electric field of the light mode of the cavity. As follows from the Pekar conditions (2.3.8), the exciton centre of mass wave-function always has

zeros at the boundaries of the cavity. For the photon mode this is true only if the phase of the reflection coefficient of the Bragg mirror for light incident from the inside is π. This is the case if $n_1 > n_2$, where n_1 is the refractive index of the layer nearest to the cavity, and n_2 is the refractive index of the next layer of the Bragg mirror (we will refer to this kind of mirror as "metallic-like"). In the opposite case (which is the usual one in most samples studied to date, and which will be referred to as the "dielectric-like" mirror), the phase of the reflection coefficient of the mirror is zero, and the photon mode has antinodes at the boundaries of the cavity. In the case of "metallic-like" mirrors, only one exciton state is coupled to the cavity mode. The overlap integrals of the cavity mode with all the other exciton states are equal to zero. For a $\lambda/2$-microcavity it is the ground exciton state with $N = 1$ (where $N = 1, 2, 3, \ldots$ denotes quantum confined exciton states in the cavity layer). For commonly-used "dielectric-like" mirrors, all the exciton states with even N are coupled to light in a $\lambda/2$-cavity. This is the case in our model structure, where one can see the exciton resonances with $N = 2, 4, 6, 8, 10$.

To obtain a well-defined discrete excitonic spectrum we assume the exciton mass $M = 0.07m_0$ in this case, which is an order of magnitude less than the realistic exciton effective mass in GaAs. Comparing s- and p-polarised spectra, one can see that they are very similar, except for one additional resonance seen in p-polarisation at a frequency of 1.517 eV. This is the so-called longitudinal (L) polariton, resulting from interaction of the $N = 2$ exciton state and p-polarised light. This polariton mode can only be activated by light with a non-zero normal to the plane component of the electric field. In the absence of coupling with the cavity photon, the longitudinal and transverse (T) polariton energies almost coincide. However, the T-polariton has a much larger oscillator strength, and consequently interacts more strongly with the cavity mode. For our model structure the cavity mode is resonant with the $N = 2$ exciton resonance at an incidence angle of 55°. At the anticrossing point, splitting of T-polaritons reaches 6 meV. For the L-polariton the weak-coupling regime holds, so that the L-polarised mode remains in between two split T-modes.

Figure 2.7 shows the energies of polariton resonances in reflection spectra as a function of the incidence angle in p-polarisation (solid lines) and s-polarisation (triangles). These are in fact the polariton dispersion curves that can be obtained from angle-resolved optical experiments. One can see a series of anticrossings of the cavity mode with various exciton states. In p-polarisation a double-anticrossing is seen when the optical mode passes through the $N = 2$ exciton resonance. Consider anticrossings of different T-polarised exciton states with the optical mode. Note that for T-polarised modes the strong coupling regime and anticrossings are seen even for exciton states with high values of N. Splitting of polariton modes (Rabi splitting) as a function of N is shown in Figure 2.8. One can see that the splitting decreases with increasing N. For $N = 2$, the splitting in s-polarisation is less than in p-polarisation because of the additional repul-

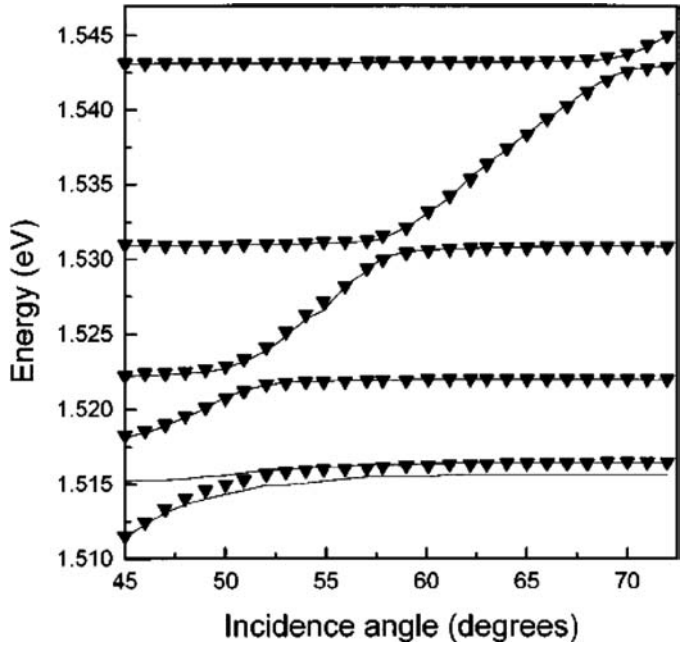

Fig. 2.7. In-plane dispersion of s- and p-polarized exciton–polariton modes in the same bulk GaAs microcavity as in Figure 2.6 (triangles and solid lines, respectively).

sion of T-polarised polaritons from the L-polarised polariton in the latter case. For $N > 2$, Rabi splitting in s-polarised spectra is somewhat larger than in p-polarised spectra because of the higher reflectivity of Bragg mirrors in s-polarisation (see Section 1.2.2).

Numerical solution of the dispersion equations (2.3.23), (2.3.24) allows one to also obtain the lifetimes of polariton modes. The lifetime is inversely proportional to the imaginary part of the eigenenergy of a polariton mode. For our model structure, the lifetime of a bare photon mode is 6×10^{-14} s and that of a bare exciton state is 3.3×10^{-12} s. In the anticrossing regions the lifetime changes between these two values. At the anticrossing point, the exciton radiative damping is always approximately twice as fast as out of the resonance with the cavity mode.

It is instructive to compare the splittings of polariton eigenmodes at the anticrossing points obtained from the spectral resonances with those found from the dispersion equations. The ground-state Rabi splitting can be estimated by neglecting the spatial dispersion. In this case, the dispersion equations (2.3.23), (2.3.24) are reduced to:

$$\left[r_B \exp(ikd)\right]^2 = 1, \tag{2.3.25}$$

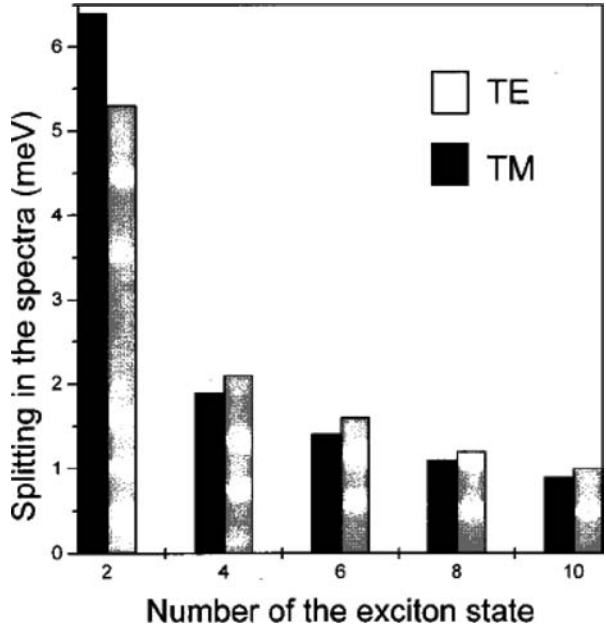

Fig. 2.8. Vacuum-field Rabi splittings for different pairs of exciton–polariton modes formed by a quantum confined exciton state in a central cavity layer and the cavity photon mode. N is the index of quantum confined exciton state. All cavity parameters are the same as in Figures 2.6, 2.7.

where r_B is the amplitude reflection coefficient of the Bragg mirror for light incident from the cavity layer (here, r_B is assumed to be the same for both mirrors). Near the frequency $\overline{\omega}$, which is the centre of the stop-band of the mirrors, r_B can be approximated by:

$$r_B = \sqrt{R}\exp\left[i\frac{n_c L_{\mathrm{DBR}}}{c}(\omega - \overline{\omega})\right], \tag{2.3.26}$$

where L_{DBR} is the effective length of the mirror (see Section 1.2). Assuming $\omega_0 = \overline{\omega}$, ω_{LT}, $\Gamma \ll \omega_0$, and $1 - R \ll 1$, one can obtain from Eq. (2.3.25) the value of the Rabi splitting:

$$\Omega = \left(\frac{2\omega_0\omega_{LT}d}{L_{\mathrm{DBR}} + d}\right)^{1/2}. \tag{2.3.27}$$

For our model structure $\hbar\Omega = 6$ meV. This value is close to that obtained from the spectra for $N = 2$.

To estimate the Rabi splitting for higher exciton states (Ω_N), one can use the simple quantum-mechanical relation:

$$\frac{\Omega_N}{\Omega_2} = \left[\frac{P_N}{P_2}\right]^2, \tag{2.3.28}$$

where P_N is the overlap integral of the exciton wave-function and the light mode. In our case

$$P_N \propto \int_{-\pi/2}^{\pi/2} \sin Nx \sin x \, dx. \tag{2.3.29}$$

Splittings obtained in this way are summarised in the following table:

Index of exciton state	2	4	6	8	10
Polariton splitting, meV	6.0	0.96	0.40	0.22	0.14

There exists an obvious disagreement between these numbers and the splittings seen in the spectra (Figure 2.8) for $N = 4, 6, 8, 10$, which are much larger. The reason is that the dips in the reflection spectra in general *do not correspond* to the frequencies of the polariton eigenmodes. Absorption of light at the frequencies of bare exciton states manifests itself as a series of maxima in the reflection spectra. If the exciton broadening is small these maxima are extremely narrow. In their presence, even in the weak-coupling regime, reflection spectra exhibit two minima near the resonance of the exciton and the cavity mode. In the strong-coupling regime, the splitting between dips in reflectivity accurately reproduces the splitting of the eigenmodes only if it is much larger than the width of the exciton peak in absorption. Otherwise, the reflection spectra always yield over-estimated values of the Rabi splitting. This is true for any kind of microcavity.

Experimentally, bulk GaAs-microcavities have been studied by Tredicucci et al. [13] in the normal incidence geometry. Typical reflection spectra observed by these authors show a pronounced multi-peak structure, resulting from the spatial dispersion of exciton–polaritons. All the experimental observations can be easily interpreted within the formalism presented here.

In conclusion to this section, the method developed here allows one to obtain the in-plane dispersion of exciton–polaritons in microcavities tuned to the bulk exciton resonance in the cavity layer. The strong-coupling regime is expected to be observed only for polariton modes with a transverse polarisation, while resonances originating from L-polarized polaritons may be seen in reflection experiments at oblique incidence in p-polarisation. Angle-resolved reflection spectra allow one to obtain the polariton dispersion curves with a good accuracy, while observed reflection values of Rabi splitting are often over-estimated. Many exciton states in bulk microcavities remain uncoupled with the cavity mode for symmetry reasons. These states form so-called *dark exciton–polaritons* in the cavities.

2.4. Regular Gratings of Quantum Wires and Quantum Dots in a Microcavity

Introduction of a regular in-plane structure inside a microcavity allows the coupling of different in-plane modes, which results in a variety of peculiar optical phenomena. From the point of view of applications, gratings of quantum wires are of interest for lasers with a distributed positive feedback. From the fundamental point of view, microcavity structures with in-plane modulation of the optical response are at the interface between planar cavities and photonic crystals. The density of photonic (polaritonic) states in these structures can be strongly altered by changing the lateral modulation, and formation of a three-dimensional photonic band-gap is not excluded.

Here we shall consider interaction of a light wave with regular structures of quantum wires and quantum dots in order to obtain reflection and diffraction coefficients of these structures. We then address the peculiarities of light coupling with such gratings in microcavities.

2.4.1. REGULAR GRATING OF QUANTUM WIRES

Consider a grating of parallel infinitely long quantum wires (QWRs). All wires are identical. Each contains a single exciton resonance having a frequency ω_0 and a homogeneous nonradiative broadening γ. The period of the grating is d. We chose the system of coordinates such as y-axis is parallel to the wires, z-axis is normal to the plane of the grating. We shall consider only oblique incidence of light in the xz-plane. For a general consideration of resonant reflection of light from a grating of QWRs we address the reader to Refs. [14–16].

To obtain a complex amplitude of light incident on a regular grating of QWRs we use the same approach as one in Section 1.1, i.e., we solve Maxwell equations taking into account the non-local contribution of exciton resonances to the dielectric polarization. This contribution can always be represented in form

$$4\pi P_{\text{exc}}(z) = \int_{-\infty}^{\infty} dx' \int_{-\infty}^{\infty} dz' \, \chi(x, z, x', z') E(x', z'), \tag{2.4.1}$$

while the non-local dielectric susceptibility $\chi(z, z')$ is given by

$$\chi(x, z, x', z') = \tilde{\chi}(\omega) \sum_n \Phi\big((x - x_n), (z - z_n)\big) \Phi\big((x' - x_n)(z' - z_n)\big). \tag{2.4.2}$$

Here $\tilde{\chi}(\omega) = Q/(\omega_0 - \omega - i\gamma)$, $Q = \varepsilon_B \omega_{LT} \pi a_B^3$, $\Phi(x, z)$ is the exciton wavefunction in a quantum wire taken with equal electron and hole coordinates, ω_{LT} and a_B are exciton longitudinal-transverse splitting and Bohr radius, respectively. Using the Bloch theorem, one can represent the electric field of a light-wave prop-

agating within the structure as

$$\vec{E}(x,z) = \vec{E}_{\mathrm{QWR}}(x,z)e^{ik_x x}, \tag{2.4.3}$$

where k_x is a projection of the wave-vector of light $k = \sqrt{\varepsilon_B}k_0$ on x-axis, $\vec{E}_{\mathrm{QWR}}(x,z)$ has the same periodicity as the grating:

$$\vec{E}_{\mathrm{QWR}}(x+nd,z) = \vec{E}_{\mathrm{QWR}}(x,z). \tag{2.4.4}$$

Using the Green-function method in the same manner as in Section 1.1 one can express

$$\begin{aligned} E_\alpha(x,z) &= E_{0\alpha}e^{i(k_x x + k_z z)} \\ &\quad + 4\pi k_0^2 \tilde{\chi}(\omega) \sum_n e^{ink_x d} \iint dx'\,dz'\, G_{\alpha\beta}^{\mathrm{QWR}}\big((x - x_n - x'),(z - z_n - z')\big) \\ &\qquad \times \Phi(x',z') \int dx''\,dz''\,\Phi(x'',z'')E_\beta(x'',z''), \end{aligned} \tag{2.4.5}$$

where $\vec{E}_0$ is an electric field of the incident light,

$$G_{\alpha\beta}^{\mathrm{QWR}}(x,z) = \left(\delta_{\alpha\beta} + \frac{1}{k^2}\frac{\partial^2}{\partial r_\alpha \partial r_\beta}\right)\overline{G}^{\mathrm{QWR}}(x,z), \tag{2.4.6}$$

$\alpha, \beta = x, y, z$.

$$\overline{G}^{\mathrm{QWR}}(x,z) = \frac{i}{4}H_0^{(1)}(k_x x + k_z z), \tag{2.4.7}$$

$H_0^{(1)}(x)$ is the Hankel function. $\overline{G}(x,z)$ satisfies an equation

$$-(\Delta + k^2)\overline{G}^{\mathrm{QWR}}(x,z) = \delta(x,z). \tag{2.4.8}$$

Eq. (2.4.5) can be solved in the same way as Eqs. (1.1.27) and (1.1.28) for a quantum well. For s-polarized light $\vec{E} \| y$, the indices α, β can be omitted, and the Green function (2.4.6) reduces to (2.4.7). In this case Eq. (2.4.5) can be easily solved using the same technique as one we already applied to solve Eq. (1.1.7) for a QW. Namely, both parts of the equation should be multiplied by $\Phi(x,z)$ and integrated over x and z. Then the left part of resulting equation should be substituted to the right part of Eq. (2.4.5). This allows to obtain an expression for the electric field. The amplitude back- and forward-scattering coefficients of the grating of QDs can be obtained in the same way as those for QWRs. In the important limit of no diffraction

$$r_j = \frac{i\beta_j}{\widetilde{\omega}_0 - \omega - i(\gamma + \sum_{j'}\Gamma_{j'})}, \qquad t_j = \delta_{0j} + r_j, \tag{2.4.9}$$

where

$$\Gamma_j = \frac{k^2 Q}{2\varepsilon_B d k_{jz}} I_j^2, \qquad \beta_j = \frac{I_0}{I_j}\Gamma_j,$$

$$I_j = \int dx\, dz\, \Phi(x,z) \cos k_{jx} x \cos k_{jz} z,$$

$$k_{jx} = k_x + 2\pi j/d, \qquad k_{jz} = \sqrt{k^2 - k_{jx}^2}, \qquad \delta_{00} = 1,$$

$\widetilde{\omega}_0$ is the exciton resonance frequency renormalized because of the polariton effects, $\delta_{0j} = 0$ if $j \neq 0$.

For $j = 0$, Eq. (2.4.9) describes reflected and transmitted light. $j \neq 0$ denotes diffracted modes whose number is limited by a condition $|k_{jx}| < k$. The exciton lifetime with respect to emission of y-polarized light in all allowed directions is

$$\tau_y = \left(2 \sum_{j'} \Gamma_{j'}\right)^{-1}. \tag{2.4.10}$$

This lifetime is zero if $d = (2\pi N c)/(\sqrt{\varepsilon_B}\omega_0)$ (N is an integer). In this case a standing wave appears in x-direction with nodes at the centers of the wires. Because of Bragg interference of the secondary light waves emitted by wires, the exciton radiative damping rate in this mode becomes larger proportionally to the quantity of the wires. In the model case of an infinite grating of QWRs the exciton radiative life-time vanishes. In the limit of no diffraction ($kd < \pi$) Eq. (2.4.9) becomes similar to the formulas (1.1.15), (1.1.16) for a QW. Note however, that the oscillator strength of a grating of wires is smaller than that of a QW by a factor L/d, where L is the typical lateral size of the wire.

2.4.2. RECTANGULAR GRATING OF QUANTUM DOTS

The same method allows to calculate diffraction of light on a rectangular grating of quantum dots (QDs). Let us consider an infinite grating of identical QDs characterized by the exciton resonance frequency ω_0. The periods of the grating in x and y directions will be d_x and d_y, respectively. z-axis will be normal to the grating. We shall consider diffraction of a light-wave propagating in the xz-plane.

The exciton contribution to the dielectric polarization writes in this case

$$4\pi P_{\text{exc}}(\vec{r}) = \int d\vec{r}\,' \chi(\vec{r}, \vec{r}\,') E(\vec{r}\,'), \tag{2.4.11}$$

where

$$\chi(\vec{r}, \vec{r}\,') = \tilde{\chi}(\omega) \sum_{n,m} \Phi\big(\vec{r} - \vec{R}_{nm}\big) \Phi\big(\vec{r}\,' - \vec{R}_{nm}\big), \tag{2.4.12}$$

$\vec{R}_{nm} = nd_x\vec{x} + md_y\vec{y}$, $\vec{x}$ and $\vec{y}$ are the unit vectors along the x- and y-axes. Bloch theorem allows us to write

$$\vec{E}(\vec{r}) = \vec{E}_{\mathrm{QD}}(\vec{r})e^{ik_x x}, \tag{2.4.13}$$

where

$$\vec{E}_{\mathrm{QD}}(x + nd_x, y, z) = \vec{E}_{\mathrm{QD}}(x, y + md_y, z) = \vec{E}_{\mathrm{QD}}(x, y, z). \tag{2.4.14}$$

This allows to express the electric field of the light-wave as

$$\vec{E}(\vec{r}) = \vec{E}_0 e^{i\vec{k}\vec{r}} + 4\pi k_0^2 \tilde{\chi}(\omega) \sum_{n,m} e^{ink_x d} \int d\vec{r}\,' \vec{G}^{\mathrm{QD}}\big(\vec{r} - \vec{R}_{nm} - \vec{r}\,'\big)\Phi(\vec{r}\,') \times \int d\vec{r}\,'' \Phi(\vec{r}\,'')\vec{E}(x'', z''), \tag{2.4.15}$$

where $\vec{E}_0$ is an electric field of the incident light,

$$G^{\mathrm{QD}}_{\alpha\beta}(\vec{r}) = \left(\delta_{\alpha\beta} + \frac{1}{k^2}\frac{\partial^2}{\partial r_\alpha \partial r_\beta}\right)\overline{G}^{\mathrm{QD}}(\vec{r}), \tag{2.4.16}$$

$\alpha, \beta = x, y, z$.

$$\overline{G}^{\mathrm{QD}}(\vec{r}) = \frac{e^{ikr}}{4\pi r}. \tag{2.4.17}$$

$\overline{G}(\vec{r})$ satisfies an equation

$$-(\Delta + k^2)\overline{G}^{\mathrm{QD}}(\vec{r}) = \delta(\vec{r}). \tag{2.4.18}$$

For s-polarized light ($\vec{E} \| y$), Eq. (2.4.15) can be resolved in the same way as Eq. (2.4.5) for the wires. In an important limit of no diffraction ($kd_x, kd_y < \pi$), reflection and transmission coefficients of the grating of dots are

$$r^{\mathrm{QD}} = \frac{i\Gamma^{\mathrm{QD}}}{\widetilde{\omega}_0 - \omega - i(\gamma + \Gamma^{\mathrm{QD}})}, \qquad t^{\mathrm{QD}} = 1 + r^{\mathrm{QD}}, \tag{2.4.19}$$

where

$$\Gamma^{\mathrm{QD}} = \frac{k_0 Q}{2\sqrt{\varepsilon_B} d_x d_y}\left[\int d\vec{r}\,\Phi_{\mathrm{QD}}(\vec{r})\cos kr\right]^2,$$

$\widetilde{\omega}_0$ is the exciton resonance frequency renormalized because of the polariton effects. The difference between Γ_{QD} and the exciton radiative broadening in a QW is approximately given by $S/d_x d_y$, where S is the lateral size of the QD.

2.4.3. CAVITY MODE INTERACTION WITH A PERIODIC GRATING OF WIRES OR DOTS

For a short-period grating of QWRs or QDs ($kd, kd_x, kd_y < \pi$), diffraction is absent, which means that under resonant condition between light and exciton modes, 2D polariton dispersion is obtained from the solution of an equivalent problem of two coupled harmonic oscillators. In this case, light reflection and transmission for the whole structure can be readily obtained by use of 2×2 transfer matrices (see Section 1.3). The same formalism is applicable for $kd, kd_x, kd_y > \pi$, if the in-plane projection of the wave vector k_x is far enough from the multiples of π/d ($d = d_x$ in the case of dots). However, if k_x is close to $\pi m/d$, where m is an integer one has to take into account the mixing between four excitations, namely, two photon modes A and B with in-plane wave-vectors $k_A = k_x$ and $k_B = k_x - 2\pi m/d$ and two excitonic waves with corresponding wave-vectors.

We shall consider the mixing of reflected, transmitted and diffracted modes on an example of a microcavity with an embedded grating of QWRs (Figure 2.9).

In order to obtain the dispersion of 2D exciton polaritons in this system, let us introduce for each layer of the structure a 4×4 matrix $\widehat{T}$ describing the transfer of the vector $(A, \tilde{A}, B, \tilde{B})$ across the layer, where A, $\tilde{A}$, B, and $\tilde{B}$ are the amplitudes of the incoming and outgoing waves for two photon modes considered. For each nonabsorbing dielectric layer the transfer matrix is diagonal; for each interface it is quasi-diagonal (see Appendix B, Ch. 1). The mixing between two photon modes arises only in the transfer matrix across the layer of quantum wires, which has the form

$$\widehat{T}_{\mathrm{QWR}} = \frac{1}{\Xi}\begin{bmatrix} 2\Theta - t_0^B & \Theta - t_0^B & t_1^B & t_1^B \\ t_0^B - \Theta & t_0^B & -t_1^B & -t_1^B \\ t_{-1}^A & t_{-1}^A & 2\Theta - t_0^A & \Theta - t_0^A \\ -t_{-1}^A & -t_{-1}^A & t_0^A - \Theta & t_0^A \end{bmatrix}, \tag{2.4.20}$$

where the transmission coefficients $t_j^{A,B}$ for the photon modes A and B are the same as in Eq. (2.4.9), $\Theta = t_0^A t_0^B - t_1^B - t_{-1}^A$. The boundary conditions for eigenmodes in a microcavity are as follows: there is no light incident on the structure from left and right sides. The resulting dispersion equation for 2D exciton–polaritons reads

$$\left[\frac{t_0^A}{\Theta} - \left(\frac{\tilde{r}_L^B}{1+\tilde{r}_L^B} + \frac{\tilde{r}_R^B}{1+\tilde{r}_R^B}\right)\right]\left[\frac{t_0^B}{\Theta} - \left(\frac{\tilde{r}_L^A}{1+\tilde{r}_L^A} + \frac{\tilde{r}_R^A}{1+\tilde{r}_R^A}\right)\right] = \frac{t_1^B t_{-1}^A}{\Theta^2}, \tag{2.4.21}$$

where $\tilde{r}_{L,R}^{A,B} = r_{L,R}^{A,B} \exp(2i\Phi_{L,R}^{A,B})$, $r_{L(R)}^{A(B)}$ is the amplitude reflection coefficient of the A (B) light wave incident from the central layer on the left (right) Bragg mirror, and $\Phi_{L(R)}^{A(B)}$ is the phase gained by the corresponding wave of light between the layer of wires and corresponding Bragg mirror. For the symmetric λ-cavity

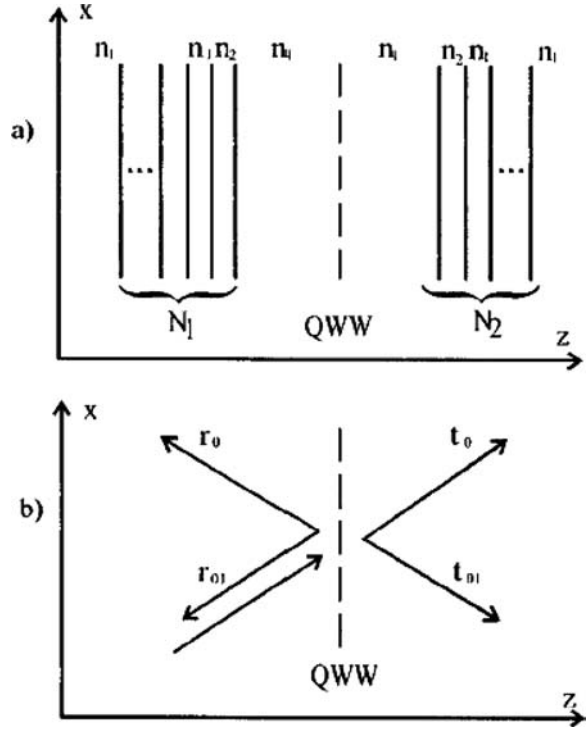

Fig. 2.9. The microcavity with an embedded periodical array of quantum wires (a). Light reflection, transmission, and diffraction scattering at the grating of quantum wires (b); the scattering angle is close to the angle of incidence. r_0 and t_0 are the amplitude reflection and transmission coefficients, r_{01} and t_{01} are the amplitudes of scattered waves in reflection and transmission, respectively.

with quantum wires in the center, neglecting the difference between $I_{\pm 1}$ and I_0 in (2.4.9) and approximating the reflection coefficient of the Bragg mirror as in Section 1.2

$$r_{L,R}^{A,B} = \bar{r}_{A,B} \exp\left[i\alpha_{A,B}(\omega - \overline{\omega})\right], \tag{2.4.22}$$

one can represent Eq. (2.4.21) in a simplified form:

$$\det\begin{bmatrix} \Omega_{\text{exc}} & 0 & V_A & V_B \\ 0 & \Omega_{\text{exc}} & V_A & V_B \\ V_A & V_A & \Omega_A & 0 \\ V_B & V_B & 0 & \Omega_B \end{bmatrix} = 0, \tag{2.4.23}$$

where $\Omega_{\text{exc}} = \widetilde{\omega}_0 - \omega - i\gamma$, $\Omega_{A,B} = \omega_{A,B} - \omega - i\gamma_{A,B}$,

$$V_{A,B} = \left[\gamma_0^{A,B}(1 + \bar{r}_{A,B})/(2\alpha_{A,B}\bar{r}_{A,B})\right]^{1/2}, \tag{2.4.24}$$

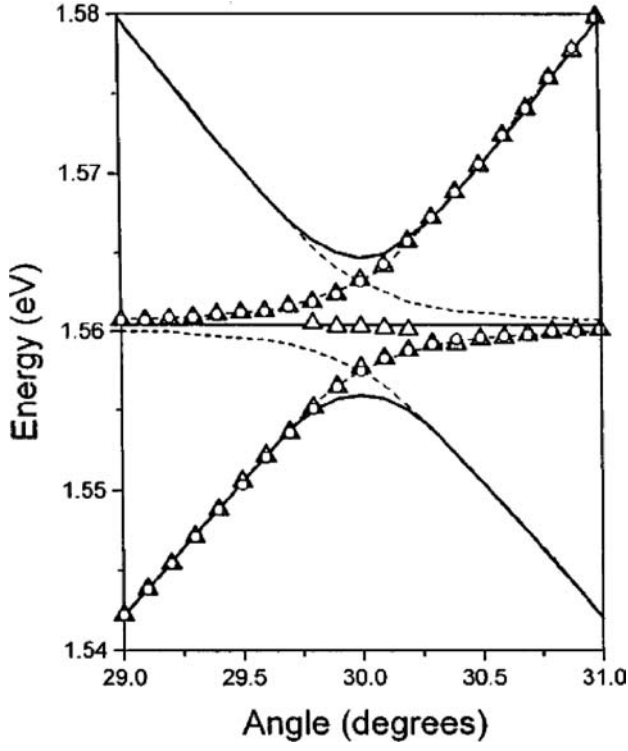

Fig. 2.10. Eigen-frequencies of exciton–polariton modes in a microcavity containing a grating of quantum wires. The first diffraction beam is tuned to the back-scattering direction. Dashed lines, triangles, and circles show the resonant features in calculated diffraction, absorption, and reflection spectra, respectively.

and $\omega_{A,B}$ and $\gamma_{A,B}$ are eigenfrequencies and broadenings of the photon modes A and B in the empty cavity, respectively.

Eq. (2.4.23) in general has four solutions, one of which corresponds to the bare exciton resonance. This is unlike the microcavities with bulk or 2D excitons where the exciton state interacting with a cavity mode is shifted in energy at the anticrossing point by a half of the Rabi splitting. Figure 2.10 shows angle-dependencies of the polariton eigen-energies in comparison with resonances in calculated reflection, absorption and back-scattering diffraction spectra for a model microcavity structure (for details, see Ref. [17]). Interestingly, the spectral features not necessarily coincide with polariton eigen mode positions. The most stricking effects of the wire grating are seen in diffraction which exhibits four resonances. The four-mode spectrum indicates superposition of two exciton anticrossings with photon modes A and B. Note that the resonant diffraction of

light on a grating of quantum wires is strongly polarization-dependent. In particular, it vanishes in the x-polarization. Another remark is that the scattered intensity remains extremely weak in comparison with the intensity of light reflected by a microcavity (less than 1% in realistic structures). In order to increase the scattering amplitudes, one should increase the area occupied by wires in the plane, keeping constant the period of the grating. For these reasons the system which seems to be optimum for observation of resonant diffraction effects consists of rather wide (100–150 nm) quantum stripes separated by barriers of a comparable thickness. To observe diffraction effects in a grating of QDs one should also try to increase as much is possible the exciton oscillator strength of the dots. As will be shown in Section 3.1 it can also be achieved by increasing the dot size up to some limit.

Finally, non-resonant diffraction gratings are widely used to excite cavity- or wave-guide modes propagating at very oblique angles. In semiconductor lasers, diffraction of light by a dielectric grating is used to provide a positive feedback. Gratings are very widely applied in spectrometers, optical filters, etc. All these applications are far beyond the scope of this book.

2.5. Magnetic Field Effect. Kerr and Faraday Rotation

A magnetic field strongly affects excitons in quantum wells, and thus it also affects exciton–polaritons in microcavities. One can distinguish between three kinds of magneto-exciton effects in cavities:

(1) The energies of electron and hole quantum-confined levels change as a function of the magnetic field, following the so-called *Landau fan diagram*. As a result, the energies of electron–hole transitions increase by

$$\delta E = (l + 1/2)\hbar\omega_c, \tag{2.5.1}$$

where the cyclotron frequency $\omega_c = eB/\mu c$ depends on the reduced electron–hole effective mass μ and magnetic field B, and $l = 0, 1, 2, \ldots$ is the Landau quantum index.

(2) Zeeman splitting of the exciton resonance. Excitons with spins parallel or antiparallel to the magnetic field have different energies. The splitting is given by:

$$\Delta E = \mu_B g B, \tag{2.5.2}$$

where $\mu_B \approx 0.062$ meV/T is the Bohr magneton, and g is the exciton g-factor, which depends on the materials composing the quantum well and the magnetic field orientation with respect to the QW. In the following we shall consider the so-called *Faraday geometry*, i.e., the magnetic field parallel to

the wave-vector of the light and, consequently, normal to the QW plane (normal incidence case). Note that g can be positive or negative; in most non-magnetic semiconductor materials it varies between -2 and 2, and in GaAs/AlGaAs QWs it changes sign as the QW width changes.

(3) An increase of the exciton binding energy and oscillator strength due to the shrinkage of the exciton wave-function in a magnetic field. This effect is important for strong enough magnetic fields, for which the magnetic length $L = \sqrt{c\hbar/eB}$ is comparable to the exciton Bohr diameter (typically about 100 Å).

In microcavities, all these effects have a strong impact on the energy spectrum and polarisation properties of exciton–polaritons. Landau quantisation results in the appearance of a fine-structure of polariton eigenstates and gives the possibility of tuning of different Landau levels into resonance with the cavity mode [18]. Exciton Zeeman splitting leads to an effect known as *resonant Faraday rotation*, i.e., rotation of the polarisation plane of linearly polarised light passing through a QW. In microcavities, this effect is strongly amplified due to the fact that light makes a series of round trips, each time crossing the QW before escaping from the cavity [19]. Giant Faraday rotation in microcavities has recently been discovered experimentally [20]. Finally, an increase of the exciton oscillator strength in a magnetic field enhances the vacuum-field Rabi splitting by about 30%, as demonstrated experimentally in the mid-1990s [21].

2.5.1. LANDAU QUANTISATION AND RENORMALISATION OF RABI SPLITTING

Consider an exciton confined in a QW and subject to a magnetic field normal to the QW plane. Separating the exciton centre of mass motion and relative electron–hole motion in the QW plane as in [22], and assuming that the exciton does not move as a whole in the QW plane, we obtain the following exciton Hamiltonian:

$$\widehat{H} = \widehat{H}_e + \widehat{H}_h + \widehat{H}_{\rm ex}, \tag{2.5.3}$$

where

$$\widehat{H}_\nu = -\frac{\hbar^2}{2m_\nu}\frac{\partial^2}{\partial z_\nu^2} + V_\nu(z_\nu) - \mu_B g_\nu \vec{s}_\nu \vec{B} + (l_\nu + 1/2)\hbar\omega_c^\nu,$$

$$\nu = e, h, \tag{2.5.4}$$

$$\widehat{H}_{\rm ex} = -\frac{\hbar^2}{2\mu}\left[\frac{1}{\rho}\frac{\partial}{\partial\rho}\left(\rho\frac{\partial}{\partial\rho}\right) - \frac{\rho^2}{4L^4}\right] - \frac{e^2}{\varepsilon\sqrt{\rho^2 + (z_e - z_h)^2}}, \tag{2.5.5}$$

ρ is the coordinate of electron–hole relative motion in the QW plane, $L = \sqrt{c\hbar/eB}$, $\vec{B}$ is the magnetic field, $m_{e(h)}$ is the electron (hole) mass normal to

the plane, $V_{e(h)}$ is the QW potential for an electron (hole), $g_{e(h)}$ and $\omega_c^{e(h)}$ are the electron (hole) g-factor and cyclotron frequency, respectively, $l = 0, 1, 2, \ldots$, $\mu = m_e m_h^{\parallel}(m_e + m_h^{\parallel})^{-1}$, $m_h^{\parallel}$ is the in-plane hole mass, and ε is the dielectric constant. Hereafter we neglect the heavy-light hole mixing. The excitonic Hamiltonian (2.5.5) was first derived by Gor'kov and Dzyaloshinskii [23]. It contains a parabolic term dependent on the magnetic field. If the field increases, the magnetic length L decreases, which leads to the shrinkage of the wave-function of the electron–hole relative motion. Thus, the probability of finding the electron and hole at the same point increases, leading to an increase of the exciton oscillator strength. In order to estimate this effect, let us solve Eq. (2.5.3) variationally using, as a trial function

$$\Psi_{\text{exc}}(z_e, z_h, \rho) = U_e(z_e)U_h(z_h)f(\rho); \tag{2.5.6}$$

where $z_{e(h)}$ is the electron (hole) coordinate in the direction normal to the plane, and ρ is the coordinate of electron–hole in-plane relative motion. If the conduction band offsets are large in comparison to the exciton binding energy, which is the case in conventional GaAs/AlGaAs QWs, we find $U_{e,h}(z_{e,h})$ as a solution of single-particle problems in a rectangular QW. We separate variables in the excitonic Schrödinger equation [22], and choose

$$f(\rho) = \sqrt{\frac{2}{\pi}}\frac{1}{a_\perp}\exp(-\rho/a_\perp), \tag{2.5.7}$$

where $a_\perp$ is a variational parameter. Substituting this trial function into the Schrödinger equation for electron–hole relative motion with a Hamiltonian (2.5.3), we obtain the exciton binding energy

$$E_B = -\frac{3}{16}\frac{\hbar^2 a_\perp^2}{\mu L^4} - \frac{\hbar^2}{2\mu a_\perp^2} + \frac{4}{a_\perp^2}\int_0^\infty \rho\, d\rho\, e^{-2\rho/a_\perp} V(\rho)$$
$$- \hbar\omega_c^e\left(l_e + \frac{1}{2}\right) - \hbar\omega_c^h\left(l_h + \frac{1}{2}\right), \tag{2.5.8}$$

where

$$V(\rho) = \frac{e^2}{\varepsilon}\int_{-\infty}^{\infty}\int_{-\infty}^{\infty} dz_e\, dz_h \frac{U_e^2(z_e)U_h^2(z_h)}{\sqrt{\rho^2 + (z_e - z_h)^2}}. \tag{2.5.9}$$

The parameter $a_\perp$ should maximise the binding energy. Differentiating Eq. (2.5.8) with respect to $a_\perp$ we obtain:

$$\frac{\hbar^2}{8\mu}\left[1 - 6\left(\frac{a_\perp}{2L}\right)^4\right] = \int_0^\infty \rho\, d\rho\, V(\rho)\left(1 - \frac{\rho}{a_\perp}\right)e^{-2\rho/a_\perp}. \tag{2.5.10}$$

The exciton radiative damping rate Γ_0, defined in Section 1.1, can be expressed in terms of exciton parameters as

$$\Gamma_0 = \frac{\omega_0}{c}\omega_{LT}\sqrt{\varepsilon}a_B^3 a_\perp^{-2} J_{eh}^2. \tag{2.5.11}$$

Here, $J_{eh} = \int dz\, U_e(z)U_h(z)$, ω_0 is the exciton resonance frequency, and ω_{LT} and a_B are the longitudinal-transverse splitting and Bohr radius of the bulk exciton, respectively. (For GaAs one can use $\hbar\omega_{LT} = 0.08$ meV, $a_B = 14$ nm.) The vacuum-field Rabi splitting in a microcavity is

$$\Omega \propto \sqrt{\Gamma_0} \propto \frac{1}{a_\perp}. \tag{2.5.12}$$

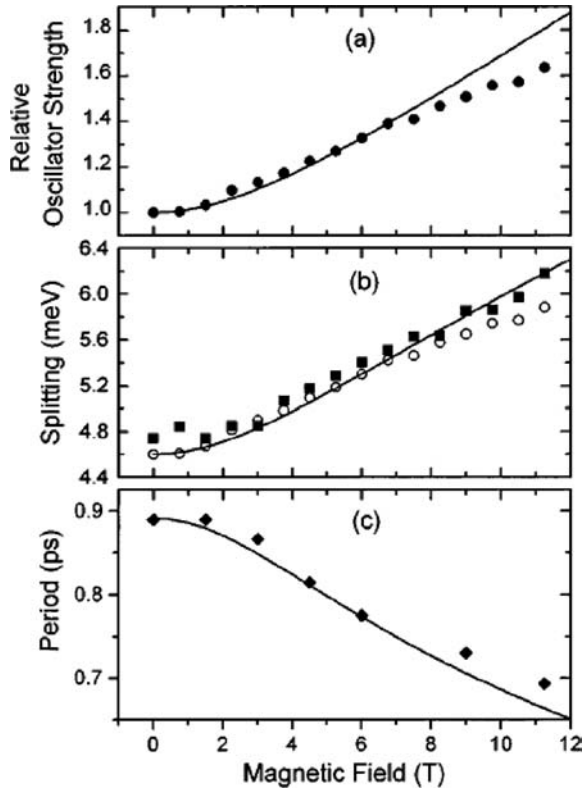

Fig. 2.11. Relative exciton radiative broadening, Rabi-splitting and period of Rabi-oscillations (i.e., oscillations in time-resolved reflection due to beats between two exciton–polariton modes in the cavity) measured experimentally from a GaAs-based microcavity with InGaAs/GaAs QWs ([21], rectangles and circles), and calculated (lines).

Shrinkage of the wave-function of electron–hole relative motion in the magnetic field becomes essential if the magnetic length L is comparable with the exciton Bohr radius a_B, i.e., for magnetic fields of about 3 T and more in the case of GaAs QWs. Taking into account the fact that $L \approx 70$ Å at $B = 10$ T, the exciton Bohr radius can be realistically reduced by a factor of two. Figure 2.11 shows the relative exciton radiative broadening (oscillator strength), Rabi splitting and period of Rabi oscillations (i.e., oscillations in time-resolved reflection due to beats between two exciton–polariton modes in the cavity) measured experimentally in Ref. [21], and calculated within the same formalism as here. One can see that the oscillator strength increases by about 80% with the magnetic field changing from 0 to 12 T, which results in the Rabi splitting increasing by more than 30% and a corresponding decrease in the period of Rabi oscillations.

2.5.2. FARADAY ROTATION

Faraday rotation is rotation of the electric field vector of a linearly polarised light wave propagating in a medium in the presence of a magnetic field oriented along the light propagation direction. Consider the propagation of linearly (X) polarised light, whose initial polarisation is described by a vector

$$\begin{bmatrix} 1 \\ 0 \end{bmatrix} = \frac{1}{2}\begin{bmatrix} 1 \\ i \end{bmatrix} + \frac{1}{2}\begin{bmatrix} 1 \\ -i \end{bmatrix}, \tag{2.5.13}$$

where the upper and lower components of the vectors correspond to the electric field projections in the x- and y-directions, respectively, and the two terms on the right-hand side describe σ^+ (right-circular) and σ^- (left-circular) polarised waves, respectively. If the structure is placed in a magnetic field, the transmission coefficients for σ^+ and σ^- polarised waves become different, so that the transmitted light can be represented as

$$\hat{I} = \frac{1}{2}A\exp(i\varphi_+)\begin{pmatrix} 1 \\ i \end{pmatrix} + \frac{1}{2}B\exp(i\varphi_-), \tag{2.5.14}$$

where the amplitudes A and B and phases φ_+ and φ_- coincide in the absence of the field, but may be different in the presence of the field. $\hat{I}$ is elliptically polarised light, which can be conveniently represented as a sum of waves linearly polarised along the main axes of the ellipse:

$$\hat{I} = \frac{i}{2}(B - A)\exp(i\psi)\begin{bmatrix} \sin\phi \\ -\cos\phi \end{bmatrix} + \frac{1}{2}(A + B)\exp(i\psi)\begin{bmatrix} \cos\phi \\ \sin\phi \end{bmatrix}, \tag{2.5.15}$$

where $\psi = (\varphi_+ + \varphi_-)/2$ and $\phi = (\varphi_- - \varphi_+)/2$ is the *Faraday rotation* angle.

The transmission coefficient of the structure for light detected in x-polarisation is

$$T_x = \frac{1}{4}\left|A\exp(i\varphi_+) + B\exp(i\varphi_-)\right|^2, \tag{2.5.16}$$

and in y-polarisation it is

$$T_y = \frac{1}{4}\left|A\exp(i\varphi_+) - B\exp(i\varphi_-)\right|^2. \tag{2.5.17}$$

In σ^+ and σ^- polarisation the amplitude of light transmitted across the quantum well at the exciton resonance frequency is given by

$$t_{\sigma^+,\sigma^-} = 1 + \frac{i\Gamma_0}{\omega_0^{\sigma^+,\sigma^-} - \omega - i(\gamma+\Gamma_0)}, \tag{2.5.18}$$

where $\omega_0^{\sigma^+,\sigma^-}$ is the exciton resonance frequency in the two circular polarisations, whose splitting in a magnetic field is referred to as exciton Zeeman splitting, Γ_0 is the exciton radiative decay rate and γ is the exciton non-radiative decay rate. Hereafter we shall neglect the exciton inhomogeneous broadening. The polarisation plane of linearly polarised light passing through the QW rotates by the angle

$$\begin{aligned}\phi &= \frac{1}{2}\left[\arctan\frac{(\omega_0^- - \omega)\Gamma_0}{(\omega_0^- - \omega)^2 + (\gamma+\Gamma_0)^2} - \arctan\frac{(\omega_0^+ - \omega)\Gamma_0}{(\omega_0^+ - \omega)^2 + (\gamma+\Gamma_0)^2}\right] \\ &\approx \frac{(\omega_0^{\sigma^-} - \omega_0^{\sigma^+})\Gamma_0}{(\gamma+\Gamma_0)^2}.\end{aligned} \tag{2.5.19}$$

In the case of a microcavity, the Faraday rotation can be greatly amplified. Let us first analyse the expected effects in the framework of simplified "ray optics". Consider a cavity-polariton mode as a ray of light travelling backwards and forwards inside the cavity within its lifetime. At the anticrossing point of the exciton and photon modes the lifetime of cavity polaritons τ is

$$\tau = \frac{1}{\kappa + \gamma + \Gamma_0}, \tag{2.5.20}$$

where κ is the cavity decay rate, dependent on the reflectivity of the Bragg mirrors. The average number of round trips of light inside the cavity is

$$N = \frac{\tau c}{2n_c L_c}, \tag{2.5.21}$$

where n_c is the cavity refractive index and L_c is its length. In high-quality GaAs-based microcavities this factor reaches 70–80. While circulating between the mirrors the light accumulates a rotation, before escaping the cavity. The amplitude of the emitted light can be found as

$$E = t_1 + t_1 r_1 e^{i\phi} + t_1 r_1^2 e^{2i\phi} + \cdots = \frac{t_1}{1 - r_1 e^{i\phi}}, \tag{2.5.22}$$

where r_1 and t_1 are the amplitude reflection and transmission coefficients of the Bragg mirror, respectively. The angle of resulting rotation of the linear polarisa-

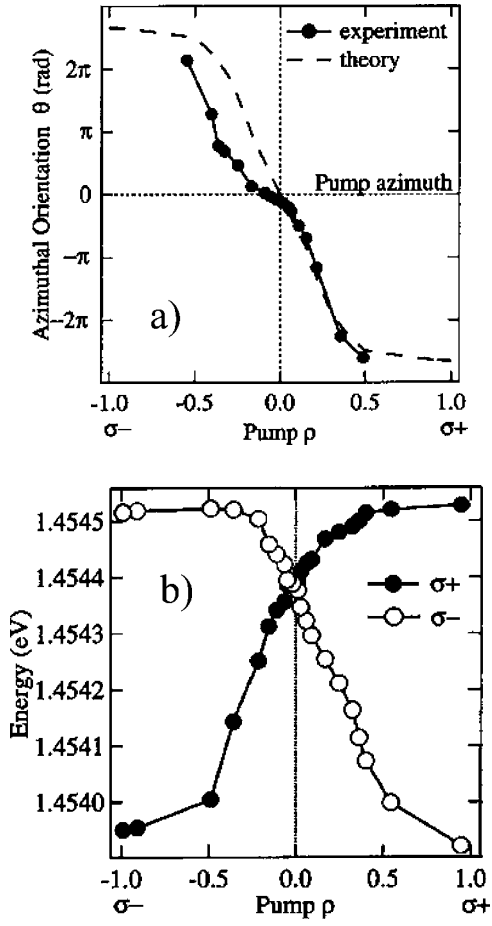

Fig. 2.12. Rotation angle of the linear polarisation of emission of a microcavity vs circular polarization degree of the pumping light experimentally measured by a pump-probe technique by Lagoudakis et al. [20] (solid lines) in comparison with theoretical calculation (dashed lines) (a). The theory used the dependence of the spin-splitting of the exciton resonance on pump polarization degree measured experimentally (b).

tion is

$$\theta = \arg(E) = \frac{r_1 \sin\phi}{1 - r_1 \cos\phi}. \tag{2.5.23}$$

Note that this consideration neglects reflection of light by a QW exciton, since the amplitude of the QW reflection coefficient is more than an order of magnitude smaller than the transmission amplitude.

To observe a giant Faraday rotation a peculiar experimental configuration is needed. In the reflection geometry only a very small rotation of the polarisation plane can be observed (Kerr effect). Actually, the reflection signal is dominated by a surface reflection from the upper Bragg mirror which does not experience any polarisation rotation. To observe the giant effect predicted by Eq. (2.5.13), either the measurement should be carried out in the transmission geometry, which would imply etching the absorbing substrate, or a pump-probe technique should be used to introduce the light into the cavity at an oblique angle and then to probe emission at the normal angle.

This kind of measurement has been performed by Lagoudakis et al. [24]. An effect of *stimulated scattering* (addressed in Chapter 5 of this book), has been used to induce emission of coherent linearly polarised light by a QW embedded in a cavity, in a direction normal to the plane of the structure. Zeeman splitting of the exciton resonance has been optically induced in this experiment. Its value is proportional to the circular polarisation degree of the pump-pulse, $\rho = (I^+ - I^-)/(I^+ + I^-)$, where I^+ and I^- are the intensities of the pump pulse measured in σ^+ and σ^- polarisations. Figure 2.12(a) shows the evolution of θ calculated using Eq. (2.5.13) against the circular polarisation degree of the pump pulse. The splitting $(\omega_0^- - \omega_0^+)$ is taken from the experimental data shown in Figure 2.12(b). The points show the experimentally measured polarisation rotation angle. One can see rotation of the polarisation plane by more than 2π.

Finally, the effect of a magnetic field on the dynamics of relaxation of exciton–polaritons in microcavities is of significant interest. It will be addressed in the second part of this book.

References

1. M. R. Vladimirova, E. L. Ivchenko, A. V. Kavokin, Exciton polaritons in long-period quantum-well structures, *Semiconductors* 32, 90 (1998).
2. S. Pashkovskiy, "Applications of Chebyshev Polynomials and Series". Nauka, Moscow, 1983.
3. M. Markus, H. Mink, "Review on Matrix Theory and Matrix Inequalities". Nauka, Moscow, 1972.
4. E. L. Ivchenko, A. I. Nesvizhskii, S. Jorda, Resonant Bragg reflection from quantum well structures, *Superlatt. & Microstruct.* 16, 17 (1994).
5. A. Armitage, M. S. Skolnick, V. N. Astratov, D. M. Whittaker, G. Panzarini, L. C. Andreani, T. A. Fischer, J. S. Roberts, A. V. Kavokin, M. A. Kaliteevski, M. R. Vladimirova, Optically induced splitting of bright excitonic states in coupled quantum microcavities, *Phys. Rev. B* 57, 14 877 (1998).
6. S. I. Pekar, *Zh. Eksper. Teoret. Fiz.* 33, 1022 (1957).
7. V. A. Kiselev, I. N. Uraltsev, B. S. Razbirin, *JETP Lett.* 18, 296 (1973).
8. D. Frölich, A. Kulik, B. Uebbing, A. Mysyrowicz, V. Langer, H. Stolz, W. von der Osten, Coherent propagation and quantum beats of quadrupole polaritons in Cu_2O, *Phys. Rev. Lett.* 67, 2343 (1991).

9. E. L. Ivchenko, Spatial dispersion effects in exciton resonance region, in "Excitons" (E. I. Rashba and M. D. Sturge, Eds.). Elsevier, North-Holland, 1982.
10. V. M. Agranovich, V. L. Ginzburg, "Spatial Dispersion in Crystal Optics and the Theory of Excitons". Interscience Publ., London, 1966.
11. M. R. Vladimirova, A. V. Kavokin, M. A. Kalitevski, Dispersion of bulk exciton polaritons in a semiconductor microcavity, *Phys. Rev. B* 54, 14566 (1996).
12. Y. Chen, A. Tredicucci, F. Bassani, Bulk exciton polaritons in GaAs microcavities, *Phys. Rev. B* 52, 1800 (1995).
13. A. Tredicucci, Y. Chen, V. Pellegrini, M. Börger, L. Sorba, F. Beltram, F. Bassani, Controlled exciton–photon interaction in semiconductor bulk microcavities, *Phys. Rev. Lett.* 75, 3906 (1995).
14. A. D'Andrea, R. Del Sole, Excitons in semiconductor confined systems, *Solid State Commun.* 74, 1121 (1990).
15. E. L. Ivchenko, A. V. Kavokin, Light reflection from quantum well, quantum wire and quantum dot structures, *Sov. Phys. Solid State* 34, 1815 (1992).
16. A. V. Kavokin, E. L. Ivchenko, M. R. Vladimirova, M. A. Kaliteevski, S. V. Goupalov, *Superlatt. & Microstr.* 23, 389 (1998).
17. A. V. Kavokin, M. A. Kaliteevski, M. R. Vladimirova, Coupling between one-dimensional excitons and two-dimensional photons: Quantum wires in a microcavity, *Phys. Rev. B* 54, 1490 (1996).
18. J. Tignon, P. Voisin, C. Delalande, M. Voos, R. Houdré, U. Oesterle, R. P. Stanley, From Fermi's golden rule to the vacuum Rabi splitting: Magnetopolaritons in a semiconductor optical microcavity, *Phys. Rev. Lett.* 74, 3967 (1995).
19. A. V. Kavokin, M. R. Vladimirova, M. A. Kaliteevski, O. Lyngnes, J. D. Berger, H. M. Gibbs, G. Khitrova, Resonant Faraday rotation in a semiconductor microcavity, *Phys. Rev. B* 56, 1087 (1997).
20. A. V. Kavokin, G. Malpuech, P. Lagoudakis, J. J. Baumberg, K. V. Kavokin, Polarization rotation in parametric scattering of polaritons in semiconductor microcavities, *Phys. Stat. Sol. (a)* 195, 579 (2003).
21. J. D. Berger, O. Lyngnes, H. M. Gibbs, G. Khitrova, T. R. Nelson, E. K. Lindmark, A. V. Kavokin, M. A. Kaliteevski, V. V. Zapasskii, Magnetic field enhancement of the exciton–polariton splitting in a semiconductor quantum well microcavity, *Phys. Rev. B* 54, 1975 (1996).
22. A. V. Kavokin, A. I. Nesvizhskii, R. P. Seisyan, Exciton in a semiconductor quantum well subjected to a strong magnetic field, *Sov. Phys. Semicond.* 27, 530 (1993).
23. L. P. Gor'kov, I. E. Dzialoshinskii, *JETP* 53, 717 (1967).
24. P. G. Lagoudakis, P. G. Savvidis, J. J. Baumberg, D. M. Whittaker, P. R. Eastham, M. S. Skolnick, J. S. Roberts, Stimulated spin dynamics of polaritons in semiconductor microcavities, *Phys. Rev. B* 65, 161310 (R) (2002).

This page intentionally left blank

Chapter 3
Disorder Effect on Cavity Polaritons

3.1. Reflection and Elastic Scattering of Light by Localised Excitons 88
3.1.1. Multiple Scattering of Light and Weak-Localization of Exciton–Polaritons 95
3.2. Motional Narrowing of Cavity Polaritons 95
3.2.1. Single QW Case 97
3.2.2. Reflection of Light from Microcavities 99
3.3. Photoluminescence and Resonant Rayleigh Scattering from Microcavities (Linear Regime) 101
3.4. Time-Resolved Reflection of Light from Quantum Wells and Microcavities 107
3.4.1. Free Homogeneously Broadened Exciton Resonance in a QW 107
3.4.2. Inhomogeneous Broadening Effect on Time-Resolved Spectra of QWs 108
3.4.3. Vertical Motional Narrowing in Time-Resolved Spectra of Multiple QWs 110
3.4.4. Inhomogeneous Broadening Effect on Time-Resolved Reflection Spectra of Microcavities 111
References 113

In this chapter we address a series of phenomena caused by in-plane potential fluctuations in microcavities. These potential fluctuations are always present in real samples. They come from inevitable structure imperfections, monolayer fluctuations of quantum-well boundaries, impurities, alloy fluctuations, spontaneous polarization fields, etc. The resulting disorder potential localizes excitons in the plane of the structure, which leads to relaxation of the wave-vector conservation law and causes elastic (Rayleigh) scattering of light. On the other hand, photonic modes are not confined in the plane of the microcavity. They interact with localized excitons that leads to formation of extended exciton–polariton modes for which the in-plane wave-vector is still a good quantum number in many cases. The interplay between disorder scattering and polariton effect governs the linear optical properties of realistic microcavities and has an important impact on their non-linear properties, as well. In this chapter we consider light interaction with a single localized exciton state, with an ensemble of localized excitons, and finally calculate eigen-energies of microcavity polaritons in the presence of the disorder scattering. We address also the time-resolved response of the microcavities limiting ourselves to the linear regime, however. Optical spectroscopies relevant to the theory we are going to present here are: reflection, transmission, resonant Rayleigh scattering, linear pump-probe technique, and photoluminescence under low pumping.

3.1. Reflection and Elastic Scattering of Light by Localised Excitons

A free exciton in a QW does not scatter light; it only participates in wave-vector conserving optical processes such as reflection and transmission. This is why the model we developed in Chapter 1 does not describe any scattering of light. On the other hand, in reality, semiconductor QWs are not uniform in their plane. There are always fluctuations of the QW width or alloy concentration that produce a potential disorder, leading to the appearance of a huge number of excitonic states localised in the QW plane. The energies of these states are statistically distributed with a function that usually reminds one of a Gaussian, while other shapes are also possible in particular cases. Each localised excitonic state can scatter the incident light in any direction, as the wave-vector conservation rule no longer applies. Formally, it interacts with light in the same way as a quantum dot (QD) containing an exciton resonance. The optical properties of the entire structure are governed by interfering waves scattered by different localised excitons, so that the QW acts as an array of QDs.

Here we present a model that describes all types of coherent optical experiment (reflection, transmission and scattering) on confined localised excitons in the framework of a unified formalism. The model properly takes into account the exciton–polariton effect in a disordered QW, modelled by an array of QDs.

Analogous to what has been done to find the reflection and transmission coefficients of a QW containing free excitons, we shall use the Green's function approach to the problem of light–exciton coupling in low-dimensional structures (see Section 1.1). We consider N QDs, which represent shallow potential islands distributed in the QW plane that weakly localise exciton wave-functions, so that the wave-functions attributed to neighbouring QDs may overlap. Each QD is characterised by a given exciton resonance frequency ω_n, and radius vector $\vec{R}_n$ that denotes the centre of the localised exciton wave-function in the dot. We assume ω_n to be distributed with a function

$$f(\omega_n) = \left[\pi\,\Delta \cosh\left(\frac{\omega_n - \omega_0}{\Delta}\right)\right]^{-1}, \tag{3.1.1}$$

where Δ describes the exciton inhomogeneous broadening.

Neglecting deviations in the shape of exciton wave-functions localised in different dots, we solve the Maxwell equation:

$$\nabla \times \nabla \times \vec{E} = k_0^2 \vec{D} \tag{3.1.2}$$

where

$$\vec{D} = \varepsilon_b \vec{E} + 4\pi \vec{P}_{\text{exc}} \tag{3.1.3}$$

and

$$4\pi \vec{P}_{\text{exc}} = \sum_{n=1}^{N} T_n \Phi\big(\vec{r} - \vec{R}_n\big) \int \vec{E}(\vec{r}\,')\Phi\big(\vec{r}\,' - \vec{R}_n\big)\, d\vec{r}\,', \tag{3.1.4}$$

with

$$T_n = \frac{\varepsilon_b \omega_{LT} \pi a_B^3}{\omega_n - \omega - i\gamma},$$

where k_0 is the wave-vector of the incident light in a vacuum, ω_{LT} is the longitudinal-transverse splitting, ε_b is the background dielectric constant, a_B is the Bohr radius of the exciton in the bulk, γ is the homogeneous broadening, and $\Phi(\vec{r})$ is the localised exciton wave-function taken with equal electron and hole coordinates. Further, we assume equal (Gaussian) shapes of $\Phi(\vec{r})$ for all QDs. The distribution of QD sizes would result in a distribution in the exciton oscillator strength that may slightly influence the scattered signal. Solving Eq. (3.1.2), we represent the electric field as

$$\vec{E}(\omega, \vec{r}) = \vec{E}_0 \exp\big(i\vec{k}\vec{r}\big) + k_0^2 \sum_{n=1}^{N} T_n \int d\vec{r}\,' \, \Phi\big(\vec{r}\,' - \vec{R}_n\big) G_0(\vec{r} - \vec{r}\,') \times \int \vec{E}(\vec{r}\,'')\Phi\big(\vec{r}\,'' - \vec{R}_n\big)\, d\vec{r}\,'', \tag{3.1.5}$$

where $G_0(\vec{r} - \vec{r}\,') = e^{ik|\vec{r} - \vec{r}\,'|}/(4\pi|\vec{r} - \vec{r}\,'|)$ is the Green's function for a zero-dimensional system and $\vec{k} = \vec{k}_0\sqrt{\varepsilon_b}$ is the wave-vector of the incident light in the medium. Neglecting the fluctuations of the electric field from dot to dot, we obtain

$$\vec{E}(\omega, \vec{r}) = \vec{E}_0 \exp\big(i\vec{k}\vec{r}\big) + k_0^2 \sum_{n=1}^{N} T_n \int d\vec{r}\,' \, \Phi\big(\vec{r}\,' - \vec{R}_n\big) G_0(\vec{r} - \vec{r}\,') \times \frac{\int \vec{E}_0 e^{i\vec{k}\vec{r}}\, \Phi(\vec{r})\, d\vec{r}}{1 - \sum_{m=1}^{N} \Theta_{nm}}, \tag{3.1.6}$$

where $\Theta_{nm} = k_0^2 T_n \int\int G_0(\vec{r} - \vec{r}\,')\Phi_{\text{QD}}(\vec{r}\,' - \vec{R}_n)\Phi_{\text{QD}}(\vec{r} - \vec{R}_m)\, d\vec{r}\,' \, d\vec{r}$.

The Fourier transform of the electric field (3.1.6) yields its directional dependence, which can be represented in the form

$$\vec{E}_d(\omega, \vec{k}_s) = \vec{E}_0 \delta_{\vec{k},\vec{k}_s} + \vec{E}_0 \sum_{m=1}^{N} \frac{i\Gamma_0^{\text{QD}}}{\omega_m - \omega - i\gamma} \frac{1}{1 - \sum_{n=1}^{N} \Theta_{nm}} \times \exp\big(i\vec{k}_s . \vec{R}_m\big), \tag{3.1.7}$$

where

$$\Gamma_0^{\mathrm{QD}} = \frac{1}{6}\omega_{LT} k_0^3 a_B^3 \left(\int d\vec{r} \cos(\vec{k}.\vec{r}) \Phi(\vec{r}) \right)^2, \tag{3.1.8}$$

$\delta_{\vec{k},\vec{k}_s} = 1$ if $\vec{k}_s = \vec{k}$, $\delta_{\vec{k},\vec{k}_s} = 0$ if $\vec{k}_s \neq \vec{k}$.

Note that in the oblique incidence case, Eq. (3.1.7) should be slightly modified. In particular, Θ_{nm} should be multiplied by $\cos\alpha$ in the *s*-polarisation and divided by $\cos\alpha$ in the *p*-polarisation, where α is the light propagation angle in the medium [1]. Eq. (3.1.8) describes all kinds of coherent optical experiments (reflection, transmission and Rayleigh scattering) within the same semiclassical formalism, properly taking into account the polariton effect. The ratio of reflected and average scattered intensities can be estimated from Eqs. (3.1.7), (3.1.8), assuming that the light waves scattered by QDs lying within a Γ_r vicinity interfere positively in the reflection direction (where Γ_r is the radiative broadening of the exciton resonance in reflection):

$$I_r / I_s \approx N \left(\frac{\Gamma_r}{\Delta} \right)^2, \tag{3.1.9}$$

where N is given by the number of QDs within the light spot. To estimate the ratio of the angle-integrated scattered intensity $\bar{I}_s$ to the reflected intensity, assuming negligible microscopic dephasing, one has to divide the value of I_r / I_s by the total number of *speckles* (inside and outside the light cones). This procedure yields

$$I_r / \bar{I}_s = \lambda^2 / \pi d^2, \tag{3.1.10}$$

where λ is the wavelength of light in the medium and d is the average distance between QDs.

Figure 3.1 shows experimentally measured reflected and scattered intensities by a single QW in the vicinity of an exciton resonance taken from Ref. [2] in comparison with a theoretical calculation by Eq. (3.1.7). One can see pronounced variation of the scattered intensity as a function of angle that is a signature of *speckles* in the Rayleigh scattering. The ratio of average reflected and scattered intensities is about 10^6, which gives an order of magnitude of the number of localized excitons contributing to the spectra.

In the specular reflection direction, one can neglect the small portion of scattered light and assume $\Theta_{nm} = \Theta_{nn}$. Substituting summation by integration in Eq. (3.1.7) we obtain the reflection and transmission coefficients of a QW, r_{QW} and t_{QW}, as

$$r_{\mathrm{QW}} = \frac{\beta}{1-\beta}, \qquad t_{\mathrm{QW}} = \frac{1}{1-\beta}, \tag{3.1.11}$$

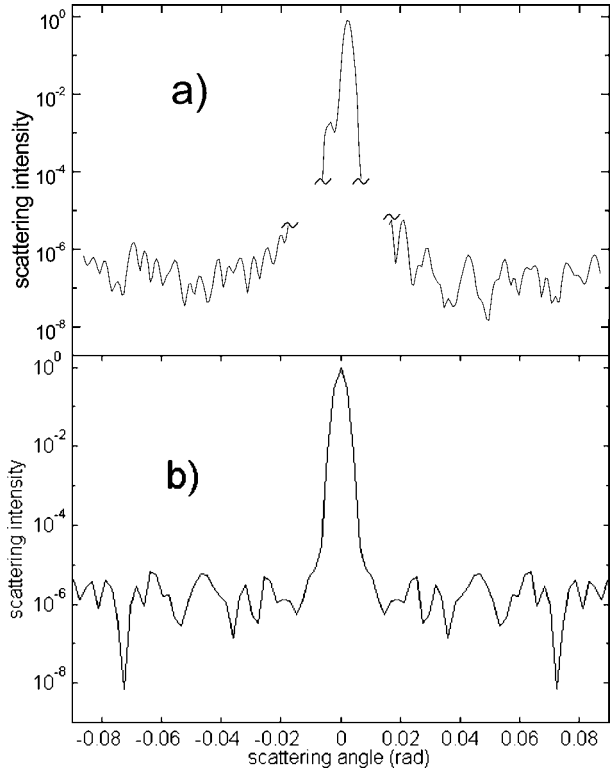

Fig. 3.1. Intensity of the scattered (reflected) light by the GaAs/AlGaAs single QW as a function of the scattering angle in the reflection plane: experiment (a) and theory (b). Zero angle corresponds to the specular reflection.

where

$$\beta = i\Gamma_r \int d\nu \, \frac{f(\nu)}{\nu - \omega - i\gamma},$$

$$\Gamma_r = \frac{k}{2d^2}\omega_{LT}\pi a_B^3 \left[\int \Phi(\vec{r}) \cos(\vec{k}\vec{r}) \, d\vec{r} \right]^2. \qquad (3.1.12)$$

Note, that the radiative broadening Γ_r obtained here coincide with one of a regular grating of QDs having a period d in no-diffraction regime (see Section 2.4). In real systems, $\Gamma_r \gg \Gamma_0^{\mathrm{QD}}$, which means that optically coupled QDs emit light much faster than single QDs. In GaAs/AlGaAs QWs of about 10 nm width, $\hbar\Gamma_r \approx 25$ μeV, which corresponds to an exciton radiative lifetime $\tau = 1/2\Gamma_r \approx 10$ ps. The radiative lifetime of an exciton in a single QD varies be-

tween wide limits as a function of the QD size. Here we analyse it by assuming that a QD has a spherical shape, which is, of course, far from reality in QWs but is exactly the case in nanospheres [3]. The form factors introduced by a non-spherical shape of potential islands in a QW do not change qualitatively the tendencies described below.

Three different cases should be distinguished.

(1) In the case of a nanosphere smaller than the Bohr diameter of the exciton, $2a_B$, (due to the small value of a_B, one may deal with very small objects in the case of wide-band-gap semiconductors), Eq. (3.1.8) reduces to:

$$\Gamma_0^{\mathrm{QD}} = \frac{1}{6}\hbar\omega_{LT}k_0^3 a_B^3. \tag{3.1.13}$$

(2) In the second case, where the nanosphere is "bigger" than the exciton, but nevertheless remains "smaller" than the wavelength of the light, one obtains for the radiative recombination rate from (3.1.8):

$$\Gamma_0^{\mathrm{QD}} = \frac{1}{6}\omega_{LT}k_0^3 V. \tag{3.1.14}$$

In this equation, V represents the volume of the nanosphere that comes from the normalization condition

$$\left[\int d^3r\, \Phi(\vec{r})\right]^2 = \frac{V}{a_B^3} = \frac{4\pi R^3}{3a_B^3}, \tag{3.1.15}$$

where R is the radius of the considered nanosphere.
Eq. (3.1.14) predicts an increase of the light–matter coupling strength with an increase of the size of the QD. This is a manifestation of the Rashba–Gurgenishvili effect [4], which consists in an enhancement of the oscillator strength of a localised exciton proportional to the spreading of its wavefunction.

(3) We now consider dots with sizes comparable to the wavelength of the light, and look for a tractable analytical formula for the oscillator strength. To do so we approximate $\Phi(\vec{r})$ by a Gaussian function:

$$\Phi(\vec{r}) = \frac{1}{\sqrt{\pi a_B^3}}\frac{1}{\langle r\rangle^{3/2}}\left(\frac{2}{\pi}\right)^{3/4}\exp\left(-\frac{r^2}{\langle r\rangle^2}\right). \tag{3.1.16}$$

The normalisation condition (3.1.15) yields

$$\langle r\rangle = R\left(\frac{\sqrt{2\pi}}{3}\right)^{1/3} \approx R. \tag{3.1.17}$$

Table 3.1. Exciton Bohr radius, dielectric constant, longitudinal transverse splitting and optimal QD radius for eleven semiconductors

	GaAs	InP	CdTe	ZnTe	CdSe	ZnSe	CdS	ZnS	GaN	β-GaN	β-ZnO
a_B (nm)	13.6	11.9	7.2	5.8	5.3	4.4	3.2	3.5	25	30	14
ε_B	12.6	12.1	9.3	8.7	9.5	7.6	8.1	8	8	9	8.36
ω_{LT} (meV)	0.13	0.17	0.67	0.62	1	1.63	2.05	2.1	2.5	2.5	1.5
λ_0 (nm)	816	873	772	518	674	439	484	325	380	356	368

Substituting the wave-function (3.1.16) into the general formula (3.1.8), we obtain

$$\Gamma_0^{\mathrm{QD}} = \frac{1}{6}\omega_{LT}k_0^3 a_B^3 \left(\frac{1}{\sqrt{\pi a_B^3}} \frac{1}{\langle r\rangle^{3/2}} \left(\frac{2}{\pi}\right)^{3/4} \int r^2\, dr\, \sin\theta\, d\theta\, d\varphi \right.$$
$$\left. \times \cos\left(\frac{2\pi}{\lambda} r\cos\theta\right) \exp\left(-\frac{r^2}{\langle r\rangle^2}\right)\right)^2 \tag{3.1.18}$$

that yields, after integration:

$$\Gamma_0^{\mathrm{QD}} = \frac{\sqrt{2\pi}}{3}\omega_{LT}\left(\frac{2\pi}{\lambda_0}\right)^3 \langle r\rangle^3 \exp\left(-8\varepsilon_b \frac{\pi^2\langle r\rangle^2}{\lambda_0^2}\right). \tag{3.1.19}$$

This function is non-monotonic and has a maximum at

$$\langle r\rangle = \frac{\sqrt{3}}{2}\frac{\lambda_0}{2\pi\sqrt{\varepsilon_b}}. \tag{3.1.20}$$

We have calculated the nanosphere size that leads to the strongest coupling of the individual QD with the electromagnetic field for several semiconductors, using the parameters collected in Table 3.1, which were taken from the documented literature dedicated to excitons in semiconductors. The results are shown in Figure 3.2.

The exciton radiative decay time in a QD is $\tau_r^{\mathrm{QD}} = \hbar/2\Gamma_0^{\mathrm{QD}}$. The results are shown in Figure 3.3 for eleven semiconductors of technological interest.

Individual QDs with substantial exciton oscillator strength are of particular importance for microcavity physics. Indeed, in laterally confined *pillar* microcavities [5] or in *photonic* cavities [6] (cavities in photonic crystals) a strong coupling of a fully localised photon mode with a single QD exciton may be possible. Eigenmodes of a spherical microcavity containing a single nanosphere at the centre have been found analytically by generalisation of the transfer matrix method for spherical light waves [7]. These systems are very peculiar, because an exciton in a single QD is a fermion in the sense that only one exciton can be created in a given quantum state. This makes a microcavity with a QD a strongly non-linear optical

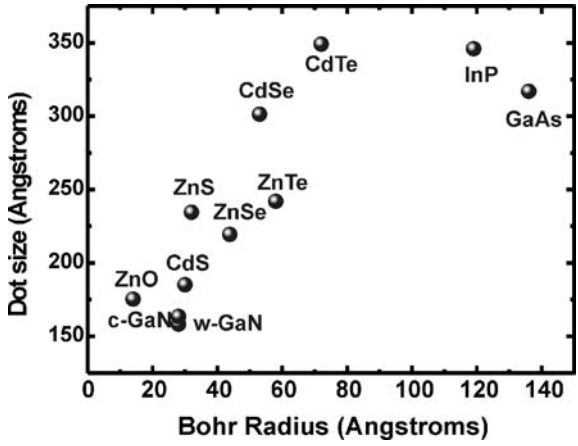

Fig. 3.2. Evolution of the dot radius giving the optimized coupling with the electromagnetic field for some typical direct bandgap II–VI and III–V semiconductors. For the wurtzite semiconductors, we took an average value for the dielectric constant and chose the longitudinal-transverse splitting for the lowest exciton having Γ_5 symmetry.

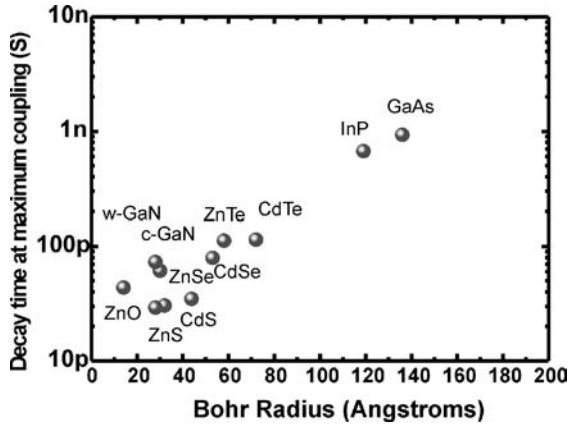

Fig. 3.3. Plot of the radiative decay time computed at maximum coupling for eleven semiconductors.

system. Actually, the microcavity changes its optical properties once *one* photon is absorbed. This is why such a system is widely discussed in relation to the *optical entanglement* problem [8], and possible applications for *quantum cryptography* and *quantum computing*. A discussion of all these intriguing perspectives is beyond the scope of the present book. The reader is advised to consult the reviews available [9].

While a QW itself can be considered as an array of QDs, experimental efforts have been made to realise microcavities containing specially fabricated arrays of dots. Reflection of light from planar microcavities containing many QDs is conveniently described with the use of Eq. (3.1.12). A huge exciton inhomogeneous broadening Δ in most presently available microcavities with QDs prevents observation of the strong-coupling regime.

3.1.1. MULTIPLE SCATTERING OF LIGHT AND WEAK-LOCALIZATION OF EXCITON–POLARITONS

The *multiple scattering of light* by QDs is not included in the model presented here. Obviously, it is a second order process that does not influence strongly the intensity of reflected or scattered light in multiple QD systems. However, in a particular case of resonant *back-scattering* of light, multiple scatterings become important. In this case, the initial and the final in-plane wave vectors of exciton polaritons are different just by sign. That is why, if only elastic scattering is taken into account, the system is subject to time-inversion symmetry. Let us consider a chain of scattering acts during which, an exciton polariton changes its wave vector in the following order:

$$\vec{k}_1 \to \vec{k}_2 \to \vec{k}_3 \to \cdots \to \vec{k}_n \to -\vec{k}_1. \tag{3.1.21}$$

The symmetry of the system to time reversal means that this process has exactly the same probability as the following one

$$\vec{k}_1 \to -\vec{k}_n \to \cdots \to -\vec{k}_3 \to -\vec{k}_2 \to -\vec{k}_1. \tag{3.1.22}$$

Moreover, the phase of light at the end of these two processes must be the same. Thus, polaritons going by these two chaines of scattering acts positively interfere at the end. That is why, a probability of resonant elastic backscattering appears to exceed the scattering probabilities in all other directions. This is a manifestation of so-called *weak-localization* of exciton–polaritons. Theoretically, resonant back-scattering of exciton–polaritons has been described by Savona and Zimmermann [10], and experimentally it has been evidenced by Langbein [11]. A detailed analysis of weak-localization of polaritons in microcavities can be found in a paper by Litinskaia et al. [12].

3.2. Motional Narrowing of Cavity Polaritons

Motional narrowing is the narrowing of a distribution function of a quantum particle propagating in a disordered medium due to averaging of the disorder potential over the size of the wave-function of a particle. In other words, a quantum particle, which is never localised at a given point in space but always occupies some

non-zero volume, has a potential energy that is the average of the potential within this volume. This is why, in a random fluctuation potential, the energy distribution function of a quantum particle is always narrower than the potential distribution function.

Motional narrowing of exciton–polaritons in microcavities was the subject of scientific polemics at the end of the 1990s. The polemics were initiated by an experimental finding of the M. Skolnick group [13]. Measuring the sum of full widths at half minimum (FWHM) for two exciton–polariton resonances in reflection spectra of microcavities as a function of incidence angle, the experimentalists found a minimum of this function at the anticrossing of exciton and cavity modes. This result contradicts what one could expect from a simple model of two coupled oscillators (Section 1.3). Actually, if the dispersion of microcavity polaritons is given by an equation

$$(\omega_0 - \omega - i\gamma)(\omega_c - \omega - i\gamma_c) = V^2, \tag{3.2.1}$$

then the sum of the imaginary parts of the two solutions of this equation is always $-(\gamma + \gamma_c)$, independent of the detuning $\delta \equiv \omega_0 - \omega_c$. This follows from a more general property of any system of coupled harmonic oscillators to keep the sum of eigenfrequencies constant independent of the coupling strength (see Eq. (2.1.15)).

Clearly, Eq. (3.2.1) is no longer valid if, instead of a single free exciton transition, one has an infinite number of resonances distributed in energy. This is what happens in realistic QWs, where in-plane potential fluctuations caused by the QW width and alloy fluctuations induce the so-called *inhomogeneous broadening* of an exciton resonance. An idea has been proposed that exciton–polaritons, having a lighter effective mass than bare excitons, are less sensitive to the disorder potential. Thus, the inhomogeneous broadening of exciton–polariton modes is less than that of a pure exciton state, which is a consequence of the polariton motional narrowing effect. At the anticrossing point this effect is especially strong, since at this point both polaritons are half-exciton half-photon. Hence, an attempt has been made to interpret the experimental data [13] in terms of motional narrowing.

Further analyses [14,15] have shown, however, that experimentally observed narrowing of polariton lines at the anticrossing point is indeed caused by exciton inhomogeneous broadening, but not by the motional narrowing effect. On the other hand, the motional narrowing may manifest itself in resonant Rayleigh scattering or even photoluminescence.

Here, we consider first of all the effect of exciton inhomogeneous broadening on optical spectra of QWs. We then show that the inhomogeneous distribution of the exciton resonance frequency is sufficient to explain the effects observed in Ref. [13]. Finally, we address the issue of motional narrowing and discuss experimental configurations in which this effect can be important.

3.2.1. SINGLE QW CASE

We shall suppose that the in plane wave-vector of any exciton interacting with the incident light is the same as the in-plane wave-vector of light q, while the frequency of exciton resonance ω_0 is distributed with a Gaussian function. Note that this model is a particular case of a microscopic model considering all exciton states as quantum-dot like and assuming no wave-vector conservation. This more general model has been presented in Section 3.1. The present model is adapted for description of reflection or transmission, i.e., experiments that conserve the in-plane component of the wave-vector of light. Note that most scattered light does not contribute to reflection and transmission spectra, while a small part of it can re-obtain the initial value of q after a second, third, etc. scattering act. The main reason why motional narrowing has almost no influence on reflection spectra is that it is an effect which originates from the finite in-plane size of the exciton–polariton wave-function, or, in other words, implies scattering of exciton–polaritons in the plane of the structure. The impact of scattering is, however, negligibly small in reflection and transmission experimental geometries.

As in Section 1.1, we shall operate with the dielectric susceptibility (1.1.6), while also taking into account that the exciton resonance frequency is distributed with some function $f(\nu - \omega_0)$. We assume that in this case the dielectric susceptibility of a QW can be written in the form

$$\tilde{\chi}(\omega) \equiv \int d\nu\, \chi(\omega - \nu) f(\nu - \omega_0). \tag{3.2.2}$$

If f is a Gaussian function, this integral can be obtained analytically:

$$\tilde{\chi}(\omega) \equiv \frac{1}{\sqrt{\pi}\Delta} \int d\nu\, \chi(\omega - \nu) \exp\left[-\left(\frac{\nu - \omega_0}{\Delta}\right)^2\right] = \frac{i\pi^{1/2}\Theta}{\Delta} e^{-z^2} \operatorname{erfc}(-iz), \tag{3.2.3}$$

where

$$\chi(\omega - \omega_0) = \frac{\varepsilon_\infty \omega_{LT} \pi a_B^3 \omega_0^2 / c^2}{\omega_0 - \omega - i\gamma},$$

$$\Theta = \varepsilon_B \omega_{LT} \pi \omega_0^2 a_B^3 / c^2, \qquad z = \frac{\omega - \omega_0 + i\gamma}{\Delta}, \tag{3.2.4}$$

$\operatorname{erfc}(z)$ is the complementary error function, and Δ is a width parameter of the Gaussian distribution that describes exciton inhomogeneous broadening. We assume $\Delta, \gamma > 0$ and consider a normal incidence case for simplicity. Substituting the susceptibility (3.2.2) into Eq. (1.1.12) and carrying out the same transformations as in Section 1.1, we obtain finally the amplitude reflection and transmission

coefficients of a QW in the form:

$$r = \frac{i\alpha\tilde{\chi}}{1 - i\alpha\tilde{\chi}}, \qquad t = 1 + r, \tag{3.2.5}$$

where $\alpha = \Gamma_0/\Theta$ and Γ_0 is the radiative damping rate of the exciton in the case of no inhomogeneous broadening. This yields, using Eq. (3.2.3):

$$r = -\frac{\sqrt{\pi}\Gamma_0 e^{-z^2}\,\mathrm{erfc}(-iz)}{\Delta + \sqrt{\pi}(\Gamma_0 + i(\widetilde{\omega}_0 - \omega_0))e^{-z^2}\,\mathrm{erfc}(-iz)}, \qquad t = 1 + r, \tag{3.2.6}$$

where Γ_0 is the same as in Section 1.1. We shall neglect renormalisation of the exciton resonance frequency due to the polariton effect, since it is much less than Γ_0, and also assume $\widetilde{\omega}_0 - \omega_0 \approx 0$. In the limit of small inhomogeneous broadening, the complementary error function becomes:

$$e^{-z^2}\,\mathrm{erfc}(-iz) \to \frac{i}{\sqrt{\pi}z}, \quad |z| \to \infty, \tag{3.2.7}$$

which allows one to reduce Eq. (3.2.5) to the "homogeneous" formula (1.1.15).

Moreover, Eq. (3.2.6) formally coincides with the expressions for reflection and transmission coefficients obtained from a micromodel considering a QW as an ensemble of QDs (see Section 3.1). Actually, Eqs. (3.1.11), (3.1.12) reduce to Eq. (3.2.5) if one takes the average distance between QDs and the in-plane size of a QD equal to the in-plane Bohr radius of a free exciton in a QW. This confirms the validity of Eq. (3.2.3).

In realistic narrow QWs, the distribution of the exciton resonance frequency may have a more complex non-Gaussian distribution. Quite often it is asymmetric due to the so-called excitonic motional narrowing effect (to be distinguished from the motional narrowing of exciton–polaritons). This effect comes from the blue-shift of the lower-energy wing of the excitonic distribution due to the lateral quantum confinement of localised excitons. In many cases it is convenient to represent the dielectric susceptibility of a QW in the form

$$\begin{aligned}\tilde{\chi}(\omega) &\equiv \frac{\Delta_1 + \Delta_2}{2\sqrt{\pi}\Delta_1\Delta_2}\left[\int_0^\infty d\nu\,\chi(\omega - \nu)\exp\left[-\left(\frac{\nu - \omega_0}{\Delta_1}\right)^2\right]\right. \\ &\qquad \left. + \int_{-\infty}^0 d\nu\,\chi(\omega - \nu)\exp\left[-\left(\frac{\nu - \omega_0}{\Delta_2}\right)^2\right]\right] \\ &= \frac{i\pi^{1/2}\Theta}{2\Delta_1\Delta_2}(\Delta_1 + \Delta_2)e^{-z^2}\,\mathrm{erfc}(-iz),\end{aligned} \tag{3.2.8}$$

with

$$z = \begin{cases} \dfrac{\omega - \omega_0 + i\gamma}{\Delta_1}, & \omega < \omega_0, \\ \dfrac{\omega - \omega_0 + i\gamma}{\Delta_2}, & \omega \geqslant \omega_0. \end{cases}$$

Here Δ_1 and Δ_2 are the inhomogeneous broadenings of the lower- and higher-energy wings of the excitonic distribution. Because of the excitonic motional narrowing effect $\Delta_1 < \Delta_2$. Even with this more complex form of $\tilde{\chi}$, the expressions in Eq. (3.2.4) for the reflection and transmission coefficients of a QW are still valid, while Eq. (3.2.5) can no longer be used.

Exciton inhomogeneous broadening of any shape necessarily modifies the equation for exciton–polariton eigenmodes in a microcavity. Eq. (3.2.1) obtained for the model of two coupled oscillators is no longer valid, and one should use the general formula (1.3.6) instead. For the coupled exciton and photon modes it reduces to

$$r_B(2r + 1)e^{ikL_c} = 1. \tag{3.2.9}$$

Using the same representation for the reflection coefficient of the Bragg mirror as in Section 1.3, and Eq. (3.2.5) for r with $\tilde{\chi}$ given by Eq. (3.2.2), we obtain after transformations analogous to those in Section 1.3:

$$\omega_c - \omega - i\gamma_c = V^2 \int_{-\infty}^{\infty} d\nu \, \frac{f(\nu - \omega_0)}{\nu - \omega - i\gamma}. \tag{3.2.10}$$

In the limit (3.2.7) of a small inhomogeneous broadening, Eq. (3.2.10) reduces to Eq. (3.2.1).

Eq. (3.2.10) has from zero to two complex solutions depending on the shape of the distribution function $f(\nu - \omega_0)$. In the general case, the sum of the imaginary parts of its eigenfrequencies varies as a function of detuning, which is not the case for the pure two coupled oscillator problem.

3.2.2. REFLECTION OF LIGHT FROM MICROCAVITIES

In order to understand the experimentally observed narrowing of polariton resonances near the anticrossing point, let us consider light reflection by a microcavity containing a QW with an inhomogeneously broadened exciton resonance. As before, we shall use the transfer matrix method described in Appendices A and B to calculate the reflectivity of the entire structure. In the transfer matrix for a QW we substitute the reflection and transmission coefficients (3.2.5). Figure 3.4 shows the dependencies of the FWHM of two polariton resonances on detuning $\delta = \omega_0 - \omega_c$, in calculated reflection spectra of a GaAs-based microcavity with an embedded QW, in comparison with experimental data from [13]. One can see that

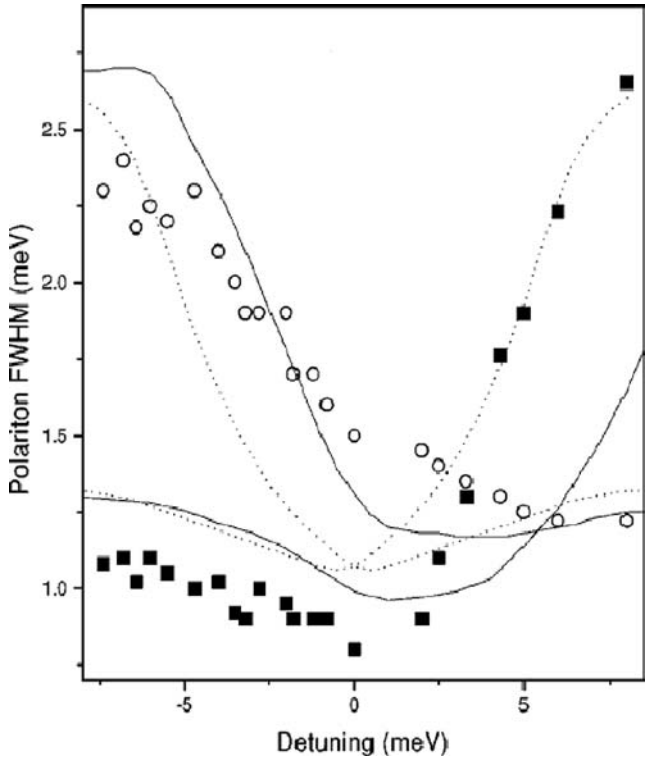

Fig. 3.4. Full width at half minimum of two polariton resonances in reflectivity spectra of a GaAs-based microcavity with an embedded QW [13] as a function of the detuning $\delta = \omega_0 - \omega_c$ (circles correspond to the upper branch, squares correspond to the lower branch) in comparison with a theoretical calculation accounting for or neglecting asymmetry in the exciton frequency distribution (solid and dashed lines, respectively).

the broadenings of the two polariton modes coincide near the zero-detuning point. At this point, both in calculation and experiment, the sum of the two FWHM has a pronounced minimum.

This minimum is a specific feature of an inhomogeneously broadened exciton state coupled to the cavity mode. It can be interpreted in the following way. The coupling to light has a different strength for excitons from the centre and from the tails of an inhomogeneous distribution. As the density of states of excitons has a maximum at $\omega = \omega_0$, these excitons have the highest radiative recombination rate and the strongest coupling to light. This statement is in a perfect agreement with the result of a micromodel (Section 3.1, Eq. (3.1.12)), since the maximum of the density of states corresponds to the minimum of the average distance d between localised excitons. Now, the strong-coupling regime holds only for excitons situ-

ated in the vicinity of ω_0, while the tails remain in the weak-coupling regime. The central part of the excitonic distribution is of course less broadened than the entire distribution. Therefore, the two polariton modes that arise due to its coupling with the cavity photon are also narrower than one would expect for the case of all excitons equally coupled to light. At zero detuning, both polariton modes are far enough from the bare exciton energy, so that the tails of the exciton resonance give no contribution to the FWHM of polariton resonances. On the contrary, for strong negative or positive detunings, one of two polariton states almost coincide in energy with a bare exciton state, so that the line-shape of the corresponding spectral resonance is necessarily affected by the tails of the excitonic distribution.

Note that this interpretation does not involve any motional narrowing. On the other hand, specific effects of motional narrowing play a role in resonant Rayleigh scattering of the cavity polaritons, and may also provide narrowing of the photoluminescence lines. Only wave-vector conserving optical spectroscopies such as reflection and transmission are not sensitive to the motional narrowing.

Another remark concerns the asymmetric behaviour of the broadenings of the two polariton peaks in Figure 3.4. This comes from the asymmetry of the excitonic distribution that is given by the difference between Δ_1 and Δ_2. It is a manifestation of the *exciton* motional narrowing that we have described above. Actually, the lower polariton branch is the result of mixing between the photon mode and the lower part of the excitonic distribution, which is sharper than the upper part. This is why the lower branch has a narrower line-width at the anticrossing condition.

3.3. Photoluminescence and Resonant Rayleigh Scattering from Microcavities (Linear Regime)

Emission of light in a microcavity in the strong-coupling regime is essentially different from light emission by conventional semiconductor structures. Photoluminescence (PL) in conventional QWs is usually referred to as incoherent spectroscopy. Actually, the standard optical set-up used to detect the PL spectra assumes non-resonant optical pumping of the structure (i.e., pumping at some frequency far above the exciton resonance). Optically excited electron–hole pairs relax in energy and form excitons, which in turn relax until the lowest energy states that are localised states. The in-plane localisation in QWs takes place because of QW width and alloy fluctuations, as discussed in Section 3.1. During their energy relaxation, excitons lose the memory of their initial phase, and emit light with some random phases. Obviously, excitons localised on different potential islands know nothing about each other if their wave-functions are not overlapping. Thus, the resulting PL signal is incoherent. To find its intensity I_{PL}, one should sum the intensities of light waves emitted by all individual excitons. Using Eq. (3.1.7) one

finds

$$I_{\rm PL} = |\vec{E}_0| \sum_{m=1}^{N} \frac{(\Gamma_0^{\rm QD})^2}{(\omega_m - \omega)^2 + \gamma^2} \left[\frac{1}{1 - \sum_{n=1}^{N} \Theta_{nm}} \right]^2 . \qquad (3.3.1)$$

This function has a weak directional dependence via $\Gamma_0^{\rm QD}$.

The situation in a microcavity is drastically different. If the coupling constant V exceeds the exciton inhomogeneous broadening, the localised exciton states remain optically coupled, so that the PL spectra are dominated by exciton–polaritons with an infinite (or at least large compared to the scale of potential fluctuations) in-plane size. This means that all individual light waves emitted by localised excitons interfere, and that the intensity of the signal emitted by a QW embedded in a microcavity is given by

$$I_{\rm PL}(\vec{k}_s) = \left| \vec{E}_0 \sum_{m=1}^{N} \frac{i\Gamma_0^{\rm QD}}{\omega_m - \omega - i\gamma} \frac{1}{1 - \sum_{n=1}^{N} \Theta_{nm}} \exp(i\vec{k}_s . \vec{R}_m) \right|^2 . \qquad (3.3.2)$$

Thus, PL from microcavities in the strong-coupling regime has similar spectral properties to Rayleigh scattering, and the most essential of these is that it preserves coherence, at least partly. Polariton relaxation in a microcavity and its impact on the PL spectra will be discussed in detail in the second part of the book. Here we assume that the light wave emitted by a QW has some amplitude and some phase (coherent emission), and we shall study the effect of photonic confinement in a microcavity on this emission. Note that Eq. (3.3.2) only describes light emitted inside a microcavity. Before travelling outside, this light makes many round trips in the cavity, is reflected many times at different interfaces, interferes with itself, and finally escapes from the structure; as a result it has peculiar spectral properties imposed by the geometry of the microcavity, and detuning between the exciton resonance and the cavity mode. In order to calculate PL spectra of microcavities taking into account all these effects we shall use the transfer matrix method.

Let us consider a QW embedded in the center of microcavity as an emitter of light. We neglect the spatial distribution of the emitter, which is the usual assumption in the non-local model. We take into account the polariton effect within the QW, i.e., the possibility of emission and absorption of a photon by the same exciton. Using the transfer matrix method for a given in-plane wave-vector of light q, we calculate the reflection and transmission coefficients of the right part of the structure (between $z = z_{\rm QW}$ and $z = d$, where $z_{\rm QW}$ is the coordinate of the QW, and d is the total length of the microcavity structure), labeled r_r and t_r, respectively, as well as those of the left part of the structure (between $z = z_{\rm QW}$ to $z = 0$), labeled r_l and t_l, respectively.

Formally, we consider our structure as a Fabry–Perot resonator with an infinitely thin central layer, where the emitter is placed. Let us describe first the prop-

agation of a light-wave emitted by the QW in the positive z-direction. Taking into account all multiple reflections in the resonator, we can write the electric field just to the right of the source as:

$$\widetilde{E}_{+}^{+}(\omega, z_{\mathrm{QW}}) = \frac{1}{1 - r_r r_l}, \tag{3.3.3}$$

and the field just to the left of the emitter as:

$$\widetilde{E}_{+}^{-}(\omega, z_{\mathrm{QW}}) = \frac{r_r}{1 - r_r r_l}. \tag{3.3.4}$$

We calculate the electric field at the end and at the beginning of the entire structure as:

$$\widetilde{E}_{+}^{+}(\omega, d) = \frac{t_r}{1 - r_r r_l}, \tag{3.3.5}$$

$$\widetilde{E}_{+}^{-}(\omega, 0) = \frac{r_r t_l}{1 - r_r r_l}, \tag{3.3.6}$$

respectively. In the same way we calculate the amplitudes $\widetilde{E}_{-}^{+}(\omega, z_{\mathrm{QW}})$, $\widetilde{E}_{-}^{-}(\omega, z_{\mathrm{QW}})$, $\widetilde{E}_{-}^{-}(\omega, 0)$, $\widetilde{E}_{-}^{+}(\omega, d)$, in the case of a pulse emitted from $z = z_{\mathrm{QW}}$ in the negative direction. The lower indices "+" or "−" mean that the wave is emitted by a QW in the positive or negative direction, respectively. The upper indices "+" and "−" mean that these are amplitudes of waves propagating in positive and negative directions, respectively.

The field just to the left of the emitter is:

$$\widetilde{E}_{-}^{-}(\omega, z_{\mathrm{QW}}) = \frac{1}{1 - r_r r_l}, \tag{3.3.7}$$

and the field just to the right of the emitter is:

$$\widetilde{E}_{-}^{+}(\omega, z_{\mathrm{QW}}) = \frac{r_l}{1 - r_r r_l}. \tag{3.3.8}$$

We calculate the electric field at the end and at the beginning of the entire structure as:

$$\widetilde{E}_{-}^{-}(\omega, 0) = \frac{t_l}{1 - r_r r_l}, \tag{3.3.9}$$

$$\widetilde{E}_{-}^{+}(\omega, d) = \frac{r_l t_r}{1 - r_r r_l}, \tag{3.3.10}$$

respectively.

The amplitude of a light-pulse with a spectral function $A_s(z_Q, \omega)$, emitted by a QW in positive and negative directions simultaneously at the upper surface of the structure ($z = 0$), is:

$$\widetilde{E}_A(\omega, 0) = A_s(z_{\mathrm{QW}}, \omega)\big(\widetilde{E}_{+}^{-}(\omega, 0) + \widetilde{E}_{-}^{-}(\omega, 0)\big). \tag{3.3.11}$$

The time-resolved photoluminescence signal is given by:

$$I_{\mathrm{PL}}(t) = \left| \frac{1}{2\pi} \int_{-\infty}^{+\infty} E_A(\omega, 0) \exp(-i\omega t)\, d\omega \right|^2. \tag{3.3.12}$$

This model includes all coherent reflection-transmission processes in the cavity for the light emitted by a QW. In order to take into account within this local model a non-local effect of secondary absorption (i.e., absorption of light in the same QW from which it has been emitted), one can include formally a "half-well" (i.e., a QW having an exciton resonance with radiative damping $\Gamma_0' = \Gamma_0/2$) in the left and right parts of our model structure, immediately before and after the point-like emitter, respectively. This trick allows us to correctly take into account absorption in a QW of light reflected by Bragg mirrors.

The model can be easily extended to microcavities containing multiple QWs. In this case, the amplitude of light emitted by each QW should be calculated independently following the scheme described above. Then, if PL from different QWs is not correlated (the weak-coupling regime), one should sum the intensities of light waves emitted by them to find the overall intensity of photoluminescence:

$$I_{nc}^{\mathrm{ALL}} = \sum_j I_{\mathrm{PL}}^j, \tag{3.3.13}$$

where j is the index of the QW.

In the strong-coupling regime all QWs within the cavity emit a coherent light. The overall intensity is dependent in this case on the interference of light waves emitted by different QWs. It can be found as:

$$I_c^{\mathrm{ALL}}(\omega) = \left| \sum_j E_A^j(\omega, 0) \right|^2, \tag{3.3.14}$$

where E_A^j is the complex amplitude of light emitted by jth QW. Note that in this case the spectral functions of the emitted light A_s contain in general phase factors for each QW, taking into account the phase of the polariton mode of each QW. Thus, the picture becomes rather complicated. However, it simplifies if all QWs are situated at the antinodes of the electric field of the bare cavity photon mode. In this case, all QWs emit light of the same amplitude and phase, and thus the functions A_S are the same for all wells.

Figure 3.5 shows a series of PL spectra measured from a typical GaAs-based microcavity with QWs at the centre for different values of the detuning of the exciton and photon modes [16]. Both polariton modes are very well seen in the spectra. The PL emission peak of the lower mode is stronger than one of the upper mode in the negative detuning case while the situation is inversed in the case of positive detuning. While positions of PL emission peaks are well described by a simple linear model presented above, to describe correctly the intensity of

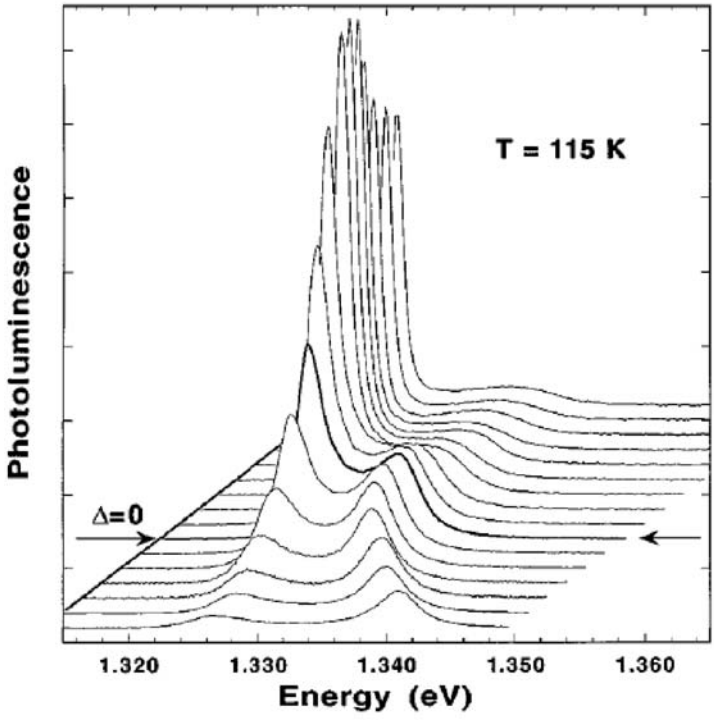

Fig. 3.5. Experimental photoluminescence spectra of a GaAs-based microcavity containing QWs (Ref. [16]) measured for different detunings between exciton and photon modes. The detuning changes between $\delta = -10$ meV and $\delta = 12$ meV.

peaks one should account for the complex dynamics of exciton–polariton energy relaxation (see Chapter 6).

Within the approach described here, the difference between PL and resonant Rayleigh scattering (RRS) is contained in the shape of the complex amplitude of the emitted light A_S. In the case of RRS it is given by Eq. (3.1.7), while for the PL in any case the first term in the right part of (3.1.7) describing the transmitted light wave must be omitted. Then, the spectral function $A_s(z_Q, \omega)$ is different, in general, for PL and RRS. In both cases it strongly depends on the regime of optical coupling in a system of consideration.

Figure 3.6 shows directional images of the scattered intensity from a lower-polariton branch of a GaAs-microcavity resonantly excited by a laser pulse at $q = 1.85\ \mu\text{m}^{-1}$ [17]. The time on the figure corresponds to the delay between the excitation pulse and the detection. One can see that the most part of light escapes from the structure keeping the same absolute value of q, and therefore

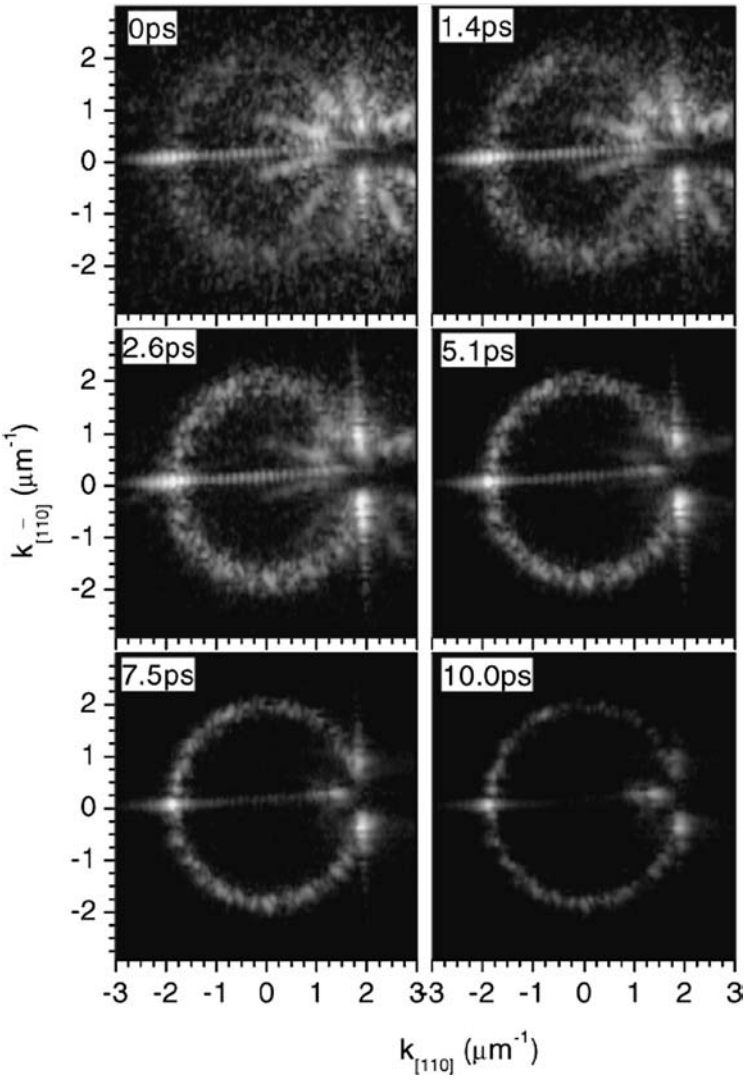

Fig. 3.6. Experimentally measured intensity of scattered light as a function of angle for a GaAs-based microcavity whose lower-polariton branch was resonantly excited by a laser pulse having an in-plane wave-vector $q = 1.85\ \mu\text{m}^{-1}$ [17].

keeping the same energy as the exciting light. Only direction of q changes, which is a signature of the elastic Rayleigh scattering. Due to elastic scattering, exciton–polaritons are distributed along so-called *elastic circle* in the reciprocal space (i.e.,

a circle having q as a radius). The straight lines on the figure come from the scattering by imperfections of the Bragg mirrors and are not related to the exciton–polariton dynamics. Note also a strongly preferential back-scattering direction.

3.4. Time-Resolved Reflection of Light from Quantum Wells and Microcavities

The radiative properties of excitons and the strength of their coupling with light have a very important impact on the time-resolved reflection (transmission, Rayleigh scattering) spectra of quantum structures. Here we consider the time-resolved reflection of a single QW, MQWs and microcavities, paying special attention to the exciton inhomogeneous broadening effect.

First, we focus on the simplest case of a free single exciton resonance in a single QW, and then we address the inhomogeneous broadening effect on time-resolved spectra of QWs and microcavities.

3.4.1. FREE HOMOGENEOUSLY BROADENED EXCITON RESONANCE IN A QW

For a single QW surrounded by an infinite medium with the same background refractive index as the QW, the time-resolved reflection is given by:

$$r(t) = \frac{1}{2\pi} \int_{-\infty}^{\infty} d\omega\, r(\omega) g(\omega) e^{-i\omega t}, \tag{3.4.1}$$

where $r(\omega)$ is the frequency-dependent amplitude reflection coefficient of the QW and $g(\omega)$ is a spectral function of the incident pulse. In the following we shall assume $g(\omega) \equiv 1$, which corresponds to a delta-function-like pulse in the time space. If there is no inhomogeneous broadening, $r(\omega)$ at the exciton resonance is given by (see Section 1.1):

$$r(\omega) = \frac{i\Gamma_0}{\omega_0 - \omega - i(\Gamma_0 + \gamma)}. \tag{3.4.2}$$

Using the pole theorem, one can easily carry out the integration (3.4.1) in this case. The result is

$$r(t) = -\Gamma_0 e^{-i\omega_0 t} e^{-(\Gamma_0+\gamma)t}. \tag{3.4.3}$$

One can see that the reflected intensity $R \equiv |r|^2$ decays with an exponent $t = 1/2(\Gamma_0 + \gamma)$. If $\gamma \to 0$ we obtain the radiative decay time of a free exciton in a QW:

$$\tau = \frac{1}{2\Gamma_0}. \tag{3.4.4}$$

In a more complex system, such as a microcavity or a MQW structure, there are two or more exciton–polariton modes. Each of these is characterised by a complex eigenfrequency

$$\omega_j = \omega_{0j} + i\gamma_j. \tag{3.4.5}$$

The radiative lifetime of the corresponding polariton state is

$$\tau = \frac{1}{2\gamma_j}. \tag{3.4.6}$$

3.4.2. INHOMOGENEOUS BROADENING EFFECT ON TIME-RESOLVED SPECTRA OF QWS

Let us now consider the effect of exciton inhomogeneous broadening on time-resolved reflection of light from a single QW. In this subsection we will follow Ref. [18]. To calculate this we have to substitute into Eq. (3.4.1) the reflection coefficient (3.2.5).

The integral (3.4.1) cannot be found analytically, in general. However, if we approximate the reflection coefficient by a simpler function, the time-resolved reflection of a QW can be easily analysed. Let us assume that the reflected signal is a superposition of plane waves, whose amplitudes are proportional to $\exp(-((\omega - \omega_0)/\Delta)^2)$. Here we neglect the possible asymmetry of the excitonic distribution and refer to the simplified form of the reflection coefficient (3.2.6). This corresponds to the Gaussian broadening of the exciton resonance. As a zeroth-order approximation, assume that all these plane waves have the same phase. Bearing in mind that

$$e^{i(\omega_0+\nu)t} + e^{i(\omega_0-\nu)t} = 2e^{i\omega_0 t}\cos\nu t, \tag{3.4.7}$$

and choosing $\nu = \omega - \omega_0$, we easily find the time-resolved reflection as

$$r(t) \propto \int_{-\infty}^{\infty} d\nu\, e^{-\nu^2/\Delta^2}\cos\nu t = \sqrt{\pi}\,\Delta\exp\left(\frac{-\Delta^2 t^2}{4}\right), \tag{3.4.8}$$

which describes a monotonous Gaussian decay of the reflected signal. It shows that the reflected intensity decays by a factor of e at

$$t = \frac{\sqrt{2}}{\Delta}. \tag{3.4.9}$$

More complex behaviour of the time-resolved reflection can be obtained if the dependence of the phase of the reflection coefficient on frequency is taken into account. The phase of $r(\omega)$ changes by π while crossing the exciton resonance [18]. If the disorder is strong enough, this dependence can be approximated by:

$$\varphi \approx \operatorname{arctg}\frac{\nu}{\Delta}. \tag{3.4.10}$$

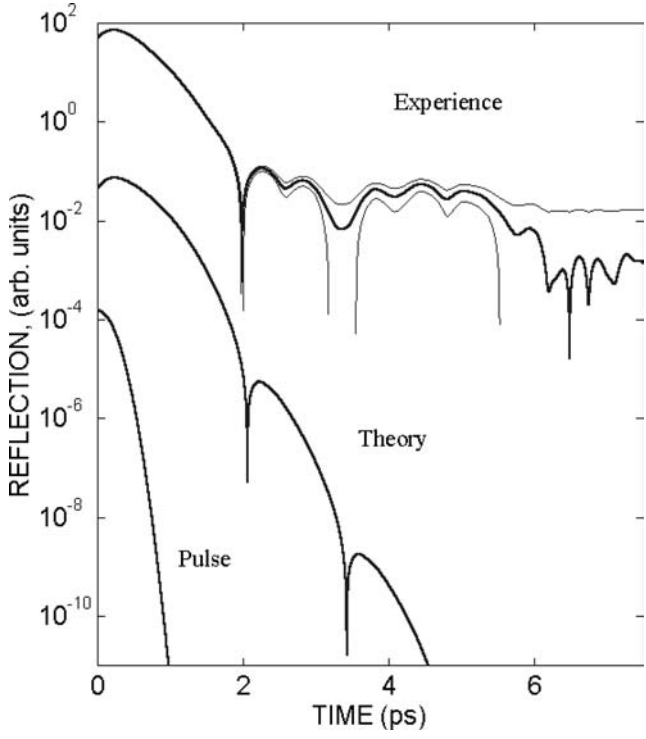

Fig. 3.7. Time-resolved reflectivities of a single InGaAs/GaAs QW obtained with use of Eq. (3.2.7) from theoretical and experimental complex functions. An incident pulse $g(\omega)$ with a temporary length of $\tau = 1.5$ ps has been assumed. The experimental one is sandwiched by two error lines which assume a relative experimental noise of 1.5×10^{-3}. For clarity, the theoretical curve and the pulse are shifted of 10^3 and 10^6 with respect to the experimental one.

In this case

$$r(t) \propto \Delta^{-1} \int_{-\infty}^{\infty} d\nu\, e^{-\nu^2/\Delta^2} (\Delta \cos \nu t - \nu \sin \nu t)$$
$$= \sqrt{\pi}\Delta \exp\left(-\frac{\Delta^2 t^2}{4}\right)\left[1 - \frac{t\Delta}{2}\right]. \tag{3.4.11}$$

Thus, the reflected signal becomes non-monotonic. It has a minimum (zero) at $t = 2/\Delta$. An indirect experimental confirmation of predicted theoretically oscillations in time-resolved reflection spectra of single QWs has been obtained by numerical Fourier transformation of the complex reflection coefficient $r(\omega)$, extracted from reflectivity and absorption spectra of a single $In_{0.06}Ga_{0.94}As/GaAs$ QW of width 172 Å, as shown in Figure 3.7 [19]. The oscillations are originated

from the interference between low-energy and high-energy tails of the inhomogeneous exciton distribution.

3.4.3. VERTICAL MOTIONAL NARROWING IN TIME-RESOLVED SPECTRA OF MULTIPLE QWS

Time-resolved reflection of a multiple QW structure or a microcavity is more complex. Note that to calculate $r(t)$ for any complex multilayer structure one can always use Eq. (3.4.1), where the frequency-resolved coefficient $r(\omega)$ can be found by a standard transfer matrix technique described in Appendices A, B and Ch. 1. Each layer containing a QW is described by a matrix (A.14) or (B.10) dependent on the basis we use, where reflection and transmission coefficients of a QW are given by Eq. (3.2.5), in general. Exciton inhomogeneous broadening can be easily accounted for in this formalism by choosing a proper form of the dielectric susceptibility $\tilde{\chi}$ to be substituted into Eq. (3.2.5).

Figure 3.8 shows calculated in this way time-resolved reflection spectra from periodic structures containing 1, 10, 50, and 100 identical QWs having an inhomogeneously broadened exciton resonance. The period of 70 nm has been taken for all the structures. Excitonic parameters assumed in this calculation are typical for $GaN/Al_xGa_{1-x}N$ QWs ($\hbar\omega_0 = 3.6$ eV, $\hbar\Gamma_0 = 0.4$ meV, $\hbar\gamma = 0.1$ meV [20]). The inhomogeneous broadening parameter $\hbar\Delta$ has been taken to be 5 meV for all the structures (curves (a)–(d)). For comparison, a time-resolved reflection spectrum of a single QW calculated with $\hbar\Delta = 0$ is shown by the curve (e). Comparing the curves (a) and (e), one can see that the exciton inhomogeneous broadening induces a dramatic decrease of the decay time of the signal. This reflects appearance of additional channels of energy relaxation for excitons as the disorder increases in the structure. Note the strong decrease of the exciton decay time with increase of the number of QWs in the structure (curves (a)–(d)). This is a manifestation of the *vertical motional narrowing* effect which consists in reduction of the disorder effect on radiative properties of excitons in MQWs because of coupling of QW excitons via light. It can be qualitatively described in the following way. An exciton–polariton mode in MQWs is extended over the entire structure. That is why the polariton averages disorder potential fluctuations across the structure, and the resulting broadening of the polariton resonance decreases with increase of the number of wells within the structure. One can see that in the limit of a huge number of QWs the decay time of time-resolved reflection in a MQW structure approaches the single QW exciton decay time *in the absence* of inhomogeneous broadening.

The oscillations seen in time-resolved reflection spectra of MQW structures mostly come from the interference of different polariton eigenmodes thus representing a kind of quantum beats between discrete polariton states. In the limit of strong inhomogeneous broadening ($\Delta \gg N\Gamma_0$, where N is the number of QWs

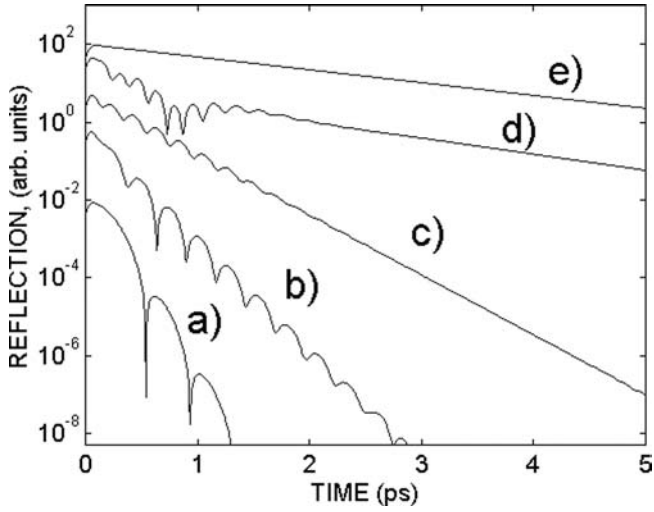

Fig. 3.8. Calculated time-resolved reflection of GaN/AlGaN quantum well structures: (a) single QW with $\hbar\Delta = 5$ meV; (b) MQW, $N = 10$, $\hbar\Delta = 5$ meV; (c) MQW, $N = 50$, $\hbar\Delta = 5$ meV; (d) MQW, $N = 100$, $\hbar\Delta = 5$ meV; (e) single QW with $\hbar\Delta = 0$ meV.

in the structure), one can observe the oscillations caused by exciton inhomogeneous distribution which have been discussed in Section 3.4.2. In the opposite limit, $\Delta \ll N\Gamma_0$ a MQW structure can be conveniently described as a layer of bulk semiconductor having some effective dielectric function containing an exciton resonance [20]. Oscillations in $r(t)$ come in this case from the interference of upper and lower branches of the bulk exciton–polaritons.

It is important to note that time-resolved transmission spectra of MQWs or thin layers of bulk semiconductors can be rather different from time-resolved reflection spectra. They exhibit normally the same decay time, but oscillations may have a different period than in reflection. This is because of a finite time needed for a light to cross the structure in transmission geometry. In bulk layers or in MQWs with a huge N the period of oscillations in transmission increases as a square root of time while in reflection it does not vary with time [21].

3.4.4. INHOMOGENEOUS BROADENING EFFECT ON TIME-RESOLVED REFLECTION SPECTRA OF MICROCAVITIES

Time-resolved coherent spectroscopies of microcavities allow to detect so-called Rabi-oscillations, i.e., oscillations coming from beats between two polariton branches whose period T is related to the vacuum-field Rabi-splitting Ω as

$$T = 2\pi / \Omega. \tag{3.4.12}$$

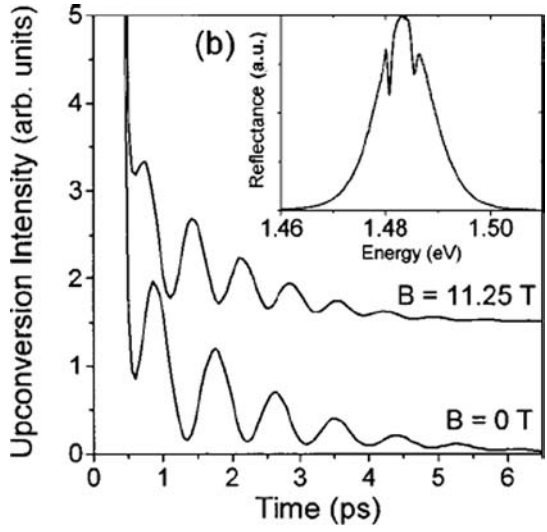

Fig. 3.9. Time-resolved reflection from a microcavity at magnetic field $B = 0$ (lower curve) and $B = 11.25$ T (upper curve, vertical offset by 1.5). The inset shows the time-averaged reflected pulse spectrum at $B = 0$ [19].

Exciton inhomogeneous broadening influences Ω, that is why it affects the period of Rabi-oscillations. In the absence of inhomogeneous broadening,

$$\Omega = 2\sqrt{V^2 - \gamma\gamma_c}, \tag{3.4.13}$$

where V is the exciton-cavity mode coupling constant (see Eq. (1.3.9)), γ and γ_c are broadenings of the exciton resonance and the cavity mode, respectively.

Figure 3.9 shows Rabi-oscillations in time-resolved reflection from a GaAs-based microcavity containing InGaAs QWs subjected to an external magnetic field normal to the cavity plane [22]. The period of oscillations decreases with increase of the magnetic field reflecting magnetic field induced enhancement of the Rabi-splitting, as described in Section 2.5.

In the presence of inhomogeneous broadening, Ω is given by the splitting between real parts of two solutions of Eq. (3.2.10) for eigenfrequencies of exciton–polaritons with $\omega_0 = \omega_c$:

$$\omega_0 - \omega - i\gamma_c = V^2 \int_{-\infty}^{\infty} d\nu \, \frac{f(\nu - \omega_0)}{\nu - \omega - i\gamma}. \tag{3.4.14}$$

In zeroth order approximation, one can assume $\gamma \to \gamma + \Delta$ in Eq. (3.4.13) where Δ is a parameter of inhomogeneous broadening. Clearly, in this case the period of Rabi-oscillations increases with increase of the broadening. If $\Delta \gg V$, the

weak coupling regime is hold, and the reflectivity of a microcavity is given by a single QW reflectivity filtered by a cavity mode. In this case, oscillations typical for a single QW having an inhomogeneously broadened exciton resonance can appear in time-resolved spectra. Their period decreases with increase of Δ (see Eq. (3.4.11)). These oscillations are much less pronounced than Rabi-oscillations.

References

1. E. L. Ivchenko, A. V. Kavokin, Light reflection from quantum well, quantum wire and quantum dot structures, *Sov. Phys. Solid State* 34, 1815 (1992).
2. A. V. Kavokin, G. Malpuech, W. Langbein, Theory of propagation and scattering of exciton–polaritons in quantum wells, *Solid State Commun.* 120, 259 (2001).
3. B. Gil, A. V. Kavokin, Giant exciton–light coupling in ZnO quantum dots, *Appl. Phys. Lett.* 81, 748 (2002).
4. E. I. Rashba, G. E. Gurgenishvili, *Sov. Phys. Solid State* 4, 759 (1962).
5. G. Panzarini, L. C. Andreani, Quantum theory of exciton polaritons in cylindrical semiconductor microcavities, *Phys. Rev. B* 60, 16 799 (1999).
6. C. M. Soukoulis, Ed., "Photonic Band Gap Materials". Kluwer, Dordrecht, 1996.
7. M. A. Kaliteevski, S. Brand, R. Abram, V. V. Nikolaev, M. V. Maximov, C. M. Sotomayor-Torres, A. V. Kavokin, Electromagnetic theory of the coupling of zero-dimensional exciton and photon states: A quantum dot in a spherical microcavity, *Phys. Rev. B* 64, 115305 (2001).
8. G. Panzarini, U. Hohenester, E. Molinari, Self-induced transparency in semiconductor quantum dots, *Phys. Rev. B* 65, 165322 (2002).
9. A. Steane, *Rep. Prog. Phys.* 61, 117 (1998).
10. V. Savona, E. Runge, R. Zimmermann, Enhanced resonant backscattering of light from quantum-well excitons, *Phys. Rev. B* 62, R4805 (2000).
11. W. Langbein, E. Runge, V. Savona, R. Zimmermann, Enhanced resonant backscattering of excitons in disordered quantum wells, *Phys. Rev. Lett.* 89, 157401 (2002).
12. M. Litinskaia, G. C. La Rocca, V. M. Agranovich, Inhomogeneous broadening of polaritons in high-quality microcavities and weak localization, *Phys. Rev. B* 64, 165316 (2001).
13. D. M. Whittaker, P. Kinsler, T. A. Fisher, M. S. Skolnick, A. Armitage, A. M. Afshar, M. D. Sturge, J. S. Roberts, Motional narrowing in semiconductor microcavities, *Phys. Rev. Lett.* 77, 4792 (1996).
14. C. Ell, J. Prineas, T. R. Nelson, Jr., S. Park, H. M. Gibbs, G. Khitrova, S. W. Koch, R. Houdré, Influence of structural disorder and light coupling on the excitonic response of semiconductor microcavities, *Phys. Rev. Lett.* 80, 4795 (1998).
15. A. V. Kavokin, Motional narrowing of inhomogeneously broadened excitons in a semiconductor microcavity: Semiclassical treatment, *Phys. Rev. B* 57, 3757 (1998).
16. R. P. Stanley, R. Houdré, C. Weisbuch, U. Oesterle, M. Ilegems, Cavity-polariton photoluminescence in semiconductor microcavities: Experimental evidence, *Phys. Rev. B* 53, 10 995 (1996).
17. W. Langbein, J. M. Hvam, Elastic scattering dynamics of cavity polaritons: Evidence for time-energy uncertainty and polariton localization, *Phys. Rev. Lett.* 48, 47 401 (2002).
18. L. C. Andreani, G. Panzarini, A. V. Kavokin, M. R. Vladimirova, Effect of inhomogeneous broadening on optical properties of excitons in quantum wells, *Phys. Rev. B* 57, 4670 (1998).
19. G. Malpuech, A. Kavokin, J. Leymarie, P. Disseix, A. Vasson, Optical spectroscopy study of the phase of the reflection coefficient of a single quantum well in the exciton resonance region, *Phys. Rev. B* 60, 13 298 (1999).

20. G. Malpuech, A. Kavokin, Vertical motional narrowing of exciton–polaritons in GaN based multiple quantum wells, *Appl. Phys. Lett.* 76, 3049 (2000).
21. A. Kavokin, G. Malpuech, G. Panzarini, Propagation of excitons–polariton in inhomogeneous semiconductor films, *Phys. Rev. B* 60, 16 788 (1999).
22. J. D. Berger, O. Lyngnes, H. M. Gibbs, G. Khitrova, T. R. Nelson, E. K. Lindmark, A. V. Kavokin, M. A. Kaliteevski, V. V. Zapasskii, Magnetic field enhancement of the exciton–polariton splitting in a semiconductor quantum well microcavity: The strong coupling threshold, *Phys. Rev. B* 54, 1975 (1996).

Part II

Non-Linear Properties of Microcavities

This page intentionally left blank

Chapter 4

Photoluminescence of Strongly Coupled Microcavities

4.1. Qualitative Features 120
4.1.1. First PL Experiments Performed on Microcavities 120
4.1.2. Relaxation of Cavity Polaritons: Qualitative Features 120
4.2. Semi-Classical Treatment of the Relaxation Kinetics of Cavity Polaritons 124
4.2.1. The Semi-Classical Boltzmann Equation 124
4.2.2. Polariton–Structural Disorder Interaction 125
4.2.3. Polariton Decay 125
4.2.4. Polariton–Phonon Interaction 126
4.2.5. Polariton–Electron Interaction 129
4.2.6. Polariton–Polariton Interaction 131
4.2.7. Numerical Solution of Boltzmann Equations, Practical Aspects 131
4.3. Relaxation Kinetics of Cavity Polariton 133
4.3.1. Quantitative Analysis of Polariton Relaxation Kinetics 133
4.3.2. Presentation of Recent PL Results, Comparison with Theory 138
4.4. Conclusions 143
References 144

Photoluminescence (PL) experiments have been in recent decades the most widely used optical spectroscopy technique to characterise semiconductors. It is by definition a non-linear technique, since the semiconductor emission is recorded in a frequency range different from the exciting laser frequency. The physical processes involved can be summarised as follows:

(1) A semiconductor sample is excited by a laser which generates coherent electron–hole pairs. Because of the strong carrier–carrier interaction, these electron–hole pairs lose coherence and are redistributed in reciprocal space. They self-thermalise at their own temperature on a time scale of a few femtoseconds. This initial carrier temperature can be of the order of thousands of Kelvin.
(2) These carriers, referred in the literature as hot carriers, exchange their kinetic energy with the lattice, namely with optical phonons on a subpicosecond time-scale. They rapidly thermalise at a temperature smaller than the creation energy of optical phonons (typically a few hundreds of Kelvin). During this relaxation process, carriers may or may not form excitons depending on their density and the lattice temperature.
(3) Excitons or carriers relax along their dispersion branch by interacting with acoustic phonons. The time scale to reach the lattice temperature is of the

order of hundreds of picoseconds. Carriers which reach the central part of the reciprocal space can emit light, which gives information on the electronic states of the structure.

All these characteristic steps have been carefully described theoretically, and are still the subject of intense research activity [1]. With the exception of the initial relaxation stage, where the correlations induced by the laser excitation still play a role, the main hypothesis assumed to describe these phenomena is that the carrier gas can be characterised by a temperature because of the strong carrier–carrier interaction.

In microcavities, the two first relaxation steps can be described in the framework of the general picture presented above. The third step is, however, much more original. Usually, in semiconductors the emission of light comes from localised states that are red-shifted in energy with respect to absorption states, namely states where the density of states is a maximum. This energy shift, mainly due to structural imperfections, is the well-known Stokes shift. In a QW the absorption line-width and the Stokes shift are linked, and are both due to exciton inhomogeneous broadening. This means that the light is emitted once via spontaneous emission by localized carriers and is never reabsorbed. This picture is not valid in microcavities. The light emitted, even far below the QW absorption edge, is reflected by the mirrors and is reabsorbed by a free exciton state with a large probability. The criterion is that the Stokes shift should be smaller than the half Rabi splitting, which is always fulfilled in a strongly-coupled microcavity. The light emitted by microcavities in PL experiments does not come from pure electronic states, but from polariton modes. This statement is clearly supported by the first PL experiments performed on microcavities [2], where the authors have deduced the in-plane polariton dispersion, recording angle-resolved PL emission. Therefore, the correct theoretical way to describe microcavity PL is to consider relaxation of particles along the lower polariton branch (LPB). This relaxation process is extremely original and constitutes a large part of the beauty of polariton physics, because of the distortion of the central zone of the dispersion relation induced by the strong light–matter coupling. As one can see in Figure 4.1, the central zone of the polariton dispersion exhibits a deep and sharp minimum. In principle, polaritons should easily accumulate in this “polariton trap”. This accumulation should result in a wide range of temperature and densities to a Bose condensation of polaritons, accompanied by a laser-like emission of light [3]. However, it is hard for polaritons to drop into the trap by resonant exciton–exciton or exciton–phonon scattering. The photon fraction of polaritons is very large in the central zone of the dispersion curve, and consequently polariton life-time is quite short. That is why the polariton trap is often less populated than expected from an equilibrium situation. This kinetic limitation of polariton relaxation has been called the “bottleneck effect” [4]. Most PL experiments performed on microcavities and their associated theoretical description have concerned the study of the

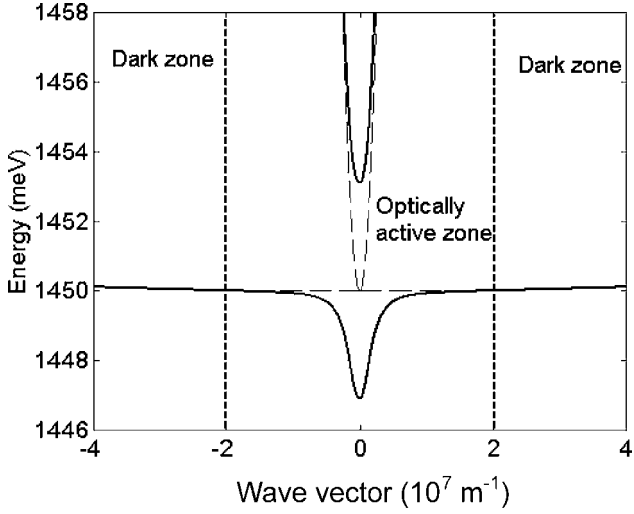

Fig. 4.1. Bare exciton and bare cavity photon dispersion (dashed line). Polariton dispersion (solid line). In the dark zone, excitons wave vector is larger than the light wave vector in the media.

bottleneck effect and the possibilities to overcome it in order to achieve polariton Bose condensation in the trap, as will be discussed later.

Our objective in this chapter is to emphasise the specifics of microcavity PL rather than general features of semiconductor PL, which have already been widely discussed in the literature [1]. These specifics are:

- Light is emitted from polariton states and not from pure electronic (or excitonic) states.
- The polariton distribution function is mostly non-equilibrium.
- Collective effects, linked with the bosonic character of polaritons, can take place.

This last aspect is extremely rich from a fundamental and application point of view. It will be addressed specifically in Chapters 5 and 6.

In Section 4.1 we present qualitatively the main exciton relaxation processes and discuss their relative efficiencies. In Section 4.2 we present the semi-classical Boltzmann equation allowing one to describe polariton relaxation. Scattering rates associated with the main relaxation processes are calculated. A practical way to numerically solve these equations is presented. In Section 4.3 we present numerical and experimental results. Finally we remind that a simple linear model of the PL from microcavities has been addressed in Section 3.3.

4.1. Qualitative Features

4.1.1. FIRST PL EXPERIMENTS PERFORMED ON MICROCAVITIES

One of the first experimental papers that reported on PL of microcavities in the strong-coupling regime was entitled "*Measurements of cavity-polariton dispersion curve from angle resolved photoluminescence experiments*" [2]. This title already indicates the great specificity of strongly-coupled microcavity emission, which is completely dominated by coherent light–matter coupling, i.e., the polariton effect. In the bulk, it has already been shown that luminescence can be affected by the polariton effect [5].

Typical dispersion curves of bulk polaritons are shown in Figure 2.5. Excitons created by an initial laser excitation relax along the lower polariton dispersion, which is essentially the bare exciton dispersion, except near the exciton–photon resonance. In this region, the polariton density of states is strongly reduced and the excitonic contribution to the polariton is decreased. One should note that strictly speaking, a $k = 0$ photon does not exist, and that consequently, the $k = 0$ polaritonic state of the LPB does not exist. The polariton dispersion has no minimum and polaritons accumulate in a large number of states in the so-called bottleneck region, from where the light is mainly emitted. In this respect, PL experiments performed on the bulk can be viewed as being influenced by the polaritonic effect. More simply, the bulk bottleneck effect is induced by the sharpness of the energy/wave-vector region where an exciton can emit a photon considering energy and wave-vector conservation conditions. In microcavities, polariton dispersion is completely different and the LPB has a minimum at $k = 0$. A bottleneck effect still arises because of the sharpness of this minimum, but light is clearly emitted from the whole polariton dispersion including the ground state. The polaritonic effect is from this point of view much clearer than in the bulk, as the PL signal comes from polariton modes, which are easily distinguishable from bare exciton and photon modes. States which emit light in a strongly-coupled microcavity are polariton states, despite the localisation effect. The consequences are twofold. First, PL gives direct access to the polariton dispersion as pointed out in [2]. Second, a theoretical description of PL experiments should account for the polariton effect and the particle relaxation should be described within the polariton base (more details on this point are given in Section 5.2).

4.1.2. RELAXATION OF CAVITY POLARITONS: QUALITATIVE FEATURES

The initial process is a non-resonant optical excitation or an electrical excitation of the semiconductor. At our level, the differences between the two kinds of excitation are only qualitative. This excitation generates non-equilibrium electron–hole pairs which self thermalise on a sub-picosecond time scale. A typical temperature

of this electron–hole gas is of the order of hundreds or even thousands of Kelvin. This electron–hole gas strongly interacts with optical phonons and is cooled down to a temperature smaller than $\hbar\omega_{\mathrm{LO}}/k_b$ on a picosecond time scale. During these few picoseconds excitons may form and populate the exciton dispersion. The exact ratio between excitons and electron–hole pairs and their relative distribution in reciprocal space is still the object of intense research activity [6]. For simplicity we choose to completely neglect these early-stage processes. Rather, we choose to consider as an initial condition the direct injection of excitons in a particular region of reciprocal space. We assume that the typical time scale needed to achieve such a situation is much shorter than the typical relaxation time of polaritons within their dispersion relation. Therefore, our objective is to describe the relaxation of particles (polaritons) moving in a dispersion relation composed of two branches (the upper polariton mode and the lower polariton mode), as shown in Figure 4.2(a). We moreover assume for simplicity that the upper branch plays only a minor role, and that polaritons only relax within the LPB. The peculiar shape of the dispersion relation plays a fundamental role in the polariton relaxation kinetics. The LPB is composed of two distinct areas. In the central zone, excitons are coupled to the light (weakly or strongly coupled, see Section 4.2.3 for details). In the rest of reciprocal space, excitons have a wave-vector larger than the light wave-vector in the medium and are therefore dark. In the active zone, the polariton lifetime is mainly associated with radiative decay and is of the order of a few picoseconds. In the dark zone polaritons only decay non-radiatively with a decay time of the order of hundreds of picoseconds. The dark zone has a parabolic dispersion associated with the heavy-hole exciton mass, which is of the order of the free electron mass. The optically active zone is strongly distorted by strong exciton–light coupling. The central part of this active zone can be associated with a very small effective mass (about $10^{-4}m_0$). This mass rapidly increases with wave-vector to reach the exciton mass at the frontier between the optically active and dark zones.

The physical processes involved in polariton relaxation towards lower energy states are:

4.1.2.1. Polariton–Acoustic Phonon Interaction

Interaction between excitons and acoustic phonons is much less efficient than optical phonon–exciton interaction. Each relaxation step needs about 10 ps and no more than 1 meV can be exchanged. About 100–200 ps are therefore needed for a polariton to dissipate 10–20 meV of excess kinetic energy and to reach the frontier zone between dark and active areas. This relaxation time is shorter than the particle lifetime within the dark zone and some thermalisation can take place in this region of reciprocal space. Once polaritons have reached the edge of the active zone they still need to dissipate about 5–10 meV to reach the bottom of the

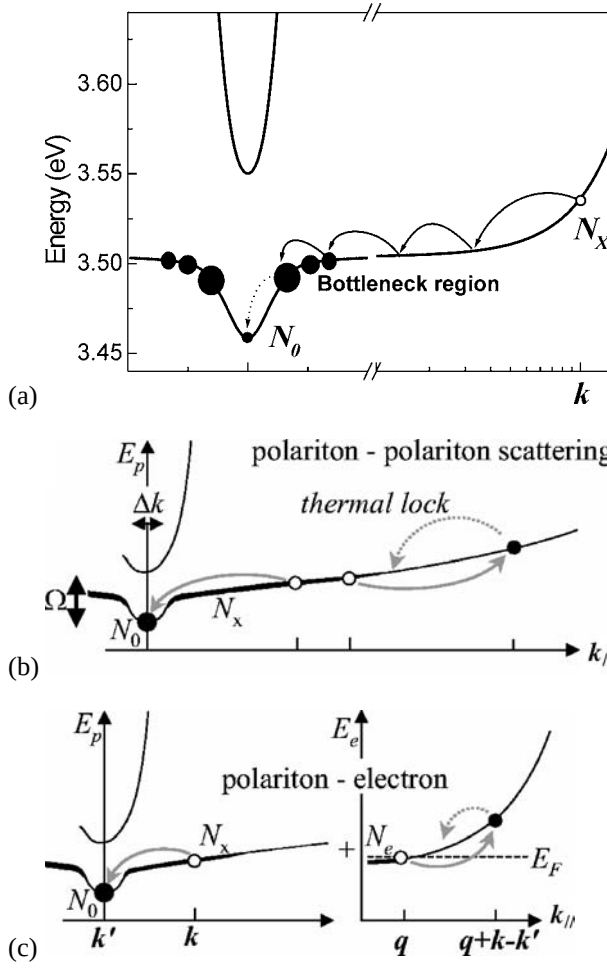

Fig. 4.2. (a) Sketch of the polariton relaxation within the lower polariton branch. (b) Sketch of polariton–polariton scattering process. (c) Sketch of polariton–electron scattering process (the curve on the right-hand side sketch the free electron dispersion.

polariton trap. This process assisted by the acoustic phonon needs about 50 ps, which is at least ten times longer than the polariton lifetime in this region. Therefore, polaritons cannot strongly populate the states of the trap. The distribution function takes larger values in the dark zone and at the edge of the active zone than in the trap. It cannot achieve thermal equilibrium values because of the slow relaxation kinetics. This effect has been called the “bottleneck effect” [4], since it is induced by the existence of a “neck” in the dispersion relation. Such a phe-

nomenon does not take place in a single QW with a parabolic dispersion. The energy difference between the dark–active zone frontier is only 0.05 meV and a dark exciton can reach the ground state by a single scattering event.

4.1.2.2. Polariton–Polariton Interaction

Such an elastic scattering mechanism is sketched in Figure 4.2(b). It is a dipole–dipole interaction with a typical time scale of a few ps. It is very likely to happen because of the non-parabolic shape of the dispersion relation. Each scattering act can provide an energy dissipation of a few meV. It is the main available process allowing population of the polariton trap and overcoming of the "bottleneck effect". All experimental results in this field confirm that polariton–polariton interaction strongly affects polariton relaxation. However, polariton–polariton interaction does not dissipate energy and does not reduce the temperature of the polariton gas. If one considers the process sketched in Figure 4.2(b), one polariton drops into the active zone where it will rapidly decay, whereas the other polariton gains energy and stays in a long-living zone. Altogether, this process heats the polariton gas substantially and may generate a non-equilibrium distribution function as we shall see in Section 4.3.

4.1.2.3. Polariton–Free Carrier Interaction (see Figure 4.2(c))

As stated above, optical pumping generates hot free carriers, which may interact with polaritons. Actually, the formation time of excitons or of strongly-correlated electron–hole pairs is much shorter than the polariton lifetime. It is reasonable to assume that they do not play a fundamental role in polariton relaxation. However, a free carrier excess may exist in modulation-doped structures, or may even be photo-induced if adapted structures are used [7]. A large free-carrier excess destroys excitonic correlations. However, at moderate density it can keep polaritons alive and provide a substantial relaxation mechanism. Polariton–electron interaction is a dipole-charge interaction and the associated scattering process has a sub-picosecond timescale. Electrons are moreover quite light particles in semiconductors (typically 7–8 times lighter than heavy-hole excitons). An electron is therefore able to exchange more energy by exchanging a given wave-vector amount than an exciton. This aspect is extremely helpful in providing polariton relaxation in the steepest zone of the polariton dispersion. An electron–polariton scattering event is moreover a dissipative process for the polariton gas. It may be argued that the electron system can be heated by such an interaction. This is only partially true, and we assume that the two-dimensional electron gas covering the entire sample represents a thermal reservoir. In this framework, an electron gas plays a role similar to acoustic phonons in polariton relaxation, but with a considerably enhanced efficiency. This efficiency could allow a thermal polariton distribution function [8,9] to be achieved, as we shall see in Chapter 6.

4.2. Semi-Classical Treatment of the Relaxation Kinetics of Cavity Polaritons

4.2.1. THE SEMI-CLASSICAL BOLTZMANN EQUATION

The classical Boltzmann equation describes the relaxation kinetics of classical particles. In reciprocal space this equation reads:

$$\frac{dn_{\vec{k}}}{dt} = P_{\vec{k}} - \Gamma_{\vec{k}} n_{\vec{k}} - n_{\vec{k}} \sum_{\vec{k}'} W_{\vec{k}\to\vec{k}'} + \sum_{\vec{k}'} W_{\vec{k}'\to\vec{k}} n_{\vec{k}'}, \tag{4.2.1}$$

where $P_{\vec{k}}$ is the generation term, due to optical pumping or to any other physical process, $\Gamma_{\vec{k}}$ is the particle decay rate, and $W_{\vec{k}\to\vec{k}'}$ is the total scattering rate between the states $\vec{k}$ and $\vec{k}'$ due to any kind of physical process. Uhlenbeck and Gropper first proposed [10] to include the quantum character of the particles involved, taking into account their fermionic or bosonic nature. Eq. (4.2.1) written for fermions reads:

$$\frac{dn_{\vec{k}}}{dt} = P_{\vec{k}} - \Gamma_{\vec{k}} n_{\vec{k}} - n_{\vec{k}} \sum_{\vec{k}'} W_{\vec{k}\to\vec{k}'}(1 - n_{\vec{k}'}) + (1 - n_{\vec{k}}) \sum_{\vec{k}'} W_{\vec{k}'\to\vec{k}} n_{\vec{k}'}, \tag{4.2.2}$$

whereas for bosons it is:

$$\frac{dn_{\vec{k}}}{dt} = P_{\vec{k}} - \Gamma_{\vec{k}} n_{\vec{k}} - n_{\vec{k}} \sum_{\vec{k}'} W_{\vec{k}\to\vec{k}'}(1 + n_{\vec{k}'}) + (1 + n_{\vec{k}}) \sum_{\vec{k}'} W_{\vec{k}'\to\vec{k}} n_{\vec{k}'}. \tag{4.2.3}$$

Eqs. (4.2.2) and (4.2.3) are called the semi-classical Boltzmann equations. The main task to describe the relaxation kinetics of particles in this framework is to calculate scattering rates. One should first identify the main physical processes which provoke scattering of particles. Then, scattering rates can be calculated using the Fermi Golden Rule. This procedure is usable only if the scattering processes involved are weak and can be treated in a perturbative way. Interactions should provoke scattering of particles within their dispersion relation and not provoke energy renormalisation. For example, the coupling of particles with the light should be a weak coupling, only responsible for a radiative decay. In a strongly-coupled microcavity one cannot describe relaxation of excitons using a Boltzmann equation. One should first treat non-perturbatively the exciton–photon coupling giving rise to the polariton base. Then, polaritons weakly interact with their environment. This weak interaction provokes scattering of polaritons within their dispersion relation and Eq. (4.2.3) can be used. The scattering rates can indeed be calculated in a perturbative way (Fermi Golden Rule) because they are induced by weak interactions.

In a semiconductor microcavity the main scattering mechanisms identified are:

- Polariton decay (mainly radiative).
- Polariton–phonon interaction.
- Polariton–free carrier interaction.
- Polariton–polariton interaction.
- Polariton–structural disorder interaction.

4.2.2. POLARITON–STRUCTURAL DISORDER INTERACTION

This scattering process is mainly associated with the excitonic part of polaritons. Structural disorder induces coherent elastic (Rayleigh) scattering with a typical time scale of about 1 ps. It couples very efficiently all polaritons situated on the same "elastic circle" in reciprocal space [11] (see Section 3.3 and Figure 3.6). This allows one to simplify the description of polariton relaxation by assuming cylindrical symmetry of the polariton distribution function. Also, disorder induces a broadening of the polariton states, which should be accounted for when scattering rates are calculated.

4.2.3. POLARITON DECAY

There are three different regions in reciprocal space: $[0, k_{sc}]$, $]k_{sc}, k_L]$, $]k_L, \infty]$.

- $[0, k_{sc}]$ is the region where the exciton–photon anticrossing takes place. Indeed, cavity mirrors reflect the light only within a finite angular cone, which corresponds to an in-plane wave-vector k_{sc}. k_{sc} of course depends on the detuning. In this central region the polariton decay is mainly due to the finite cavity photon lifetime:

$$\Gamma_k = \frac{c_k}{\tau_c},$$

  where c_k is the photon fraction of the polariton and τ_c is the cavity photon lifetime. k_{sc} values are typically of the order of 4 to 8×10^6 m^{-1} and τ_c is in the range 1–10 ps.
- $]k_{sc}, k_L]$, where k_L is the wave-vector of light in the medium. In this region excitons are only weakly coupled to the light and polariton decay is $\Gamma_k = \Gamma_0$, which is the radiative decay rate of QW excitons (see Section 1.1).
- $]k_L, \infty]$. Beyond k_L excitons are no longer coupled to the light. They only decay non-radiatively with a decay rate Γ_{nr}. We do not wish to enter into the details of the mechanism involved in this decay, which can be considered as constant in the whole reciprocal space for simplicity. This quantity is given by the decay time measured in time-resolved luminescence experiments performed in the low excitation density regime, and is typically in the range 100 ps–1 ns.

4.2.4. POLARITON–PHONON INTERACTION

The theoretical description of carrier–phonon or of exciton–phonon interaction has received considerable attention throughout the history of semiconductor heterostructures. Here we present a simplified picture which is, however, well suited to our problem. Cavity polaritons are two-dimensional particles with only an in-plane dispersion. They are scattered by phonons which are in the QWs we consider, mainly three-dimensional (acoustic phonons) or two-dimensional (optical phonons). Scattering events should conserve the wave-vector in the plane. We call $\vec{q}$ the phonon wave-vector and $\vec{q}_{\text{II}}$ and $\vec{q}_z$ the in-plane and z-component of $\vec{q}$. Using the Fermi Golden Rule, the scattering rate between two discrete polariton states of wave-vector $\vec{k}$ and $\vec{k}'$ reads:

$$W^{\text{phon}}_{\vec{k}\to\vec{k}'} = \frac{2\pi}{\hbar}\sum_{\vec{q}}\left|M(\vec{q})\right|^2\left(0, 1 + N^{\text{phon}}_{\vec{q}=\vec{k}-\vec{k}'+\vec{q}_z}\right)\delta\left(E(k') - E(k) \mp \hbar\omega_{\vec{q}}\right), \quad (4.2.4)$$

where $N^{\text{phon}}_{\vec{q}}$ is the phonon distribution function. If one considers an equilibrium phonon distribution, $N^{\text{phon}}_{\vec{q}} = 1/(\exp(-E(\vec{q})/k_bT) - 1)$, where $E(\vec{q})$ is the phonon dispersion. The sum on the right-hand side of Eq. (4.2.4) is over the phonon states. The 0 and the $-$ in (4.2.4) hold for the absorption of a phonon (if $E(k) < E(k')$). The 1 and the $+$ hold for emission. M is the matrix element of interaction between phonons and polaritons. If one considers polariton states with a finite energy width $\hbar\gamma_{k'}$, the δ function can be replaced by a Lorentzian and Eq. (4.2.4) becomes:

$$W^{\text{phon}}_{\vec{k}\to\vec{k}'} = \frac{2\pi}{\hbar}\sum_{\vec{q}}\left|M(\vec{q})\right|^2\left(0, 1 + N^{\text{phon}}_{\vec{q}=\vec{k}-\vec{k}'+\vec{q}_z}\right) \times \frac{\hbar\gamma_{k'}/\pi}{(E(k') - E(k) \pm \hbar\omega_{\vec{q}})^2 + (\hbar\gamma_{k'})^2}. \quad (4.2.5)$$

The energy width of a state can be defined as the imaginary part of its eigen energy. It is the half of the decay rate Γ_k associated with the state. The wave-vector conservation in the plane actually limits the sum (4.2.5) to the z-direction.

In the framework of the Born approximation the matrix element of interaction reads:

$$\left|M(\vec{q})\right| = \left|\left\langle\psi^{\text{pol}}_k\middle|H^{\vec{q}}_{\text{pol-phon}}\middle|\psi^{\text{pol}}_{k'}\right\rangle\right| = \sqrt{x_k x_{k'}}\left|\left\langle\psi^{\text{exc}}_k\middle|H^{\vec{q}}_{\text{exc-phon}}\middle|\psi^{\text{exc}}_{k'}\right\rangle\right|, \quad (4.2.6)$$

where ψ^{pol}_k is the polariton wave function, ψ^{exc}_k is the exciton wave function, and x_k is the exciton fraction of the polariton. The exciton wave-function reads:

$$\psi_{\vec{k}}(\vec{r}_e, \vec{r}_h) = f_e(z_e)\,f_h(z_h)\frac{1}{\sqrt{S}}e^{i\vec{k}(\beta_e\vec{r}_e + \beta_h\vec{r}_h)}\sqrt{\frac{2}{\pi}}\frac{1}{a^{\text{2D}}_b}e^{-|\vec{r}_e - \vec{r}_h|/a^{\text{2D}}_b}, \quad (4.2.7)$$

where z_e, z_h are electron and hole coordinates along the growth axis and $\vec{r}_e$ and $\vec{r}_h$ their coordinates in the plane, f_e and f_h are the electron and hole wave-functions in the growth direction, a_b^{2D} is the two-dimensional exciton Bohr radius, $\beta_e = m_e/(m_e + m_h)$, $\beta_h = m_h/(m_e + m_h)$, where $m_{e(h)}$ are the electron (hole) masses, S is a normalisation area.

4.2.4.1. Interaction with Longitudinal Optical Phonons

This interaction is mainly mediated by the Frölich interaction [12]. In three dimensions the exciton–LO phonon matrix element reads:

$$M^{\mathrm{LO}}(\vec{q}) = \frac{-e}{q}\sqrt{\frac{\hbar\omega_{\mathrm{LO}}}{2SL}\left(\frac{1}{\varepsilon_\infty} - \frac{1}{\varepsilon_s}\right)} = \frac{M_0^{\mathrm{LO}}}{q\sqrt{SL}}, \tag{4.2.8}$$

where $\hbar\omega_{\mathrm{LO}}$ is the energy for creation of a LO-phonon, ε_∞ is the optical dielectric constant, ε_s the static dielectric constant, L is the dimension along the growth axis. In two dimensions one should consider confined optical phonons with quantised wave-vector in the z-direction. L becomes the QW width and $q_z^m = m\pi/L$, where m is an integer. Moreover, the overlap integral between exciton and phonon wave-functions quickly vanishes while m increases. Therefore, we consider only the first confined phonon state and the matrix element (4.2.8) becomes:

$$M^{\mathrm{LO}}(\vec{q}) = \frac{M_0^{\mathrm{LO}}}{\sqrt{|\vec{q}_{\mathrm{II}}|^2 + (\pi/L)^2}\sqrt{SL}}. \tag{4.2.9}$$

The wave-vectors exchanged in the plane are typically much smaller than π/L and (4.2.9) can be approximated by:

$$M^{\mathrm{LO}}(\vec{q}) = \frac{M_0^{\mathrm{LO}}}{\pi}\sqrt{\frac{L}{S}}. \tag{4.2.10}$$

Considering a dispersionless phonon dispersion for LO phonons, the LO phonon contribution to (4.2.5) reads:

$$W_{\vec{k}\to\vec{k}'}^{\mathrm{phon-LO}} = \frac{2}{\pi^2\hbar}\frac{L}{S}x_k x_{k'}\left|M_0^{\mathrm{LO}}\right|^2\left(0, 1 + \frac{1}{\exp(-\hbar\omega_{\mathrm{LO}}/k_bT) - 1}\right) \times \frac{\hbar\gamma_{k'}}{(E(k') - E(k) \mp \hbar\omega_{\mathrm{LO}})^2 + (\hbar\gamma_{k'})^2}. \tag{4.2.11}$$

Optical phonons interact very strongly with carriers. They allow a fast exciton formation. Their energy of formation $\hbar\omega_{\mathrm{LO}}$ is, however, of the order of 20 to 90 meV, depending on the nature of the semiconductor involved. An exciton with a kinetic energy smaller than 20 meV can no longer emit an optical phonon. The probability of absorbing an optical phonon remains extremely small at low temperature. This implies that an exciton gas cannot cool down at a temperature lower than 100–200 K by interacting only with optical phonons. Optical phonons are

therefore extremely efficient at relaxing a hot-carrier gas (optically or electrically created) towards an exciton gas with a temperature 100–300 K in a few picoseconds. The final cooling of this exciton gas towards the lattice temperature should, however, be assisted by acoustical phonons or other scattering mechanisms. The semiconductor currently used to grow microcavities, and where optical phonons play the largest role, is CdTe. In such a material, $\hbar\omega_{\mathrm{LO}}$ is only 21 meV, namely larger than the exciton binding energy in CdTe-based QWs. Moreover, the Rabi splitting is of the order of 10–20 meV in CdTe-based cavities. This means that the direct scattering of a reservoir exciton towards the polariton ground state is a possible process which may play an important role.

4.2.4.2. Interaction with Acoustic Phonons

This interaction is mainly mediated by the deformation potential.

The exciton–acoustic phonon matrix element reads:

$$M^{\mathrm{ac}}(\vec{q}) = \sqrt{\frac{\hbar q}{2\rho c_s SL}}\, G(\vec{q}_{\mathrm{II}}, q_z), \tag{4.2.12}$$

where ρ is the density and c_s is the speed of sound in the medium. Assuming isotropic bands, G reads

$$\begin{aligned} G(\vec{q}_{\mathrm{II}}, q_z) &= D_e I_e^{\perp}(\vec{q}_z) I_e^{\mathrm{II}}(\vec{q}_{\mathrm{II}}) + D_h I_h^{\perp}(\vec{q}_z) I_h^{\mathrm{II}}(\vec{q}_{\mathrm{II}}) \\ &\approx D_e I_e^{\mathrm{II}}(\vec{q}_{\mathrm{II}}) + D_h I_h^{\mathrm{II}}(\vec{q}_{\mathrm{II}}). \end{aligned} \tag{4.2.13}$$

D_e, D_h are the deformation coefficients of the conduction band and valence band, respectively, and $I_{e(h)}^{\perp\,(\mathrm{II})}$ are the overlap integrals between the exciton and phonon mode in the growth direction and in the plane, respectively:

$$\begin{aligned} I_{e(h)}^{\mathrm{II}}(q_{\mathrm{II}}) &= \left(\sqrt{\frac{2}{\pi}}\frac{1}{a_b^{\mathrm{2D}}}\right)^2 \int d^2\vec{r}\, e^{-(2|r|/a_b^{\mathrm{2D}})} \exp\!\left(i m_{h(e)} \vec{q}_{\mathrm{II}}.\vec{r}/(m_e + m_h)\right) \\ &= \left(1 + \left(\frac{m_{h(e)} q_{\mathrm{II}} a_b^{\mathrm{2D}}}{2M_x}\right)\right)^{-3/2}, \end{aligned} \tag{4.2.14}$$

$$I_{e(h)}^{\perp}(q_z) = \int dz \left| f_{e(h)}(z)\right|^2 e^{iq_z z} \approx 1. \tag{4.2.15}$$

Using this matrix element and moving to the thermodynamic limit in the growth direction, the scattering rate (4.2.5) becomes

$$\begin{aligned} W_{\vec{k}\to\vec{k}'}^{\mathrm{phon}} = \frac{2\pi}{\hbar}\frac{L}{2\pi} x_k x_{k'} \int_{q_z} \frac{\hbar q}{2\rho c_s SL} \left|G(\vec{k} - \vec{k}')\right|^2 \left(0, 1 + N_{\vec{k}-\vec{k}'+\vec{q}_z}^{\mathrm{phon}}\right) \\ \times \frac{\hbar\gamma_{k'}/\pi}{(E(k') - E(k) \mp \hbar\omega_{\vec{k}-\vec{k}'+\vec{q}_z})^2 + (\hbar\gamma_{k'})^2}\, dq_z. \end{aligned} \tag{4.2.16}$$

Moving to the thermodynamic limit means that we have let the system size in a given direction (here the z-direction) go to infinity, substituting the summation with an integral, using the formula: $\sum_{q_z} \to \frac{L}{(2\pi)} \int dq_z$.

Eq. (4.2.16) can be easily simplified:

$$W^{\text{phon}}_{\vec{k}\to\vec{k}'} = \frac{|G(\vec{k}-\vec{k}')|^2}{2\pi S\rho c_s} x_k x_{k'} \int_{q_z} \left|\vec{k}-\vec{k}'+\vec{q}_z\right| \left(0, 1+N^{\text{phon}}_{\vec{k}-\vec{k}'+\vec{q}_z}\right) \times \frac{\hbar\gamma_{k'}}{(E(k')-E(k)\mp\hbar\omega_{\vec{k}-\vec{k}'+\vec{q}_z})^2+(\hbar\gamma_{k'})^2}\, dq_z. \tag{4.2.17}$$

4.2.5. POLARITON–ELECTRON INTERACTION

The polariton–electron scattering rate is calculated using the Fermi Golden Rule as

$$W^{\text{el}}_{\vec{k}\to\vec{k}'} = \frac{2\pi}{\hbar} \sum_{\vec{q}} \left|M^{\text{el}}_{\vec{q},\vec{k},\vec{k}'}\right|^2 x_k x_{k'} N^e_{\vec{q}} \left(1-N^e_{\vec{q}+\vec{k}'-\vec{k}}\right) \times \frac{\hbar\gamma_{k'}/\pi}{\left(E(k')-E(k)+\frac{\hbar^2}{2m_e}(q^2-|\vec{q}+\vec{k}-\vec{k}'|^2)\right)^2+(\hbar\gamma_{k'})^2}, \tag{4.2.18}$$

where $N^e_{\vec{q}}$ is the electron distribution function and m_e the electron mass. If one considers electrons at thermal equilibrium, it is given by the Fermi–Dirac electron distribution function with a chemical potential

$$\mu_e = k_b T \ln\left(\exp\left(\frac{\hbar^2 n_e}{2\pi k_b T m_e}\right)-1\right),$$

where n_e is the electron concentration. M^{el} is the matrix element of interaction between an electron and an exciton. A detailed calculation of the electron–polariton matrix element can be found in [13] and [8]. M^{el} is composed of a direct contribution and of an exchange contribution.

$$M^{\text{el}} = M^{\text{el}}_{\text{dir}} \pm M^{\text{el}}_{\text{exc}}. \tag{4.2.19}$$

The $+$ in (4.2.19) corresponds to a triplet configuration (parallel electron spins), and the $-$ to a singlet configuration (antiparallel electron spins). If both electrons have the same spin, the total exciton spin is conserved through the exchange process. However, if both electron spins are opposite, an active exciton state of spin $+1$, for example, will be scattered towards a dark state of spin $+2$ through the exchange process. Here and in what follows we shall consider only the triplet configuration for simplicity.

In order to calculate M^{el} we adopt the Born approximation and write:

$$M^{\mathrm{el}}_{\mathrm{dir}} = \iiint d\vec{r}_e\, d\vec{r}_h\, d\vec{r}'_e\, \psi^*_{\vec{k}}(\vec{r}_e,\vec{r}_h) f^*_{\vec{q}}(\vec{r}'_e)\big[V\big(|\vec{r}_e-\vec{r}'_e|\big) - V\big(|\vec{r}_h-\vec{r}'_e|\big)\big] \times \psi_{\vec{k}'}(\vec{r}_e,\vec{r}_h) f_{\vec{q}+\vec{k}-\vec{k}'}(\vec{r}'_e), \tag{4.2.20}$$

$$M^{\mathrm{el}}_{\mathrm{exc}} = \iiint d\vec{r}_e\, d\vec{r}_h\, dr'_e\, \psi^*_{\vec{k}}(\vec{r}_e,\vec{r}_h) f^*_{\vec{q}}(\vec{r}'_e)\big[V\big(|\vec{r}_e-\vec{r}'_e|\big) - V\big(|\vec{r}_h-\vec{r}'_e|\big)\big] \times \psi_{\vec{k}'}(\vec{r}'_e,\vec{r}_h) f_{\vec{q}+\vec{k}-\vec{k}'}(\vec{r}_e), \tag{4.2.21}$$

where the Coulomb potential $V(r) = -e^2/\varepsilon r$, with ε being the dielectric susceptibility of the QW. The free-electron wave-function f is

$$f_{\vec{q}}(\vec{r}'_e) = \frac{1}{\sqrt{S}} e^{i\vec{q}\vec{r}'_e}. \tag{4.2.22}$$

The integrals (4.2.20), (4.2.21) can be done analytically, which yields:

$$M^{\mathrm{el}}_{\mathrm{dir}} = \frac{2\pi e^2}{S\varepsilon|\vec{k}-\vec{k}'|}\big[\big(1+\xi_h^2\big)^{-3/2} - \big(1+\xi_e^2\big)^{-3/2}\big], \tag{4.2.23}$$

$$M^{\mathrm{el}}_{\mathrm{exc}} = \frac{8\pi e^2}{S\varepsilon}\frac{[(1+\xi_c^2)^{-3/2} - (1+4\xi_h^2)^{-3/2}]}{[a^{-2}+|\vec{q}-\beta_e\vec{k}'|^2]^{1/2}}, \tag{4.2.24}$$

where $\xi_{e,h} = \frac{1}{2}\beta_{e,h}|\vec{k}'-\vec{k}|a_b^{2\mathrm{D}}$, $\xi_c = |\beta_e\vec{k}+\vec{k}'-\vec{k}-\vec{q}|a_b^{2\mathrm{D}}$.

Passing to the thermodynamic limit, (4.2.18) becomes

$$W^{\mathrm{el}}_{\vec{k}\to\vec{k}'} = \frac{S}{2\pi^2\hbar}\int_{\vec{q}} \big|M^{\mathrm{el}}_{\mathrm{dir}} + M^{\mathrm{el}}_{\mathrm{exc}}\big|^2 x_k x_{k'} N^e_{\vec{q}}\big(1 - N^e_{\vec{q}+\vec{k}'-\vec{k}}\big) \times \frac{\hbar\gamma_{k'}}{\big(E(k') - E(k) + \frac{\hbar^2}{2m_e}(q^2 - |\vec{q}+\vec{k}-\vec{k}'|^2)\big)^2 + (\hbar\gamma_{k'})^2}. \tag{4.2.25}$$

The polariton–electron interaction is a dipole-charge interaction which takes place on a picosecond time scale. An equilibrium electron gas can thermalise a polariton gas quite efficiently. A more complex effect may, however, take place such as trion formation or exciton dephasing. These effects are out of our scope.

4.2.6. POLARITON–POLARITON INTERACTION

The polariton–polariton scattering rate reads:

$$W^{\mathrm{pol}}_{\vec{k}\to\vec{k}'} = \frac{2\pi}{\hbar}\sum_{\vec{q}} |M_{\mathrm{ex}}|^2 x_k x_{k'} x_q x_{\vec{q}+\vec{k}'-\vec{k}} N^{\mathrm{pol}}_{\vec{q}} \left(1 + N^{\mathrm{pol}}_{\vec{q}+\vec{k}'-\vec{k}}\right) \times \frac{\hbar\gamma_{k'}/\pi}{(E(k') - E(k) + E(\vec{q}+\vec{k}'-\vec{k}) - E(q))^2 + (\hbar\gamma_{k'})^2}. \tag{4.2.26}$$

The exciton–exciton matrix element of interaction is also composed of a direct and an exchange term. Ref. [14] is entirely devoted to its derivation. Here and in what follows we shall use a numerical estimate [15] of this quantity, which we shall assume constant over the whole reciprocal space:

$$M_{\mathrm{ex}} \approx 6\frac{(a_b^{\mathrm{2D}})^2}{S} E_b = \frac{1}{S} M^0_{\mathrm{exc}}, \tag{4.2.27}$$

where E_b is the exciton binding energy. Passing to the thermodynamic limit in the plane, (4.2.26) becomes:

$$W^{\mathrm{pol}}_{\vec{k}\to\vec{k}'} = \frac{1}{2\pi^2\hbar S}\int d^2\vec{q} \left|M^0_{\mathrm{exc}}\right|^2 x_k x_{k'} x_q x_{\vec{q}+\vec{k}'-\vec{k}} N^{\mathrm{pol}}_{\vec{q}} \left(1 + N^{\mathrm{pol}}_{\vec{q}+\vec{k}'-\vec{k}}\right) \times \frac{\hbar\gamma_{k'}}{(E(k') - E(k) + E(\vec{q}+\vec{k}'-\vec{k}) - E(q))^2 + (\hbar\gamma_{k'})^2}. \tag{4.2.28}$$

As one can see, the *a priori* unknown polariton distribution function is needed to calculate scattering rates. This means that in any simulation these scattering rates should be updated dynamically throughout the simulation time, which can be extremely time consuming.

Polariton–polariton scattering has been shown to be extremely efficient when a microcavity is resonantly excited (see Chapter 5). It also plays a fundamental role in the case of non-resonant excitation. Depending on the excitation condition and on the nature of the semiconductor used, the exciton–exciton interaction may be strong enough to self-thermalise the exciton reservoir at a given temperature.

4.2.7. NUMERICAL SOLUTION OF BOLTZMANN EQUATIONS, PRACTICAL ASPECTS

4.2.7.1. Choice of the Grid

In order to solve numerically the Boltzmann equations one should discretise the reciprocal polariton space. As mentioned in Section 4.2.2, it is reasonable to assume cylindrical symmetry for the distribution function. The elementary cells of

the chosen grid should reflect this cylindrical symmetry, and therefore these cells should be annular. The cell number i, $C(i)$ should contain all states with wavevectors satisfying $|\vec{k}| \in [k_i, k_{i+1}[$. The question of the choice of a scale for the k_i (linear scale, quadratic scale, etc.) has been widely debated in the literature [4,8,15,16]. Actually, the only requirement is that the distribution function does not varies too abruptly from cell to cell. Therefore, one should use small cells in the steep zone of the polariton dispersion, whereas very large cells can be used in the flat excitonic area. The only state which requires particular attention is the ground state, especially if one wishes to describe "condensation-like phenomena", namely a discontinuity of the polariton distribution function. If such a discontinuity takes place the actual size of the cells plays a role. We cannot choose infinitely small cells numerically. This means that one cannot solve numerically the Boltzmann equations in the thermodynamic limit in the case of Bose condensation. What can be done is to account for a finite system size R. The spacing between states becomes finite ($2\pi/R$). The grid size plays a role, but it is no longer arbitrary but related to a real physical quantity. In such a case the cell size should follow the real state spacing in the region where the polariton distribution function varies abruptly.

4.2.7.2. Effective Scattering Rates

The total scattering rate from a discrete state $\vec{k}$ to another discrete state $\vec{k}'$ is the sum of all the scattering rates:

$$W_{\vec{k}\to\vec{k}'} = \frac{w_{\vec{k}\to\vec{k}'}}{S} = W^{\text{phon}}_{\vec{k}\to\vec{k}'} + W^{\text{pol}}_{\vec{k}\to\vec{k}'} + W^{\text{el}}_{\vec{k}\to\vec{k}'}. \tag{4.2.29}$$

We now need to calculate two kinds of transition rate. The first is the transition rate between a discrete initial state $\vec{k}$ and all the states belonging to a cell of the grid, indexed by a natural number i.

$$W^{\text{escape}}_{\vec{k}\to\vec{k}'\in C(i)} = \sum_{\vec{k}'\in C(i)} \frac{w_{\vec{k}\to\vec{k}'}}{S}. \tag{4.2.30}$$

We pass to the thermodynamic limit, changing the sum to an integral:

$$W^{\text{escape}}_{\vec{k}\to\vec{k}'\in C(i)} = \frac{S}{(2\pi)^2}\int_{\vec{k}'\in C(i)} d^2\vec{k}'\,\frac{w_{\vec{k}\to\vec{k}'}}{S} = \frac{1}{(2\pi)^2}\int_{\vec{k}'\in C(i)} d^2\vec{k}'\,w_{\vec{k}\to\vec{k}'}. \tag{4.2.31}$$

Here the integration takes place over final states. The cells have cylindrical symmetry, which means that the scattering rate does not depend on the direction of $\vec{k}$. The total scattering rate towards cell i is therefore the same for any state belonging

to cell j. So:

$$\text{If } \vec{k} \in C(j), \quad W^{\text{escape}}_{j\to i} = W^{\text{escape}}_{\vec{k}\to\vec{k}'\in C(i)}. \tag{4.2.32}$$

One also needs to calculate the number of particles reaching a state $\vec{k}'$ from the cell $C(i)$.

$$W^{\text{reach}}_{\vec{k}\in C(i)\to\vec{k}'} = W^{\text{reach}}_{i\to j} = \frac{1}{(2\pi)^2}\int_{\vec{k}\in C(i)} d^2\vec{k}\, w_{\vec{k}\to\vec{k}'}. \tag{4.2.33}$$

Here the integration takes place over initial states.

If one wishes to describe condensation in a finite-size system, the ground-state cell is constituted by a single state and no integration takes place when the final state is the ground state:

$$W^{\text{escape}}_{\vec{k}\to 0} = W^{\text{escape}}_{i\to 0} = \frac{w_{\vec{k}\to 0}}{S}. \tag{4.2.34}$$

This scattering rate is inversely proportional to the system size.

4.2.7.3. The Practical Equation Set to Solve

In this framework, Eq. (4.2.3) is written:

$$\frac{dn_i}{dt} = P_i - \Gamma_i n_i - n_i \sum_{j\neq i} W^{\text{escape}}_{i\to j}(1+n_j) + (1+n_i)\sum_{j\neq i} W^{\text{reach}}_{i\to j} n_j. \tag{4.2.35}$$

It is an ensemble of coupled first-order differential equations which can be easily solved. One should point out that despite the cylindrical symmetry hypothesis, and despite the one-dimensional nature of the final equation, all two-dimensional scattering processes are correctly accounted for.

4.3. Relaxation Kinetics of Cavity Polariton

4.3.1. QUANTITATIVE ANALYSIS OF POLARITON RELAXATION KINETICS

Figure 4.3 shows polariton distribution functions calculated using Eq. (4.2.35). The structure considered is a CdTe-based microcavity with a Rabi splitting of 11 meV. We consider non-resonant *cw* pumping and only acoustic phonon scattering is taken into account. The structural disorder is assumed to be responsible for an inhomogeneous broadening of 1 meV. The distribution functions achieved keep the same aspect for the three lower pumping powers used. It is strongly modified for the higher pumping power, for which a stimulation threshold is achieved for the state $k = 2\times 10^6$ m^{-1}. One should note that the polariton density achieved in this last case is much larger than the exciton bleaching density,

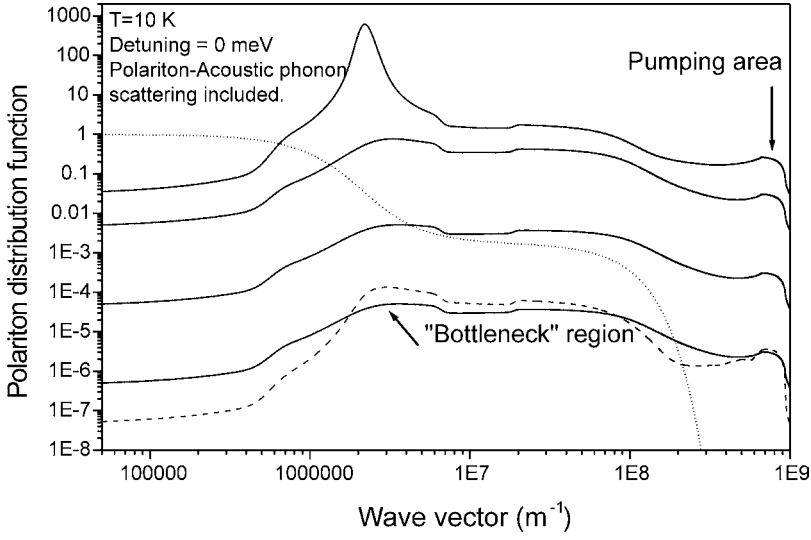

Fig. 4.3. Calculated polariton distribution function for a CdTe microcavity at zero detuning and 10 K. Solid lines are obtained using an inhomogeneous broadening of 1 meV and the dashed line is obtained using an inhomogeneous broadening of 0.1 meV. Only polariton–acoustic phonon scattering is included. The pumping powers absorbed are 0.0001 (solid and dashed lines), 0.01, 1, 10 W/cm^2 (solid lines, from bottom to top). The corresponding polariton concentrations are (solid lines): 9.2×10^8, 9.2×10^{10}, 8.92×10^{12}, 6.55×10^{13} cm^{-2}. The dotted line shows the Boltzmann distribution function with zero chemical potential.

even considering microcavities containing several QWs. The ground-state population evolves linearly with pumping for the three lower pumpings used, and sublinearly once a stimulation threshold is reached. Kinetic distributions functions are compared with a Boltzmann distribution having a null chemical potential, which corresponds to a density of 8×10^8 cm^{-2} at this temperature (10 K). Differences between Boltzmann and Bose distributions occur only for wave-vectors smaller than 10^6 m^{-1}. The specific features of a Bose distribution around $k = 0$ will be addressed in Chapter 6. Now let us describe in detail the kinetic distribution functions. The region where excitons are introduced (around 10^9 m^{-1}) shows large values of the distribution function. This is rather unrealistic. It happens because we neglect exciton–exciton scattering, which rapidly redistributes excitons in reciprocal space. Going down within reciprocal space, distribution functions increase between 4×10^8 and 2×10^7 m^{-1}, as should occur for a thermal distribution function. The wave-vector of light in the medium is 2×10^7 m^{-1}. Between 8×10^6 and 2×10^7 m^{-1} excitons are weakly coupled to the light and their lifetime is only 3 ps in CdTe QWs. This short lifetime provokes a depletion which is clearly observable. Strong coupling holds in the region between 2×10^6 and

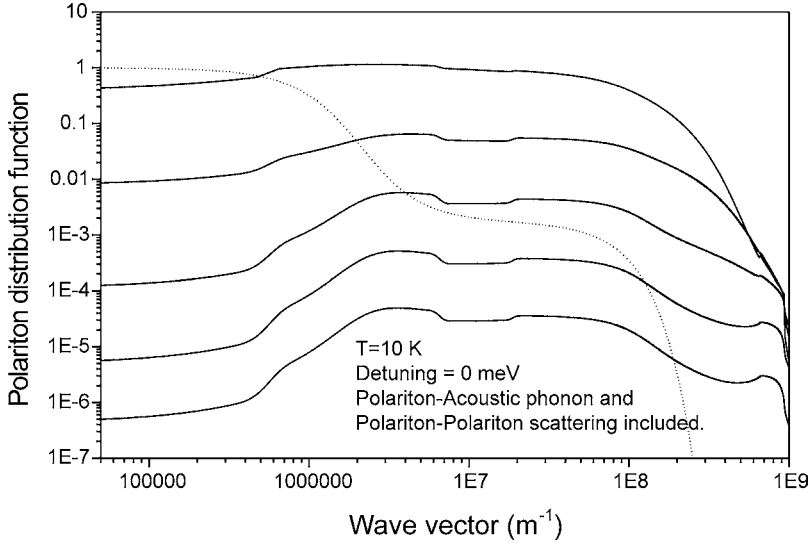

Fig. 4.4. Solid lines: Calculated polariton distribution function for a CdTe microcavity at zero detuning, 10 K, and using an inhomogeneous broadening of 1 meV. Scattering processes included are polariton–acoustic phonon scattering and polariton–polariton scattering. The pumping powers absorbed are (from bottom to top) 0.00001, 0.0001, 0.001, 0.1, 1 W/cm^2. The corresponding polariton concentration are: 9×10^8, 9×10^9, 8.7×10^{10}, 8.06×10^{11}, 5.68×10^{12} cm^{-2}. The dotted line shows the Boltzmann distribution function with zero chemical potential.

8×10^6 m^{-1}, but there polaritons are exciton-like and their lifetime is rather long. In this region polariton dispersion is not strongly distorted (see Figure 4.1) and the states are easily accessible to particles through acoustic phonon scattering. As a result, polaritons accumulate in this area of reciprocal space, which is called the "bottleneck region". Further down in wave-vector space, the polariton lifetime rapidly decreases and the dispersion becomes steep, which increases the relaxation time. The increase of the relaxation time combined with the decrease of the lifetime provokes a depletion of the ground state and the surrounding region. As a result, values achieved by the distribution function at the ground state are two orders of magnitude smaller than in the bottleneck region. The dashed curve has been calculated considering a small inhomogeneous broadening (0.1 meV). The qualitative description presented above remains valid, but irregularities of the distribution function are still amplified. There is no comparison between kinetic and thermodynamic distribution functions. In the framework we consider, the system properties are completely dominated by polariton relaxation kinetics.

Figure 4.4 is the same as Figure 4.3, but exciton–exciton scattering is included. For the lower pumping power used, the distribution function remains essentially the same as in Figure 4.3. The influence of exciton–exciton scattering increases

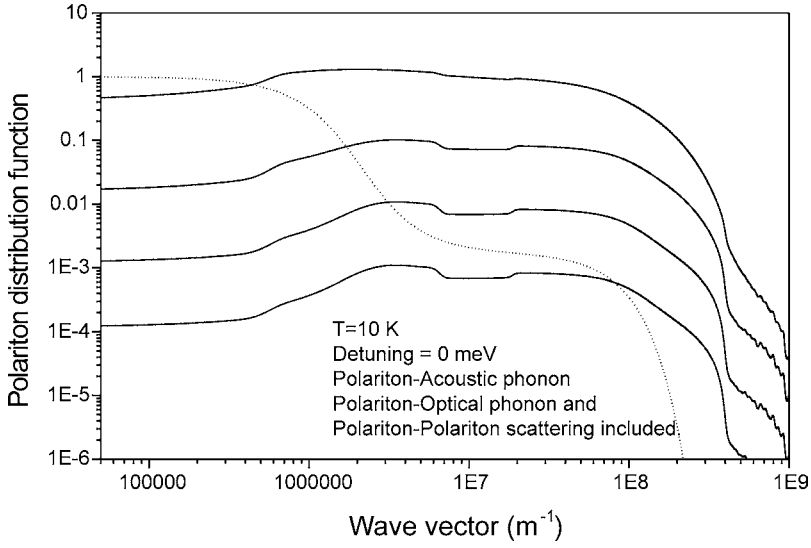

Fig. 4.5. Solid lines: calculated polariton distribution function for a CdTe microcavity at zero detuning, 10 K, and using an inhomogeneous broadening of 1 meV. Scattering processes included are polariton–acoustic phonon scattering, polariton–optical phonon scattering and polariton–polariton scattering. The pumping powers absorbed are 0.0001, 0.001, 0.1, 1 W/cm^2 (from bottom to top). The corresponding polariton concentrations are: 6.86×10^9, 6.85×10^{10}, 6.68×10^{11}, 5.3×10^{12} cm^{-2}. The dotted line shows the Boltzmann distribution function with a null chemical potential.

quadratically with pumping power and its role appears for high pumping power. Because of this scattering process, large wave-vector excitons self-thermalise at a temperature much larger than the lattice temperature (about 100 K). The bottleneck flattens to almost disappear for the largest pumping power used. The ground-state emission versus pumping power changes gradually from a linear to a quasi-quadratic dependence. Such behaviour is in agreement with existing experimental data, as we shall see in Section 4.3.2. Here we point out that a super-linear dependence is not a signature of a stimulation threshold [17], which is characterised by a super-exponential dependence (not shown).

Figure 4.5 is the same as Figures 4.3 and 4.4, but optical phonon scattering is included. The bottleneck is reduced with respect to previous cases in the low excitation density range. Also, distribution functions are more thermal in the dark zone. However, in the higher excitation case, the distribution function remains essentially similar to the one in Figure 4.4. This shows that exciton–exciton scattering dominates the polariton relaxation dynamics in the high-density range. Figures 4.6, 4.7 and 4.8 are the same as Figure 4.5, but for negative detuning (-5 meV), positive detuning (5 meV) and high temperature (100 K). Distribution functions achieved at low temperature are similar whatever the detuning, except

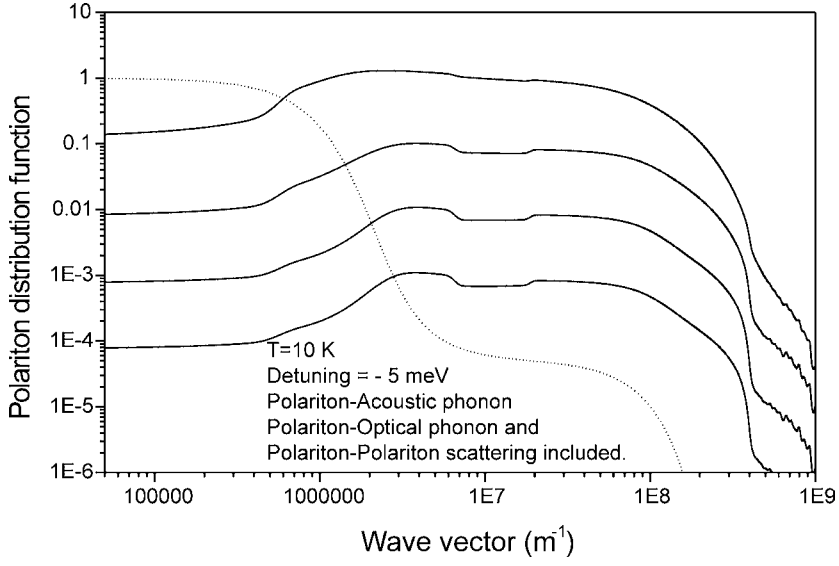

Fig. 4.6. Same as Figure 4.5, but for a detuning -5 meV. Densities achieved are 6.85×10^9, 6.83×10^{10}, 6.67×10^{11}, 5.3×10^{12} cm^{-2}, respectively.

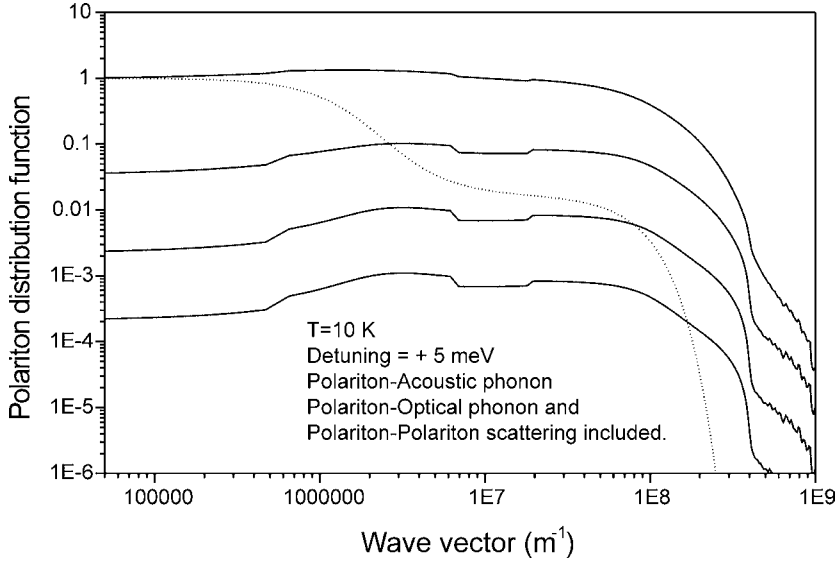

Fig. 4.7. The same as Figure 4.5, but with for a positive detuning $+5$ meV. Densities achieved are 6.87×10^9, 6.85×10^{10}, 6.7×10^{11}, 5.33×10^{12} cm^{-2}, respectively.

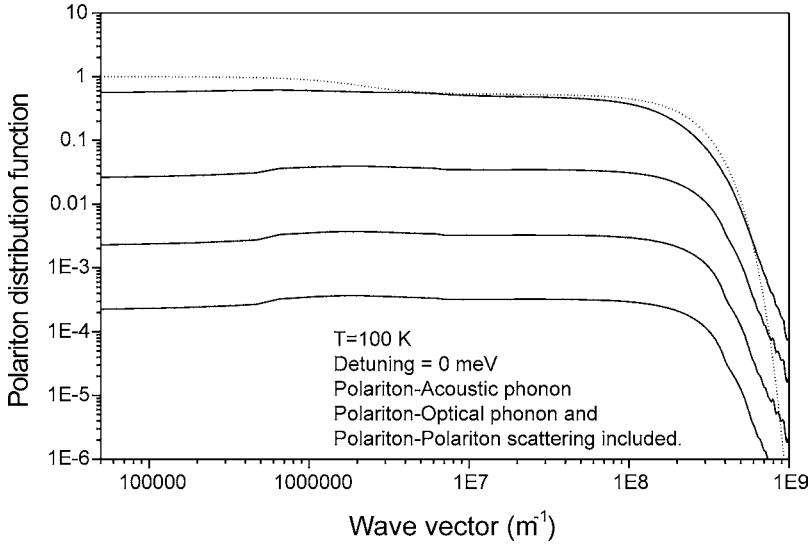

Fig. 4.8. Same as Figure 4.5 but using $T = 100$ K. Densities achieved are: 8.78×10^9, 8.76×10^{10}, 8.66×10^{11}, 7.84×10^{12} cm^{-2}, respectively.

around $k = 0$. The ground-state depletion is indeed larger when one goes towards negative detuning. There is an optimum detuning at each temperature which provides a maximum ground-state population. Empirically, the condition is that the deepness of the polariton trap should be roughly equal to $k_B T$ (if $k_B T$ is larger than the inhomogeneous broadening). At 10 K, $k_B T$ is of the order of 1 meV, comparable with the inhomogeneous broadening we consider. The deepness of the trap should therefore be of the order of 1 meV which is less than the half of the Rabi splitting and corresponds to a positive detuning in the range 5–10 meV. At 100 K, $k_B T$ is of the order of 8 meV, which corresponds to a small negative detuning. An interesting feature of Figure 4.8 is that the distribution functions are thermal at the lattice temperature in the large wave-vector region. However, a bottleneck effect remains visible, that points out the weak efficiency of phonon-assisted relaxation in the central zone.

4.3.2. PRESENTATION OF RECENT PL RESULTS, COMPARISON WITH THEORY

PL experiments give direct access to the polariton distribution function in the strongly-coupled zone. The rest of the distribution function is inaccessible from classical optical spectroscopy techniques and remains unknown. This represents a huge difficulty. Figures 4.9 and 4.10 show angular-dependent PL experiments

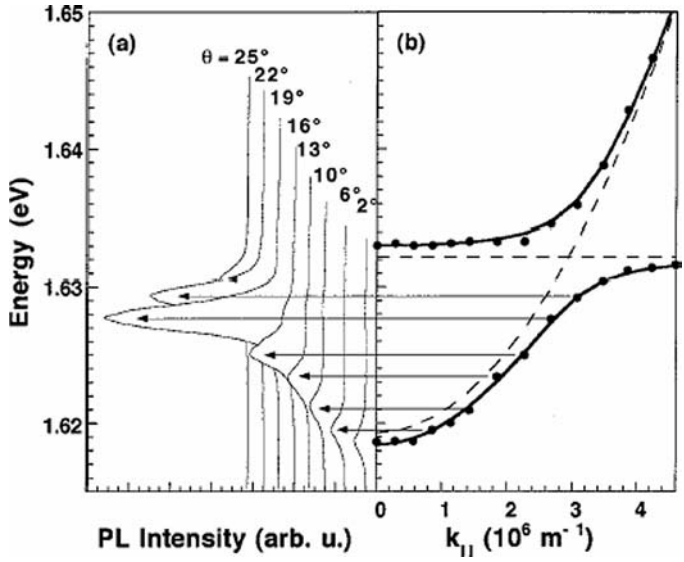

Fig. 4.9. Angle-resolved PL emission spectra of a CdTe based microcavity for a negative detuning of 12.9 meV. Note the sharp intensity maximum around 20 degrees. From [18].

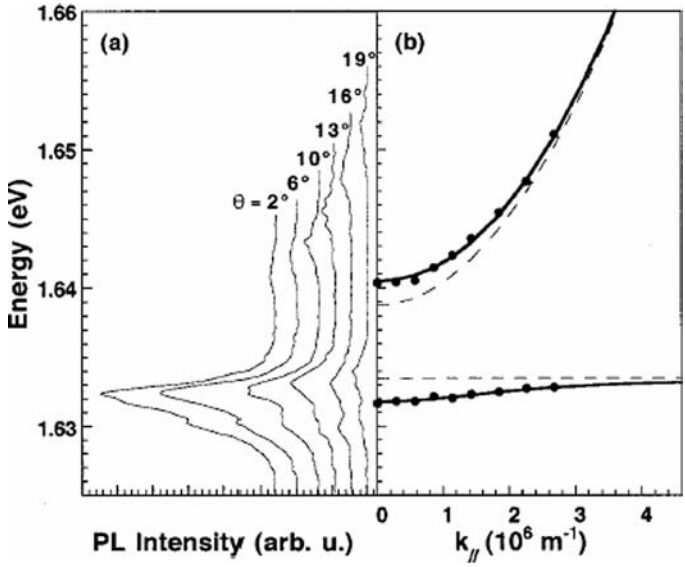

Fig. 4.10. The same as Figure 4.9 but for a positive detuning of 5.3 meV. The distribution function looks thermalised. From [18].

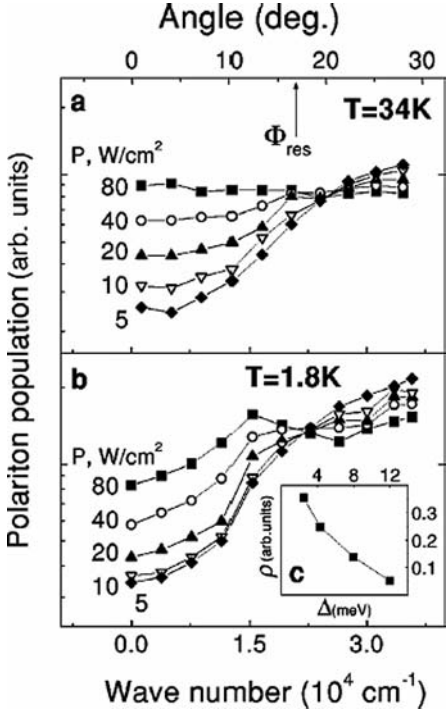

Fig. 4.11. Polariton distribution function for different excitation densities at (a) $T = 34$ K, (b) $T = 1.8$ K. (c) Ratio of polariton populations at the ground state and in the reservoir versus detuning, for low excitation and $T = 1.8$ K. The structure is a GaAs-based cavity at negative detuning. From [19].

[18] recorded for negative and positive detuning on a CdTe microcavity. A pronounced bottleneck effect is present in the negative detuning case (Figure 4.9), whereas it is relaxed for positive detuning, in qualitative agreement with numerical simulations. Similar experiments have been performed on GaAs-based microcavities for various excitation powers, detuning and temperatures [19,20]. Figures 4.11 and 4.12 concern both the same GaAs-based cavity with a splitting of 6.8 meV. Figure 4.11 shows the polariton distribution function versus pumping for two different temperatures, and for a negative detuning. In agreement with the theory, the bottleneck reduces when pumping increases. Also, the bottleneck is much weaker at higher temperature. Figure 4.12 shows polariton distribution functions versus pumping power for three different negative detunings (-13, -8 and -3 meV). Once again, the bottleneck reduces when moving to less negative detuning. The maximum of the distribution function also goes to a lower emission angle when pumping or detuning increases. However, strong coupling always col-

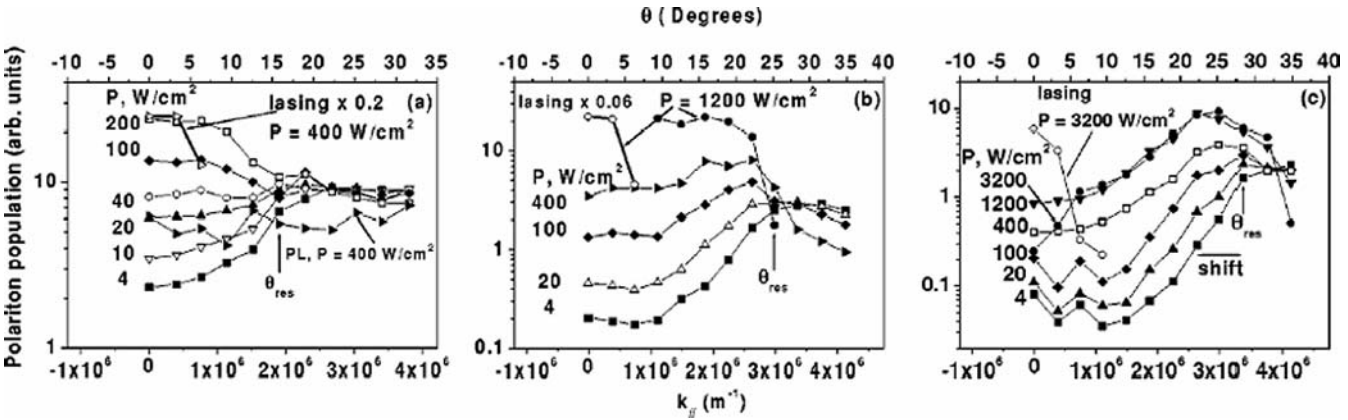

Fig. 4.12. Polariton distribution functions for detunings equal −3, −8.7 and −13.5 meV for (a), (b) and (c), respectively. The bottleneck is suppressed well below the lasing threshold in (a), only very close to threshold in (b), whereas in (c) the low k states are still depleted relative to the states with high k even above the stimulation threshold. The structure considered is the same GaAs based cavity as for Figure 4.11. From [20].

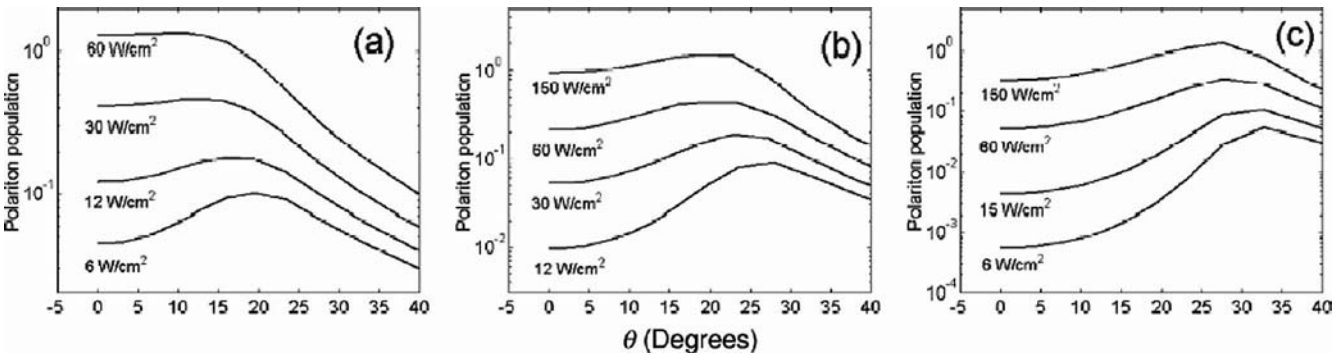

Fig. 4.13. Calculated polariton distribution functions for detunings equal -3, -8.7 and -13.5 meV for (a), (b) and (c), respectively. Polariton–acoustic phonon and polariton–polariton scattering are included in the calculation. The structure is the same as for Figures 4.11 and 4.12. From [20].

lapses before a complete bottleneck removal. Also, stimulated scattering is not observed within the strong-coupling regime. Normal lasing takes place for the higher pumping power used. The emission versus pumping dependence is found to be super-linear but not quadratic, showing the combined influence of phonon–polariton and polariton–polariton scattering processes. These experimental results have been directly compared with simulations based on Boltzmann equations [20] (Figure 4.13). Polariton–acoustic phonon and polariton–polariton scattering were taken into account. The agreement between theory and experiment is extremely good. However, one should bear in mind that only a very small part of the dispersion relation is compared. An important question is to ask whether a temperature can be associated with the dark exciton gas, and what is this temperature. Results of simulation seem to show that a temperature is not so easy to define and that such a temperature is nevertheless much higher than the lattice temperature. Once again, such a statement cannot be supported by direct measurements of the distribution function. Other works than those presented here have been performed in this field. They address more precisely the achievement of polariton stimulated scattering and will be addressed in Chapter 6.

4.4. Conclusions

PL experiments represent one of the most common ways to access information on relaxation processes in heterostructures. The peculiar shape of the polariton dispersion leads to the originality and beauty of these processes in microcavities. In this chapter we have emphasised these specifics, neglecting early processes following optical excitation such as exciton formation. The shape of the dispersion, the finite particle lifetime, their self-interaction, and their interaction with the lattice are described in the framework of a semi-classical formalism based on the numerical solution of the Boltzmann equations. Results obtained are in agreement with existing experimental data. These data show that a pronounced kinetic blocking of the particle relaxation takes place at the edge of the strongly-coupled zone of reciprocal space. This kinetic blocking is called the bottleneck effect. It represents a huge difficulty on the way to achieving polariton Bose condensation and polariton lasing (see Chapter 6). Another interesting result presented in this chapter is that dark excitons are not thermalised at the lattice temperature when experiments are performed at liquid helium temperature. This result cannot be directly confirmed by optical measurements. This statement is, however, supported by the fast destruction of the strong-coupling regime when pumping power is increased. All these results clearly demonstrate that polariton Bose condensation is hardly achievable in existing GaAs- or CdTe-based microcavities that are non-resonantly pumped. Such an achievement would require the use of alternative

spectroscopy techniques or of alternative structures. The solutions that have been proposed, and which we will develop in Chapter 6, are:

(1) Resonant injection of cold polaritons within the lower polariton branch [21].
(2) The use of higher temperature and densities in microcavities made of larger band-gap materials (ZnSe, GaN, ZnO) [3,22].
(3) The use of structures specifically designed to speed up relaxation processes, such as microcavities containing a cold carrier gas [8,9].

References

1. See, for example, J. Shah, "Ultrafast Spectroscopy of Semiconductors and Semiconductor Nanostructures", 2nd edition. Springer, 1999.
2. R. Houdré, C. Weisbuch, R. P. Stanley, U. Oesterle, P. Pellandini, M. Ilegems, Measurements of cavity–polariton dispersion curve from angle resolved photoluminescence experiments, *Phys. Rev. Lett.* 73, 2043 (1994).
3. A. Kavokin, G. Malpuech, F. P. Laussy, Polariton lasers and polariton superfluidity in microcavities, *Phys. Lett. A* 306, 187 (2003).
4. F. Tassone, C. Piermarocchi, V. Savona, A. Quattropani, P. Schwendimann, Bottleneck effects in the relaxation and photoluminescence of microcavity polaritons, *Phys. Rev. B* 56, 7554 (1997).
5. V. M. Agranovich, V. L. Ginzburg, "Spatial Dispersion in Crystal Optics and the Theory of Excitons". Interscience Publ., London, 1966.
6. See, for example, P. E. Selbmann, M. Gulia, F. Rossi, E. Molinari, P. Lugli, Coupled free-carrier and exciton relaxation in optically excited semiconductors, *Phys. Rev. B* 54, 4660 (1996); M. Gurioli, P. Borri, M. Colocci, M. Gulia, F. Rossi, E. Molinari, P. E. Selbmann, P. Lugli, Exciton formation and relaxation in GaAs epilayers, *Phys. Rev. B* 58, R13 403 (1998).
7. R. Harel, E. Cohen, E. Linder, A. Ron, L. N. Pfeiffer, Absolute transmission, reflection, and absorption studies in GaAs/AlAs quantum wells containing a photoexcited electron gas, *Phys. Rev. B* 53, 7868–7875 (1996); R. Rapaport, R. Harel, E. Cohen, A. Ron, E. Linder, L. N. Pfeiffer, Negatively charged quantum well polaritons in a GaAs/AlAs microcavity: An analog of atoms in a cavity, *Phys. Rev. Lett.* 84, 1607 (2000).
8. G. Malpuech, A. Kavokin, A. Di Carlo, J. J. Baumberg, Polariton lasing by exciton–electron scattering in semiconductor microcavities, *Phys. Rev. B* 65, 153310 (2002).
9. A. Qarry, G. Ramon, R. Rapaport, E. Cohen, A. Ron, A. Mann, E. Linder, L. N. Pfeiffer, Nonlinear emission due to electron–polariton scattering in a semiconductor microcavity, *Phys. Rev. B* 67, 115320 (2003); A. I. Tartakovskii, D. N. Krizhanovskii, G. Malpuech, M. Emam-Ismail, A. V. Chernenko, A. V. Kavokin, V. D. Kulakovskii, M. S. Skolnick, J. S. Roberts, Giant enhancement of polariton relaxation in semiconductor microcavities by polariton–free carrier interaction: Experimental evidence and theory, *Phys. Rev. B* 67, 165302 (2003); P. G. Lagoudakis, M. D. Martin, J. J. Baumberg, A. Qarry, E. Cohen, L. N. Pfeiffer, Electron–polariton scattering in semiconductor microcavities, *Phys. Rev. Lett.* 90, 206401 (2003).
10. G. E. Uhlenbeck, L. Gropper, The equation of state of a non-ideal Einstein–Bose or Fermi–Dirac gas, *Phys. Rev.* 41, 79 (1932).
11. T. Freixanet, B. Sermage, J. Bloch, J. Y. Marzin, R. Planel, Annular resonant Rayleigh scattering in the picosecond dynamics of cavity polaritons, *Phys. Rev. B* 60, R8509 (1999); W. Langbein, J. M. Hvam, Elastic scattering dynamics of cavity polaritons: Evidence for time-energy uncertainty and polariton localization, *Phys. Rev. Lett.* 88, 047401 (2002).

12. H. Frolich, *Proc. Roy. Soc. A* 160, 230 (1937).
13. G. Ramon, A. Mann, E. Cohen, Theory of neutral and charged exciton scattering with electrons in semiconductor quantum wells, *Phys. Rev. B* 67, 045323 (2003).
14. C. Ciuti, V. Savona, C. Piermarocchi, A. Quattropani, P. Schwendimann, Role of the exchange of carriers in elastic exciton–exciton scattering in quantum wells, *Phys. Rev. B* 58, 7926 (1998).
15. F. Tassone, Y. Yamamoto, Exciton–exciton scattering dynamics in a semiconductor microcavity and stimulated scattering into polaritons, *Phys. Rev. B* 59, 10 830 (1999).
16. D. Porras, C. Ciuti, J. J. Baumberg, C. Tejedor, Polariton dynamics and Bose–Einstein condensation in semiconductor microcavities, *Phys. Rev. B* 66, 085304 (2002).
17. P. Senellart, J. Bloch, B. Sermage, J. Y. Marzin, Microcavity polariton depopulation as evidence for stimulated scattering, *Phys. Rev. B* 62, R16 263 (2000).
18. M. Müller, J. Bleuse, R. André, Dynamics of the cavity polariton in CdTe-based semiconductor microcavities: Evidence for a relaxation edge, *Phys. Rev. B* 62, 16 886 (2000).
19. A. I. Tartakovskii, M. Emam-Ismail, R. M. Stevenson, M. S. Skolnick, V. N. Astratov, D. M. Whittaker, J. J. Baumberg, J. S. Roberts, Relaxation bottleneck and its suppression in semiconductor microcavities, *Phys. Rev. B* 62, R2283 (2000); A. I. Tartakovskii, D. N. Krizhanovskii, V. D. Kulakovskii, Polariton–polariton scattering in semiconductor microcavities: Distinctive features and similarities to the three-dimensional case, *Phys. Rev. B* 62, R13298 (2000).
20. R. Butté, G. Delalleau, M. S. Skolnick, V. N. Astratov, J. J. Baumberg, G. Malpuech, A. Di Carlo, A. V. Kavokin, J. S. Roberts, Transition from strong to week coupling and the onset of lasing in semiconductor microcavities, *Phys. Rev B* 65, 205310 (2002).
21. P. G. Savvidis, J. J. Baumberg, D. Porras, D. M. Whittaker, M. S. Skolnick, J. S. Roberts, Ring emission and exciton-pair scattering in semiconductor microcavities, *Phys. Rev. B* 65, 073309 (2002); H. Deng, G. Weihs, C. Santori, J. Bloch, Y. Yamamoto, Condensation of semiconductor microcavity exciton polaritons, *Science* 298, 199 (2002).
22. G. Malpuech, A. Di Carlo, A. Kavokin, J. J. Baumberg, M. Zamfirescu, P. Lugli, Room-temperature polariton lasers based on GaN microcavities, *Appl. Phys. Lett.* 81, 412 (2002); M. Zamfirescu, A. Kavokin, B. Gil, G. Malpuech, M. Kaliteevski, ZnO as a material mostly adapted for the realization of room-temperature polariton lasers, *Phys. Rev. B* 65, 161205 (2002).

This page intentionally left blank

Chapter 5

Resonant Excitation Case and Parametric Amplification

5.1. Experimental Aspects 148
5.1.1. Early Stage 148
5.1.2. The Savvidis–Baumberg Breakthrough. Experimental Details 151
5.1.3. The *cw* Excitation Case 155
5.1.4. Dressing of the Polariton Dispersion Induced by Stimulated Scattering 156
5.1.5. Spin Selection Rules 158
5.1.6. A Few Other Experimental Results 161
5.2. Theoretical Approach: Semi-Classical Model 164
5.2.1. The Boltzmann Equation 164
5.2.2. Threshold 165
5.3. Theoretical Approach: Quantum Model 166
5.3.1. Diagonalisation of the Exciton–Photon Hamiltonian 166
5.3.2. Polariton–Polariton Interaction 169
5.3.3. Equation of Motion for the Operators $p_{\vec{k}}^{-}$ and $p_{\vec{k}}^{+}$ 170
5.3.4. Three-Level Model 170
5.3.5. Analytical Solution of the Three-Level Model in the Case of *cw* Pumping: The Parametric Oscillation Model 172
5.3.6. Coherence Evolution and Symmetry Breaking 174
5.3.7. Dressing of the Dispersion Induced by Polariton Condensates 178
References 179

The first pump-probe experiments on semiconductor microcavities were performed with two beams under normal or quasi normal incidence [1–3]. The basic idea was to modify the system using an intense pump pulse and to record the resulting polarisation by measuring the reflection, transmission, absorption or scattering of a weak probe pulse. The main objective of these first investigations [1,2] was to elucidate the mechanisms responsible for the loss of the strong-coupling regime. After this early stage, the understanding of non-linear optical properties of microcavities has progressed considerably in the last three years. This progress has been mainly due to use of advanced spectroscopy techniques, allowing one to tune the angle, energy and time delay between pulses independently. The breakthrough came from an experiment performed in 2000 by Savvidis et al. [4], in which a remarkable and unexpected non-linear effect was reported. They excited resonantly with a 1 ps pump pulse in the vicinity of the lower polariton branch inflexion point. In their microcavity this corresponded to an excitation angle of 16.5°. With a controlled delay they excited the lower branch ground state with a weak probe pulse at normal incidence and measured its reflection. This probe

pulse was found to be amplified more than 70 times. The physical process involved in this amplification is the resonant scattering of two pumped polaritons into one "signal polariton" and one "idler polariton". The amplification was found to be huge because the stimulated polariton scattering is resonant, i.e., it conserves both energy and wave-vector. This experiment has shown the bosonic behaviour of cavity polaritons. It has also shown the main mechanisms governing optical non-linearity in microcavities. This discovery has really given a new impulse to the whole microcavity research field. An avalanche of experimental and theoretical work has followed that of Savvidis, revealing rich and deep physical phenomena. The first established results of this ongoing process are reported in this chapter.

In Section 5.1 we review the experimental results obtained in the last ten years. Section 5.1.1 briefly presents the results obtained before 1999 [1–3] using resonant excitation techniques, and what were the main research interests at that time. Section 5.1.2 describes in details the Savvidis experiment [4]. Sections 5.1.3 to 5.1.6 review all further results that have been obtained using the related experimental geometry. Section 5.1.3 describes experiments showing parametric amplification under *cw* excitation. The effect of polariton dispersion dressing is addressed in Section 5.1.4, whereas spin properties are presented in Section 5.1.5. Other interesting results such as temperature and material dependence, disorder impact and future realisation of polariton based devices are discussed in Section 5.1.6. Section 5.1 does not contain many equations but favours a qualitative overview of the current understanding in the field. It is written in order to be easily accessible to non-specialists.

Sections 5.2 and 5.3 present two theoretical models developed to describe the above-mentioned experiments. Section 5.2 shows that the semi-classical Boltzmann equation presented in Chapter 4 can be adapted to describe most of the results obtained experimentally in a very simple and intuitive way. Section 5.3 is devoted to the presentation of the quantum formalism developed by Ciuti and co-workers [5–7]. The main advantage of this formalism with respect to the semi-classical one is that it allows one to account for the dressing of the polariton dispersion correctly, i.e., dressing induced by the strong polariton–polariton interaction.

5.1. Experimental Aspects

5.1.1. EARLY STAGE

The first works [1–3,8], carried out in the second half of the 1990s, mainly addressed the problem of the transition between strong-coupling and weak-coupling regimes. Jahnke et al. [2] performed *cw* resonant pump-probe measurements of

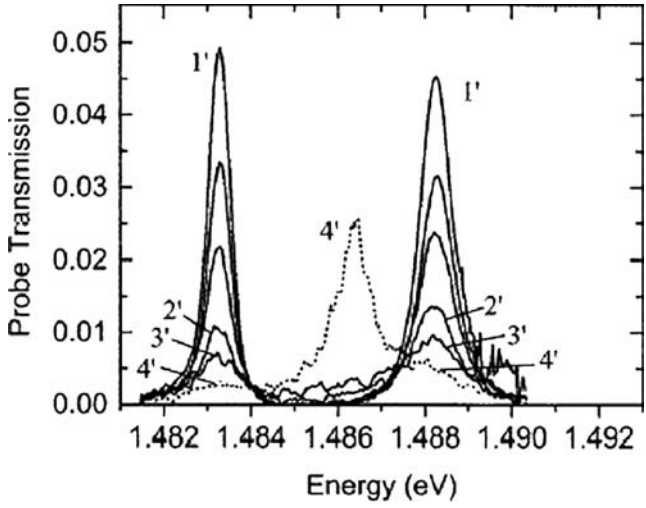

Fig. 5.1. Experimental probe transmission spectra with increasing pumping from $1'$ to $4'$. The pumping is at 787 nm. The sample is a GaAs based microcavity with $In_{0.04}Ga_{0.96}As$ QWs. Stronger pumping than $4'$ results in lasing at a wavelength close to the 40 peak. From [2].

a strongly-coupled GaAs based microcavity. The result is shown in Figure 5.1. The height of the two polariton peaks decreases and their width increases with pump power. Rabi splitting also remains constant up to a critical pumping, where the strong coupling suddenly collapses. This experiment shows that for this particular sample, containing InGaAs QWs, the strong-coupling collapse is due to a carrier-induced exciton line broadening, rather than to a decrease of the oscillator strength. This finding is in agreement with a theoretical model based on the solution of Maxwell's equations including a non-linear QW susceptibility. For a detailed review on the theoretical and experimental aspects of this problem we refer the reader to the work of Khitrova et al. [1] and references therein.

Another interesting effect reported in 1998 [3] is the transition from the polariton doublet to an AC Stark triplet in a strongly-driven microcavity. The experiment consisted in the resonant excitation of the polariton modes with a 100 fs pump of varying intensity and recording the transmission of a 100 fs probe pulse. The results are shown in Figure 5.2. Without pump, one can observe a clear polariton doublet. Then, as the pumping power increases, a third peak appears between the two original peaks, which progressively stray apart. This three-peak spectrum has been interpreted as a Mollow triplet [9]. Qualitatively, this observation can be explained as follows. As discussed in Chapter 3, the QW excitonic state is composed of a collection of localised excitonic states coupled by light.

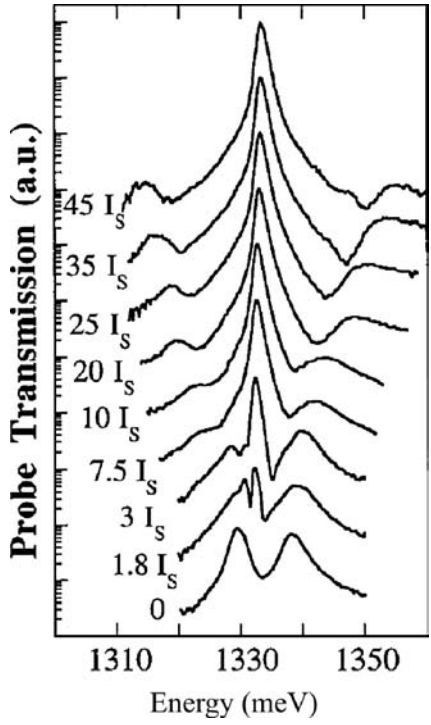

Fig. 5.2. The structure studied is a GaAs based microcavity. The figure shows the transmission spectra of the structure as measured by a weak 100 fs-long probe pulse for different excitation intensities of the 100 fs long pump pulse. From [3].

Individually, these localised states behave as fermions. A localised state cannot be filled by more than two electron–hole pairs (taking into account the spin degeneracy). The QW contains, however, millions of localised states of about the same energy. The light couples these millions of localised states so that polariton states are created. Polariton quantum states can therefore be populated by much more than one polariton, and thus they behave like bosons up to some critical density. In the experiment [3] this critical density is achieved. Localised exciton states having the largest oscillator strength are populated by the pump pulse and cannot absorb light any more. This is why the probe pulse just propagates freely in the optical mode. However, excitons which are in the tail of the dispersion have the smallest oscillator strength. They are less populated and are not saturated, and so they are still able to absorb the light of the probe pulse. This is manifested by two lateral peaks that can be seen in the probe transmission spectra. With pump power increase, the farther from resonance the more excitons that are saturated, accounting for the spreading of the lateral peaks. It

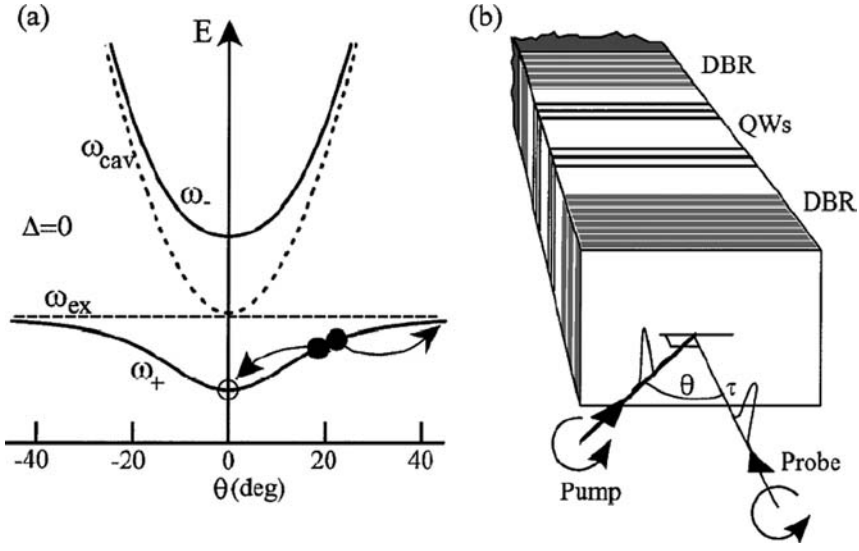

Fig. 5.3. (a) Polariton dispersion relation ($\omega_\pm$) vs incident angle θ at zero detuning. Cavity (exciton) energies $\omega_{\rm cav}, \omega_{\rm ex}$ shown dashed. Probe polariton (○) stimulates the scattering of pump polaritons (●). (b) Sample structure and experimental geometry probed at normal incidence and time delay τ, while changing the pump angle θ. The microcavity was grown by metalorganic vapor-phase epitaxy and consists of two pairs of three 100 Å $In_{0.06}Ga_{0.94}As$ quantum wells separated by 100 Å GaAs barriers, sandwiched between 17 (20) pairs of distributed Bragg reflectors $GaAsAl_{0.18}$ $Ga_{0.98}As$ on top (bottom). The optical cavity length is $3\lambda/2$ and varies across the sample allowing access to both positive and negative detunings. The Rabi splitting is 6.7 meV. From [4].

should be noted that the conclusions of Refs. [2] and [3] are rather contradictory, since in the first case, the pump pulse is found to provoke a line broadening, while in the second case it is found to provoke an oscillator strength screening. The difference probably comes from the different experimental geometries. In [3], pump and probe are pulses and the detection is time-resolved. The triplet is indeed only observable for a pump-probe delay smaller than 1 ps. In [2], however, pump and probe are *cw* and such dynamical effects are not observable.

5.1.2. THE SAVVIDIS–BAUMBERG BREAKTHROUGH [4]. EXPERIMENTAL DETAILS

The microcavity sample used in [4] is sketched in Figure 5.3(b). Figure 5.3(a) shows the experimental geometry used. A pump pulse of 1 ps duration excites resonantly the lower polariton branch with a varying excitation angle. At the same time, a 100 fs probe pulse excites the cavity under normal incidence. The

delay between pump and probe can be modified in a few ps range. The pump intensity has been tuned in order to inject about one million polaritons at the k_p-point of the polariton dispersion curve, whereas the probe pulse injects only a few thousands polaritons within the ground state. What is recorded is the light emitted by the sample under normal incidence, i.e., the reflection of the probe pulse and the eventual non-linear contribution coming from the pump pulse. The physical process which is expected to take place is sketched in Figure 5.3(a). Polaritons with an in-plane wave-vector k_p are resonantly created by the pump pulse near the inflection point of the polariton dispersion relation. Two polaritons from this state can therefore resonantly scatter into one signal polariton ($k = 0$) and one idler polariton ($k = 2k_p$). This process is resonant because it conserves both energy and wave-vector. The driving force of the scattering is the Coulomb interaction between excitons that compose the polaritons (see Chapter 4). We recall that exciton–polaritons represent a superposition of two bosonic states (exciton and photon), and are therefore supposed to be bosons. This means that the scattering towards a state k is amplified by the final state population by a factor $(1 + N_k)$. In the present experiment, the scattering process considered is supposed to be stimulated by the $k = 0$ populations induced by the probe pulse. Figure 5.4 shows on the two bottom curves the reflection of the probe pulse alone and of the pump and probe when pulses are cross-circularly polarised (σ^+, σ^-). In both cases the transmission just shows two unperturbed polariton dips. However, when pulses are co-circularly polarised (σ^+, σ^+) an enormous sharp emission line appears, slightly blue-shifted with respect to the reflection dip. A striking point is that both polariton dips remain perfectly visible while the nonlinear emission takes place, showing that this amplification process happens in the strong-coupling regime. A nonlinear emission coming from the $2k_p$ or "idler" state was also detected. The inset in Figure 5.4 shows the relative intensity of the pump PL, of the probe reflection, and of the pump + probe emission. This last curve shows a gain of about 40 with respect to the bare probe reflection. Figure 5.5 shows, for different exciton–photon detuning, the value of the gain versus pumping angle. For all detuning values the curves have a sharp maximum if the pumping is near the inflexion point of the dispersion relation. The pronounced angular dependence of the gain, together with the existence of a strong idler emission, indicates that the resonant scattering of two pumped polaritons into one signal and one idler polariton is the physical process responsible for this effect. The gain dependence on the probe, and on the probe polarisation, clearly demonstrates that the process is stimulated by the final state population as expected from bosonic scattering. The sharpness of the signal emission shows that the probe laser's induced coherence is kept by polaritons, which also confirms the stimulated character of polariton scattering towards their ground state.

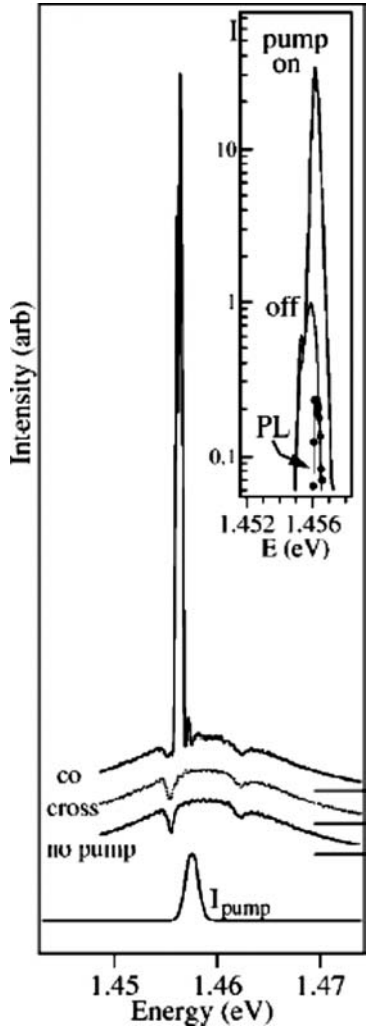

Fig. 5.4. The sample studied is the same as for Figure 5.3. Reflected probe spectra at $\tau = 0$ ps for pump off, co-, and cross-circularly polarized to the probe. Spectral oscillations are caused by interference between reflections from front and back of the sample. Pump spectrum on lower trace. *Inset*: Reflected narrow band probe spectra at $\tau = 0$ ps, with pump pulse on/off, together with pump PL without probe pulse (•). From [4].

5.1.2.1. Results

– This experiment has clearly demonstrated that polaritons behave as bosons in the low-density limit. As we shall discuss in Chapter 6, numerous groups of sci-

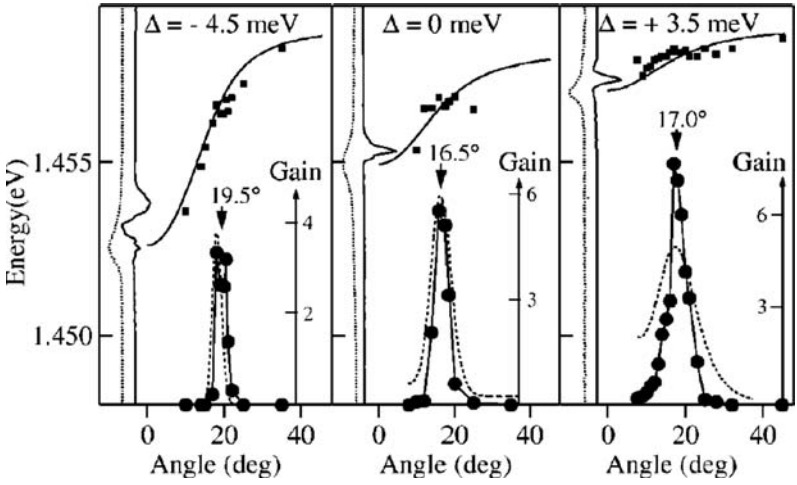

Fig. 5.5. Parametric gain (•) vs angle for detunings $\Delta = -4.5, 0, +3.5$ meV. The energy of the pump pulse (■) is tuned to achieve maximum gain. Fitted dispersion relations (lines) match the reflected probe spectra shown solid (dashed) on the left side for pump on (off). The gain peaks are at $19.5 \pm 1.5°$, $16.5 \pm 2°$, and $17 \pm 2.5°$, respectively, compared to the predicted curves shown dashed, which are at 18.0°, 16.3°, and 17.2°. Pump (probe) powers are 20 W/cm^2 (0.4 W/cm^2). All data are taken on the same sample as in Figures 5.3, 5.4. From [4].

entists have attempted to show evidence of bosonic behavior of excitons since the 1960s (see Chapter 6, or for recent reviews, [10,11]). Exciton and polariton BEC discoveries have been claimed scores of times in the most well-known journals. Most have since been retracted. Finally, the Savvidis–Baumberg experiment represents without any doubt the clearest evidence of the bosonic behavior of an excitonic molecule. It should be mentioned that gains of an order of 5000, together with amplification up to 200 K, have recently been observed [12]. We shall briefly review these results in Section 5.1.4.

– This experiment also provided evidence that polaritons behave as whole particles characterised by a specific dispersion relation. The very peculiar shape of the polariton dispersion is a key element of microcavity physics. Also, phonon scattering is not the only way for polaritons to move along this dispersion relation. Resonant polariton–polariton scattering may play a dominant role in the relaxation processes.
– The origin of the blue shift of the signal line was not understood at that time. It was shown in experimental and theoretical works, which we shall discuss later in the chapter, that this energy renormalisation is a characteristic feature of the parametric scattering of polaritons. It is caused by inter-particle interactions which are strongly enhanced in the resonant configurations and “dress” the polariton dispersion.

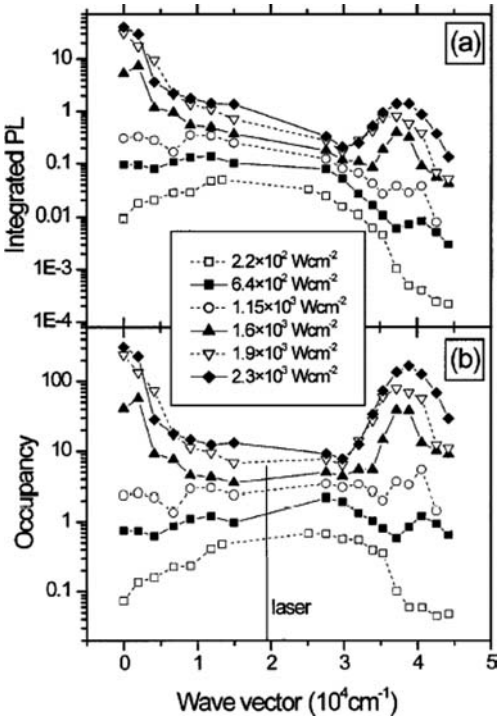

Fig. 5.6. The same GaAs microcavity as for Figures 5.3–5.5 is excited resonantly at the "magic angle" by a *cw* laser. (a) Integrated intensities of PL peaks as a function of in plane k (angle), (b) as (a) but corrected for the photon fraction of the lower branch as a function of k. By normalizing to the measured power of the $k = 0$ feature above threshold, the vertical axis is labeled in terms of state occupancy. From [13].

5.1.3. THE *cw* EXCITATION CASE

A similar experiment has been reported by Stevenson et al. [13], but using a *cw* pump laser, and without a probe. The microcavity used was the same as in [4], and the pump laser resonantly excited the lower polariton branch at the so-called "magic angle", for which a resonant polariton–polariton scattering towards the ground state $k = 0$ is possible. The measured PL intensity as a function of the emission angle and for different exciting power is shown in Figure 5.6(a), while the deduced energy distribution function of polaritons is shown in Figure 5.6(b). The strong-coupling regime has been kept throughout the measurements. One can see at $k = 0$ and $k = 4 \times 10^4$ cm^{-1}, the emission intensity increases by a factor of 10 000, while the pumping power increases only by a factor of 10 (exponential increase). The resonant dissociation of two polaritons excited by pumping light into

one signal polariton and one idler polariton is once again clearly identified. The stimulated nature of the process is also evident. The novelty with respect to the Savvidis–Baumberg results is that the ground state seed is not brought by a probe but spontaneously builds up. A pronounced line-sharpening of the signal has been observed above threshold to stimulation, demonstrating that a large ground state population is achieved. A 1 meV blue shift of the emission line, similar to the one observed in the Savvidis–Baumberg experiment, has also been observed. It was argued [10] that the coherence build-up was induced by the exciting laser through a "parametric amplification phenomena". This interpretation seems to us misleading. Spontaneous scattering of two pumped polaritons populates the ground state. Above some threshold the spontaneous scattering is strong enough to make the ground-state population larger than one, which switches on the stimulated scattering. Below the threshold, the ground-state emission line is wide and incoherent. Above the threshold, the seed forms spontaneously and has presumably a random phase. The phase of the seed varies from experiment to experiment and is unrelated to the pump laser phase. In our opinion, this experimental finding manifests the "spontaneous symmetry breaking" [10], and therefore represents experimental evidence of the spontaneous build up of the Bose coherence. It is an out-of-equilibrium phase transition in much the same way as the laser and by definition cannot be considered as a Bose–Einstein condensation. We shall further comment on this in Section 5.3.6, and we shall also return to the notion of "spontaneous symmetry breaking" and the Bose phase transition in Chapter 6.

5.1.4. DRESSING OF THE POLARITON DISPERSION INDUCED BY STIMULATED SCATTERING

As mentioned in Sections 5.1.2 and 5.1.3, an important feature of the experiments of Savvidis–Baumberg and Stevenson that was not immediately understood was the blue shift of the signal line above threshold. At first glance, this shift may be attributed to a decrease of the Rabi splitting induced by the high carrier density introduced in the QWs by optical pumping. This explanation is, however, ruled out by the fact that the upper polariton branch does not move. This shift can rather be attributed to the energy renormalisation induced by inter-exciton interactions. Let us consider $N \gg 1$ particles whose interaction is described by a potential M. The interaction energy of a single particle with all the others is simply given by $(N-1)M \approx NM$. M is the polariton–polariton matrix element of interaction and is given by the formula (4.2.27). It is approximately equal to $1.25 \times 10^{-11}/S$ in meV in GaAs, where S is a normalisation area (in cm^2). So, the ground state is shifted by $1.25 \times 10^{-11} n$ meV, where n is the total polariton density. The shift is equal to 1 meV for $n = 8 \times 10^{10}$ polaritons/cm^2, which corresponds to 1.3×10^{10} excitons/cm^2 and per QW in the six-QW structure of [4,13]. This density is below the bleaching threshold for excitons, i.e., approximately

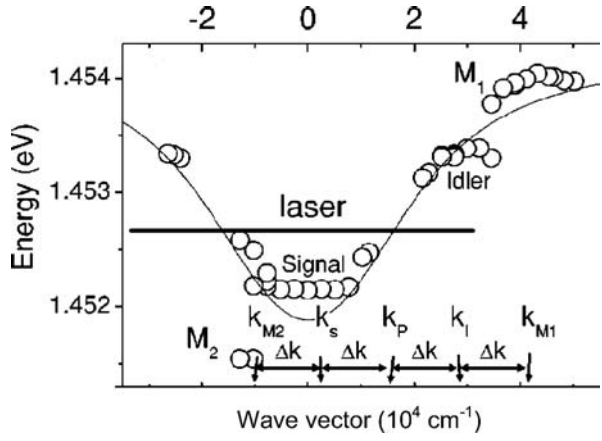

Fig. 5.7. The solid line is the lower polariton branch of a GaAs based cavity. Open circles show the dispersion of emission maxima detected. The bold line shows the laser energy. From [14].

5×10^{10} excitons/cm^2 per well in such structures. It is also in good agreement with the density estimated experimentally. However, precise measurements of the whole dispersion have shown that interactions between particles do not only lead to a shift, but rather to a complete change of the dispersion relation. Figure 5.7 shows the dispersion followed by emission peaks during an experiment performed under *cw* excitation [14]. One can observe a flattening of the dispersion around the ground state, and the appearance of off-branch extra peaks, having wave-vectors $3k_{\text{pump}}$ and $-k_{\text{pump}}$. A quite complete theoretical description of these phenomena has been given in [7] and will be presented in Section 5.3.7. For now we just give a qualitative interpretation. Stimulated scattering macroscopically populates the signal and idler states while the pump state is strongly populated by the laser pump. Therefore, a process:

2 polaritons (0) $\rightarrow$ 1 polariton (k_p) + 1 polariton $(-k_p)$ can conserve energy only if the polariton state $(-k_p)$ is completely out of the dispersion (see Figure 5.7). This non-resonant process may, however, occur if it is fast enough. In such a case the energy conservation rule no longer strictly applies. Following the fourth Heisenberg inequality, the time energy relation reads $\Delta E/R \geqslant \hbar$, where ΔE is the energy distance between the emitting polariton state $-k_p$ and the dispersion relation, and R is the transition rate of the scattering process. This rate is given by (see Chapter 4 and Section 5.2)

$$R = N_0^2 N_p \frac{4\pi}{\hbar} \frac{|M|^2}{\pi\hbar\Gamma}, \tag{5.1.1}$$

where Γ is the decay rate of the polariton state, which is, as mentioned in Section 4.2.4, twice larger than the energy width γ of the polariton state.

Considering realistic parameters: $N_0 = 4 \times 10^3$, $N_p = 10^6$, $\hbar\Gamma = 2$ meV and an exciting laser spot size of 100 μm, we find $\Delta E \geqslant 6$ meV. This means that such strongly-driven scattering can give rise (and actually gives rise) to an emission line 6 meV from the dispersion. The flattening of the dispersion has the same origin. The renormalisation of the dispersion relation by a macroscopically populated state is well known in the theory of Bose condensation of interacting particles. In the Bose condensation case only the ground state is macroscopically populated. Because of the inter-particle interaction, the elementary excitations of the ground state are no longer single excited particles, but rather collective modes. These collective modes behave like sound waves and have a linear dispersion around the ground state rather than a quadratic one [15]. Here the situation is more complicated since there are *a priori* three strongly-occupied states which are interacting and dressing the polariton dispersion. We shall return to consider this more fully in Section 5.3.7 and Chapter 6.

5.1.5. SPIN SELECTION RULES

In [4], a circularly-polarised (σ^+) pump excited the cavity at the "magic angle", while a circularly-polarised (σ^+) probe pulse generated polaritons in the ground state that stimulated resonant scattering of polaritons created by the pump pulse to the probed state (at $k = 0$). At first glance, it seemed that the scattering of polaritons from the pumped state towards the ground state could only happen if the pump and the probe were co-circularly polarised (both σ^+, for example). In case of cross-circularly polarised light no stimulation happened. It thus seemed possible to describe all the intermediate situations where both pump and probe are elliptically polarised by simply decomposing the pulse pump into σ^+ and σ^-. However, this picture has been completely ruled out by recent experimental results of Lagoudakis et al. [16], who have reported extremely unusual polarisation properties of a microcavity excited resonantly at the "magic angle". Throughout their experiment the polarisation of the probe pulse was kept right circular, whereas the pump polarisation was changed from right- to left-circular passing through elliptical and linear polarisation, hence varying linearly the relative spin populations of the pump-injected polaritons while keeping the pump intensity constant. In order to keep track of the polarisation of the different injected and emitted beams they have analysed each polarization state using three Stokes parameters, which correspond to the following polarisation degrees:

$$S^x = \frac{I_x - I_y}{I_x + I_y}, \qquad S^y = \frac{I_{x+y} - I_{x-y}}{I_{x+y} + I_{x-y}}, \qquad S^z = \frac{I_{\sigma^+} - I_{\sigma^-}}{I_{\sigma^+} + I_{\sigma^-}}, \tag{5.1.2}$$

where I_x, I_y, I_{x+y}, I_{x-y} are the intensities of light in x, y, $x + y$, $x - y$ linear polarisations, respectively, and I_{σ^+}, I_{σ^-} are the circular components. In this way, one can express any polarisation state as a vector in an orthogonal basis and

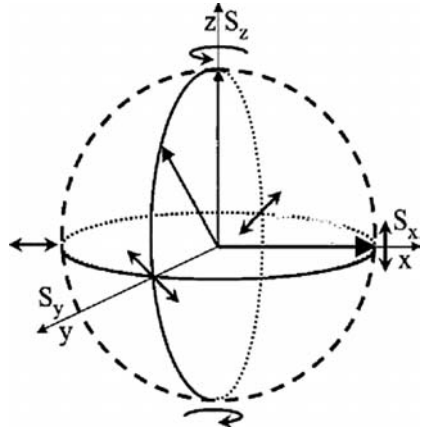

Fig. 5.8. A Poincaré sphere with a pseudospin. The equator of the sphere corresponds to different linear polarisations, while the poles correspond to two circular polarisations.

project it in the 3D polarisation space, also known as Poincaré sphere, as shown in Figure 5.8. Each of the Stokes parameters can be associated with a pseudospin S projection on three coordinate axes. Thus, throughout the experiment the polarisation vector of the probe pulse lies on the north pole of the Poincaré sphere. The polarisation state of the pump pulse moves along the meridian of the Poincaré sphere which passes through the equator at the states that corresponds to the horizontal and vertical linear polarisations. The pumping light is characterised by its circular polarisation degree (circularity)

$$\rho = \frac{I^+ - I^-}{I^+ + I^-}, \tag{5.1.3}$$

where I^+ is the intensity of the σ^+ component of pump pulse and I^- is the intensity of its σ^- component. The experimental values of the components that correspond to the three polarisation degrees versus ρ for the emitted signal are presented in Figure 5.9 (a)–(c). To briefly summarise these results, in the case of a linearly-polarised pump pulse and circularly-polarised probe pulse the observed signal was linearly polarised, but with a plane of polarisation rotated by 45 degrees with respect to the pump polarisation. In the case of elliptically-polarised pump pulse the signal also became elliptical, while the direction of the main axis of the ellipse rotated as a function of the circularity of the pump. In the case of a purely circular pump, the polarisation of the signal was also circular, but its intensity was half that found for a linear pump. The polarisation of the idler emission emerging at roughly twice the magic angle showed a similar behaviour, although in the case of a linearly-polarised pump the idler polarisation was rotated by 90 degrees with respect to the pump polarisation. We mentioned a part of these experimental ob-

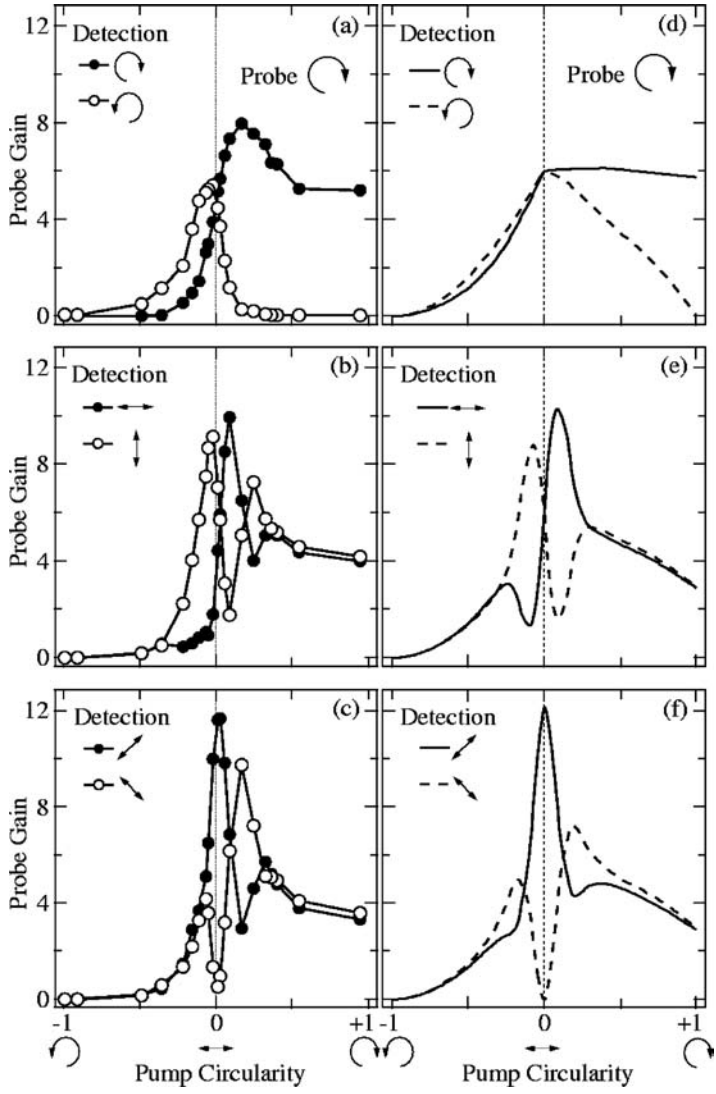

Fig. 5.9. Experimental (a–c) and theoretical (d–f) intensities of circularly (a, d) and linearly (b, c, e, f) polarized components of the light emitted by a microcavity in normal to the surface direction as a function of circular polarisation degree of the pumping light. From [17].

servations in Section 2.5. The very fast rotation of the signal polarisation versus pump circularity is a manifestation of the resonant Faraday rotation effect. Indeed, while the pump is diagonal σ^+ and σ^- populations are unbalanced. This splitting

has been detected experimentally and is shown in Figure 2.12(b). This splitting provokes a dephasing of the components of the elliptically-polarised light which are propagating inside the cavity. This dephasing finally results in a fast polarisation rotation. An attempt to describe theoretically these data has been presented in [17], from where Figure 5.9 (d)–(f) are taken. The main ingredient of this formalism is the accounting of the splitting shown in Figure 2.12(b). The complexity of other polarisation effects revealed in this experiment, as well as in polarised photoluminescence under non-resonant excitation [18], will be commented on in Section 6.4.

5.1.6. A FEW OTHER EXPERIMENTAL RESULTS

5.1.6.1. Influence of Polariton–Polariton Scattering on the Upper Branch Ground-State Emission [19]

The experiment performed by Huang et al. is sketched in Figure 5.10. They have resonantly pumped two points of the lower polariton branch with excitation angles of 45 and -45 degrees. Simultaneously, a probe pulse seeded the lower-branch ground state. The resonant scattering process that was expected to be stimulated was

$$1\ \text{LP}\ (45\ \text{degrees}) + 1\ \text{LP}\ (-45\ \text{degrees}) \rightarrow 1\ \text{LP}\ (0\ \text{degrees}) + 1\ \text{UP}\ (0\ \text{degrees}).$$

This process conserves both energy and in-plane wave-vector, and is expected to enhance the upper branch emission. The effect observed was rather weak, however. An increase of a few tens of percent has been obtained in the best case.

5.1.6.2. Temperature and Material Dependence [12]

The authors of [12] reproduced the experiment [4], but using four different cavities and making temperature-dependent measurements. One structure contained InGaAs QWs, two others contained GaAs QWs, and the last one contained CdTe QWs. Due to the large number of QWs embedded, the Rabi splitting was larger than 15 meV in all samples. Figure 5.11(a) shows the temperature dependences of the parametric gain versus temperature reported in [12]. The parametric gain in the cavities having large polariton splittings is robust enough to survive up to 125 K in the GaAlAs samples and up to 220 K in the CdTe one. Remarkably, the two GaAlAs samples with 12 and 36 wells show a very similar temperature cutoff of the gain, although they have a different polariton splitting. This feature indicates that beyond a certain point the cutoff temperature no longer enhances with the polariton splitting, and is limited by some intrinsic parameter of the material. The CdTe sample, having a polariton splitting only 25% larger than the GaAlAs one, sustained the parametric amplification up to almost twice the temperature.

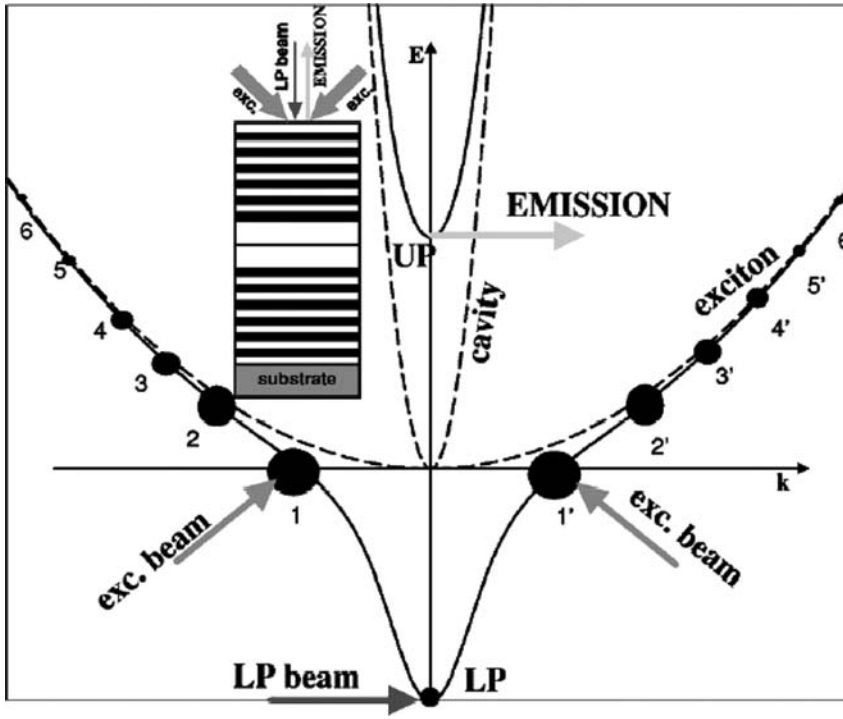

Fig. 5.10. Dispersion of the polariton branches. Exciton (not to scale) and cavity photon (dashed lines) dispersions are shown. The exciton population is depicted by solid circles of proportional size. *Inset*: the cross section of the microcavity structure. Quarter wavelength dielectric stacks DBR's confine the photon inside the cavity, into which a GaAs quantum well, confining the exciton, is embedded. The experimental excitation scheme is also shown. From [19].

What is very different in GaAs and CdTe materials is the exciton binding energy, i.e., the energy separating the quasi-bosonic bound exciton states from the fermionic continuum of unbound electron–hole pairs. In the 7 nm-wide GaAs quantum well the exciton binding energy is about 13.5 meV, while in the CdTe wells it is about 25 meV. The curve recorded from a InGaAs-based microcavity with a 5 meV exciton binding energy only shows the gain up to 50 K, which confirms the tendency mentioned. The dependence of the cutoff temperature (temperature at which gain falls to unity, highest possible operation temperature for the device) on the exciton binding energy appears to be linear, as shown in Figure 5.11(b). Suitable materials to achieve a polariton gain in microcavities at room temperature are II–VI microcavities, based on ZnSe, for instance, which have exciton binding energies as high as 40 meV and can exhibit very large Rabi splittings [20]. GaN-based semiconductor compounds have attracted even more attention

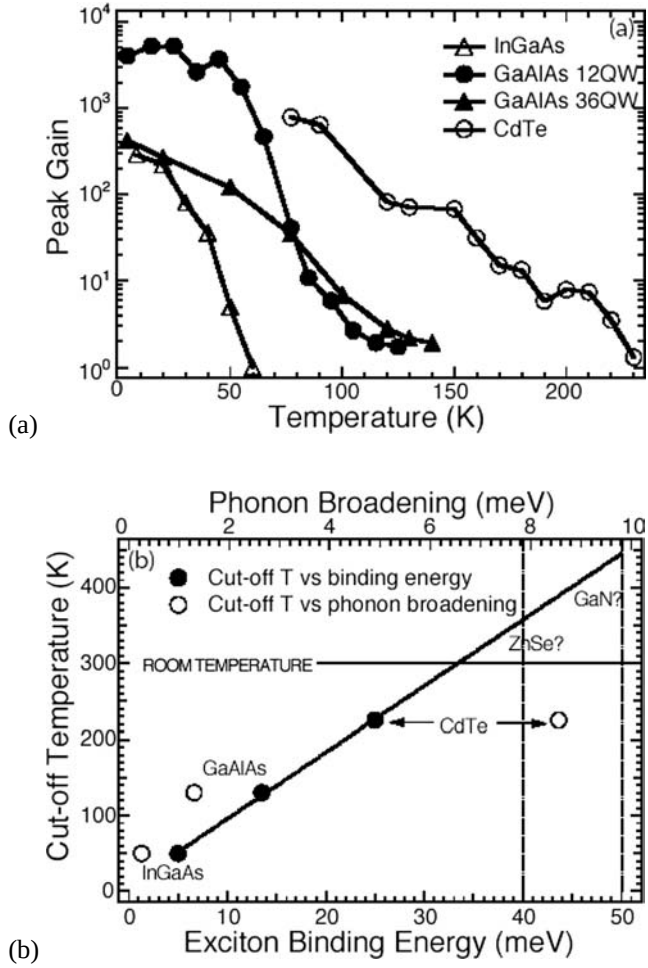

Fig. 5.11. Temperature dependence of parametric gain. (a) Peak gain versus temperature for the different samples. The CdTe cavity is designed to match the exciton energy at high temperatures and below 77 K the exciton–photon resonance is no more achieved. The measurements are taken for the same pump fluence for both GaAlAs samples, but due to the greater threshold for the 36-well sample, at low temperatures the gain is lower than in the 12-well one. (b) Cut-off temperatures for the gain in different materials as a function of the exciton binding energy (lower x-axis, full dots). The dotted line is a linear fit to the data. The inverse logarithmic slope of the last points on each curve has the same dependence on the binding energy. The vertical dashed lines mark the typical exciton binding energies in ZnSe and GaN-based quantum wells. In contrast the cut-off temperature seems not to scale with the exciton-phonon coupling rate (upper x-axis, empty dots). From [12].

due to very large exciton oscillator strengths in them [21]. Intense efforts are concentrating on growth technology in order to improve the sample quality and achieve strong coupling in these microcavities. Realisation of ZnO-based cavities also appears to be a promising direction to follow [22]. The strong-coupling regime at room temperature has already been demonstrated in organic microcavities [23], with huge polariton splittings (100 meV or more). Even if the coherence time of optical excitations in such compounds is very short, the low material cost and simplicity of sample preparation will encourage studies of the ultrafast polaritonic nonlinearities. One should also mention that the impact of the structural disorder on exciton–polariton properties has been carefully studied experimentally [24,25]. A theory describing the disorder effects is presented in Chapter 3 of this book.

5.2. Theoretical Approach: Semi-Classical Model

The goal of this section is to describe parametric amplification experiments [4, 12,13] using the semi-classical Boltzmann equations presented in Chapter 4. The advantages of such a description with respect to the parametric amplifier model (classical or quantum), which will be presented in the later section, is that it allows one to account for stimulated scattering, and to include easily all types of interactions affecting exciton–polariton relaxation. The disadvantage is that dispersion dressing of polaritonic energies, an important feature of parametric amplification, cannot be easily accounted for in this model. It should be mentioned that to our knowledge, this kind of modelling has never before been used to describe the results of parametric amplification experiments.

5.2.1. THE BOLTZMANN EQUATION

The generic Boltzmann equation for a state of wave-vector k is (see Chapter 4, Section 4.2.1):

$$\frac{dn_{\vec{k}}}{dt} = P_{\vec{k}} - \Gamma_{\vec{k}} n_{\vec{k}} - n_{\vec{k}} \sum_{\vec{k}'} W_{\vec{k}\to\vec{k}'}(n_{\vec{k}'}+1) + (n_{\vec{k}}+1)\sum_{\vec{k}'} W_{\vec{k}'\to\vec{k}} n_{\vec{k}'}. \quad (5.2.1)$$

The equation to be solved describing the polariton dynamics is formed by the ensemble of Boltzmann equations written for all allowed values of the in-plane wave-vector. It can be solved numerically as described in Chapter 4, choosing suitable initial conditions. These conditions are, for a pump-probe experiment, $n_0(0) = n_{\text{probe}}$, $n_{\vec{k}_p}(0) = n_{\text{pump}}$ and $P_{\vec{k}} = 0$. For *cw* experiments, these initials conditions are $n_{\vec{k}}(0) = 0$, $P_{\vec{k}_p}(t) = P_0$.

In Chapter 4, cylindrical symmetry of the distribution function was assumed. In the parametric amplification experiments, the resonant excitation conditions

used break this symmetry and a two-dimensional polariton distribution function should be assumed. However, it is clear that just below and above the amplification threshold a good description of the ground-state population can be performed assuming only three states: the ground or signal state, the pump state and the idler state. The main loss processes for these states are therefore the radiative losses and the elastic scattering processes driven by disorder, which can both be included in the same loss constant even if their nature is very different. The radiative loss means disappearance of the particles, while the disorder scattering implies transfer of a particle towards other states that are neglected in this model. The interaction with phonons is in this framework similar to the disorder interaction, and it can also be included as such a loss with its appropriate constant. The phonon contribution is often negligible at low temperatures in typically-used cavities. It may cause a significant broadening of the polariton states in experiments performed at high temperatures. The broadening, or loss parameter, can be written as:

$$\frac{1}{\Gamma_k} = \frac{x_k}{\Delta + \Gamma_{\text{phonons}}} + \frac{(1 - x_k)}{\Gamma_c}, \tag{5.2.2}$$

where Δ is the exciton inhomogeneous broadening, Γ_{phonons} is the phonon-induced broadening, and Γ_c is the cavity photon broadening. At low temperature, $\Gamma_{\text{phonons}} \ll \Delta$. Moreover, in the most of cavity samples studied experimentally, $\Delta \approx \Gamma_c$, which yields $\Gamma_0 \approx \Gamma_p \approx \Gamma_i = \Gamma$. In this framework, the system can be described by a set of three coupled equations:

$$\begin{aligned}
\dot{n}_0 &= P_0 - \Gamma n_0 - \alpha n_0 n_i (n_p + 1)^2 + \alpha (n_0 + 1)(n_i + 1) n_p^2, \\
\dot{n}_p &= P_p - \Gamma n_p + 2\alpha n_0 n_i (n_p + 1)^2 - 2\alpha (n_0 + 1)(n_i + 1) n_p^2, \\
\dot{n}_i &= P_i - \Gamma n_i - \alpha n_0 n_i (n_p + 1)^2 + \alpha (n_0 + 1)(n_i + 1) n_p^2,
\end{aligned} \tag{5.2.3}$$

where $\alpha = \frac{2\pi}{\hbar} \frac{|M|^2}{\pi \hbar \Gamma/2}$. M is the polariton–polariton matrix element of interaction (see Chapter 4), which is here approximately equal to one fourth of the exciton–exciton matrix element of interaction. This system of equations can be easily solved numerically. Moreover, if one consider the *cw* excitation case, $P_0 = P_i = 0$, this gives $n_0 = n_i$. The system (5.2.3) thus becomes:

$$\dot{n}_0 = n_0 \left(-\Gamma - \alpha n_0 (n_p + 1)^2 + \alpha (n_0 + 1) n_p^2 \right) + \alpha n_p^2, \tag{5.2.4a}$$

$$\dot{n}_p = P - \Gamma n_p + 2\alpha n_0^2 (n_p + 1)^2 - 2\alpha (n_0 + 1)^2 n_p^2. \tag{5.2.4b}$$

5.2.2. THRESHOLD

In the stationary regime $\dot{n}_0 = \dot{n}_p = 0$. Before proceeding further with the formalism, we have to discuss how to define correctly the threshold condition for amplification in the stationary case. Very often, it is believed that a good empirical

criterion is that the population of a given state reaches one. Indeed, the evolution equation for the ground-state population formally reads:

$$\dot{n}_0 = W_{\text{in}}(n_0 + 1) - W_{\text{out}} n_0.$$

W_{in} is supposed to include all channels used by incoming polaritons, and W_{out} all channels for their departure from the ground state. The $+1$ in the brackets corresponds to the spontaneous scattering process, n_0 in the brackets describes the stimulated scattering, and $-W_{\text{out}} n_0$ the loss term. Therefore, the condition $n_0 = 1$ means that the stimulation term is as large as the spontaneous scattering term, and that the amplification threshold is reached. This point of view is, however, quite misleading. The equation for the ground-state population can indeed be rewritten as

$$\dot{n}_0 = n_0(W_{\text{in}} - W_{\text{out}}) + W_{\text{in}}.$$

W_{in} remains the spontaneous term, but it is clear the relevant stimulated part of the equation is now $n_0(W_{\text{in}} - W_{\text{out}})$. We shall return to this point in Chapter 6, which is devoted to the study of BEC phenomena. Thus, the threshold is given by the condition $W_{\text{in}} - W_{\text{out}} = 0$. Eq. (5.2.4a) yields in this case:

$$-\Gamma - \alpha n_0 (n_p + 1)^2 + \alpha(n_0 + 1) n_p^2 = 0 \tag{5.2.5}$$

which implies:

$$n_0 = \frac{\alpha n_p^2 - \Gamma}{\alpha(2n_p + 1)}. \tag{5.2.6}$$

n_0 is a population so it should be positive or zero. In the latter case

$$n_p = \sqrt{\frac{\Gamma}{\alpha}}. \tag{5.2.7}$$

Below threshold $n_p \approx P/\Gamma$, which gives:

$$P_{\text{thres}} = \Gamma \sqrt{\frac{\Gamma}{\alpha}} = \Gamma \frac{\hbar\Gamma}{2|M|}. \tag{5.2.8}$$

Assuming an exciting laser spot size of 50 microns, $\hbar\Gamma = 1$ meV and typical GaAs parameters, $P_{\text{threshold}} \approx 10^6 \Gamma \approx 50$ μW. This is in good agreement with experimental data [13].

5.3. Theoretical Approach: Quantum Model

5.3.1. DIAGONALISATION OF THE EXCITON–PHOTON HAMILTONIAN

In this section we derive the exciton–polariton dispersion, treating the exciton–photon system as a quantum two-level system. Effects of the polarisation of light

are neglected here. This method is completely equivalent to the semi-classical description presented in Chapter 1 (Section 1.3). A quantum-mechanical description is convenient to introduce interactions between free polaritons (in Section 5.3.2) and to describe their energy relaxation.

5.3.1.1. Free Excitons and Free Photons

The Hamiltonian for free excitons and cavity photons is:

$$H_0 = \sum_{\vec{k}} E_X(\vec{k}) b_{\vec{k}}^+ b_{\vec{k}} + \sum_{\vec{k}} E_C(\vec{k}) a_{\vec{k}}^+ a_{\vec{k}}. \tag{5.3.1}$$

Operators $b_{\vec{k}}^+$, $b_{\vec{k}}$, $a_{\vec{k}}^+$, $a_{\vec{k}}$ are creation and annihilation operators for excitons and photons, respectively. The in-plane dispersion relation of excitons is

$$E_X(\vec{k}) = E_X(0) + \frac{\hbar^2 k^2}{2m_X} - \frac{i\hbar}{2}\Gamma_X(\vec{k}), \tag{5.3.2}$$

where m_X is the free in plane exciton mass, and Γ_X is a phenomenological decay rate that accounts for the finite linewidth of the exciton resonance.

$$E_C(\vec{k}) = \sqrt{E_C(0)^2 + \frac{\hbar^2 c^2 k^2}{n_C^2}} - \frac{i\hbar}{2}\Gamma_C(\vec{k}), \tag{5.3.3}$$

n_C is the cavity refractive index. $E_C(0) = hc/\lambda_0$ with λ_0 the resonant wavelength of the cavity. $\Gamma_C(\vec{k})$ is the cavity photon escape rate taking into account the possibility of photon tunnelling across the cavity mirrors. Around $k = 0$ the cavity photon dispersion can be approximated by a parabola:

$$E_C(\vec{k}) \approx E_C(0) + \frac{\hbar^2 k^2}{2m_C} - \frac{i\hbar}{2}\Gamma_C(\vec{k}), \tag{5.3.4}$$

where

$$m_C = E_C(0)\frac{n_C^2}{c^2} = \frac{hn_c}{c\lambda}. \tag{5.3.5}$$

This is identical to Eq. (1.3.14).

It should be noted that an Hamiltonian containing dissipative terms (imaginary part of the energy) is not Hermitian, that is in principle incorrect. Such way to treat dissipative processes can nevertheless be used with caution. In the Heisenberg picture which we will use later, one can write equations of motion of annihilation operators using the standard Heisenberg equation. However equations of motion of creation operators must be written using a corrected Hamiltonian H^* where all scalars are replaced by their complex conjugated.

5.3.1.2. Linear Exciton–Photon Coupling

The linear exciton–photon coupling formally reads:

$$H_{XC} = \sum_{\vec{k}} \hbar\Omega a_{\vec{k}}^{+} b_{\vec{k}} + H.c., \tag{5.3.6}$$

$$\Omega = \frac{d}{2\pi a_b^{2D}} \sqrt{\frac{N E_X}{\hbar^2 n_c \lambda_0}}, \tag{5.3.7}$$

where d is the exciton dipole moment and N is the number of QWs within the cavity. Ω is the coupling strength between an exciton and a photon, which is proportional to the exciton oscillator strength and to the number of QWs embedded in the cavity (see Sections 1.3 and 2.1). Coupling between an exciton and a photon state with an in-plane wave-vector $\vec{k}$ can be reduced to a two-level problem, so that the eigenenergies of resulting states can be found by diagonalisation of the matrix:

$$M(\vec{k}) = \begin{pmatrix} E_X(\vec{k}) & \hbar\Omega \\ \hbar\Omega & E_C(\vec{k}) \end{pmatrix}. \tag{5.3.8}$$

The eigenvalues of this matrix are given by

$$\det(M - \lambda I) = 0 \Rightarrow (E_X - \lambda)(E_C - \lambda) - \hbar^2\Omega^2 = 0. \tag{5.3.9}$$

Solutions of this equation are:

$$\begin{aligned} E_U(k) &= \frac{E_C(k) + E_X(k)}{2} + \frac{1}{2}\sqrt{(E_C(k) - E_X(k))^2 + 4\hbar^2\Omega^2}, \\ E_L(k) &= \frac{E_C(k) + E_X(k)}{2} - \frac{1}{2}\sqrt{(E_C(k) - E_X(k))^2 + 4\hbar^2\Omega^2}. \end{aligned} \tag{5.3.10}$$

E_U and E_L are the energies of the upper and lower polariton branches, respectively.

The corresponding eigenvectors are then given by the solutions of:

$$M(k) \begin{pmatrix} X_U(k) \\ C_U(k) \end{pmatrix} = E_U(k) \begin{pmatrix} X_U(k) \\ C_U(k) \end{pmatrix} \tag{5.3.11}$$

with

$$X_U^2 + C_U^2 = 1, \tag{5.3.12}$$

$$\begin{aligned} X_U E_X + C_U \hbar\Omega &= E_U X_U, \\ C_U E_C + X_U \hbar\Omega &= E_U C_U. \end{aligned} \tag{5.3.13}$$

Solving Eqs. (5.3.12), (5.3.13) easily yields:

$$\begin{aligned} C_U &= \frac{2\hbar\Omega}{\sqrt{4\hbar^2\Omega^2 + (E_U - E_X)^2}}, \\ X_U &= \frac{E_U - E_X}{\sqrt{4\hbar^2\Omega^2 + (E_U - E_X)^2}}. \end{aligned} \tag{5.3.14}$$

The same procedure repeated for C_L and X_L yields:

$$X_L = C_U, \qquad C_L = -X_U.$$

$X_{L(U)}$ and $C_{L(U)}$ are the Hopfield coefficients for the upper (lower) polariton branch. $|X|^2$ and $|C|^2$ describe weights of excitonic and photonic parts in each branch. One can check that

$$\begin{aligned} \left|X_U(k)\right|^2 + \left|X_L(k)\right|^2 &= \left|C_U(k)\right|^2 + \left|C_L(k)\right|^2 = \left|X_U(k)\right|^2 + \left|C_U(k)\right|^2 \\ &= \left|X_L(k)\right|^2 + \left|C_L(k)\right|^2 = 1. \end{aligned}$$

One can define upper and lower polariton creation and annihilation operators as:

$$\begin{aligned} p_k &= X_L(k) b_k + C_L(k) a_k^+, \\ p_k^+ &= X_L(k) b_k^+ + C_L(k) a_k, \\ pu_k &= X_U(k) b_k + C_U(k) a_k^+, \\ pu_k^+ &= X_U(k) b_k^+ + C_U(k) a_k. \end{aligned} \tag{5.3.15}$$

Therefore, the polariton Hamiltonian reads:

$$H_p = \sum_{\vec{k}} E_L(k)\, p_k^+ p_k + \sum_{\vec{k}} E_U(k)\, pu_k^+ pu_k. \tag{5.3.16}$$

The Hamiltonian is now diagonal, and its eigenstates are cavity polaritons.

5.3.2. POLARITON–POLARITON INTERACTION

An exciton–polariton wave-function is a linear superposition of photon and exciton eigenfunctions. Photons do not interact with each other directly. The Coulomb interaction between carriers is responsible for an effective exciton–exciton interaction that can be described by a Hamiltonian:

$$H_{XX} = \frac{1}{2} \sum_{\vec{k},\vec{k}',\vec{q}} V_{\vec{q}}\, b_{\vec{k}+\vec{q}}^+ b_{\vec{k}'-\vec{q}}^+ b_{\vec{k}} b_{\vec{k}'}. \tag{5.3.17}$$

It is often considered that this interaction is negligible for the upper polariton branch, which is mainly photon-like. Therefore, in the polariton basis the

polariton–polariton interaction Hamiltonian reads:

$$H_{PP} = \frac{1}{2} \sum_{\vec{k},\vec{k}',\vec{q}} V^{PP}_{\vec{q},\vec{k},\vec{k}'} p^{+}_{\vec{k}+\vec{q}} p^{+}_{\vec{k}'-\vec{q}} p_{\vec{k}} p_{\vec{k}'}, \tag{5.3.18}$$

with

$$V^{PP}_{\vec{q},\vec{k},\vec{k}'} = V_{\vec{q}} X_L(\vec{k}+\vec{q}) X_L(\vec{k}'-\vec{q}) X_L(\vec{k}) X_L(\vec{k}'), \tag{5.3.19}$$

and the total Hamiltonian reads:

$$H = H_p + H_{PP}. \tag{5.3.20}$$

It should be noted that the interaction of polaritons with phonons is neglected here.

5.3.3. EQUATION OF MOTION FOR THE OPERATORS $p_{\vec{k}}$ AND $p^{+}_{\vec{k}}$

To obtain the equation of motion for polariton operators $p_{\vec{k}}$ and $p^{+}_{\vec{k}}$ we write the Heisenberg equation:

$$\begin{aligned} i\hbar \frac{dp_{\vec{k}}}{dt} &= [p_{\vec{k}}, H] = E_L(k) p_{\vec{k}} + \sum_{\vec{k}',\vec{k}''} E^{\text{int}}_{\vec{k},\vec{k}',\vec{k}''} p^{+}_{\vec{k}'+\vec{k}''-\vec{k}} p_{\vec{k}'} p_{\vec{k}''} + P(\vec{k}), \\ i\hbar \frac{dp^{+}_{\vec{k}}}{dt} &= \left[p^{+}_{\vec{k}}, H^{*}\right] \\ &= -E^{*}_{L}(k) p^{+}_{\vec{k}} - \sum_{\vec{k}',\vec{k}''} E^{\text{int}^{*}}_{\vec{k},\vec{k}',\vec{k}''} p^{+}_{\vec{k}'} p^{+}_{\vec{k}''} p_{\vec{k}'+\vec{k}''-\vec{k}} + P^{+}(\vec{k}), \end{aligned} \tag{5.3.21}$$

where

$$E^{\text{int}}_{\vec{k},\vec{k}',\vec{k}''} = \frac{1}{2}\left(V^{PP}_{\vec{k}',\vec{k}'',\vec{k}-\vec{k}'} + V^{PP}_{\vec{k}',\vec{k}'',\vec{k}''-\vec{k}}\right), \tag{5.3.22}$$

and $P(\vec{k})$ is an operator describing the polarisation amplitude induced by an external pumping field.

5.3.4. THREE-LEVEL MODEL

The three-level model was proposed by Ciuti et al. [5] in the first theoretical paper devoted to the description of the Savvidis–Baumberg [4] experiment. It used Eqs. (5.3.21), (5.3.22) as a starting point. Then, only the three most important states were considered, namely the pumped state k_p, the ground or signal state 0, and the idler state $2k_p$. They assumed these three states to be coherently and macroscopically populated. In other words, they assumed these states to behave as classical coherent states, and they replaced the operators

$p_0, p_{k_p}, p_{2k_p}, p_0^+, p_{k_p}^+, p_{2k_p}^+$ by complex-numbers $P_0, P_{k_p}, P_{2k_p}, P_0^*, P_{k_p}^*, P_{2k_p}^*$. This Ansatz was proposed in the 1950s by Bogoliubov [15] (see also Chapter 6 of this book) to describe Bose condensation phenomena. Bogoliubov diagonalised a Hamiltonian equivalent to the Hamiltonian (5.3.20), considering the existence of a macroscopically occupied ground state. He assumed that only interactions involving the ground state were important. He also proposed to neglect fluctuations of the ground state because it was macroscopically occupied. The argument was that for the ground state $[a, a^+] = 1 = aa^+ - a^+a \ll a^+a \sim N$, where N is the ground state population. Therefore, the non-zero value of the commutator can be neglected and the ground-state operators can be replaced by complex numbers. In [5] the same kind of approximation was proposed, but three condensates instead of one were assumed to be present inside the system.

In this section, we consider that only the pumped state operators reduce to complex numbers, keeping the operator nature of signal and idler. In this framework, the system of Eqs. (5.3.21) can be reduced to just three equations:

$$\frac{\hbar}{i}\dot{p}_0 = \widetilde{E}_L(0)\,p_0 + E_{\text{int}}\,p_{2k_p}^+\,P_{k_p}^2 + \text{Probe}(t), \tag{5.3.23}$$

$$\frac{\hbar}{i}\dot{P}_{k_p} = \widetilde{E}_L(k_p)\,P_{k_p} + E_{\text{int}}\,P_{k_p}^*\,p_0\,p_{2k_p} + \text{Pump}(t), \tag{5.3.24}$$

$$\frac{-\hbar}{i}\dot{p}_{2k_p}^+ = \widetilde{E}_L^*(2k_p)\,p_{2k_p}^+ + E_{\text{int}}^*\,p_0\,P_{k_p}^{*2}, \tag{5.3.25}$$

where

$$\begin{aligned}
\widetilde{E}_L(0) &= E_L(0) + 2V_{0,k_p,0}^{PP}|P_{k_p}|^2,\\
\widetilde{E}_L(k_p) &= E_L(k_p) + 2V_{k_p,k_p,0}^{PP}|P_{k_p}|^2,\\
\widetilde{E}_L(2k_p) &= E_L(2k_p) + 2V_{2k_p,k_p,0}^{PP}|P_{k_p}|^2,
\end{aligned} \tag{5.3.26}$$

and

$$E_{\text{int}} = \frac{1}{2}\left(V_{k_p,k_p,k_p}^{PP} + V_{k_p,k_p,-k_p}^{PP}\right). \tag{5.3.27}$$

The advantage of this formalism with respect to the Boltzmann equations is that it allows one to account for the energy renormalisation processes driven by interparticle interactions. Here a blue shift of the three considered states is induced by the pump intensity. Replacing all operators by complex numbers, this equation system can be solved numerically for any pump and probe configuration.

5.3.5. ANALYTICAL SOLUTION OF THE THREE-LEVEL MODEL IN THE CASE OF *cw* PUMPING: THE PARAMETRIC OSCILLATION MODEL

Here we shall consider the steady-state excitation case. We assume that a stationary pump of frequency ω_p excites the system, without a probe. This pump drives the pump polarisation given by:

$$P_{k_p}(t) = \overline{P}_{k_p} e^{i\omega_p t}, \tag{5.3.28}$$

where $\overline{P}_{k_p}$ is a complex number. The system (5.3.23)–(5.3.25) reduces to two coupled equations:

$$\frac{\hbar}{i}\dot{p}_0 = \widetilde{E}_L(0)\, p_0 + E_{\text{int}} p^+_{2k_p} \overline{P}^2_{k_p} e^{2i\omega_p t}, \tag{5.3.29}$$

$$\frac{\hbar}{i}\dot{p}^+_{2k_p} = -\widetilde{E}^*_L(2k_p)\, p^+_{2k_p} - E_{\text{int}} p_0 \overline{P}^{*2}_{k_p} e^{-2i\omega_p t}. \tag{5.3.30}$$

We define:

$$\omega_0 = \frac{1}{\hbar}\,\text{Re}\big(\widetilde{E}_L(0)\big), \qquad \omega_i = \frac{1}{\hbar}\,\text{Re}\big(\widetilde{E}_L(2k_p)\big),$$

$$\Gamma_0 = \frac{2}{\hbar}\,\text{Im}\big(\widetilde{E}_L(0)\big), \qquad \Gamma_i = \frac{2}{\hbar}\,\text{Im}\big(\widetilde{E}_L(2k_p)\big).$$

We introduce the two rescaled quantities: $\tilde{p}_0 = p_0 e^{-i\omega_0 t}$, $\tilde{p}^+_{2k_p} = p^+_{2k_p} e^{i\omega_i t}$. These conditions together with (5.3.28) mean that we place ourselves in a rotating frame for signal, pump, and idler. We shall also introduce $\hbar\beta = \hbar|\beta| e^{i2\varphi_p} \equiv E_{\text{int}} \overline{P}^2_{k_p}$, which is a complex number. The two previous equations become:

$$\frac{\hbar}{i}\dot{\tilde{p}}_0 = -\frac{\Gamma_0}{2} p_0 + \hbar\beta p^+_{2k_p} e^{i(2\omega_p - \omega_0)t}, \tag{5.3.31}$$

$$\frac{\hbar}{i}\dot{\tilde{p}}^+_{2k_p} = -\frac{\Gamma_i}{2}\tilde{p}^+_{2k_p} - \hbar\beta^* p_0 e^{i(2\omega_i - \omega_p)t}. \tag{5.3.32}$$

This equation is nothing but a quantum mechanical equation for parametric processes first written and solved by Louisell et al. [26]. Replacing all quantum operators in this equation system by complex numbers is equivalent to treating the classical parametric oscillator studied in the last century by Faraday and Lord Rayleigh, as has been recently pointed out by Whittaker [27]. This equation system has been widely studied in recent decades. It can be solved in the Heisenberg representation in the time domain [26,28] or in the frequency domain [5,29].

5.3.5.1. Time Domain Solution

For simplicity, we assume that the resonance conditions are satisfied and that the loss coefficients are the same for signal and idler:

$$\omega_0 + \omega_i - 2\omega_p = 0,$$
$$\Gamma_0 = \Gamma_p = \Gamma_i = \Gamma.$$

Eqs. (5.3.31) and (5.3.32) become

$$\dot{\tilde{p}}_0 = -\frac{\Gamma}{2}\tilde{p}_0 + i\beta\,\tilde{p}^+_{2k_p}, \tag{5.3.33}$$

$$\dot{\tilde{p}}^+_{2k_p} = -\frac{\Gamma}{2}\tilde{p}^+_{2k_p} - i\beta^*\tilde{p}_0. \tag{5.3.34}$$

Eq. (5.3.33) implies:

$$\tilde{p}^+_{2k_p} = \frac{1}{i\beta}\left(\dot{\tilde{p}}_0 + \frac{\Gamma}{2}\tilde{p}_0\right), \tag{5.3.35}$$

$$\ddot{\tilde{p}}_0 + \Gamma\dot{\tilde{p}}_0 + \left(\frac{\Gamma^2}{4} + |\beta|^2\right)\tilde{p}_0 = 0. \tag{5.3.36}$$

The solutions of the characteristic equation associated with (5.3.36) are:

$$r\pm = -\frac{\Gamma}{4} \pm |\beta|. \tag{5.3.37}$$

The solutions of the system (5.3.35), (5.3.36) are:

$$\tilde{p}_0(t) = e^{-\frac{\Gamma}{2}t}\left(a_0\,\mathrm{ch}(|\beta|t) - i a^+_{2k_p}\,\mathrm{sh}(|\beta|t)e^{i2\varphi_p}\right), \tag{5.3.38}$$

$$\tilde{p}^+_{2k_p}(t) = e^{-\frac{\Gamma}{2}t}\left(a^+_{2k_p}\,\mathrm{ch}(|\beta|t) + i a_0\,\mathrm{sh}(|\beta|t)e^{-i2\varphi_p}\right), \tag{5.3.39}$$

where a_0 is the Schrödinger annihilation operator acting on the subspace formed by the ground state, and $a^+_{2k_p}$ is the Schrödinger creation operator acting on the subspace formed by the idler state. For $t \gg 1/|\beta|$, ch and sh can be approximated by exponentials with positive argument. Therefore:

$$\tilde{p}_0\left(t \gg 1/|\beta|\right) = \frac{1}{2}e^{(|\beta|-\Gamma/2)t}\left(a_0 - i a^+_{2k_p}e^{i2\varphi_p}\right), \tag{5.3.40}$$

$$\tilde{p}^+_{2k_p}\left(t \gg 1/|\beta|\right) = \frac{1}{2}e^{(|\beta|-\Gamma/2)t}\left(a^+_{2k_p} + i a_0 e^{-i2\varphi_p}\right). \tag{5.3.41}$$

5.3.5.2. Threshold to Stimulated Scattering

The threshold condition to stimulated scattering is given by:

$$\Gamma = 2|\beta| \quad \Rightarrow \quad |P_{k_p}|^2 = \frac{\hbar\Gamma}{2E_{\text{int}}}. \tag{5.3.42}$$

With such a pump polarisation, the energy shift of the signal at threshold is equal to the polariton linewidth. This theoretical result is in a good agreement with available experimental data. It is instructive to compare the criterion (5.3.42) with the threshold condition obtained from a semi-classical Boltzmann equation (Section 5.2).

The relation between the pumping power and the coherent polarisation is $\Gamma|P_{k_p}|^2 \approx P$ and the threshold condition for the pump power is:

$$P = \frac{\hbar\Gamma^2}{2E_{\text{int}}}. \tag{5.3.43}$$

If one assumes, as in Section 5.2, that the broadening Γ is independent of the wave-vector, and that $E_{\text{int}} \approx |M|$, the polariton–polariton matrix element of interaction, (5.3.43) becomes:

$$P_{\text{thres}} = \Gamma\frac{\hbar\Gamma}{2|M|}. \tag{5.3.44}$$

This value is exactly the same as the one obtained in Section 5.2, illustrating the equivalence of the semi-classical and quantum models on this aspect.

5.3.6. COHERENCE EVOLUTION AND SYMMETRY BREAKING

The "particle number" operator for the signal is:

$$\tilde{p}_0^+\tilde{p}_0(t) = \frac{1}{4}e^{(2|\beta|-\Gamma)t}\left(a_0^+a_0 + a_{2k_p}a_{2k_p}^+ - i\left(a_0^+a_{2k_p}^+e^{i2\varphi_p} - a_{2k_p}a_0e^{-i2\varphi_p}\right)\right). \tag{5.3.45}$$

If the signal and idler states are initially in the vacuum state, the average number of particles is

$$\langle 0,0|\tilde{p}_0^+\tilde{p}_0(t)|0,0\rangle = \left\langle\tilde{p}_0^+\tilde{p}_0(t)\right\rangle = \frac{1}{4}e^{(2|\beta|-\Gamma)t}. \tag{5.3.46}$$

However

$$\langle 0,0|\tilde{p}_0(t)|0,0\rangle = \langle\tilde{p}_0(t)\rangle = 0. \tag{5.3.47}$$

Eqs. (5.3.46) and (5.3.47) show that a ground state, initially symmetric in the phase space, will have its population growing exponentially while its amplitude remains zero. This shows that the symmetry of the ground state is not broken by

the pumping laser. To illustrate our purpose we consider that the system is initially in a state other than a vacuum.

5.3.6.1. Two-Beam Experiment

We assume that a *cw* pump laser excites the sample, together with an ultrashort probe pulse which seeds the probe state. Therefore, at $t = 0$ the probe state is a coherent state $|\alpha_0\rangle$ [30], with $\alpha_0 = |\alpha_0|e^{i\varphi_0}$. The idler state is initially unpopulated (vacuum state). The initial state of the signal $\otimes$ idler system is denoted $|\alpha_0, 0\rangle$. With such initial states:

$$\langle \tilde{p}_0^+ \tilde{p}_0(t)\rangle = \frac{1}{4}\big(1 + |\alpha_0|^2\big)e^{(2|\beta|-\Gamma)t}, \tag{5.3.48}$$

$$\langle \tilde{p}_0(t)\rangle = \frac{1}{2}\alpha_0 e^{(|\beta|-\Gamma/2)t}. \tag{5.3.49}$$

The phase φ_0 of the order parameter does not depend on the value of the pump phase φ_p and is determined by the probe phase. We define the coherence of the system as

$$\eta = \frac{|\langle \tilde{p}_0(t)\rangle|^2}{\langle \tilde{p}_0^+ \tilde{p}_0(t)\rangle}. \tag{5.3.50}$$

We obtain:

$$\eta = \frac{|\alpha_0|^2}{1 + |\alpha_0|^2}. \tag{5.3.51}$$

This coherence is constant for any phase relationship between pump and probe. It is close to one if the probe introduces a coherent seed population much larger than one. In this case, the symmetry of the system is broken by the probe.

5.3.6.2. One Beam Experiment and Spontaneous Symmetry Breaking

We have seen in the previous paragraph that the wave-function of the initially symmetrical system will remain symmetrical during its temporal evolution. Now we are going to artificially break this symmetry, assuming that the initial state is a coherent state characterised by a small but finite amplitude. Since the signal and idler are now completely identical, we consider that they are both initially in a coherent state with the same amplitude $\alpha_0 = |\alpha|e^{i\varphi_0}$, $\alpha_{2k_p} = |\alpha|e^{i\varphi_{2k_p}}$ but different phases. The average signal polarisation and population are:

$$\begin{aligned}\langle \tilde{p}_0(t)\rangle &= \frac{1}{2}e^{(|\beta|-\Gamma/2)t}\big(\alpha_0 - i\alpha_{2k_p}^* e^{i2\varphi_p}\big) \\ &= \frac{1}{2}|\alpha|e^{(|\beta|-\Gamma/2)t}e^{i\varphi_0}\big(1 - e^{i(2\varphi_p-\varphi_0-\varphi_{2k_p})}\big).\end{aligned} \tag{5.3.52}$$

The signal polarisation strongly depends on the phase relation between pump, probe and idler. Namely, it vanishes if

$$\Phi = 2\pi n, \tag{5.3.53}$$

where $\Phi = 2\varphi_p - \varphi_0 - \varphi_{2k_p}$, $n = 0, \pm 1, \pm 2, \ldots$.

It achieves its maximum if

$$\Phi = \pi + 2\pi n. \tag{5.3.54}$$

This last equation is the phase-matching condition for the parametric oscillation to take place. A similar equation can be written for the signal population:

$$\begin{aligned}\left\langle \tilde{p}_0^+ \tilde{p}_0(t)\right\rangle &= \frac{1}{4} e^{2(|\beta|-\Gamma/2)t} \\ &\quad \times \left(|\alpha_0|^2 + 1 + |\alpha_{2k_p}|^2 - i\left(\alpha_0^* \alpha_{2k_p}^* e^{i2\varphi_p} - \alpha_{2k_p}\alpha_0 e^{-i2\varphi_p}\right)\right), \\ \left\langle \tilde{p}_0^+ \tilde{p}_0(t)\right\rangle &= \frac{1}{4} e^{2(|\beta|-\Gamma/2)t}\left(1 + 2|\alpha|^2(1-\cos\Phi)\right).\end{aligned} \tag{5.3.55}$$

One can see that the population has a minimum (but does not vanish) if the condition (5.3.53) is fulfilled, while it has a maximum if the condition (5.3.54) is fulfilled, similar to what happens with the polarisation. The coherence then reads:

$$\eta = \frac{2|\alpha|^2(1-\cos\Phi)}{1 + 2|\alpha|^2(1-\cos\Phi)}. \tag{5.3.56}$$

An initial coherent state is expected to appear because of the system fluctuations. It is hard to describe such fluctuations theoretically and to quantify $|\alpha|$. It is, however, clear that the system will choose to grow on the most "favourable" fluctuation, respecting the constructive phase-matching condition (5.3.54). It is essential to note that the phase of the signal and idler is not fixed by the phase φ_p of the pumping laser together with the phase matching condition, as was proposed in Ref. [10]. One can see that only the quantity $\varphi_0 + \varphi_{2k_p}$ is actually fixed. Therefore, there is a well defined phase relation between signal and idler, but all the values of the signal phase are equivalent for the system. This signal phase is not *a priori* determined by the pump phase, but it is randomly chosen by the system from experiment to experiment. Choosing its phase, the system "breaks its symmetry" [10,31]. This symmetry breaking effect is common to the laser phase transition, superconducting phase transition, and BEC. To summarise, it is a common feature of phase transitions induced by the bosonic character of the particles involved. This is not a BEC, however, because, as is the case with lasers, it is

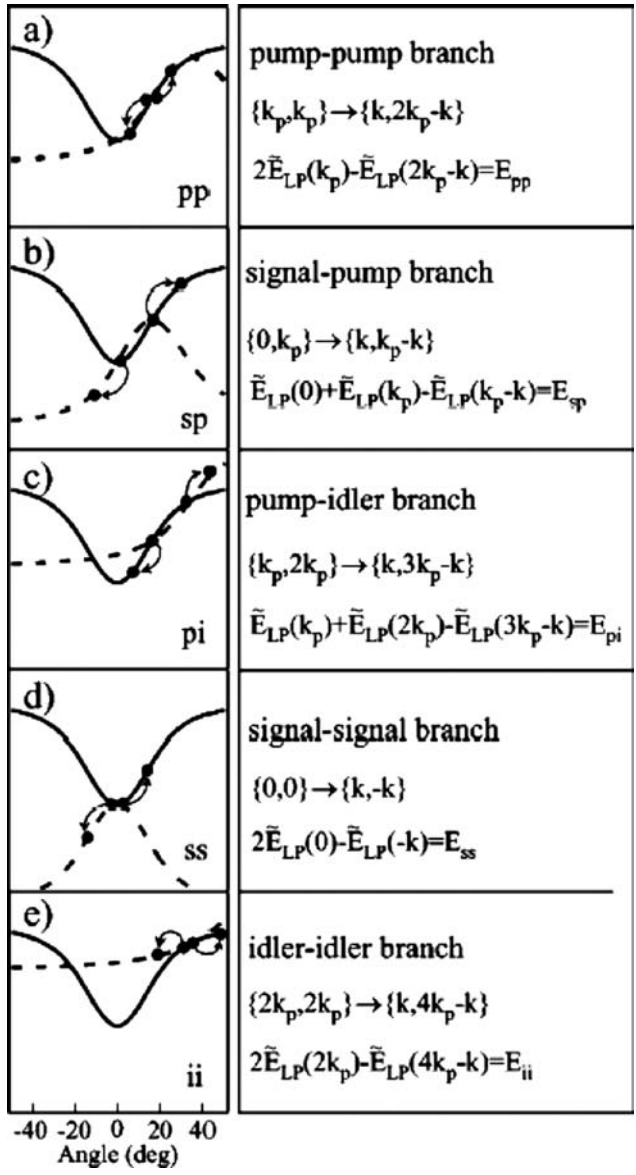

Fig. 5.12. Scattering channels starting from two polaritons in macroscopically occupied states and their corresponding induced off branches dispersion (dashed). From [7].

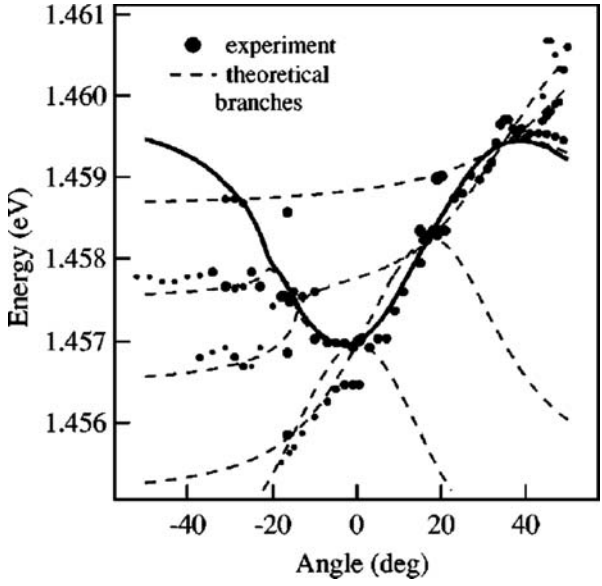

Fig. 5.13. Peak emission energy positions extracted from the time integrated spectra. Circle size represents the logarithmic intensity each peak. The dashed line shows the multibranch energy dispersion. From [7].

an out-of-equilibrium phase transition, so that, for example, a chemical potential cannot be defined. We shall return in more detail to the theory of bosonic phase transitions in semiconductors in Chapter 6.

5.3.7. DRESSING OF THE DISPERSION INDUCED BY POLARITON CONDENSATES

As mentioned in Section 5.1.4, stimulated scattering experiments have shown new emission peaks surprisingly far from the polariton dispersion. This "off branch emission" is induced by strong interactions taking place between macroscopically populated states, which are the pump, signal and idler states. Interaction between these states is not only a perturbation in the sense that it leads to a dressing of the polariton dispersion. The reader is referred to Ref. [7] for detailed description of the experiment showing this effect, as well as for its theoretical interpretation. In this section we briefly summarise this theory. We shall consider all scattering processes which involve two macroscopically populated states as initial states, and, as final states, one state on the polariton branch and one off-branch state. We shall require conservation of energy and wave-vector. As an example

of such a transition, one can consider scattering events having two pump polaritons as initial states. The wave-vector and energy conservation laws give in this case:

$$\begin{aligned} &\{k_p, k_p\} \rightarrow \{k, 2k_p - k\}, \\ &2E_L(k_p) = E_L(k) + E_{pp}^{\text{off}}(2k_p - k). \end{aligned} \tag{5.3.57}$$

Eq. (5.3.57) defines a new dispersion branch $E_{pp}^{\text{off}}(2k_p - k)$. Appearance of a polariton on this branch is possible because the corresponding scattering event is fast enough (see Section 5.1.4). Four other branches corresponding to signal-pump, pump-idler, signal-signal and idler-idler scattering can be defined, as shown in Figure 5.12. Figure 5.13 shows these five new dispersion branches together with the experimental points detected in a pump-probe experiment. The observation of off-branch emission, which can be associated with the existence of macroscopically populated polariton sates, is a characteristic feature of phase transitions of weakly interacting bosons. Its experimental observation confirms once again that microcavity polaritons are quasiparticles suitable for the observation of collective bosonic effects.

References

1. G. Khitrova, H. M. Gibbs, F. Jahnke, M. Kira, S. W. Koch, Non-linear optics of normal-mode-coupling semiconductor microcavities, *Rev. Mod. Phys.* 71, 1591 (1999) and ref. therein.
2. F. Jahnke, M. Kira, S. W. Koch, G. Khitrova, E. K. Lindmark, T. R. Nelson, Jr., D. V. Wick, J. D. Berger, O. Lyngnes, H. M. Gibbs, Excitonic nonlinearities of semiconductor microcavities in the non-perturbative regime, *Phys. Rev. Lett.* 77, 5257 (1996).
3. F. Quochi, C. Bongiovanni, A. Mura, J. L. Staehli, B. Deveaud, R. P. Stanley, U. Oesterle, R. Houdré, Strongly driven microcavities: from the polariton doublet to an AC Stark triplet, *Phys. Rev. Lett.* 80, 4733 (1998).
4. P. G. Savvidis, J. J. Baumberg, R. M. Stevenson, M. S. Skolnick, D. M. Whittaker, J. S. Roberts, Angle resonant stimulated polariton amplifier, *Phys. Rev. Lett.* 84, 1547 (2000).
5. C. Ciuti, P. Schendimann, B. Deveaud, A. Quattropani, Theory of the angle-resonant polariton amplifier, *Phys. Rev. B* 62, R4825 (2000).
6. C. Ciuti, P. Schendimann, A. Quattropani, Parametric luminescence of microcavity polaritons, *Phys. Rev. B* 63, 041303 (R) (2001).
7. P. G. Savvidis, C. Ciuti, J. J. Baumberg, D. M. Whittaker, M. S. Skolnick, J. S. Roberts, Off-branch polaritons and multiple scattering in semiconductor microcavities, *Phys. Rev. B* 63, 041303 (R) (2001).
8. R. Houdré, J. L. Gibernon, P. Pellandrini, R. P. Stanley, U. Oesterle, C. Weisbuch, J. O'Gorman, B. Roycroft, M. Ilegems, Saturation of the strong coupling regime in a semiconductor microcavity: free carrier bleaching of cavity polaritons, *Phys. Rev. B* 52, 7810 (1995).
9. B. R. Mollow, Power spectrum of light scattered by two-level systems, *Phys. Rev.* 188, 1969 (1969).
10. D. Snoke, Spontaneous Bose coherence of excitons and polaritons, *Science* 298, 1368 (2002).

11. A. Kavokin, G. Malpuech, F. P. Laussy, Polariton lasers and polariton superfluidity in microcavities, *Phys. Lett. A* 306, 185 (2003).

12. M. Saba, C. Ciuti, J. Bloch, V. Thierry-Mieg, R. Adré, L. S. Dang, S. Kundermann, A. Mura, G. Bongiovanni, J. L. Staehli, B. Deveaud, High temperature ultrafast polariton amplification in semiconductor microcavities, *Nature* 414, 731 (2001).

13. R. M. Stevenson, V. N. Astratov, M. S. Skolnick, D. M. Whittaker, M. Emam-Ismail, A. I. Tartakovskii, P. G. Savvidis, J. J. Baumberg, J. S. Roberts, Continuous wave observation of massive polariton redistribution by stimulated scattering in semiconductor microcavities, *Phys. Rev. Lett.* 85, 3680 (2000).

14. A. I. Tartakovskii, D. N. Krizhanovskii, D. A. Kurysh, V. D. Kulakovskii, M. S. Skolnick, J. S. Roberts, Polariton parametric processes in semiconductor microcavities observed in continuous wave experiment, *Phys. Rev. B* 65, 081308 (R) (2002).

15. N. N. Bogoliubov, On the theory of superfluidity, *J. Phys. USSR* 11, 23 (1947); N. N. Bogoliubov, "Lectures on Quantum Statistics, Vol. 1. Quantum Statistics". Gordon and Breach Science Publisher, New York, London, Paris, 1970; V. A. Zagrebnov and J. B. Bru, The Bogoliubov model of weakly imperfect Bose gas, *Phys. Rep.* 350 (2001) and ref. therein.

16. P. G. Lagoudakis, P. G. Savvidis, J. J. Baumberg, D. M. Whittaker, P. R. Eastham, M. S. Skolnick, J. S. Roberts, Stimulated spin dynamics of polaritons in semiconductor microcavities, *Phys. Rev. B* 65, 161310 (2002).

17. A. Kavokin, G. Malpuech, P. G. Lagoudakis, J. J. Baumberg, K. Kavokin, Polarization rotation in resonant emission of semiconductor microcavities, *Phys. Stat. Sol. (a)* 195, 579 (2003); A. Kavokin, G. Malpuech, P. G. Lagoudakis, J. J. Baumberg, Polarization rotation in parametric scattering of polaritons in semiconductor microcavities, *Phys. Rev. B* 67, 195321 (2003).

18. M. D. Martín, G. Aichmayr, L. Viña, R. André, Polarization control of the nonlinear emission of semiconductor microcavities, *Phys. Rev. Lett.* 89, 077402 (2002).

19. R. Huang, F. Tassone, Y. Yamamoto, Experimental evidence of stimulated scattering of excitons into microcavity polaritons, *Phys. Rev. B* 61, R7854 (2000).

20. A. Pawlis, A. Khartchenko O. Husberg, D.J. As, K. Lischka, D. Schikora, Large room temperature Rabi-splitting in a ZnSe/(Zn,Cd)Se semiconductor microcavity structure, *Solid State Commun.* 123, 235 (2002).

21. G. Malpuech, A. Di Carlo, A. Kavokin, J. J. Baumberg, M. Zamfirescu, P. Lugli, Room-temperature polariton lasers based on GaN microcavities, *Appl. Phys. Lett.* 81, 412 (2002); M. Zamfirescu, B. Gil, N. Grandjean, G. Malpuech, A. Kavokin, P. Bigenwald, J. Massies, Extremely sharp dependence of the exciton oscillator strength on quantum-well width in the GaN/$Al_xGa_{1-x}N$ system: The polarization field effect, *Phys. Rev. B* 64, 121304 (2001).

22. M. Zamfirescu, A. Kavokin, B. Gi, G. Malpuech, M. Kaliteevski, ZnO as a material mostly adapted for the realization of room-temperature polariton lasers, *Phys. Rev. B* 65, 161205 (2002).

23. D. G. Lidzey, D. D. C. Bradley, M. S. Skolnick, T. Virgili, S. Walker, D. M. Whittaker, Strong exciton–photon coupling in an organic semiconductor microcavity, *Nature* 395, 53 (1998); D. G. Lidzey, D. D. C. Bradley, A. Armitage, S. Walker, M. S. Skolnick, Photon mediated hybridisation of Frenkel excitons in organic semiconductor microcavities, *Science* 288, 1620 (2000).

24. R. Houdré, C. Weisbuch, R. P. Stanley, U. Oesterle, M. Ilegems, Nonlinear emission of semiconductor microcavities in the strong coupling regime, *Phys. Rev. Lett.* 85, 2793 (2000).

25. W. Langbein, J. M. Hvam, Elastic scattering dynamics of cavity polaritons: Evidence for time-energy uncertainty and polariton localization, *Phys. Rev. Lett.* 88, 047401 (2002).

26. W. H. Louisell, A. Yariv, A. E. Siegman, Quantum fluctuations and noise in parametric processes I, *Phys. Rev.* 124, 1646 (1961).

27. D. M. Whittaker, Classical treatment of parametric processes in a strong-coupling planar microcavity, *Phys. Rev. B* 63, 193305 (2001).

28. L. Mandel and E. Wolf, "Optical Coherence and Quantum Optics". Cambridge University Press, 1995.
29. R. Loudon, "The Quantum Theory of Light". Oxford University Press.
30. See for example [28] or [29].
31. A. Griffin, D. W. Snoke, S. Stringari, Eds., "Bose Einstein Condensation". Cambridge University Press, 1995.

This page intentionally left blank

Chapter 6

Toward Polariton Bose Condensation and Polariton Lasers

6.1. Eighty Years of Research on BEC 185
6.1.1. Einstein Proposal 185
6.1.2. Experimental Realization 187
6.1.3. "Modern Definition" of Bose–Einstein Condensation 188
6.1.4. Exciton and Polariton Specifics 188
6.2. Thermodynamic Properties of Cavity Polariton Systems 190
6.2.1. Interacting Bosons and Bogoliubov Model 191
6.2.2. Polariton Superfluidity and Kosterlitz–Thouless Phase Transition 193
6.2.3. Quasi-Condensation and Local Effects 196
6.3. Relaxation Kinetics of Cavity Polaritons: Towards Polariton Lasing 198
6.3.1. Experimental Quest of the Polariton Laser (1996–2003) 198
6.3.2. Theoretical Description of the Polariton Laser 201
6.3.3. Numerical Results 205
6.4. Spin Dynamics of Exciton–Polaritons in Microcavities 211
6.5. Conclusive Remarks 220
References 221

An exciton is a Coulomb-correlated electron–hole pair. It is a neutral particle of integer spin value. At low density, excitons behave as a weakly interacting Bose gas. Cavity polaritons, a mixture of exciton and photon, also behave as bosons in the low-density range, as pointed out in Chapter 5. One would therefore expect these particles to exhibit bosonic phase transition such as Bose–Einstein condensation (BEC).

In this chapter we present experimental and theoretical work performed between 1996 and 2003 to provide evidence for a cavity polariton BEC and polariton lasing. Imamoglu [1] was the first, in 1996, to point out how the bosonic character of cavity polaritons could be used to create an exciton–polariton condensate that would emit coherent laser light. The build-up of a ground-state coherent population from an incoherent exciton reservoir can be seen as a phase transition towards a Bose condensed state, or as a polariton-lasing effect resulting from bosonic stimulated scattering. This conceptual proposal was followed in 2000 by the observation of polariton stimulated scattering in resonantly-pumped microcavities [2], which was described in detail in the previous chapter. A polariton laser is, however, different from a polariton parametric amplifier. In the former case, the system is excited non-resonantly, optically or electronically, resulting in a cloud of electrons and holes that form excitons, which subsequently thermalise

at their own temperature mainly through exciton–exciton interactions. They reduce their kinetic energy by interacting with phonons and relax along the LPB. They finally scatter to their lower-energy state, where they accumulate because of stimulated scattering. The coherence of the condensate therefore builds up from an incoherent equilibrium reservoir and the associated phase transition can be interpreted as a BEC. Once condensed, polaritons emit coherent monochromatic light. As the light emission by a polariton quasi-condensate is spontaneous, there is no population inversion condition required in polariton lasers, absorption of light does not play any role, and ideally there is no threshold for lasing. Concerning this latter point, the argument is that it is sufficient to have two polaritons in the ground state to create a condensate, which will result in its disintegration with the emission of two coherent photons. Moreover, because of the small polariton mass, critical temperatures larger than 300 K can be achieved. All these characteristics combined make polariton lasers ideal candidates for the next generation of laser-light emitting devices. The main hurdle to effectively obtain polariton condensates in microcavities is the too short lifetime of the particles: polaritons disappear before they have time to condense. This difficulty is exacerbated by the slow relaxation kinetic towards the ground state, the so-called bottleneck effect (see Chapter 4). Formation of the condensate within the polariton lifetime is only possible because of the rapidity of stimulated scattering that should be able to overcome the bottleneck effect.

At the time of writing, the most challenging objective for the microcavity field remains without doubt the clear achievement of polariton coherence in a non-resonantly pumped structure.

A few theoretical works attempting to describe these phenomena have appeared. An analysis based on the Dike model has been proposed by Eastham and Littlewood [3], to describe the 0 K properties of an arbitrary-pumped microcavity including disorder and the space-filling effect. Kavokin et al. have defined a simple criterion for polariton quasi-condensation in a finite-size 2D system, and have plotted the corresponding polariton phase diagram [4]. They have also shown that room-temperature polariton lasing is achievable in hypothetical microcavities based on large band-gap semiconductors [4–6]. Kinetic aspects of polariton relaxation have also been studied, mainly by numerical solution of the semi-classical Boltzmann equations. Tassone et al. have shown that acoustic phonon relaxation was inefficient in providing polariton relaxation toward the ground state [7], but that exciton–exciton relaxation process could overcome this inefficiency [8,9]. Malpuech et al. have proposed the introduction of a free electron gas in the cavity in order to speed up the polariton relaxation [10]. Soroko and Ivanov [11] have proposed to use microcavities at very positive detuning in order to suppress the relaxation bottleneck, keeping the advantage in this geometry of a polariton mass still smaller than the exciton one. This idea is, however, achievable only in extremely high-quality structures, probably far beyond actual growth abilities.

Finally, Porras et al. have presented a simulation [12] demonstrating that existing II–VI microcavities might exhibit polariton lasing at low temperatures. They achieved a qualitative agreement with existing experimental results [13].

In Section 6.1 we present an overview of the history of BEC from both a theoretical and experimental point of view. We emphasise the case of exciton and polariton condensation. In particular, we explain why exciton BEC has never been clearly achieved and why cavity polaritons seem more suitable candidates to exhibit such effects.

In Section 6.2 we present the basic thermodynamic properties of cavity polaritons modelled as a weakly interacting Bose gas at equilibrium. We also present the polariton phase diagram. We show that these two-dimensional quasiparticles exhibit local condensation or a Kosterlitz–Thouless phase transition towards superfluidity, allowing for polariton lasing at temperatures that could be higher than 300 K.

Section 6.3.1 reviews the main experimental results obtained between 1996 and 2003 aimed at the polariton BEC.

In Sections 6.3.2 and 6.3.3 we present an analysis of the relaxation kinetics of cavity polaritons. The dynamical evolution of the condensate in a non-resonantly pumped cavity is described by a quantum kinetic formalism. The distribution function of polaritons is described by a semi-classical Boltzmann equation. A master equation for the ground-state density matrix is derived in the framework of the Born–Markov approximation following Rubo et al. [14]. Dynamics of the ground state's population and coherence are deduced. We also discuss ways to improve polariton relaxation kinetics in real structures.

Finally, Section 6.4 addresses the spin-relaxation dynamics in microcavities and the influence of spin on energy relaxation of exciton–polaritons.

The research on polariton BEC is a rapidly evolving field. We do not claim to give either its definitive or comprehensive picture. As a result, this chapter especially is liable to become rapidly outdated.

6.1. Eighty Years of Research on BEC

6.1.1. EINSTEIN PROPOSAL

A fascinating property of bosons is their tendency to accumulate in an unlimited amount in a degenerate state [15]. Einstein made an insightful proposition based on this property in the case of an ideal Bose gas which led him to the prediction of a new kind of phase transition [16]. Let us consider N non-interacting bosons at a temperature T in a volume R^d, where R is the system size and d its dimensionality. The bosons should distribute in energy following the Bose–Einstein

distribution function:

$$f_B(\vec{k}, T, \mu) = \frac{1}{\exp[(E(\vec{k}) - \mu)/k_B T] - 1}, \tag{6.1.1}$$

where $\vec{k}$ is the particle wave-vector, $E(\vec{k})$ is the in-plane dispersion function of bosons, k_B is the Boltzmann constant and μ is the chemical potential, which is a negative number if the lowest value of E is zero. Note that $-\mu$ is the energy needed to add one particle to the system. Its value is given by the normalisation condition:

$$N(T, \mu) = \sum_{\vec{k}} f_B(\vec{k}, T, \mu). \tag{6.1.2}$$

Before going to the thermodynamic limit (i.e., making the system size and the number of particles go to infinity in such a way that the density remains constant), it is convenient to separate the ground state from the others:

$$N(T, \mu) = \frac{1}{\exp[-\mu/k_B T] - 1} + \sum_{\vec{k}, |\vec{k}| \geqslant 2\pi/R} f_B(\vec{k}, T, \mu). \tag{6.1.3}$$

In the thermodynamic limit, the total polariton density is given by the following integration over the reciprocal space:

$$n(T, \mu) = \lim_{R \to \infty} \frac{N(T, \mu)}{R^d} = n_0 + \frac{1}{(2\pi)^d} \int f_B(\vec{k}, \mu)\, d^d\vec{k}, \tag{6.1.4}$$

where

$$n_0(T, \mu) = \lim_{R \to \infty} \frac{1}{R^d} \frac{1}{\exp[-\mu/k_B T] - 1}. \tag{6.1.5}$$

If μ is non zero, the ground-state density vanishes. On the other hand, the integral on the right-hand side of Eq. (6.1.4) is an increasing function of μ. So, if one increases the particle density n in the system, the chemical potential also increases. The maximum particle density which can be accommodated following the Bose distribution function is therefore:

$$n_c(T) = \lim_{\mu \to 0} \frac{1}{(2\pi)^d} \int f_B(\vec{k}, \mu)\, d^d\vec{k}. \tag{6.1.6}$$

This function can be calculated analytically in the case of a parabolic dispersion relation [17]. It is convergent if $d > 2$ and divergent if $d \leqslant 2$. So, in two or less dimensions any finite number of non-interacting bosons can always fit the Bose distribution with $\mu < 0$: the chemical potential is never zero and there is no phase transition. In higher dimensions, however, n_c is a critical density, above which it would seem no more particles can be added. Einstein proposed that at these

higher densities the extra particles in fact collapse in the ground state only, whose density is given by:

$$n_0(T) = n(T) - n_c(T). \tag{6.1.7}$$

This is a phase transition characterised by the accumulation of a macroscopic number of particles, or equivalently by a finite density in a single quantum state. The order parameter is the chemical potential, which becomes zero at the transition.

6.1.2. EXPERIMENTAL REALIZATION

This proposal was not immediately accepted and understood by the scientific community, principally because of Uhlenbeck's thesis, wherein he argued that BEC was not realistic because it would not occur in a finite system. The interest in BEC saw a revival in 1938 with the first unambiguous report of Helium-4 superfluidity [18]. A few months after this observation, London first proposed the interpretation of this phenomenon as a manifestation of BEC [19]. This link between BEC and He-4 superfluidity marked the beginning of an incredible amount of scientific activity throughout the 20th century, which is still being pursued nowadays. Another early field where Einstein's intuition found potential and practical applications is superconductivity. However, the link was only properly understood in the 1950s with the advent of the BCS theory. In both cases (He and superconductivity) the total particle density is fixed. It is thus possible to define a critical temperature T_c given by the solution of

$$n_c(T_c) = n. \tag{6.1.8}$$

A dramatic indication of the validity of Einstein's prediction (as was immediately pointed out by London) is that its direct application yields a BEC critical temperature of 3.14 K for He, very close to the experimental value of 2.17 K. However a major difficulty is that these two systems are strongly-interacting, in fact already in their liquid phase, and therefore particles interactions are expected to play a fundamental role thus making them poor realisations of Einstein's ideal gas. Consequently, the objective of most theoretical efforts of the 1940–1960s was to describe condensation of strongly-interacting bosons. Stimulated emission of light and laser action [20] is also induced by the bosonic nature of the particles involved, the photons, which do not interact. This, however, means that they cannot self-thermalise and a photon assembly represents fundamentally a non-equilibrium system. Consequently, laser action is a non-equilibrium phase transition which cannot be directly interpreted as a BEC. In fact, the first clear manifestation of condensation in a weakly-interacting Bose gas was performed recently in 1995 with trapped alkali atoms [21]. This discovery, honoured by the 2001 Nobel prize, has given a strong revival to this field.

6.1.3. "MODERN DEFINITION" OF BOSE–EINSTEIN CONDENSATION

Research on BEC was extremely intense in the period 1938–1965, especially on the theoretical side, where it allowed for many deep advances in understanding. In particular, these efforts led to a new definition of the BEC criterion. BEC is now associated with the appearance of a macroscopic condensate wave-function $\psi(\vec{r})$, which has a non-zero mean value $\langle\psi(\vec{r})\rangle$:

$$\langle\psi(\vec{r})\rangle = \sqrt{n_{\text{cond}}(\vec{r})}e^{i\theta(\vec{r})}, \tag{6.1.9}$$

$\langle\psi(\vec{r})\rangle$ is now accepted as the order parameter of this phase transition. It is a complex number with an amplitude, the square root of the condensate density, and a phase. The system Hamiltonian is invariant under an arbitrary phase change of $\psi(\vec{r})$ (global gauge invariance). However, at the phase transition this symmetric solution becomes unstable and the system breaks this symmetry by choosing a specific phase that is assumed throughout the whole condensate, which is therefore completely phase-coherent. Penrose and Onsager proposed the following criteria for BEC [22]:

$$\left\langle\psi^{+}(\vec{r})\psi(\vec{r}')\right\rangle \xrightarrow[|\vec{r}-\vec{r}'|\to\infty]{} \left\langle\psi(\vec{r})\right\rangle^{*}\left\langle\psi(\vec{r}')\right\rangle, \tag{6.1.10}$$

which is now generally accepted. Its significance has emerged gradually through the efforts of many workers. Goldstone first advanced the idea of spontaneous symmetry breaking [23], Yang [24] termed the phenomenon "off-diagonal long-range order (ODLRO)" and Anderson [25] emphasised the notion of phase coherence. The superfluid velocity can be defined from (6.1.9) as:

$$m\vec{v}_s(\vec{r},t) = \hbar\vec{\nabla}\theta(\vec{r},t). \tag{6.1.11}$$

A system is therefore "superfluid" if two arbitrary spatial points are connected by a phase-coherent path allowing for frictionless transport.

6.1.4. EXCITON AND POLARITON SPECIFICS

Depending on their density and on temperature, excitons behave as either a weakly-interacting Bose gas, a metallic liquid, or an electron–hole plasma. It has been understood by Moskalenko [26] and Blatt [27] that excitons remain in the gas phase at low densities and low temperatures, and are therefore good candidates for observation of BEC in the way envisioned by Einstein. At that time there were no experimental examples of BEC of a weakly interacting gas, and a great deal of research effort has been dedicated to the problem of exciton BEC. A number of theoretical works on excitonic condensation and superfluidity have appeared [28–31]. In most of these the fermionic nature of excitons is also addressed. The starting point of these models is a system of degenerate electrons and holes of arbitrary densities that is treated in the spirit of the

BCS theory. A key point of all the formalisms developed is that they assume an infinite lifetime of the semiconductor excitations. In other words, these theories are looking for steady-state solutions of the Schrödinger equation of interacting excitons. It is indeed clear that to have enough time to Bose-condense, excitons must have a radiative lifetime much longer than their relaxation time. Thus, the use of "dark" (uncoupled to light) excitons seems preferable. This is the case for bulk Cu_2O paraexcitons, whose ground state spin is 2, or of excitons in coupled quantum wells [29], where the electron and hole are spatially separated. These two systems have been subject to energetic experimental studies which have sometimes claimed achievement of exciton BEC or superfluidity [17,32,33]. However, careful analysis by Lozovik and Tikhodeev [33,34] showed that clear evidence of excitonic BEC has not yet been achieved. The difficulties of Bose-condensing excitons are twofold. The first reason is linked to the intrinsic imperfections of semiconductors. Because of an unavoidable structural disorder, dark excitons non-resonantly excited are often trapped in local minima of the disorder potential and can hardly be considered as free bosons able to condense. The second source of difficulties is connected with the problem of detection of the condensed phase. The clearest signature of exciton Bose condensation should be the emission of coherent light by spontaneous recombination of condensed excitons [33]. Such emission is *a priori* forbidden for a system of dark excitons.

On the other hand, "bright" excitons directly coupled to the light might also be good candidates for condensation, despite their short lifetimes. In bulk semiconductors this coherent coupling gives rise to a polarisation wave that can be considered from a quantum-mechanical point of view as a coherent superposition of pure exciton and photon states (polaritons). Bulk polaritons are stationary states that transform into photons only at surfaces. Polaritons also being bosons, they can, in principle, form condensates that would emit spontaneously coherent light. Typical dispersion curves of bulk polaritons are shown in Figure 2.5. In the vicinity of the exciton–photon intersection point, the density of states of polaritons is strongly reduced and the excitonic contribution to the polariton is decreased. One should note that strictly speaking a $k = 0$ photon does not exist, and that consequently the $k = 0$ polaritonic state of the LPB does not exist. The polariton dispersion has no minimum so that a true condensation process is strictly forbidden. Polaritons accumulate in a large number of states in the so-called bottleneck region. The situation is drastically different in microcavities. The cavity prevents the escape of photons and allows the formation of long-lifetime cavity polaritons. Conversely to the bulk case, the in-plane cavity polariton dispersion exhibits a well-defined minimum located at $k = 0$, but since they are two-dimensional quasiparticles they cannot exhibit a strict BEC phase transition [35], but rather a local condensation or Kosterlitz–Thouless phase transition towards superfluidity [4,36–39] (see Section 6.2). They have, moreover, an extremely small effec-

tive mass around $k = 0$, allowing for polariton lasing at temperatures that could be higher than 300 K (see Section 6.2). Experimental discovery of stimulated scattering of polaritons in microcavities reviewed in Chapter 5 has proved that a microcavity is probably a very suitable system to observe effects linked to the bosonic nature of polaritons, and probably BEC. Much experimental and theoretical effort followed Imamoglu's proposal [1] of a polariton laser. We shall describe in detail these efforts in Section 6.3. This work progressed quickly in the period 1996–2003. We should repeat, however, that no clear evidence of polariton BEC has been obtained at the present time, even if it looks realistic to expect rapid success. A fundamental peculiarity and difficulty of a cavity is the finite lifetime that may be responsible for a strongly non-equilibrium polaritons distribution function. The relaxation kinetic of polaritons plays a major role in this case.

6.2. Thermodynamic Properties of Cavity Polariton Systems

In this section we discuss thermodynamic properties of microcavity polaritons considered as equilibrium particles, i.e., particles having an infinite lifetime. Even though this approximation is very far from reality, mainly governed by relaxation kinetics, it is definitely instructive to examine the BEC conditions in this limiting case. We shall, moreover, assume that polaritons behave as either ideal or weakly-interacting boson gas, so that the following analysis is valid only in the low-density limit.

As mentioned in Section 6.1.1 the critical condensation density is finite for nonzero temperature if $d > 2$. However, this density diverges in the two-dimensional case. Thus, a non-interacting Bose gas cannot condense in an infinite two-dimensional system, and the same statement turns out to be true when interactions are taken into account. A rigorous proof of the absence of BEC in two dimensions has been given by Hohenberg [35]. An equivalent statement known as the Mermin–Wagner theorem asserts that long-range order cannot exist in a system of dimensionality lower than two [35]. Finally, it has been shown that spontaneous symmetry breaking does not occur in two dimensions [35]. However, a phase transition between a normal state and a superfluid state can take place in two dimensions as predicted by Kosterlitz and Thouless in the 1970s [36] in the framework of the XY model. Such a second-order phase transition is forbidden for ideal bosons, but can take place in systems of weakly-interacting bosons [37] such as low-density excitons [38,39] or polaritons [4]. In Section 6.2.1 we describe the interaction effect on bosons through a presentation of the Bogoliubov formalism [40,41]. Section 6.2.2 presents the Kosterlitz–Thouless phase transition, and its application to the cavity polariton system is presented. The problem of local condensation is addressed in Section 6.2.3.

6.2.1. INTERACTING BOSONS AND BOGOLIUBOV MODEL [40,41]

In order to explain the properties of superfluid He, Landau introduced in the 1940s an original energy spectrum [42], which is displayed in Figure 6.1. This spectrum is composed of two kinds of quasiparticles: phonons and rotons. These quasiparticles are collective modes in the "gas of quasiparticles" [43], and are associated with the first and second sound. Such a spectrum introduced "by hand" allowed Landau to describe most of the peculiar properties of superfluid He. Bogoliubov's work of 1947 [40] was a real breakthrough. He presented a microscopic description of the condensed weakly-interacting Bose gas. As we shall see below, he showed how BEC is not much altered in a weakly-interacting Bose gas, something which was not obvious at the time. He also showed how interactions completely alter the long wavelength response of a Bose gas. He recovered exactly the spectrum assumed by Landau for the quasiparticle dispersion relation. Most of the further theoretical developments in the field are based on the Bogoliubov approach.

Bogoliubov considered a Hamiltonian similar to the one we used in Chapter 5:

$$H = \sum_{\vec{k}} E(\vec{k})\, p^{+}_{\vec{k}}\, p_{\vec{k}} + \frac{1}{2} \sum_{\vec{k},\vec{k}',\vec{q}} V_{\vec{q}}\, p^{+}_{\vec{k}+\vec{q}}\, p^{+}_{\vec{k}'-\vec{q}}\, p_{\vec{k}}\, p_{\vec{k}'}. \tag{6.2.1}$$

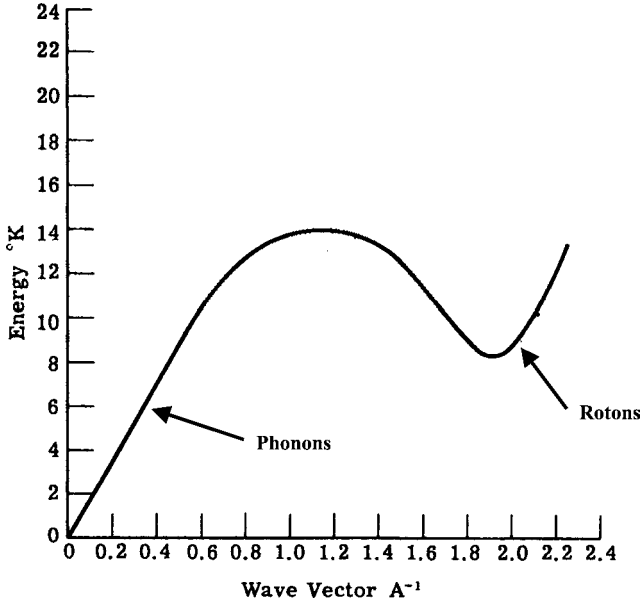

Fig. 6.1. The energy spectrum of liquid helium II.

His objective was to diagonalise this Hamiltonian making reasonable approximations. At zero Kelvin an ideal Bose gas should be completely condensed. Bogoliubov assumed that interactions are only responsible for weak condensate depletion. In other words, most system particles are assumed to be still inside the condensate. This implies:

$$p_0, p_0^+ \sim \sqrt{N_0} \gg 1 \quad \Rightarrow \quad [p_0, p_0^+] \ll p_0^+ p_0, \tag{6.2.2}$$

where N_0 is the condensate population. Bogoliubov proposed to neglect the condensate fluctuations and to replace the operators p_0^+, p_0 by complex numbers P_0^*, P_0. The condensate is thus treated classically as a particle reservoir. The second Bogoliubov approximation was to keep only the largest contributions in the interacting part of the Hamiltonian. The largest contributions are those which involve the condensate. Therefore, one keeps only the terms which involve two p_0 or more. Eq. (6.2.1) becomes:

$$\begin{aligned} H = V_0 N_0^2 + \sum_{\vec{k}\neq 0} \big(E(\vec{k}) + N_0(V_{\vec{k}} + V_0)\big) p_{\vec{k}}^+ p_{\vec{k}} \\ + N_0 \sum_{\vec{k}} V_{\vec{k}} \big(p_{\vec{k}}^+ p_{-\vec{k}}^+ + p_{\vec{k}} p_{-\vec{k}}\big). \end{aligned} \tag{6.2.3}$$

The Bogoliubov approximations conserve off-diagonal coupling terms that induce the appearance of new eigenmodes. Then, a change of basis is made through the so-called $u - v$ transformation:

$$\alpha_{\vec{k}} = u_{\vec{k}} p_{\vec{k}} - v_{\vec{k}} p_{-\vec{k}}^+, \tag{6.2.4a}$$

$$\alpha_{\vec{k}}^+ = u_{\vec{k}}^* p_{\vec{k}}^+ - v_{\vec{k}}^* p_{-\vec{k}}. \tag{6.2.4b}$$

New operators $\alpha_{\vec{k}}$, $\alpha_{\vec{k}}^+$ are bosonic operators if the transformation is canonical, namely if $u_{\vec{k}}$ and $v_{\vec{k}}$ are real numbers verifying

$$u_{\vec{k}} = u_{-\vec{k}}, \qquad v_{\vec{k}} = v_{-\vec{k}}, \qquad u_{\vec{k}}^2 = 1 + v_{\vec{k}}^2.$$

Choosing an adapted form for the $u - v$ coefficients [40,41], (6.2.3) reads:

$$H = V_0 N_0^2 + \sum_{\vec{k}\neq 0} E_{\text{bog}}(\vec{k}) \alpha_{\vec{k}}^+ \alpha_{\vec{k}} \tag{6.2.5}$$

where

$$E_{\text{bog}}(\vec{k}) = \sqrt{E(\vec{k})(E(\vec{k}) + 2N_0 V_{\vec{k}})} \tag{6.2.6}$$

is the Bogoliubov spectrum. One recovers the unperturbed dispersion if N_0 vanishes. On the other hand, if one considers the existence of a condensate, there

follows from a quadratic unperturbed dispersion $E(\vec{k}) = \hbar^2 k^2/2m$ a renormalised spectrum:

$$E_{\text{bog}}(\vec{k} \sim 0) \approx \hbar k \sqrt{\frac{N_0 V_0}{m}} \tag{6.2.7}$$

which is a phonon spectrum with a sound velocity $\sqrt{N_0 V_0/m}$. Considering a large polariton population of 10^6 and a system size of 100 microns, the typical "bogolon" velocity in a GaAs microcavity would be 5×10^5 m s^{-1}. In the same way one can estimate the reciprocal space region $[0, k_{\text{lim}}]$ where the bogolon spectrum is linear:

$$k_{\text{lim}} = \frac{2}{\hbar}\sqrt{m N_0 V_0}. \tag{6.2.8}$$

This corresponds to an angular width of about 3 degrees in the above-mentioned conditions. This rough estimate is in very good agreement with experimental results obtained so far under resonant excitation (see Section 5.1.4).

6.2.2. POLARITON SUPERFLUIDITY AND KOSTERLITZ–THOULESS PHASE TRANSITION

Superfluidity is a property deeply associated with BEC, and at first glance it seems that one of these properties cannot exist without the other. This is not exactly true [17]. BEC is linked with the appearance of a Dirac function at $k = 0$ in the distribution function of bosons. The Fourier transform of this Dirac function gives the extension in the direct space of the condensate wave-function, which is infinite and constant. BEC therefore means the appearance of a homogeneous phase in direct space. This homogeneity implies superfluidity. Particles can move throughout space along a phase-coherent, dissipationless path. Superfluidity means that statistically, two points in space are connected by a phase-coherent path, even if the whole space is not covered by a phase-coherent wave-function. As a conclusion, a superfluid state can occur without the existence of strict BEC. This is the kind of state which is taking place in two dimensions where a strict BEC is forbidden [35]. The transition between a normal state and such a superfluid state without BEC was first described by Kosterlitz and Thouless in 1973 in the framework of the XY model [36]. This second-order phase transition does not exist for an ideal gas of bosons, but it does exist in systems of weakly-interacting bosons such as low-density excitons [37–39] or polaritons [4]. We now describe qualitatively how this phase transition takes place, and we estimate the Kosterlitz–Thouless (KT) transition temperature T_{KT} for the polariton case. At temperatures higher than the critical temperature T_{KT}, the superfluid number density n_s is zero, but local condensation can take place. Condensate droplets can have quite large sizes as we shall see later, but they are characterised by an exponentially decreasing

correlation function and are not connected together. Free vortices prevent long-range ordering, i.e., percolation of the quasi-condensate droplets. However, once the critical temperature T_{KT} is reached, single vortices are no longer stable. They bind, forming pairs or clusters with the total winding number equal to zero, allowing for a sudden percolation of the quasi-condensate droplets which therefore form a superfluid. For temperatures slightly below T_{KT}, the superfluid number density is proportional to T_{KT} with a universal coefficient [44]:

$$n_s = \frac{2mk_bT_{\mathrm{KT}}}{\pi\hbar^2}, \tag{6.2.9}$$

where m is the bare polariton mass at $q = 0$, k_b is the Boltzmann constant. The pairs of vortices remain well below T_{KT} and the correlation function is not constant, but decreases as a power of distance. The superfluid wave-function has thus a finite extension in reciprocal space, and consequently is not a BEC wave-function. Complete homogeneity and true long-range order can be achieved only at $T = 0$, where vortices disappear. Below T_{KT} normal and superfluid phases coexist. The normal fluid can be characterised by a density n_n and a velocity $\vec{v}_n$, while the superfluid has a density n_s and velocity $\vec{v}_s$. The total fluid density is:

$$n = n_n + n_s, \tag{6.2.10}$$

where n_n can be calculated by following, for example, [37]. Despite the absence of BEC in two dimensions, the energies of quasiparticles (bogolons) in the superfluid phase are still given by a Bogoliubov expression:

$$E_{\mathrm{bog}}(\vec{k}) = \sqrt{E(\vec{k})(E(\vec{k}) + 2\mu)}. \tag{6.2.11}$$

We need to know the chemical potential of interacting polaritons to calculate the quasiparticle dispersion. With the meaning previously given for the chemical potential, when one considers added particles going into the ground state, the associated interaction energy yields [37–39]:

$$\mu = NV_0. \tag{6.2.12}$$

Once the quasiparticle dispersion is known, one can use the famous Landau formula [45] to calculate the normal mass density. This expression remains well-behaved in two dimensions:

$$n_n = \frac{1}{(2\pi)^2}\int E(\vec{k})\left[-\frac{\partial f_B(E_{\mathrm{bog}}(\vec{k}, T, 0))}{\partial E_{\mathrm{bog}}(\vec{k})}\right] d^2\vec{k}. \tag{6.2.13}$$

Note that the Bose distribution function (6.1.1) entering this expression is taken at zero bogolon chemical potential, while the non-zero polariton chemical potential is still present in the bogolon dispersion relation (6.2.11). Eqs. (6.2.11) to (6.2.13) yield $n_s(T, n)$. Its substitution into Eq. (6.2.9) allows one to obtain $T_{\mathrm{KT}}(n)$, and

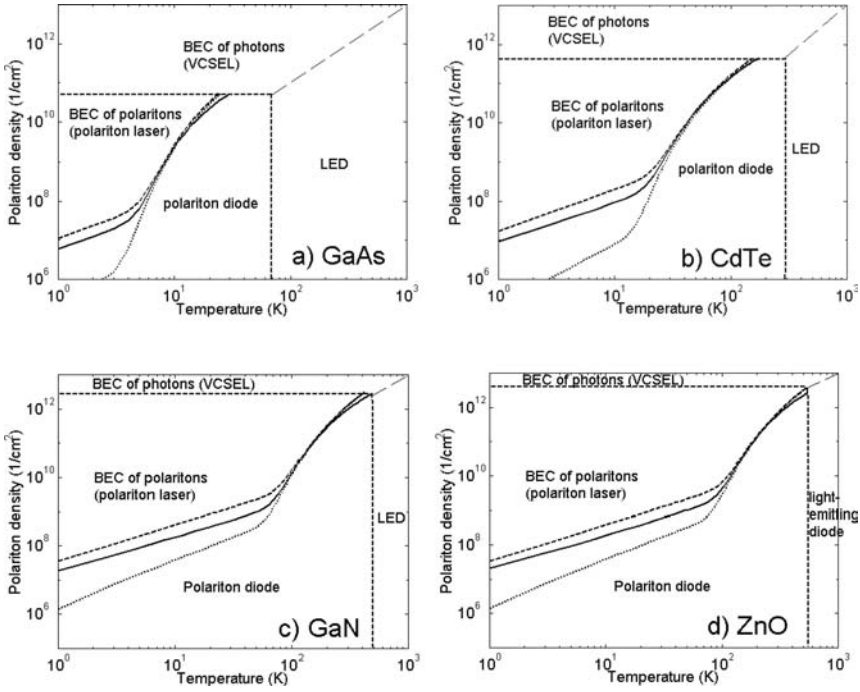

Fig. 6.2. Phase diagrams for GaAs (a), CdTe (b), GaN (c), and ZnO (d) based microcavities at zero detuning. Vertical and horizontal dashed lines show the limits of the strong-coupling regime imposed by the exciton thermal broadening and screening, respectively. Solid lines show the critical concentration N_c versus temperature of the polariton KT phase transition. Dotted and dashed lines show the critical concentration N_c for quasi condensation in 100 μm and 1 meter lateral size systems, respectively. The thin dashed line symbolizes the limit between vertical cavity surface emitting laser (VCSEL) and light-emitting diode regimes.

therefore to plot a polariton phase diagram. Such a phase diagram is shown in Figure 6.2. Solid lines (a)–(d) show the critical concentration for a KT phase transition according to the above-mentioned procedure, and calculated for typical microcavity structures based on GaAs (a), CdTe (b), GaN (c), and ZnO (d). In all cases we assume zero detuning of the exciton resonance and the cavity photon mode. For GaAs- and CdTe-based microcavities we have used the parameters of experimentally studied samples reported in Refs. [46] and [47]. Parameters of model GaN and ZnO microcavity structures can be found in Refs. [5,6]. So far, the two latter structures have only a hypothetical interest, since the strong coupling has not yet been achieved experimentally in GaN- and ZnO-based cavities. Vertical and horizontal dashed lines show the approximate limit of the strong-coupling regime in the microcavity that come from either exciton screening by

a photo-induced electron–hole plasma or from temperature-induced broadening of the exciton resonance (see discussion on the weak-strong coupling transition Section 1.3). Below the critical density, if still in the strong-coupling regime, a microcavity operates as a polariton diode emitting incoherent light, while in the weak-coupling regime the device behaves like a conventional light-emitting diode. Above the critical density, in the weak-coupling regime, the microcavity acts as a conventional laser. Thin dashed lines in Figure 6.2 indicate the limit between the latter two phases that cannot be found in the framework of our formalism limited to the strong-coupling regime. One can note that critical temperatures achieved are much higher than those which can be achieved in exciton systems. In existing GaAs- and CdTe-based cavities these temperatures are high enough for experimental observation of the KT-phase transition under laboratory conditions, but do not allow one to produce devices working at room temperature. Record critical temperatures of $T_{\mathrm{KT}} = 450$ K and 560 K for GaN- and ZnO-based model cavities are given by extremely high exciton dissociation energies in these semiconductors. It is interesting to note that even above $T_{\mathrm{KT}}(n)$, $n - n_n$ does not vanish, which reflects the existence of isolated quasi-condensate droplets. As we show below, these droplets can reach substantial size, even above the Kosterlitz–Thouless temperature or density. Their properties could dominate the behaviour of real systems.

6.2.3. QUASI-CONDENSATION AND LOCAL EFFECTS

In this section we define a rigorous criterion for boson quasi-condensation in finite-size systems. For the sake of simplicity we neglect here all kinds of interactions between particles. Let us consider a system of size R. The particle density is given by

$$n(T, R, \mu) = \frac{N_0}{R^2} + \frac{1}{R^2} \sum_{\vec{k},\ |k| \geqslant 2\pi/R} f_B(\vec{k}, T, \mu), \tag{6.2.14}$$

where N_0 is the ground-state population. We define the critical density as the maximum number of bosons which can be accommodated in all the states but the ground state:

$$n_c(R, T) = \frac{1}{R^2} \sum_{\vec{k},\ |k| \geqslant 2\pi/R} f_B(\vec{k}, T, 0). \tag{6.2.15}$$

The quasi-condensate density is thus given by $n_0 = n - n_c$. In this case, formally, the chemical potential μ is always strictly negative, but it approaches zero, allowing one to put as many bosons as desired in the ground state, while keeping concentration of bosons in all other states finite and limited by n_c. The concentration

(6.2.15) can be considered as the critical concentration for local quasi-Bose condensation in two-dimensional systems. Further, we shall refer to T_c defined in this way as the critical temperature of Bose condensation in a finite two-dimensional system. On the other hand, it appears possible, knowing the temperature and density, to deduce the typical coherent droplet size, which is given by the correlation length of the quasi-condensate.

From a practical point of view, experiments are performed on samples having a lateral size of about 1 cm. Electron–hole pairs are generated by laser light with a spot area of about 100 μm. These electron–hole pairs rapidly (typically on a timescale less than 1 ps) form excitons, which relax down to the optically active region, where they strongly interact with the light field to form polaritons. Excitons that form polaritons have a finite spatial extension in the plane of the structure, but they are all coupled to each other via light [48]. The polariton system thus covers the whole surface where excitons are generated. If the KT critical conditions are not fulfilled, but if typical droplets sizes are larger than the light spot size, the whole polariton system can be transiently phase-coherent and thus exhibits local BEC. As we shall show below, this situation is the most likely to happen in current optical experiments performed at low temperature.

Let us underline at this point an important advantage of polaritons with respect to excitons weakly coupled to light for the purposes of BEC or superfluidity. Actually, individual excitons in real structures are subject to strong localisations in inevitable potential fluctuations that prevent them from interacting and forming condensed droplets. Polaritons are basically delocalized, even though the excitons forming them could be localised. This is why their interactions are expected to be more efficient and bosonic behaviour more pronounced. The dotted and dashed lines on Figure 6.2 (a)–(d) show the critical concentration for local quasi-condensation in microcavity systems of 100 μm and 1 m lateral size, respectively. In the high-temperature (high-concentration) limit critical concentrations are very similar for both lateral sizes, and they slightly exceed critical concentrations of the KT phase transition. This means that in this limit the KT transition takes place before the droplet size reaches 100 μm. Conversely, in the low-temperature (low-concentration) limit the KT curve is between the transition curves of the 100 μm and 1 m size systems. This shows that droplets at the KT transition are larger than 100 μm but smaller than 1 m. Since the typical laser spot size is of about 100 μm, this means that local Bose condensation takes place before the KT transition at low pumping. A detailed analysis could allow one to obtain the percolating droplet size versus temperature, which is beyond the scope of our present discussion.

Note finally that inhomogeneous broadening of the exciton resonance leads to broadening of the polariton ground state in the reciprocal space. Any broadening in the reciprocal space is formally equivalent to localization in the real space. Such a localization present even in an infinite microcavity allows for quasi-condensation, in principle [49].

6.3. Relaxation Kinetics of Cavity Polaritons: Towards Polariton Lasing

As pointed out in the previous section, cavity polariton condensation represents an equilibrium state of the polariton system in a wide condition range. However, polaritons have a finite lifetime in microcavities and are therefore non-equilibrium particles. Relaxation of polaritons in the steepest zone of the polariton dispersion, and therefore towards the ground state, is a slow process compared to the polariton lifetime. Such slow relaxation results in a "bottleneck effect" (see Chapter 4). Photoluminescence mainly comes from the "bottleneck region", and the population of the ground state remains much lower than what one could expect from the equilibrium distribution function. A suitable formalism to describe polariton population dynamics is the semi-classical Boltzmann equation presented in Chapter 4. This formalism has been widely used [7,8,10–12] and has proven successful when its results were compared to experimental data [50]. A major weakness of this approach is that beyond the populations, all quantities of interest, such as the order parameter and various correlation functions, are beyond its scope. A derivation involving quantum features of the system must be undertaken [1,9]. Section 6.3.1 reviews experimental efforts performed in the years 1996–2003 in order to observe polariton lasing. A linear quantum theory of the polariton laser, only valid in the low density limit is then presented in Section 6.3.2. Section 6.3.3 presents numerical results, and discusses practical ways to improve polariton relaxation kinetics in real structures and the perspectives for polariton BEC.

6.3.1. EXPERIMENTAL QUEST OF THE POLARITON LASER (1996–2003)

A few months after Imamoglu's prediction [1] in 1996, Yamamoto's group published an experimental paper [51] claiming the observation of polariton lasing. The structure studied was a GaAs-based cavity at positive detuning. The authors observed the take-off of a sharp lasing mode from the LPB for a pumping power larger than 100 mW. They interpreted their results along the lines of some "Bose action", a disguise of polariton BEC. This "first shot" was, however, not a good one. Indeed, as pointed out by Kira et al. [52], the carrier density induced by the used pumping power was revealed to be much too high to allow strong coupling to be maintained. The authors of [51] published, less than one year after their initial paper, an experiment [53] whose result is shown in Figure 6.3. They simultaneously measured photoluminescence and reflection from a microcavity, showing that the strong sharp line they observed was due to a "normal lasing" effect rather than polariton BEC. In 1997, Tassone proposed the theoretical modeling of polariton relaxation by a numerical solution of the semi-classical Boltzmann equation [7] (see Chapter 4). Contrary to Imamoglu, Tassone did not neglect the real shape of the cavity polariton dispersion, and finally obtained a completely

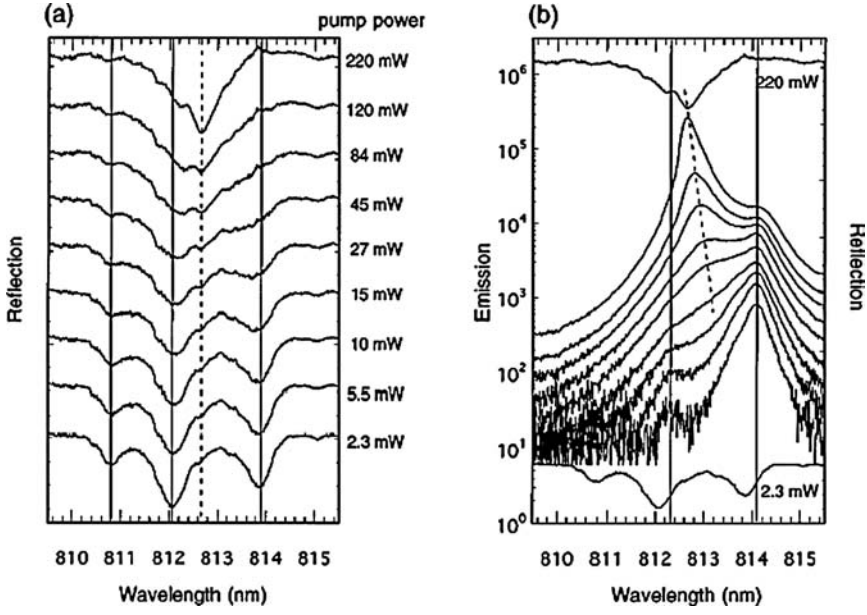

Fig. 6.3. The sample studied is a GaAs based microcavity. The structure is pumped non resonantly while a probe measure the reflection. (a) The reflection spectra of the probe at different incident pump powers. (b) The cavity emission spectra at the pump powers corresponding to (a). Two reflection spectra at low and high pump power also shown for comparison. From [52].

different conclusion. He showed that acoustic phonons cannot provide an efficient polariton relaxation toward the ground state in the steep central part of the polariton dispersion, where its slope exceeds the sound velocity. This should result in an accumulation of polaritons in the "bottleneck region". Therefore, cavity polariton BEC, only helped by acoustic phonon relaxation, appeared somewhat compromised.

Nevertheless, a nonlinear dependence of ground-state emission versus nonresonant pumping power has been observed experimentally in II–VI [47] and III–V [46] microcavities. Figure 6.4 summarizes results obtained in III–V. The superlinear dependence of PL has been found to be quadratic (Figure 6.4(a)), which shows that the dominant relaxation process is exciton–exciton scattering. However, stimulation by the final-state population should result in an exponential dependence of PL, and in a line sharpening. As pointed out in [46], this is not the case in III–V. Angle-resolved luminescence has also been performed, allowing the extraction of the polariton distribution function (Figure 6.4(b)). A bottleneck effect is visible for the lower excitation power 0.4 W/cm^2, but disappears with increasing pumping. The maximum ground-state population achieved stays, how-

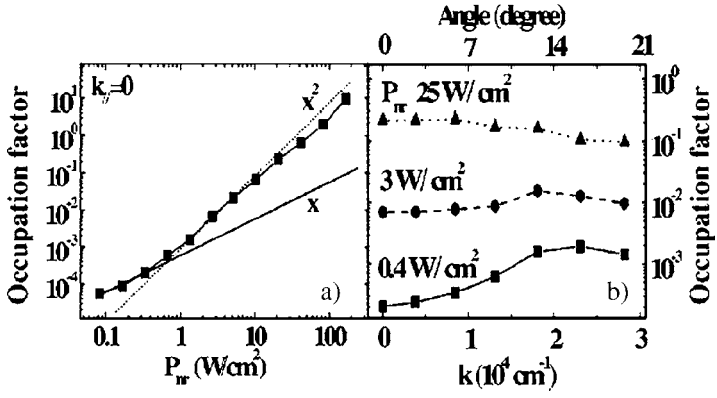

Fig. 6.4. (a) Occupation factor of the ground polariton state as a function of pumping power in a GaAs microcavity with a single InGaAs QW. The straight-dotted line shows what would be a linear-quadratic dependence. (b) Occupation factor as a function of k for three different pumping powers. From [46] (*Phys. Rev. B* paper).

ever, smaller than 1. All these data confirm that stimulation does not take place in such cavities before the weak-strong coupling transition. This conclusion has been recently confirmed by a series of experimental papers [54,50].

The situation is more promising in CdTe-based structures. Nonlinear emissions reported are accompanied by a line sharpening and the PL dependence of the emission versus pumping is exponential [47,13]. These features are accompanied by a blue shift of the emission line of about 1 meV, which remains much smaller than that which would result from a weak-strong coupling transition. One can conclude that clear evidence of polariton stimulated scattering under non-resonant excitation has been reported. A complex spin dynamics, probably a signature of strong bosonic effects, has also been observed [55] (see Section 6.4).

At the end of 2002, an increase of the second-order coherence of light emitted from the polariton ground state in a GaAs-based microcavity containing 12 QWs above some threshold has been reported [56] by the Yamamoto group, and polariton BEC claimed a second time. The time of writing is only a few months after the publication of this paper, and it is too early to give a positive or negative judgement on this work. At least, all these results clearly point out which measurements should be performed in order to definitively observe polariton BEC:

- PL versus pumping must show an exponential behavior.
- A clear line sharpening should accompany the emission take off. It may be followed by a broadening induced by a very large ground state occupation.
- The polariton distribution function should be peaked around $k = 0$.

- The quantum nature of the ground state should be probed measuring statistics of the emitted photon or second-order coherence, for example, performing Hanbury–Brown–Twiss like experiments [20].
- Strong coupling should clearly survive in a wide enough range of pumping while exponential emission takes place.

To the best of our knowledge, all these criteria have never been reported to be experimentally fulfilled together. However, results reported so far give us good hope for the near future.

6.3.2. THEORETICAL DESCRIPTION OF THE POLARITON LASER

In this section we provide a theoretical formalism for the kinetics of the various quantities involved in polariton condensation. Numerical results will be presented in Section 6.3.3.

6.3.2.1. Dissipative Linear Equation for the Polariton System

The relaxation kinetics of polaritons excited in a semiconductor microcavity are expected to be essentially classical for low polariton concentrations, when they can be regarded as weakly-interacting Bose particles. The temporal evolution of populations for the ground state N_0 and excited states $N_{\vec{k}}$ (with $N_{\vec{k}} \neq 0$) is due to random and independent scattering events, and the kinetics are well described by classical kinetic equations. However, the Boltzmann formalism should be extended in order to treat the quantum quantities of interest, rather than to shift to an altogether new realm of quantum transport theory. More precisely, we are interested in the quantum description of the evolution of the polariton ground state, i.e., the lasing mode. For all other states, apart from the stimulated scattering, which is easily taken into account with classical variables, the dynamics will be restored to that dictated by the Boltzmann equation. We fulfill the above programme by starting from a full quantum-mechanical picture in the formalism of density matrices and averaging over all degrees of freedom except the polariton ground state. This procedure is familiar from quantum optics in open systems [57], but our case presents additional features: the polariton field is (i) massive, (ii) self-interacting, and (iii) the polaritons have finite lifetime. In terms of the annihilation and creation operators $p_{\vec{k}}, p^+_{\vec{k}}$ for polaritons and $b_{\vec{k}}, b^+_{\vec{k}}$ for phonons, obeying the usual bosonic algebra, our model Hamiltonian in the interaction representation reads

$$H(t) = \sum_{\vec{k},\vec{q}\neq 0} U(\vec{k},\vec{q}) e^{\frac{i}{\hbar}(E(\vec{k})+\hbar\omega_{\vec{q}}-E(\vec{k}+\vec{q}))t} p^+_{\vec{k}} b^+_{\vec{q}} p_{\vec{k}+\vec{q}} + H.c.$$
$$+ \frac{1}{2} \sum_{\vec{k},\vec{p},\vec{q}} V(\vec{k},\vec{p},\vec{q}) e^{\frac{i}{\hbar}(E(\vec{k}+\vec{q})+E(\vec{k}-\vec{q})-E(\vec{k})-E(\vec{p}))t} p^+_{\vec{k}+\vec{q}} p^+_{\vec{p}-\vec{q}} p_{\vec{k}} p_{\vec{p}}, \tag{6.3.1}$$

where U is the Fourier transform of the interaction potential for polariton–phonon scattering and $\hbar\omega_{\vec{q}}$ is the phonon dispersion. This Hamiltonian incorporates the specific issues (i) and (ii), but does not address the finite lifetime, which is central to the physics of the polariton laser. As we shall see shortly, however, it can easily be allowed for in the final equations. It should be noted that a strong enough polariton–polariton interaction quickly destroys the applicability of the Boltzmann kinetic equation, as well as its extension presented below. In what follows, the evolution of the density matrix $\rho(t)$ of the system will be studied in the Born–Markov approximation. First, we iterate the Liouville–von Neumann equation $i\hbar\dot{\rho} = [H, \rho]$ to obtain

$$i\hbar\dot{\rho} = \big[H, \rho(-\infty)\big] + \int_{-\infty}^{t} \big[H(t), \big[H(\tau), \rho(\tau)\big]\big]\, d\tau. \tag{6.3.2}$$

Second, we apply the Born approximation, in which the density matrix of the system ρ is separable and can be written as a product of the density matrices for the polariton ground state $\rho_0(t)$, the polariton excited states $\rho_{\text{exc}}(t)$, and the phonons $\rho_{\text{phon}}(t)$, and it remains likewise uncorrelated for all times. The polariton density matrix evolves in time, while the phonon subsystem is considered as a thermal bath so that ρ_{phon} is kept equal to the equilibrium density matrix, which makes the evolution irreversible:

$$\rho(t) = \rho_0(t)\rho_{\text{exc}}(t)\rho_{\text{phon}}. \tag{6.3.3}$$

One makes the link with classical quantities $N_{\vec{k}} \equiv \langle p_{\vec{k}}^{+} p_{\vec{k}} \rangle$ and $n_{\vec{k}} \equiv \langle b_{\vec{k}}^{+} b_{\vec{k}} \rangle$, but retains the quantum character of the $k = 0$ state, by tracing over all phonon states and all $k \neq 0$ polariton states. After some lengthy but straightforward algebra, this partial trace applied to $[H(t), [H(\tau), \rho(\tau)]]$ results in the Lindblad form [58] $LL^{+}\rho_0 + \rho_0 LL^{+} - 2L^{+}\rho_0 L$ multiplied by time-dependent coefficients. The operator L coincides with p_0, p_0^{+}, or their combinations. It is at this stage that the Markov approximation is invoked: the populations are assumed to vary slowly with time and are taken out of the integral in (6.3.2) at $t = \tau$. The remaining product of exponentials, stemming from (6.3.1), is then integrated to give the energy-conservation delta functions. This procedure can be carried out easily to yield the master equation for the ground state density matrix:

$$\dot{\rho}_0 = L\rho_0. \tag{6.3.4}$$

The Liouville operator L entering this equation is given by

$$L\rho_0 = -\frac{1}{2}\left[\begin{array}{l} W_{\text{out}}(t)(p_0^{+} p_0 \rho_0 - 2p_0\rho_0 p_0^{+} + \rho_0 p_0^{+} p_0) \\ \quad + W_{\text{in}}(t)(p_0 p_0^{+}\rho_0 - 2p_0^{+}\rho_0 p_0 + \rho_0 p_0 p_0^{+}) \end{array}\right], \tag{6.3.5}$$

where $W_{\rm in}$ and $W_{\rm out}$ are obtained from the above-mentioned derivation as:

$$W_{\rm in}(t) = \frac{2\pi}{\hbar}\left[\begin{array}{l}\displaystyle\sum_{\vec{q}\neq 0}\left|U(0,\vec{q})\right|^2 N_{\vec{q}}(t)(1+n_{\vec{q}})\delta\big(E(\vec{q})-\hbar\omega_{\vec{q}}\big) \\ \quad\displaystyle+\sum_{\vec{q}} N_{\vec{q}}(t)\sum_{\vec{k}\neq 0}\left|V(\vec{q},0,\vec{k})\right|^2 N_{\vec{k}}(1+N_{\vec{k}+\vec{q}}) \\ \qquad\qquad\times\delta\big(E(\vec{k}+\vec{q})-E(\vec{k})-E(\vec{q})\big)\end{array}\right]$$

$$\equiv \sum_{\vec{q}} w_{\vec{q}\to 0} N_{\vec{q}}, \tag{6.3.6}$$

$$W_{\rm out}(t) = \frac{2\pi}{\hbar}\left[\begin{array}{l}\displaystyle\sum_{\vec{q}\neq 0}\left|U(0,\vec{q})\right|^2 \big(1+N_{\vec{q}}(t)\big) n_{\vec{q}}\delta\big(E(\vec{q})-\hbar\omega_{\vec{q}}\big) \\ \quad\displaystyle+\sum_{\vec{q}} N_{\vec{q}}(t)\sum_{\vec{k}\neq 0}\left|V(\vec{q},0,\vec{k})\right|^2 (1+N_{\vec{k}})(1+N_{\vec{q}-\vec{k}}) \\ \qquad\qquad\times\delta\big(E(\vec{q})-E(\vec{q}-\vec{k})-E(\vec{k})\big)\end{array}\right]$$

$$\equiv \sum_{\vec{q}} w_{0\to\vec{q}}(1+N_{\vec{q}}). \tag{6.3.7}$$

This approach can be easily generalised to include the polariton relaxation due to the interaction with other degrees of freedom, as long as the elementary relaxation processes are reduced to those with only one polariton at a time coming into or coming out of the condensate. In particular, the account for the polariton recombination (both radiative and non-radiative) will result in a constant correction Γ_0 added to $W_{\rm out}(t)$, such that $1/\Gamma_0$ is the lifetime of the polariton in the condensate. Eq. (6.3.5) describes a linear amplifier [20], namely a medium with a net gain allowing linear amplification of the signal, but devoid of positive feedback, like mirrors in conventional lasers. The only difference from the classical linear amplifier formalism, as it is commonly found in the literature, comes from the time dependence of $W_{\rm in}$ and $W_{\rm out}$ which may yield a non-trivial behavior for the quantities of interest. As we shall see below, such an equation is not adapted to describe a spontaneous symmetry breaking effect. To do so, one should account for either non-linear terms induced by a feedback (as in laser theory), or off-diagonal contributions (as in BEC theories).

6.3.2.2. Evolution of Average Quantities

Eq. (6.3.5) can be used to write the equation of motion of any variable $A = \langle\hat{A}\rangle$ associated with any quantum observable $\hat{A}$ referring to the ground state, with $\dot{A} = {\rm Tr}(L\rho_0 A)$. For instance, the equation for $N_0 = \langle p_0^+ p_0\rangle$ is obtained in this

way as

$$\dot{N}_0 = \big(W_{\text{in}}(t) - W_{\text{out}}(t)\big)N_0 + W_{\text{in}}(t). \tag{6.3.8}$$

This fulfills our initial goal to link to the Boltzmann theory, and Eq. (6.3.8) coincides with the semi-classical kinetic equation (see Chapter 4, Eq. (4.2.3)):

$$\dot{N}_0 = -\Gamma_0 N_0 - N_0 \sum_{\vec{q}} w_{0\to\vec{q}}(1 + N_{\vec{q}}) + (N_0 + 1)\sum_{\vec{q}} w_{\vec{q}\to 0} N_{\vec{q}}, \tag{6.3.9}$$

which is therefore rigorously demonstrated from a microscopic derivation. W_{in} is the spontaneous scattering term, whereas $(W_{\text{in}} - W_{\text{out}})N_0$ is the stimulated scattering term. An equation for the condensate order parameter $\langle p_0\rangle$ can also be derived from (6.3.5):

$$\langle \dot{p}_0\rangle = \frac{1}{2}\big(W_{\text{in}}(t) - W_{\text{out}}(t)\big)\langle p_0\rangle. \tag{6.3.10}$$

Here the spontaneous term is absent. A solution of this equation is formally written as:

$$\big\langle p_0(t)\big\rangle = \big\langle p_0(0)\big\rangle \exp\left[\int_0^t \big(W_{\text{in}}(\tau) - W_{\text{out}}(\tau)\big)\,d\tau\right]. \tag{6.3.11}$$

Another quantity of particular interest for the polariton lasing problem is the second-order correlator $A(t) = \langle p_0^+ p_0^+ p_0 p_0\rangle$, which is linked to the second-order coherence [20,56]:

$$\eta_2(t) = \frac{2N_0^2(t) - A(t)}{2N_0^2(t)}. \tag{6.3.12}$$

The coherence parameter η_2 is equal to 1 when the condensed polaritons form a coherent state, and it goes to zero for a chaotic state of the condensate. It can be measured in two-photon counting experiments [20,56], and gives information about the quantum nature of the condensate. The equation of motion of the quantity $B(t) = 2N_0^2(t) - A(t)$ reads

$$\dot{B} = \big(W_{\text{in}}(t) - W_{\text{out}}(t)\big)B. \tag{6.3.13}$$

One can note that the equation of motion for B is the same in this linear formalism as the one for the square of the order parameter. Another quantity of interest is the whole polariton system coherence, defined as

$$\eta_T = \eta_2 \frac{N_0}{N}, \tag{6.3.14}$$

where $N = \sum_{\vec{q}} N_{\vec{q}}$ is the total number of polaritons.

6.3.2.3. Analysis

We now consider the simple but instructive case where W_{in} and W_{out} do not depend on time. In such a case, the order parameter and ground state populations are:

$$\langle p_0(t)\rangle = \langle p_0(0)\rangle e^{\frac{1}{2}(W_{\text{in}}-W_{\text{out}})t}, \tag{6.3.15}$$

$$N_0(t) = \left(N_0(0) + \frac{W_{\text{in}}}{W_{\text{in}} - W_{\text{out}}}\right) e^{(W_{\text{in}}-W_{\text{out}})t} - \frac{W_{\text{in}}}{W_{\text{in}} - W_{\text{out}}}. \tag{6.3.16}$$

There are two distinct regimes depending on the sign of $W_{\text{in}} - W_{\text{out}} = \Delta W$.

If $\Delta W < 0$, the order parameter vanishes and the ground-state population reaches an equilibrium value:

$$N_0(\infty) = -\frac{W_{\text{in}}}{\Delta W}. \tag{6.3.17}$$

If $\Delta W > 0$, both ground-state population and order parameter diverge. This is the Bose condensation situation. Of course, such a situation is not realistic and some time dependence of W_{in} and W_{out} should be included to make the model converge. However, one can see that the signal rise is convex versus time for sub-critical conditions ($\Delta W < 0$), while it is concave for super-critical conditions ($\Delta W > 0$). This kind of feature can be checked experimentally in time-resolved photoluminescence experiments.

6.3.3. NUMERICAL RESULTS

6.3.3.1. How to Overcome the Bottleneck Effect?

The bottleneck region of the LPB corresponds to the transition from the exciton-like to the photon-like part of the dispersion. Exciton–exciton scattering has been proposed as an efficient relaxation process for polaritons. It remains, however, an elastic scattering process which does not dissipate the total polariton energy. It may allow stimulated scattering to take place, but as we shall see below, it hardly allows the achievement of a thermal distribution. Currently, we see two possible ways to suppress the bottleneck effect and to achieve polariton lasing. First, in future GaN-, ZnSe- or ZnO-based cavities at room temperature, if the strong-coupling regime still holds, acoustic phonon relaxation should be much more efficient than in presently-available cavities at helium temperature. Second, n-doping of microcavities is expected to allow efficient electron–polariton scattering within the photon-like part of the dispersion. The advantage of this scattering mechanism with respect to previously discussed ones is that the matrix element of electron–exciton scattering is quite large. Also, an electron has a much lighter mass than a heavy-hole exciton. Thus, the energy relaxation of a polariton from

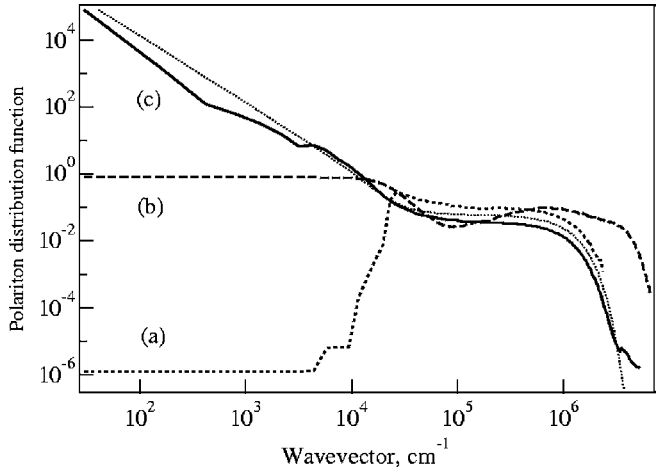

Fig. 6.5. Distribution function of polaritons in a model microcavity based on GaAs at 10 K when non-resonantly pumped with a power of 4.2 W/cm^2. Results are shown for (a) polariton–acoustic phonon scattering (dotted), (b) as (a) plus polariton–polariton scattering (dashed), and (c) as (b) plus polariton–electron scattering (solid). The thin dotted line shows the equilibrium Bose distribution function with zero chemical potential. From [10].

the bottleneck region to the ground state requires fewer scattering events than for polariton–polariton or polariton–phonon scattering. These advantages have been found theoretically to be strong enough to restore fast polariton relaxation and allow the polaritons to condense into their trapped state [10]. At the time of writing these lines, this prediction is confirmed by encouraging experimental results [59].

In order to illustrate our purpose we consider a GaAs based microcavity containing a single quantum well. We take into account a finite system size R which is assumed to be given by a 100 μm excitation spot size. This is practically done by considering a spacing of $2\pi/R$ between the ground state and the first excited states, whereas the remaining reciprocal space states are assumed to vary continuously. Figure 6.5 is extracted from [10]. The results shown here are found by solving the complete set of Boltzmann equations for all k states. Taking into account only the acoustic phonon scattering (curve (a) in Figure 6.5), a thermal distribution function is seen only beyond $k = 2 \times 10^4$ cm^{-1} (the bottleneck region) where polaritons accumulate. Equilibrium is reached 10 ns after the start of the non-resonant pumping, leaving an equilibrium polariton density of 2.5×10^{10} cm^{-2}. Including both polariton–polariton and polariton–acoustic phonon scattering processes (curve (b) in Figure 6.5) shows partial relaxation of the bottleneck and a flat polariton distribution. However, the equilibrium polariton density in the cavity remains the same, close to the saturation density for excitons (about 5×10^{10} cm^{-2}). The distribution function near the polariton ground state

approaches one. This result is in excellent agreement with experimental results obtained by Sellenart, Butté and Tartakovskii [46,50,54], which show that the amplification threshold for the distribution function at the trap state is reached when the strong-coupling regime is likely to be suppressed. To obtain an increase in the population of the lowest k state one has to increase the population of a large number of states, requiring a large density of excitons. This is due to the flat shape of the distribution function which comes from the nature of the polariton–polariton scattering process (each scattering event increases the population of the high-k states; relaxation of polaritons from these states is then assisted only by phonons and is slow). Of course, a ground-state population larger than one is achievable within the strong coupling, especially using microcavities made of larger band-gap semiconductors, such as CdTe [12]. The efficiency of exciton–exciton scattering to achieve a thermal distribution function remains low, however, and BEC hard to achieve. The radiative efficiency, which we estimate as the ratio of the concentration of photons leaving the cavity within a cone of less than 1° to the pumping intensity, is thus found to be only 1.7%. When a small free electron density of 10^{10} cm^{-2} is taken into account (curve (c) in Figure 6.5), a huge occupation number of the lowest energy state of more than 10^4 is achieved. This system thus acts as a polariton laser, in which scattering of polaritons injected at high k by optical or electrical pumping is stimulated by population of low-k states. In such a situation the light power emitted in a cone of 1° is 3.3 W/cm^2 and the efficiency of the energy transfer from pump to emitted light is about 80%. The light emitted by the cavity is much more directional and comes from a smaller number of states than in case (b). The equilibrium polariton density in the cavity is now 1.25×10^9 cm^{-2}, i.e., 20 times lower than in cases (a), (b). Pump powers at least forty times stronger can be used before the strong to weak coupling threshold is reached. The thin dotted line in Figure 6.5 shows the equilibrium polariton density from a Bose distribution function plotted for zero chemical potential. It follows quite closely curve (c), which clearly demonstrates that a thermodynamic equilibrium is practically achieved for this value of the chemical potential, which is a signature of Bose condensation of polaritons.

Another interesting feature is found in Figure 6.6, which shows the radiative efficiency of the cavity as a function of input power with (a) and without (b) polariton–electron scattering. In the first case, the emission rises quadratically up to the threshold, while in the second case it is much larger and increases linearly. The dotted line on curve (b) marks the excitation conditions for which the strong-coupling regime collapses because of the bleaching of the excitons.

6.3.3.2. Dynamical Formation of the Polariton Condensate

Before presenting the numerical results we give a qualitative analysis of the polariton condensate formation. The kinetics are characterised by a transient regime,

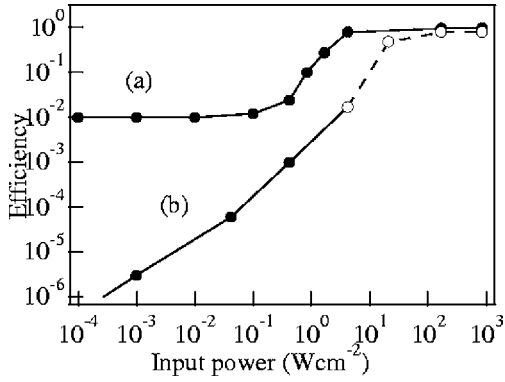

Fig. 6.6. Radiative efficiency versus power absorbed in the microcavity considered at 10 K, for (a) a doped cavity, $n_e = 10^{10}$ cm^{-2}, and (b) an undoped cavity. The dotted part of the curve (b) corresponds to a calculated exciton density $> 5 \times 10^{10}$ cm^{-2}.

during which the polaritons come to the condensate, after being excited in some $k \neq 0$ state at $t = 0$. Their relaxation speed depends nonlinearly on the pumping intensity. For strong enough pumping the stimulated scattering of polaritons into the condensate flares up at a time $t > 0$, so that the income rate increases drastically and becomes much greater than the outcome rate. In the time domain, where $W_{\text{in}}(t) > W_{\text{out}}(t)$, the $\langle p_0 \rangle = 0$ solution becomes unstable (see Eq. (6.3.10)). This instability allows the condensation to happen in a coherent quantum state. The formation of the condensate with $t \neq 0$ implies breaking the symmetry of the system, which cannot happen spontaneously in the framework of the formalism used. Therefore, to study the possibility of coherence build-up we introduce an initial seed (a coherent state with small average number of polaritons). This initial coherence can survive and be amplified for the high relaxation speed, when there exists the time domain with $W_{\text{in}}(t) > W_{\text{out}}(t)$. After the steady-state regime is reached the $\langle p_0 \rangle = 0$ point becomes stable again, since the rates reach the time-independent values $W_{\text{in}}(\infty)$ and $W_{\text{out}}(\infty)$, with $W_{\text{out}}(\infty) > W_{\text{in}}(\infty)$. However, the difference between the stationary rates is very small, inversely proportional to the system area, which corresponds to a large stationary number of condensed polaritons. If the coherence is formed its decrease is extremely slow in large cavities.

We consider the same cavity as previously, containing 10^{10} electrons/cm^{-2}. The coefficients $W_{\text{in}}(t)$ and $W_{\text{out}}(t)$ are extracted from the Boltzmann equation. We model the following experiment: at $t = 0$ an ultrashort laser pulse generates a coherent ground state containing a variable polariton number (seed). At the same time, an incoherent non-resonant *cw* pumping is turned on. Three pumping densities (0.8, 8 and 160 W/cm^2) are considered. In all cases the strong-coupling regime is maintained. Figure 6.7 shows the evolution of the ground-state pop-

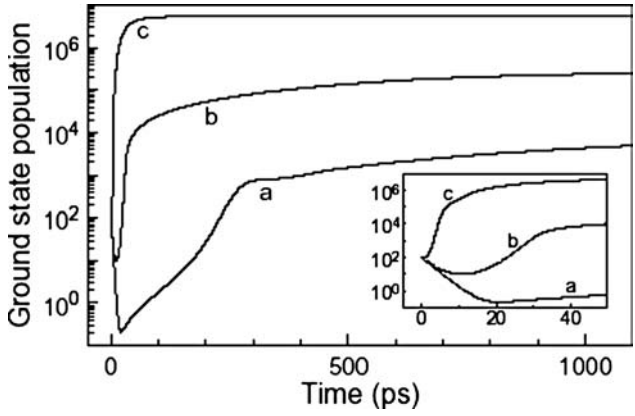

Fig. 6.7. Time dependence of the Bose-condensate occupation number N_0. The pumping densities are 0.8, 8, and 160 W/cm^2 for curves a, b, and c, respectively. The evolution of the seed at the initial stage is shown in the insert.

Table 6.1. Stationary values obtained for three different pumping powers of: the ground state (N_0), the ratio between the populations of the ground state and of the first excited state (N_0/N_1), the ratio between the population of the ground state and the total population (N_0/N) and the chemical potential (μ)

Pumping density (W/cm^2)	N_0	N_0/N_1	N_0/N	$-\mu$ (meV)
0.8	7.7×10^3	23.5	0.04	56
8	2.7×10^5	510	0.59	1.6
160	5.8×10^6	5800	0.95	0.07

ulation for different pumping densities and a seed of 100. Table 6.1 gives the parameters obtained in the steady-state regime, namely ground-state populations, the ratio of populations of the ground state and the first excited state, the ratio of the ground state population and the total populations, and the chemical potential $\mu = k_b T \ln(1 - 1/N_0)$. The steady-state distribution functions are found to be very close to the Bose distribution function.

Figure 6.8 (a)–(c) shows the evolution of the second-order coherence parameter η_2 and the whole system coherence degree η_T for the three pumping densities (seed 100). Figure 6.8(a) corresponds to a low pumping density, when the seed disappears on a time scale of a few tens of picoseconds (which is also seen in Figure 6.7). Figure 6.8(b) represents an intermediate case, when the coherence survives in part, and Figure 6.8(c) shows the Bose quasi-condensation of polaritons, which is characterised by the build-up of the order parameter and by the amplification of the initial seed coherent state. The whole system coherence also

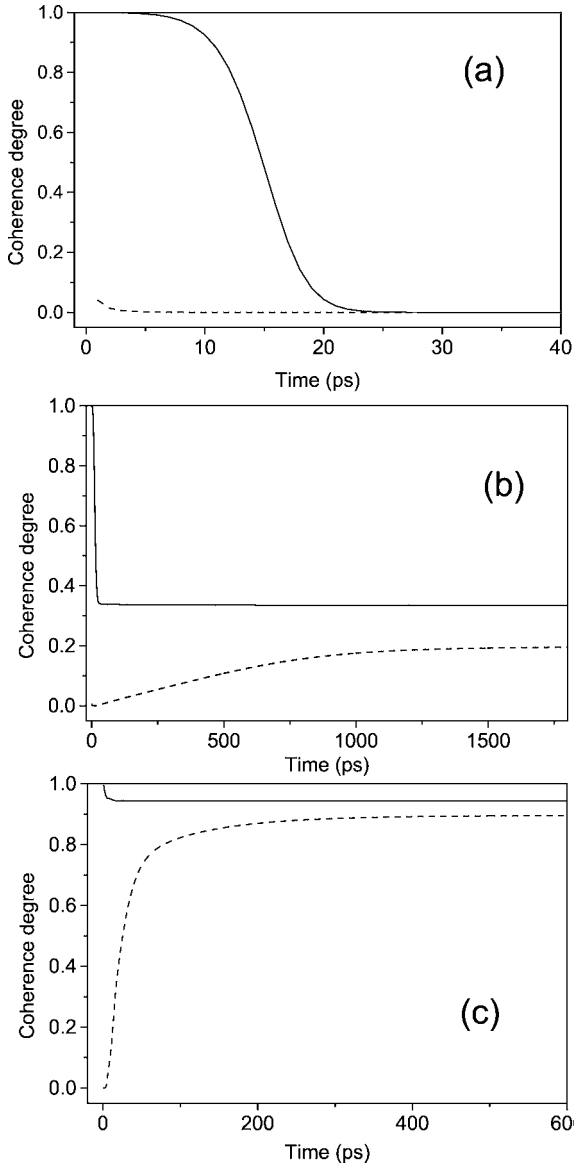

Fig. 6.8. Ground state coherence (solid lines) and total system coherence (dashed lines). The pumping densities are 0.8 W/cm^2 (a), 8 W/cm^2 (b), and 160 W/cm^2 (c).

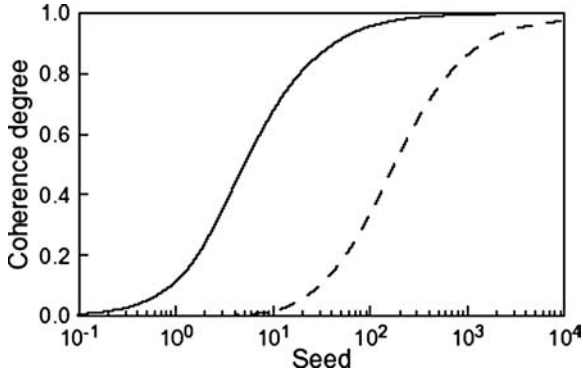

Fig. 6.9. The ground state coherence degree versus the seed population in the steady-state regime (1 ns after the pumping start). Non-resonant pumping densities are 8 W/cm^2 (dashed line) and 160 W/cm^2 (solid line).

strongly increases from 0 to more than 90%. This coherence buildup is a clear signature of polariton quasi-condensation. In the intermediate pumping densities the values of the steady-state coherence degree depend noticeably on the seed's characteristics. The dependencies of the coherence degree on the seed population are shown in Figure 6.9 for two pumping densities. One can see that the buildup of coherence takes place only if the seed population exceeds some critical value, which depends on pumping but remains always very small (from 10 to 100 polaritons as compared to $N_0 = 10^6$ in the steady-state regime).

6.4. Spin Dynamics of Exciton–Polaritons in Microcavities

An exciton is formed by an electron and hole, i.e., by two fermions having spin projections on a given axis equal to $\pm 1/2$ (for an electron), $\pm 1/2$, $\pm 3/2$ for a hole (in a zinc-blende semiconductor crystal). In quantum wells, the lowest energy level of a heavy hole lies typically lower than any light-hole energy level, and thus the exciton ground state is formed by an electron and a heavy-hole that has a spin projection of $\pm 3/2$ on the axis of the QW. Thus, the entire exciton spin has the following projections on the structure axis: ± 1 and ± 2 allowed for the ground state. Bearing in mind that the photon spin is 0 or ± 1, the excitons with spin projections equal ± 2 cannot be optically excited. These are so-called *spin–forbidden dark* states. We shall neglect them in all further consideration. σ^+ and σ^- circularly-polarised light excites $+1$ and -1 excitons, respectively. Linearly-polarized light excites a linear combination of $+1$ and -1 exciton-states, so that the total exciton spin projection on the structure axis is zero in this case. Exciton spin-dynamics in semiconductors can be experimentally studied by measurement

of time-resolved polarisation of light emitted by excitons. The polarisation degree of light $\wp$ is given by the difference between concentrations of spin $+1$ and -1 excitons (N^+ and N^-, respectively) related to the total exciton concentration:

$$\wp = \frac{N^+ - N^-}{N^+ + N^-}.$$

Among the principal mechanisms of electron spin-relaxation, the most important are Elliott–Yaffet [60], Bir–Pikus [61], and Dyakonov–Perel' [62] mechanisms connected with intrinsic symmetry properties of crystals, spin-orbit and exchange interactions. The exciton spin-relaxation may be realised via these "single-electron" mechanisms as well as via spin-flips due to collisions of excitons with structure imperfections, impurities or other excitons. As we shall see below, a specific spin-relaxation mechanism linked to the exciton longitudinal-transverse splitting plays the most important role in microcavities. There has been a huge amount of experimental activity on spin-relaxation of excitons in semiconductor heterostructures since the early 1980s [63]. Nowadays, exciton–polaritons in microcavities have offered a few new puzzles to scientists that still need to be resolved.

Exciton–polaritons have the same spin-structure as excitons. The difference between their spin-relaxation dynamics and spin-relaxation of pure (*mechanical*) excitons was expected to come from the different shape of dispersion curves and, consequently, different energy relaxation dynamics.

Between 2000 and 2002 a series of experimental works appeared that reported unusual spin-effects in microcavities, such as polarisation beats, stimulated spin-scattering, giant Faraday rotation and others both under resonant and non-resonant excitation [55,64,65]. Many of these effects remains unexplained at the moment of writing. In this section we present a formalism that allows one to incorporate the spin of polaritons in kinetic equations describing their energy relaxation. We consider only the non-resonant excitation case and assume perfect cylindrical symmetry of the polariton distribution in the reciprocal space at any moment of time (which means that all the in-plane directions are equivalent). We shall take into account only two mechanisms of spin-relaxation, namely spin-lattice relaxation and the spin-rotation mechanism caused by the longitudinal-transverse splitting of exciton–polaritons (to be addressed in detail below). We neglect the spin-flips during polariton–polariton scattering for simplicity and because these processes conserve the total spin in the system, though they are of course present in reality. Our goal is to calculate the polarisation degree of the photoluminescence from the lowest energy polariton state.

The polarisation degree of light emitted by polaritons with in-plane wavevector $\mathbf{k} = 0$ is determined as

$$\wp = \frac{I^+ - I^-}{I^+ + I^-} = \frac{N^+_{\mathbf{k}=0}(t) - N^-_{\mathbf{k}=0}(t)}{N_{\mathbf{k}=0}(t)} \tag{6.4.1}$$

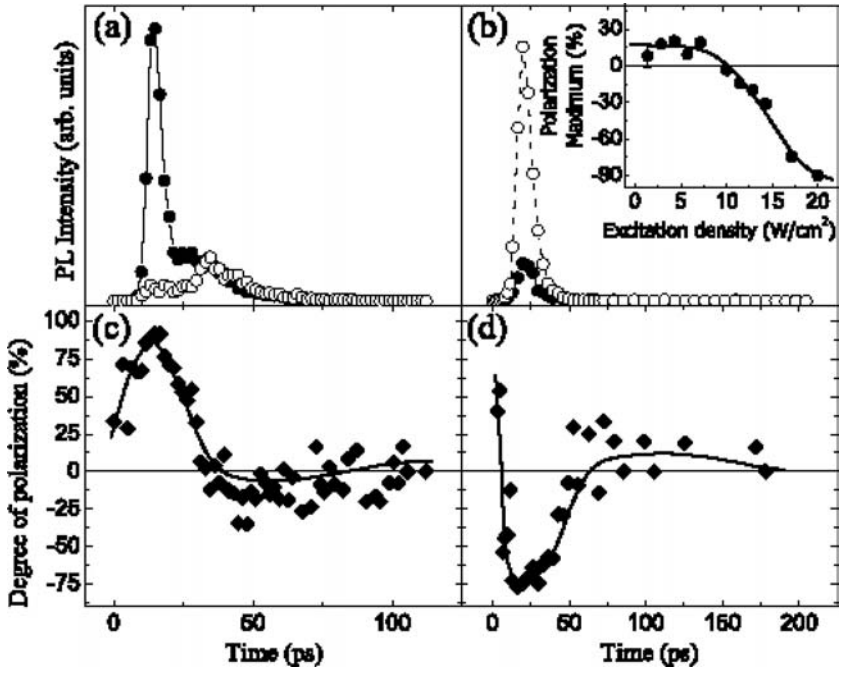

Fig. 6.10. Experimentally measured [55] temporal evolution of the photoluminescence of a CdTe-based microcavity excited by circularly-polarised light at the positive detuning, upper polariton branch (a, $\delta = 10$ meV) and negative detuning, lower polariton branch (b, $\delta = -10$ meV). The filled circles/solid line (open circles/dashed line) denote the σ^+ (σ^-) emission. The deduced time evolution of the circular polarisation degree for positive and negative detunings is shown in (c) and (d), respectively. The inset shows the maximum value of the polarisation degree at 20 ps in the negative detuning case.

where $I^{\pm}$ denote the circularly-polarised intensities that were measured. Here $N^{\pm}_{\mathbf{k}=0}$ represent the populations of polaritons with opposite spin projections in the state $\mathbf{k} = 0$, $N_{\mathbf{k}=0}(t) = N^{+}_{\mathbf{k}=0}(t) + N^{-}_{\mathbf{k}=0}(t)$. In the experimental work by Martin et al. [55], the polarisation degree has been measured as a function of time for a strong-coupling microcavity for different values of the detuning. Instead of an exponential decay due to the spin-lattice relaxation processes that one would expect, experimentally detected $\wp$ exhibited a non-trivial temporal dependence. At positive detuning, the initial polarisation of $\sim$30% first increased up to $\sim$90% and then showed damped oscillations (Figure 6.10). For negative detuning, the polarisation degree started from a positive value $\sim$50%, fast decreased down to strongly negative values, then increased showing attenuated oscillations with a period of about 50 ps.

Let us try to understand these unusual spin-dynamics of exciton–polaritons in microcavities. Consider a mechanism of exciton–polariton spin-relaxation which is similar to the well-known Dyakonov–Perel spin-relaxation mechanism [62] for electrons. In order to describe it we need to adopt the pseudospin formalism (essentially the same as in Section 5.1). Let us remind that the pseudospin is a vector that characterises the orientation of both the spin and dipole moment of an exciton (see Figure 5.8). Its z-projection is proportional to the polarisation degree of light $\wp(t)$:

$$S^z_{\mathbf{k}=0}(t) \equiv \frac{N^+_{\mathbf{k}=0}(t) - N^-_{\mathbf{k}=0}(t)}{2} = \wp(t)\frac{N^+_{\mathbf{k}=0}(t) + N^-_{\mathbf{k}=0}(t)}{2}, \qquad (6.4.2)$$

while its x- and y-components characterise the degree of linear polarisation defined as in Eq. (5.1.2).

The spin-relaxation mechanism we describe plays a role if the exciton states having dipole moments in, say, x- and y-directions have different energies. This is typically the case for excitons having non-zero in-plane wave-vectors. The splitting of exciton states with dipole moments parallel and perpendicular to the wave-vector is called *longitudinal-transverse splitting*. The longitudinal-transverse splitting of exciton–polaritons in quantum wells is a result of the long-range exchange interaction that splits energies of excitons with their dipole moment parallel to the wave-vector and perpendicular to the in-plane wave-vector $\mathbf{k}$. The splitting is zero for $\mathbf{k} = 0$ and increases as a function of k, following a square root law at large k. For more details the reader is referred to Tassone [66] (see also Section 2.3 of this book). The exciton longitudinal-transverse splitting amplified by coupling with the cavity mode creates a kind of effective magnetic field which affects the exciton pseudospin. This is a typical effect of *quantum beats*, where a coherent superposition of two quantum states split in energy exhibits oscillations in the phase of the wave-function with a period given by the energy splitting between the states. Rotation of the pseudospin of relaxing polaritons results in oscillations of the circular polarisation degree of the emitted light.

In microcavities, splitting of longitudinal and transverse polariton states is amplified due to the exciton coupling with a cavity mode. Note that the cavity mode frequency is also split in TE- and TM-light polarisations [67]. The resulting polariton splitting strongly depends on the detuning between the cavity mode and the exciton resonance and, in general, increases with k. Figure 6.11 shows the longitudinal-transverse polariton splitting Ω_k calculated for a microcavity sample from Ref. [55] for different detunings. For these calculations, polariton eigenfrequencies in the two polarisations have been found numerically by a transfer matrix method, as described in Section 1.3. One can see that the splitting is very sensitive to the detuning, and may have different signs for upper and LPBes.

To describe the dynamics of the polariton pseudospin one needs to calculate $N^{\pm}_{\mathbf{k}=0}(t)$. In the absence of spin-relaxation and if the pseudospin is oriented along

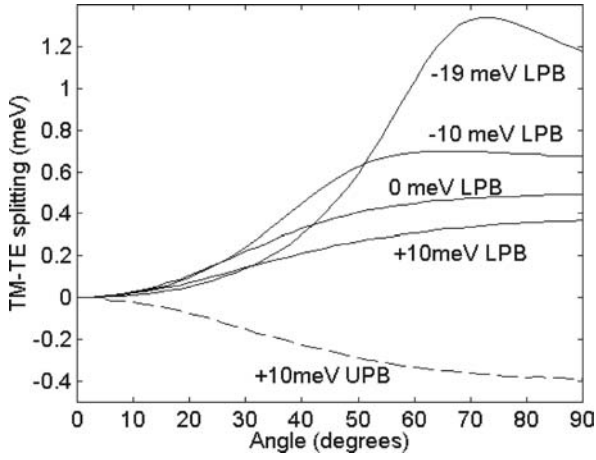

Fig. 6.11. Longitudinal-transverse (TM–TE) polariton splitting calculated for detunings: +10, 0, −10, −19 meV. Solid lines: lower polariton branch, dashed lines: upper polariton branch.

z-axis it is given by a conventional Boltzmann equation:

$$\frac{dN_{\mathbf{k}}^{\pm}}{dt} = -\frac{1}{\tau_k} N_{\mathbf{k}}^{\pm} + \sum_{\mathbf{k}'} W_{\mathbf{k}'\to\mathbf{k}} N_{\mathbf{k}'}^{\pm}\left(N_{\mathbf{k}}^{\pm}+1\right) - \sum_{\mathbf{k}'} W_{\mathbf{k}\to\mathbf{k}'} N_{\mathbf{k}}^{\pm}\left(N_{\mathbf{k}'}^{\pm}+1\right), \tag{6.4.3}$$

where τ_k is a polariton lifetime that includes the spin recombination time, and $W_{\mathbf{k}\to\mathbf{k}'}$ describes polariton scattering from the quantum state $\mathbf{k}$ to the quantum state $\mathbf{k}'$.

It is evident that relative pseudo-spin orientation of initial and final polariton states must have an influence on the probability of scattering process between these two states if final state stimulation of scattering is accounted for. Still neglecting the spin-relaxation, let us now take into account the pseudospin orientation effect on stimulated scattering process. It is convenient to do it using the spin-density matrix

$$\boldsymbol{\rho}_k = \frac{N_{\mathbf{k}}}{2} I + \mathbf{S}_{\mathbf{k}} \cdot \boldsymbol{\sigma},$$

where I is the identity matrix, $\boldsymbol{\sigma}$ is the Pauli-matrix vector. The diagonal elements of this matrix are nothing but $N_{\mathbf{k}}^{\pm}$. Its non-diagonal elements depend on the in-plane projection of the pseudospin S_k^{τ}. One can consider the evolution of the density matrix ρ_2, describing the state 2, due to the scattering from the state 1 as

a result of the unitary transformation of ρ_1

$$\left(\frac{\partial \rho_2}{\partial t}\right)_{1\to 2} = \widehat{T}\rho_1\widehat{T}^{+}.$$

Comparing this expression with Eq. (6.4.3) for the case of all pseudospins oriented along z-axis, one can find all elements of the matrix $\widehat{T}$, and thus obtain explicitly the dynamics of all elements of S_k. After summation over all allowed polariton states and angle averaging we obtain the following kinetic equations:

$$\begin{aligned}\frac{dN_k}{dt} = &-\frac{1}{\tau_k}N_k + \sum_{k'}\widetilde{W}_{k'k}\left[\left(\frac{N_{k'}}{2}+S^z_{k'}\right)\left(\frac{N_k}{2}+S^z_k+1\right)\right.\\ &\left.+\left(\frac{N_{k'}}{2}-S^z_{k'}\right)\left(\frac{N_k}{2}-S^z_k+1\right)\right]\\ &-\sum_{k'}\widetilde{W}_{kk'}\left[\left(\frac{N_k}{2}+S^z_k\right)\left(\frac{N_{k'}}{2}+S^z_{k'}+1\right)\right.\\ &\left.+\left(\frac{N_k}{2}-S^z_k\right)\left(\frac{N_{k'}}{2}-S^z_{k'}+1\right)\right]\\ &+2\sum_{k'}\left(\overline{W}_{k'k}-\overline{W}_{kk'}\right)S^\tau_{k'}S^\tau_k, \end{aligned} \tag{6.4.4}$$

$$\begin{aligned}\frac{dS^z_k}{dt} = &-\frac{1}{\tau_k}S^z_k + \frac{1}{2}\sum_{k'}\widetilde{W}_{k'k}\left[\left(\frac{N_{k'}}{2}+S^z_{k'}\right)\left(\frac{N_k}{2}+S^z_k+1\right)\right.\\ &\left.-\left(\frac{N_{k'}}{2}-S^z_{k'}\right)\left(\frac{N_k}{2}-S^z_k+1\right)\right]\\ &-\sum_{k'}\widetilde{W}_{kk'}\left[\left(\frac{N_k}{2}+S^z_k\right)\left(\frac{N_{k'}}{2}+S^z_{k'}+1\right)\right.\\ &\left.-\left(\frac{N_k}{2}-S^z_k\right)\left(\frac{N_{k'}}{2}-S^z_{k'}+1\right)\right], \end{aligned} \tag{6.4.5}$$

$$\begin{aligned}\frac{dS^\tau_k}{dt} = &-\frac{1}{\tau_k}S^\tau_k + \sum_{k'}\left[\left(\overline{W}_{k'k}-\overline{W}_{kk'}\right)\left(\frac{N_k}{2}+1\right)S^\tau_{k'} + \left(\widetilde{W}_{k'k}-\widetilde{W}_{kk'}\right)\right.\\ &\left.\times\left(\frac{N_{k'}}{2}+1\right)S^\tau_k + \overline{W}_{kk'}S^\tau_{k'} - \widetilde{W}_{k'k}S^\tau_k\right]. \end{aligned} \tag{6.4.6}$$

Here and in what follows we shall assume perfect in-plane isotropy of the polariton distribution, so that the indices **k** in all distribution functions can be considered as scalars (k).

In Eqs. (4.4.4)–(4.4.6) the scattering matrix elements are the angle-averages of $W_{\mathbf{k}\to\mathbf{k}'}$.

$$\widetilde{W}_{k\to k'} = \frac{1}{2\pi}\int_0^{2\pi} W_{\mathbf{k}\to\mathbf{k}'}\, d\phi, \tag{6.4.7}$$

$$\overline{W}_{k\to k'} = \frac{1}{2\pi}\int_0^{2\pi} W_{\mathbf{k}\to\mathbf{k}'}\cos(2\phi)\, d\phi, \tag{6.4.8}$$

where ϕ is the angle between $\mathbf{k}$ and $\mathbf{k}'$. Eqs. (6.4.4)–(6.4.6) represent a closed set of equations, which can be treated numerically if appropriate initial conditions are formulated.

Once spin-dependent stimulated relaxation is described, it is easy to introduce the spin-lattice relaxation and pseudospin dynamics coming from the longitudinal-transverse splitting of polaritons. To describe the spin-lattice relaxation one just needs to replace τ_k^{-1} in Eqs. (6.4.5), (6.4.6) by $\tilde{\tau}_k^{-1} = \tau_k^{-1} + \tau_{sl}^{-1}$, where τ_{SL} is the spin-lattice relaxation time constant. Note, that this term accounts for the spin-relaxation in course of all elastic scattering events. To account for the polariton longitudinal-transverse splitting one should add to the right-hand side of Eq. (6.4.5) and to the right-hand side of Eq. (6.4.6) the terms

$$\Omega_k S_k^{\tau}, \quad -\Omega_k S_k^{z}, \tag{6.4.9}$$

respectively. Note that Eq. (6.4.4) for the polariton population remains unchanged.

In the case of resonant excitation under an oblique angle the in-plane isotropy would be broken, and one would need to introduce an additional equation to describe the dynamics of the pseudospin vector. In vector form the kinetic equations for the polariton population and pseudospin vector write

$$\frac{dN_{\mathbf{k}}}{dt} = -\frac{1}{\tau_k}N_{\mathbf{k}} + \sum_{\mathbf{k}'}\Bigg[(W_{\mathbf{k}'\to\mathbf{k}} - W_{\mathbf{k}\to\mathbf{k}'})\left(\frac{1}{2}N_{\mathbf{k}}N_{\mathbf{k}'} + 2(\mathbf{S}_{\mathbf{k}}\mathbf{S}_{\mathbf{k}'})\right) + (W_{\mathbf{k}'\to\mathbf{k}}N_{\mathbf{k}'} - W_{\mathbf{k}\to\mathbf{k}'}N_{\mathbf{k}})\Bigg], \tag{6.4.10}$$

$$\frac{d\mathbf{S}_{\mathbf{k}}}{dt} = -\frac{1}{\tau_k}\mathbf{S}_{\mathbf{k}} + \sum_{\mathbf{k}'}\Bigg[\frac{1}{2}(W_{\mathbf{k}'\to\mathbf{k}} - W_{\mathbf{k}\to\mathbf{k}'})(N_{\mathbf{k}}\mathbf{S}_{\mathbf{k}'} + N_{\mathbf{k}'}\mathbf{S}_{\mathbf{k}}) + (W_{\mathbf{k}'\to\mathbf{k}}\mathbf{S}_{\mathbf{k}'} - W_{\mathbf{k}\to\mathbf{k}'}\mathbf{S}_{\mathbf{k}})\Bigg] + [\mathbf{\Omega}_{\mathbf{k}}\times\mathbf{S}_{\mathbf{k}}], \tag{6.4.11}$$

where the effective magnetic field $\mathbf{\Omega}_{\mathbf{k}}$ makes twice the same angle as $\mathbf{k}$ with the x-axis, $|\mathbf{\Omega}_{\mathbf{k}}| = \Omega_k$, and $\mathbf{G}_{\mathbf{k}}(t)$ describes generation of the spin polarisation. For more details on the derivation of Eqs. (6.4.10), (6.4.11) we refer the reader to a paper by Maialle [68,69].

The approach described here allows one to model numerically spin- and energy-relaxation of exciton–polaritons in microcavities. In the particular case of a strong bottleneck effect at the LPB, one can estimate the dynamics of the circular polarisation degree of microcavity emission analytically. In this regime one can approximate the polariton spectrum by a three-level system, i.e., the ground level (further indexed by 0), the state at the bottleneck (indexed by 1), and the optically pumped state (2). Furthermore, we shall assume that the relaxation between states (2) and (1) is much faster than relaxation between states (1) and (0), so that the rate equations describing spin dynamics of polaritons between levels (2) and (1) and between levels (1) and (0) can be decoupled. In the low-temperature limit the scattering matrix elements are related by $W_{10} \gg W_{01}$, $W_{21} \gg W_{12}$. Assuming $W_{01} = W_{12} = 0$ one can obtain an analytical expression for the temporal dependence of the photoluminescence polarisation ratio

$$\begin{aligned}\wp(t) = {} & \frac{2e^{-t/\tau_{\rm sl}}}{N(0)(1+\Omega_1^2\tau^2)(e^{-(1/\tau_1+W_{10})t} - e^{-t/\tau_0})} \\ & \times \Big\{ e^{-(1/\tau_1+W_{10})t}\Big[S_z(0)(\cos\Omega_1 t + \Omega_1\tau\sin\Omega_1 t) \\ & \qquad - S_\tau(0)(\Omega_1\tau\cos\Omega_1 t - \sin\Omega_1 t)\Big] \\ & - e^{-t/\tau_0}\Big[1 - \Omega_1\tau S_\tau(0)\Big]\Big\}, \end{aligned} \tag{6.4.12}$$

where $N(0)$ is the initial number of pumped polaritons, and $\tau^{-1} = \tau_0^{-1} - \tau_1^{-1} - W_{10}$. Here, the initial values of normal and tangential components of the in-plane projection of the pseudospin $\mathbf{S_k}$ are given by

$$S_z(0) = \frac{N(0)}{2}\frac{1}{1+\beta_2^2}, \qquad S_\tau(0) = \frac{N(0)}{2}\frac{\beta_2}{1+\beta_2^2}, \tag{6.4.13}$$

where $\beta_2 = \Omega_2/W_{21}$, in which Ω_2 is the effective magnetic field at level (2). If $W_{21} \gg \Omega_2$ the tangential component is initially absent, and so the initial value of $\wp$ is equal to unity. In this simplified model we neglect stimulated scattering assuming that the stimulation threshold is not reached. The high-density regime can nevertheless be accounted for through the values of the scattering rates and lifetimes which are used in calculation.

The two-level model is also valid if we consider the relaxation of polaritons pumped at the upper polariton branch (UPB) in the positive detuning case. As the UPB has a photonic character, the polaritons pumped into point 2 relax to the state $k = 0$ of the UPB via an intermediate state 1, located at the LPB (see the scheme in Figure 6.12).

The results obtained with Eq. (6.4.12) for the microcavity sample studied by D. Martin [55] are displayed in Figure 6.13. Results of this analytical model compare nicely with experimental data (Figure 6.10). One can see that the sign of

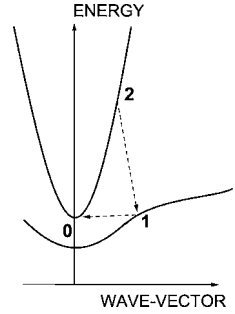

Fig. 6.12. A scheme showing the most probable mechanism of polariton relaxation in the case of positive detuning.

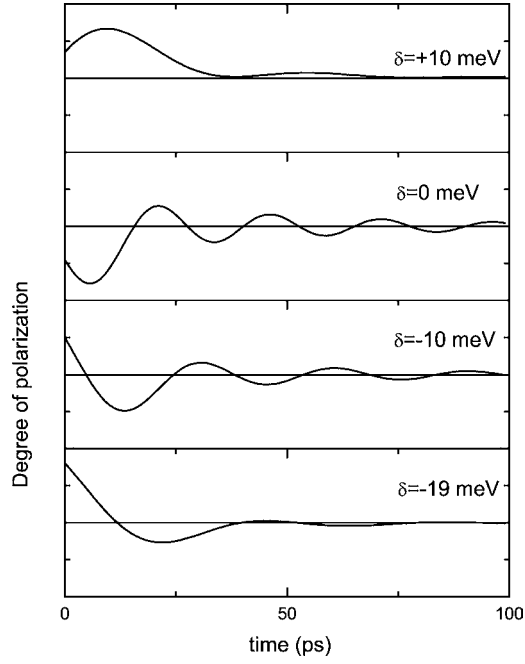

Fig. 6.13. Polarisation degree of the photoluminescence calculated according to Eq. (6.4.12) for upper and lower polariton branches (UPB and LPB, respectively), for different detuning values.

the polarisation degree can be reversed even in the absence of stimulated scattering. The change of the period of polarisation beats with the detuning comes from variation of the longitudinal-transverse splitting Ω in the bottleneck region with δ. One should mention that the model we propose is only valid if scatter-

ing rates are large enough to quickly populate the bottleneck state. Otherwise, one should rather perform accurate modelling using the complete set of spin-dependent Boltzmann equations (6.4.4)–(6.4.6).

6.5. Conclusive Remarks

In this chapter we have presented a quantum theory of the polariton phase transition in semiconductor microcavities and briefly reviewed experimental and theoretical work performed in this field. Our main conclusions on that topic are as follows:

(1) Cavity polaritons seem to be much more suitable than excitons weakly coupled to light for observation of bosonic effects because they are much less sensitive to structural imperfections of real systems. Exciton–polaritons behave as weakly interacting bosons as has been experimentally proved by Saviddis and Baumberg [2], and others (see Chapter 5).

(2) Cavity polaritons cannot Bose-condense because they are two-dimensional particles. They are subject to the Kosterlitz–Thouless phase transition towards a superfluid phase and to local quasi-condensation, which allows polariton lasing with critical temperatures larger than 300 K in wide band-gap semiconductor microcavities. These effects cannot be observed for bulk polaritons.

(3) The size of quasi-condensation droplets at their percolation transition strongly depends on the temperature and concentration of polaritons at the transition points. In the most usual experimental situation of rather low polariton concentration and low temperature, the local BEC within the laser spot takes place before the KT transition.

(4) We have presented a simple quantum kinetic theory able to describe dynamical aspects of the condensate formation in a non-resonantly pumped cavity. Evolution of the polariton distribution function is described by a semi-classical Boltzmann equation. A master equation for the ground-state density matrix is derived in the framework of the Born–Markov approximation. Evolution of the ground-state population, the order parameter, and the ground-state and whole system coherence are deduced. We show that the second-order coherence of the polariton laser is built up in the course of fast microscopic relaxation of polaritons and is maintained on a macroscopic time scale. The whole complexity of real systems, namely the peculiar polariton dispersion, finite polariton lifetime, and polariton–polariton interactions, are taken into account. Renormalisation effects induced by off-diagonal coupling have been neglected.

(5) Spin-relaxation of exciton–polaritons in microcavities is mainly governed by exciton–polariton longitudinal-transverse splitting. Spin-dependent ki-

netic equations for exciton–polaritons are essentially different from the Boltzmann equations neglecting spin.

References

1. A. Imamoglu, J. R. Ram, Nonequilibrium condensates and lasers without inversion: Exciton–polariton lasers, *Phys. Lett. A* 214, 193 (1996).
2. P. G. Savvidis, J. J. Baumberg, R. M. Stevenson, M. S. Skolnick, D. M. Whittaker, J. S. Roberts, Angle resonant stimulated polariton amplifier, *Phys. Rev. Lett.* 84, 1547 (2000).
3. P. R. Eastham, P. B. Littlewood, Bose condensation of cavity polaritons beyond the linear regime: The thermal equilibrium of a model microcavity, *Phys. Rev. B* 64, 235101 (2001).
4. A. Kavokin, G. Malpuech, F. P. Laussy, Polariton laser and polariton superfluidity in microcavities, *Phys. Lett. A* 306, 187 (2003).
5. G. Malpuech, A. Di Carlo, A. Kavokin, J. J. Baumberg, M. Zamfirescu, P. Lugli, Room-temperature polariton lasers based on GaN microcavities, *Appl. Phys. Lett.* 81, 412 (2002).
6. M. Zamfirescu, A. Kavokin, B. Gil, G. Malpuech, M. Kaliteevski, ZnO as a material mostly adapted for the realization of room-temperature polariton lasers, *Phys. Rev. B* 65, 161205 (2002).
7. F. Tassone, C. Piermarocchi, V. Savona, A. Quattropani, P. Schwendimann, Bottleneck effects in the relaxation and photoluminescence of microcavity polaritons, *Phys. Rev. B* 56, 7554 (1997).
8. F. Tassone, Y. Yamamoto, Exciton–exciton scattering dynamics in a semiconductor microcavity and stimulated scattering into polaritons, *Phys. Rev. B* 59, 10 830 (1999).
9. F. Tassone, Y. Yamamoto, Lasing and squeezing of composite bosons in semiconductor microcavities, *Phys. Rev. A* 62, 063809 (2000).
10. G. Malpuech, A. Kavokin, A. Di Carlo, J. J. Baumberg, Polariton lasing by exciton–electron scattering in semiconductor microcavities, *Phys. Rev. B* 65, 153310 (2002).
11. A. V. Soroko, A. L. Ivanov, Phonon-assisted relaxation kinetics of statistically degenerate excitons in high-quality quantum wells, *Phys. Rev. B* 65, 165310 (2002).
12. D. Porras, C. Ciuti, J. J. Baumberg, C. Tejedor, Polariton dynamics and Bose–Einstein condensation in semiconductor microcavities, *Phys. Rev. B* 66, 085304 (2002).
13. F. Boeuf, R. André, R. Romestain, Le Si Dang, E. Péronne, J. F. Lampin, D. Hulin, A. Alexandrou, Evidence of polariton stimulation in semiconductor microcavities, *Phys. Rev. B* 62, R2279 (2000); A. Alexandrou, G. Bianchi, E. Péronne, B. Hallé, F. Boeuf, R. André, R. Romestain, Le Si Dang, Stimulated scattering and its dynamics in semiconductor microcavities at 80 K under nonresonant excitation conditions, *Phys. Rev. B* 64, 233318 (2001); R. Huang, Y. Yamamoto, R. André, J. Bleuse, M. Muller, H. Ulmer-Tuffigo, Exciton–polariton lasing and amplification based on exciton–exciton scattering in CdTe microcavity quantum wells, *Phys. Rev. B* 65, 165314 (2002).
14. Y. G. Rubo, F. P. Laussy, G. Malpuech, A. Kavokin, P. Bigenwald, Dynamical theory of polariton amplifiers, *Phys. Rev. Lett.* (2003), to be published.
15. S. N. Bose, *Z. Phys.* 26, 178 (1924).
16. A. Einstein, Sitzber. Kgl. Preuss. Akad. Wiss.1 (1924) p. 26; (1925) p. 3.
17. A. Griffin, D. W. Snoke, S. Stringari, Eds., "Bose Einstein Condensation". Cambridge University Press, 1995; S. A. Moskalenko, D. W. Snoke, "Bose Einstein Condensation of Excitons and Biexcitons". Cambridge University Press, 2000.
18. J. F. Allen, D. Misener, Flow of liquid helium II, *Nature* 141, 75 (1938); P. Kapitza, Viscosity of liquid helium below the λ point, *Nature* 141, 74 (1938).
19. F. London, The *l*-phenomenon of liquid helium and the Bose–Einstein degeneracy, *Nature* 141, 74 (1938).

20. L. Mandel, E. Wolf, "Optical Coherence and Quantum Optics". Cambridge University Press, 1995.
21. M. H. Anderson, J. R. Ensher, M. R. Matthews, C. E. Wieman, E. A. Cornell, Observation of Bose–Einstein condensation in a dilute atomic vapor, *Science* 269, 198 (1995).
22. O. Penrose, L. Onsager, Bose–Einstein condensation and liquid helium, *Phys. Rev.* 104, 576 (1954).
23. J. Goldstone, *Nuovo Cimento* 19, 154 (1961); J. Goldstone, A. Salam, S. Weinberg, Broken symmetries, *Phys. Rev.* 127, 965 (1962).
24. C. N. Yang, Concept of off-diagonal long-range order and the quantum phases of liquid He and of superconductors, *Rev. Mod. Phys.* 34, 694 (1962).
25. P. W. Anderson, Considerations on the flow of superfluid helium, *Rev. Mod. Phys.* 38, 298 (1966).
26. S. A. Moskalenko, *Fiz. Tverd. Tela* 4, 276 (1962).
27. I. M. Blatt, K. W. Boer, W. Brandt, Bose–Einstein condensation of excitons, *Phys. Rev.* 126, 1691 (1962).
28. L. V. Keldysh, Kozlov, Collective properties of excitons in semiconductors, *Sov. Phys. Sol. JETP* 36, 1193 (1968).
29. Yu. E. Lozovik, V. I. Yudson, *Pis'ma Zh. Éksper. Teoret. Fiz.* 22, 26 (1975) [*JETP Lett.* 22, 26 (1975)]; *Zh. Éksper. Teoret. Fiz.* 71, 738 (1976) [*Sov. Phys. JETP* 44, 389 (1976)]; *Solid State Commun.* 18, 628 (1976).
30. H. Haug, E. Hanamura, Derivation of the two-fluid model for Bose-condensed excitons, *Phys. Rev. B* 11, 3317 (1975).
31. C. Comte, P. Nozières, Exciton Bose condensation – the ground state of an electron hole gas: Mean Field description of a simplified model, *J. Physique (Paris)* 43, 1069 (1982).
32. D. Snoke, S. Denev, Y. Liu, L. Pfeiffer, K. West, Long-range transport in excitonic dark states in coupled quantum wells, *Nature* 418, 754 (2002); L. V. Butov, C. W. Lai, A. L. Ivanov, A. C. Gossard, D. S. Chemla, Towards Bose–Einstein condensation of excitons in potential traps, *Nature* 417, 47 (2002); L. V. Butov, A. L. Ivanov, A. Imamoglu, P. B. Littlewood, A. A. Shashkin, V. T. Dolgopolov, K. L. Campman, A. C. Gossard, Stimulated scattering of indirect excitons in coupled quantum wells: Signature of a degenerate Bose-gas of excitons, *Phys. Rev. Lett.* 86, 5608 (2001).
33. Yu. E. Lozovik, I. V. Ovchinnikov, Many-photon coherence of Bose-condensed excitons: Luminescence and related nonlinear optical phenomena, *Phys. Rev. B* 66, 075124 (2002) and ref. therein.
34. S. G. Tikhodeev, Comment on "Critical velocities in exciton superfluidity", *Phys. Rev. Lett.* 84, 3502 (2000).
35. N. D Mermin, H. Wagner, Absence of ferromagnetism or antiferromagnetism in one- or two-dimensional isotropic Heisenberg models, *Phys. Rev. Lett.* 22, 1133 (1966); P. C. Hohenberg, Existence of long-range order in one and two dimensions, *Phys. Rev.* 158, 383 (1967); S. Coleman, *Comm. Math. Phys.* 31, 259 (1973).
36. J. M. Kosterlitz, D. J. Thouless, Ordering, metastability and phase transition in two-dimensional systems, *J. Phys. C* 6, 1181 (1973).
37. D. S. Fisher, P. C. Hohenberg, Dilute Bose gas in two dimensions, *Phys. Rev. B* 37, 4936 (1988).
38. Yu. E. Lozovik, O. L. Bergmann, A. A. Panfinov, The excitation spectra and superfluidity of the electron–hole system in coupled quantum wells, *Phys. Status Solidi B* 209, 287 (1998).
39. Z. G. Koinov, Bose–Einstein condensation of excitons in a single quantum well, *Phys. Rev. B* 61, 8411 (2000).
40. N. N. Bogoliubov, On the theory of superfluidity, *J. Phys. USSR* 11, 23 (1947); N. N. Bogoliubov, "Lectures on Quantum Statistics, Vol. 1. Quantum Statistics". Gordon and Breach Science Publisher, New York, London, Paris, 1970.

41. V. A. Zagrebnov, J. B. Bru, The Bogoliubov model of weakly imperfect Bose gas, *Phys. Rep.* 350 (2001) and ref. therein.

42. L. D. Landau, The theory of superfluidity of helium II, *J. Phys. USSR* 5, 71 (1941).

43. L. D. Landau, On the theory of superfluidity of helium II, *J. Phys. USSR* 11, 87 (1947).

44. D. R. Nelson, J. M. Kosterlitz, Universal jump in the superfluid density of two dimensional superfluid, *Phys. Rev. Lett.* 39 (1977).

45. See e.g. K. M. Khalatnikov, "An Introduction to the Theory of Superfluidity". Benjamin, New York, 1965.

46. P. Senellart, J. Bloch, Nonlinear emission of microcavity polaritons in the low density regime, *Phys. Rev. Lett.* 82, 1233 (1999); P. Senellart, J. Bloch, B. Sermage, J. Y. Marzin, Microcavity polariton depopulation as evidence for stimulated scattering, *Phys. Rev. B* 62, R16 263 (2000).

47. L. S. Dang, D. Heger, R. Andre, F. Boeuf, R. Romestain, Stimulation of polariton photoluminescence in semiconductor microcavity, *Phys. Rev. Lett.* 81, 3920 (1998).

48. G. Mapuech, A. Kavokin, Picosecond beats in coherent optical spectra of semiconductor heterostructures: photonic Bloch and exciton–polaritons oscillations, *Semicond., Sci. and Technol. Topical Review* 16, R1 (2001); A. Kavokin, G. Malpuech, W. Langbein, Theory of propagation and scattering of exciton–polaritons in quantum wells, *Solid State Commun.* 120, 259 (2001).

49. V. M. Agranovich, M. Litinskaia, D. G. Lidzey, Cavity polaritons in microcavities containing disordered organic semiconductors, *Phys. Rev. B* 67, 85311 (2003).

50. R. Butté, G. Delalleau, A. I. Tartakovskii, M. S. Skolnick, V. N. Astratov, J. J. Baumberg, G. Malpuech, A. Di Carlo, A. V. Kavokin, J. S. Roberts, Transition from strong to weak coupling and the onset of lasing in semiconductor microcavities, *Phys. Rev. B* 65, 205310 (2002).

51. S. Pau, H. Cao, J. Jacobson, G. Bjork, Y. Yamamoto, A. Imamoglu, Observation of a laser-like transition in a microcavity exciton polariton system, *Phys. Rev. A* 54 (3), R1789 (1996).

52. M. Kira, F. Jahnke, S. W. Koch, J. D. Berger, D. V. Wick, T. R. Nelson, Jr., G. Khitrova, H. M. Gibbs, Quantum theory of nonlinear semiconductor microcavity luminescence explaining "Boser" experiments, *Phys. Rev. Lett.* 79, 5170 (1997).

53. H. Cao, S. Pau, J. M. Jacobson, G. Björk, Y. Yamamoto, A. Imamoglu, Transition from a microcavity exciton polariton to a photon laser, *Phys. Rev. A* 55, 4632 (1997).

54. A. I. Tartakovskii, V. D. Kulakovskii, D. N. Krizhanovskii, M. S. Skolnick, V. N. Astratov, A. Armitage, J. S. Roberts, Nonlinearities in emission from the LPB of semiconductor microcavities, *Phys. Rev. B* 60, R11293 (1999); M. Emam-Ismail, R. M. Stevenson, M. S. Skolnick, V. N. Astratov, D. M. Whittaker, J. J. Baumberg, J. S. Roberts, Relaxation bottleneck and its suppression in semiconductor microcavities, *Phys. Rev. B* 62, R2283 (2000).

55. M. D. Martin, G. Aichmayr, L. Viña, R. André, Polarization control of the nonlinear emission of semiconductor microcavities, *Phys. Rev. Lett.* 89, 77 402 (2002).

56. H. Deng, G. Weihs, C. Santori, J. Bloch, Y. Yamamoto, Condensation of semiconductor microcavity exciton polaritons, *Science* 298, 199 (2002).

57. See, e.g., Y. R. Shen, Quantum statistics of non linear optics, *Phys. Rev.* 155, 921 (1967); B. Ya. Zel'dovich, A. M. Perelomov, V. S. Popov, *Zh. Eksper. Teoret. Fiz.* 65, 589 (1967).

58. G. Lindblad, On the generators of quantum dynamical semigroups, *Commun. Math. Phys.* 48, 119 (1976).

59. A. Qarry, G. Ramon, R. Rapaport, E. Cohen, Arza Ron, A. Mann, E. Linder, L. N. Pfeiffer, Nonlinear emission due to electron–polariton scattering in a semiconductor microcavity, *Phys. Rev. B* 67, 115320 (2003); A. I. Tartakovskii, D. N. Krizhanovskii, G. Malpuech, M. Emam-Ismail, A. V. Chernenko, A. V. Kavokin, V. D. Kulakovskii, M. S. Skolnick, J. S. Roberts, Giant enhancement of polariton relaxation in semiconductor microcavities by polariton–free carrier interaction: Experimental evidence and theory, *Phys. Rev. B* 67, 165302 (2003); P. G. Lagoudakis, M. D. Martin, J. J. Baumberg, A. Qarry, E. Cohen, L. N. Pfeiffer, Electron–polariton scattering in semiconductor microcavities, *Phys. Rev. Lett.* 90, 206401 (2003).

60. R. J. Elliot, Theory of the effect of spin-orbit coupling on magnetic resonance in some semiconductors, *Phys. Rev.* 96, 266 (1954); Y. Yafet, "Solid State Physics", Vol. 14, p. 1. Academic Press, New York, 1963.
61. G. E. Pikus, G. L. Bir, *Zh. Eksper. Teoret. Fiz.* 60, 195 (1971) [*Sov. Phys. JETP* 33, 108 (1971)].
62. M. I. D'yakonov, V. I. Perel, *Fiz. Tverd. Tela (Leningrad)* 13, 3851 (1971) [*Sov. Phys. Solid State* 13, 3023 (1972)].
63. See e.g. F. Meier and B. P. Zakharchenya, Eds., "Optical Orientation". North-Holland, Amsterdam, 1984.
64. P. G. Lagoudakis, P. G. Savvidis, J. J. Baumberg, D. M. Whittaker, P. R. Eastham, M. S. Skolnick, J. S. Roberts, Stimulated spin dynamics of polaritons in semiconductor microcavities, *Phys. Rev. B* 65, 161310 (2002).
65. A. Kavokin, G. Malpuech, P. G. Lagoudakis, J. J. Baumberg, K. Kavokin, Polarization rotation in resonant emission of semiconductor microcavities, *Phys. Stat. Sol. (a)* 195, 579 (2003); A. Kavokin, G. Malpuech, P. G. Lagoudakis, J. J. Baumberg, Polarization rotation in parametric scattering of polaritons in semiconductor microcavities, *Phys. Rev. B* 67, 195321 (2003).
66. F. Tassone, F. Bassani, L.C. Andreani, Quantum-well reflectivity and exciton–polariton dispersion, *Phys. Rev. B* 45, 6023 (1992).
67. G. Panzarini, L. C. Andreani, A. Armitage, D. Baxter, M. S. Skolnick, V. N. Astratov, J. S. Roberts, A. V. Kavokin, M. R. Vladimirova, M. A. Kaliteevski, Exciton–light coupling in single and coupled semiconductor microcavities: Polariton dispersion and polarization splitting, *Phys. Rev. B* 59, 5082 (1999).
68. M. Z. Maialle, D. E. de Andrada e Silva, L. J. Sham, Exciton spin dynamics in quantum wells, *Phys. Rev. B* 47, 15 776 (1993).
69. The method of Maialle has been extended by K. Kavokin in order to account for the stimulated scattering (K. V. Kavokin, I. A. Shelykh, A. V. Kavokin, G. Malpuech, P. Bigenwald, unpublished).

Appendix. Transfer Matrix Method for a Light Wave Propagating in a Planar Structure

Here we describe the transfer matrix method of solution of the wave equation for light propagating in planar structures. The most frequently used basis of tangential components of electric and magnetic fields and amplitudes of light waves propagating in positive and negative directions are considered. In these two bases the transfer matrix looks different. Note that a variety of similar techniques, such as the scattering matrix method, are used for the solution of Maxwell's equations or Schrödinger's equation in planar structures. We do not use these other methods in the present book and so do not describe them here.

A. Basis of Tangential Components of Electric and Magnetic Fields

Consider a light-wave propagating along the z-direction in a medium characterised by a refractive index n that is homogeneous in the xy-plane but possibly z-dependent. The wave equation in this case is:

$$-\frac{\partial^2 E}{\partial z^2} = k_0^2 n^2 E, \tag{A.1}$$

where k_0 is the wave-vector of light in a vacuum. We shall chose two linearly-independent solutions of Eq. (A.1), $y_1(z)$ and $y_2(z)$, subject to the set of boundary conditions:

$$y_1(0) = 1, \quad y_2(0) = 0, \quad \frac{\partial}{\partial z} y_1(0) = 0, \quad \frac{\partial}{\partial z} y_2(0) = k, \tag{A.2}$$

where $k = k_0 n$. The transfer matrix $\widehat{T}_a$ across the layer of width a is, by our definition, a 2×2 matrix with the following elements:

$$\begin{aligned} t_{11}^a &= y_1(a); \qquad t_{12}^a = \frac{i}{n} y_2(a); \\ t_{21}^a &= -\frac{in}{k} \frac{\partial}{\partial z} y_1(a); \qquad t_{22}^a = \frac{1}{k} \frac{\partial}{\partial z} y_2(a). \end{aligned} \tag{A.3}$$

If n is a constant across the layer a, $y_1(z) = \cos kz$, $y_2(z) = \sin kz$, and

$$\widehat{T}_a = \begin{bmatrix} \cos ka & \frac{i}{n} \sin ka \\ in \sin ka & \cos ka \end{bmatrix}. \tag{A.4}$$

It is easy to check that for a vector

$$\vec{\Phi}(z) = \begin{bmatrix} E(z) \\ H(z) \end{bmatrix} = \begin{bmatrix} E(z) \\ -\frac{i}{k_0}\frac{\partial E(z)}{\partial z} \end{bmatrix}, \tag{A.5}$$

where $E(z)$, $H(z)$ are the amplitudes of the electric and magnetic field of any light wave propagating in the z direction in the structure under study, the following condition is fulfilled:

$$\widehat{T}_a \vec{\Phi}|_{z=0} = \vec{\Phi}|_{z=a}. \tag{A.6}$$

Note that $\vec{\Phi}(z)$ is continuous at any point in the structure due to the fourth of Maxwell's boundary conditions. In particular, it is continuous at all interfaces where n changes abruptly. Thus, a transfer matrix across a structure composed of m layers can be found as

$$\widehat{T} = \prod_{i=m}^{i=1} \widehat{T}_i, \tag{A.7}$$

where $\widehat{T}_i$ is the transfer matrix across ith layer. The order of multiplication in Eq. (A.7) is essential. The amplitude reflection and transmission coefficients (r_s and t_s) of a structure containing m layers, and sandwiched between two semi-infinite media with refractive indices n_0, n_f before and after the structure, respectively, can be found from the relation

$$\widehat{T}\begin{bmatrix} 1+r_s \\ n_0 - n_0 r_s \end{bmatrix} = \begin{bmatrix} t_s \\ n_f t_s \end{bmatrix}. \tag{A.8}$$

One can easily obtain

$$r_s = \frac{n_f t_{11} + n_0 n_f t_{12} - t_{21} - n_0 t_{22}}{t_{21} - n_0 t_{22} - n_f t_{11} + n_0 n_f t_{12}}, \tag{A.9}$$

$$t_s = 2n_0 \frac{t_{12}t_{21} - t_{11}t_{22}}{t_{21} - n_0 t_{22} - n_f t_{11} + n_0 n_f t_{12}}. \tag{A.10}$$

The intensities of reflected and transmitted light normalised by the intensity of the incident light are given by

$$R = |r_s|^2, \qquad T = |t_s|^2 \frac{n_f}{n_0}, \tag{A.11}$$

respectively.

In its turn, the transfer matrix across a layer can be expressed via reflection and transmission coefficients of this layer. If the reflection and transmission coefficients for light incident from the right-hand side and left-hand side of the layer are the same, and $n_0 = n_f \equiv n$ (the symmetric case realised, in particular, in a

QW embedded in a cavity), the Maxwell boundary conditions for light incident from the left and right sides of the structure yield:

$$\widehat{T}\begin{bmatrix} 1+r_s \\ n-nr_s \end{bmatrix} = \begin{bmatrix} t_s \\ nt_s \end{bmatrix}, \qquad \widehat{T}\begin{bmatrix} t_s \\ -nt_s \end{bmatrix} = \begin{bmatrix} 1+r_s \\ -n+nr_s \end{bmatrix}. \tag{A.12}$$

This allows the matrix $\widehat{T}$ to be expressed as:

$$\widehat{T} = \frac{1}{2t}\begin{bmatrix} t_s^2 - r_s^2 + 1 & -\frac{(1+r_s)^2 - t_s^2}{n} \\ n((r_s-1)^2 - t_s^2) & t_s^2 - r_s^2 + 1 \end{bmatrix}. \tag{A.13}$$

For a QW, $t_s = 1 + r_s$, and Eq. (A.13) becomes

$$\widehat{T}_{QW} = \begin{bmatrix} 1 & 0 \\ -2n\frac{r_s}{t_s} & 1 \end{bmatrix}. \tag{A.14}$$

In the ***oblique incidence case***, in the s-polarisation, one can use the basis $\begin{bmatrix} E_\tau(z) \\ H_\tau(z) \end{bmatrix}$, where E_τ, H_τ are the tangential (in-plane) components of the electric and magnetic fields of the light wave. In this case, the transfer matrix (A.4) keeps its form provided that the following substitutions are made:

$$k_z = k\cos\varphi, \qquad n \to n\cos\varphi, \tag{A.15}$$

where φ is the propagation angle in the corresponding medium ($\varphi = 0$ at normal incidence).

In the p-polarisation, following Born and Wolf [1] we use the basis $\begin{bmatrix} H_\tau(z) \\ E_\tau(z) \end{bmatrix}$ which still allows the transfer matrix (A.4) to be used, and where one should substitute:

$$k_z = k\cos\varphi, \qquad n \to \frac{\cos\varphi}{n}. \tag{A.16}$$

Note that the transfer matrices across the interfaces are still identity matrices, and Eq. (A.7) for the transfer matrix across the entire structure is valid.

In the formulas for reflection and transmission coefficients (A.9)–(A.11) one should replace, in the s-polarization

$$n_0 \to n_0\cos\varphi_0, \quad n_f \to n_f\cos\varphi_f, \tag{A.17}$$

and in the p-polarization

$$n_0 \to \frac{\cos\varphi_0}{n_0}, \quad n_f \to \frac{\cos\varphi_f}{n_f}, \tag{A.18}$$

where φ_0, φ_f are the propagation angles in the first and last media, respectively. The same transformations would be applied to the transfer matrices (A.13), (A.14). Note that any two propagation angles φ_i, φ_j in the layers with refractive

indices n_i, n_j are linked by the Snell–Descartes law:

$$n_i \sin\varphi_i = n_j \sin\varphi_j, \tag{A.19}$$

which is also valid in the case of complex refractive indices, when the propagation angles formally become complex as well.

B. Basis of Amplitudes of Light Waves Propagating Towards $z = +\infty$ and $z = -\infty$

A solution of Eq. (A.1) can be formally represented as:

$$E(z) = E^+(z) + E^-(z), \tag{B.1}$$

where $E^{+(-)}(z)$ is the complex amplitude of a light wave propagating in the positive (negative) direction. One can define the transfer matrix $\widehat{M}_a$ by its property:

$$\widehat{M}_a \begin{bmatrix} E^+(0) \\ E^-(0) \end{bmatrix} = \begin{bmatrix} E^+(a) \\ E^-(a) \end{bmatrix}. \tag{B.2}$$

Consider a few particular cases.

If the refractive index n is constant across the layer a, the transfer matrix has a simple form:

$$\widehat{M}_a = \begin{bmatrix} e^{ika} & 0 \\ 0 & e^{-ika} \end{bmatrix}. \tag{B.3}$$

The transfer matrix across an interface between a medium with refractive index n_1 and a medium with refractive index n_2 is

$$\widehat{M}_a = \frac{1}{2n_2} \begin{bmatrix} n_1 + n_2 & n_2 - n_1 \\ n_2 - n_1 & n_1 + n_2 \end{bmatrix}. \tag{B.4}$$

It can be obtained using the condition (B.2) applied to the light waves incident from the left side and right side of the interface, keeping in mind the well-known expressions for the reflection and transmission coefficients of interfaces.

A transfer matrix across a structure containing m layers has the form

$$\widehat{M} = \prod_{j=2m+1}^{1} \widehat{M}_j, \tag{B.5}$$

where $j = 1, 2, \ldots, 2m + 1$ labels all the layers and interfaces of the structure from its left to right side. The amplitude reflection and transmission coefficients (r_s and t_s) of a structure containing m layers, and sandwiched between two semi-infinite media with refractive indices n_0, n_f before and after the structure, respec-

tively, can be found from the relation

$$\widehat{M}\begin{bmatrix}1\\ r_s\end{bmatrix}=\begin{bmatrix}t_s\\ 0\end{bmatrix} \tag{B.6}$$

as

$$r_s=\frac{m_{21}}{m_{11}}, \tag{B.7}$$

$$t_s=\frac{1}{m_{11}}. \tag{B.8}$$

Note that here the refractive indices n_0, n_f do not appear explicitly as they are contained in the transfer matrices across both surfaces of the structure.

If the reflection and transmission coefficients for light incident from the right-hand side and left-hand side of the layer are the same and $n_0=n_f\equiv n$, Maxwell's boundary conditions for light incident from the left and right sides of the structure yield, in addition to Eq. (B.6), the following:

$$\widehat{M}\begin{bmatrix}0\\ t_s\end{bmatrix}=\begin{bmatrix}r_s\\ 1\end{bmatrix}. \tag{B.9}$$

In this case, the transfer matrix across a symmetric object (a QW embedded in the cavity, for example) can be written as:

$$\widehat{M}=\frac{1}{t_s}\begin{bmatrix}t_s^2-r_s^2 & r_s\\ -r_s & 1\end{bmatrix}. \tag{B.10}$$

This matrix must be Hermitian if there is no absorption within the object (this follows from the symmetry of the system with respect to time inversion). As a result

$$r_c/t_c=-r_c^*/t_c^*. \tag{B.11}$$

For a QW containing an exciton resonance, Eq. (B.11) is not valid, since the exciton absorbs light.

In the case of oblique incidence, the interface matrix between a medium with refractive index n_1 and a medium with refractive index n_2 is, for the s-polarisation

$$\widehat{M}_a^{\mathrm{TE}}=\frac{n_1\cos\varphi_1+n_2\cos\varphi_2}{2n_1\cos\varphi_1}\begin{pmatrix}1 & \frac{n_1\cos\varphi_1-n_2\cos\varphi_2}{n_2\cos\varphi_2+n_1\cos\varphi_1}\\ \frac{n_1\cos\varphi_1-n_2\cos\varphi_2}{n_2\cos\varphi_2+n_1\cos\varphi_2} & 1\end{pmatrix}. \tag{B.12}$$

For the p-polarisation:

$$\widehat{M}_a^{\mathrm{TM}}=\frac{n_1\cos\varphi_2+n_2\cos\varphi_1}{2n_1\cos\varphi_1}\begin{pmatrix}1 & \frac{n_1\cos\varphi_2-n_2\cos\varphi_1}{n_1\cos\varphi_2+n_2\cos\varphi_1}\\ \frac{n_1\cos\varphi_2-n_2\cos\varphi_1}{n_1\cos\varphi_2+n_2\cos\varphi_1} & 1\end{pmatrix}, \tag{B.13}$$

where φ_1 and φ_2 are the light propagation angles inside the two different media. The transfer matrix across a layer keeps the same form as for the normal incidence

case (B.3):

$$\widehat{M}_a = \begin{bmatrix} e^{ik_z a} & 0 \\ 0 & e^{-ik_z a} \end{bmatrix}, \tag{B.14}$$

where k_z is the wave-vector in the growth direction given by:

$$k_z = \frac{n\omega}{c}\cos\varphi. \tag{B.15}$$

The transfer matrix across the structure containing m layers keeps the form (B.5) and the reflection and transmission coefficients keep the form (B.7) and (B.8), respectively.

C. Photonic Bands of 1D Periodic Structures

Consider an infinite structure whose refractive index is homogeneous in the (xy)-plane and whose dependence on the coordinate z is a periodic function with period d. The shape of this function is not essential, and we shall only assume that a transfer matrix $\widehat{T}_d$ across the period of the structure can be written as a product of a finite number of matrices of the form (A.4). Let an electromagnetic wave propagate along the z-direction. For this wave

$$\widehat{T}_d \vec{\Phi}|_{z=0} = \vec{\Phi}|_{z=d}, \tag{C.1}$$

where $\vec{\Phi}(z)$ is defined by Eq. (A.5). According to the *Bloch theorem*, it can be represented in the form:

$$\vec{\Phi}(z) = e^{iQz} \begin{bmatrix} U_E(z) \\ U_H(z) \end{bmatrix}, \tag{C.2}$$

where $U_{E,H}(z)$ have the same periodicity as the structure, and Q is a complex number in general. Note that the factor e^{iQz} is the same for electric (E) and magnetic (H) fields in a light wave because in the normal incidence case they are linked by the relation: $H(z) = -\frac{i}{k_0}\frac{\partial E(z)}{\partial z}$.

Substitution of Eq. (C.2) into Eq. (C.1) yields

$$\widehat{T}_d \vec{\Phi}|_{z=0} = e^{iQd} \vec{\Phi}|_{z=0}. \tag{C.3}$$

Thus, e^{iQd} is an eigenvalue of the matrix $\widehat{T}_d$, and therefore

$$\det\left(\widehat{T}_d - e^{iQd}\hat{I}\right) = 0, \tag{C.4}$$

where $\hat{I}$ is an identity matrix. Resolving Eq. (C.4), we use an important property of the matrix $\widehat{T}_d$ following from Eqs. (A.4), (A.7):

$$\det \widehat{T}_d = 1. \tag{C.5}$$

Thus we reduce Eq. (C.4) to

$$1 - (T_{11} + T_{22})e^{iQd} + e^{2iQd} = 0, \tag{C.6}$$

where T_{ij} are the elements of the matrix $\widehat{T}_d$. Multiplying each term by e^{-iQd} we obtain finally:

$$\cos Qd = (T_{11} + T_{22})/2. \tag{C.7}$$

The right-hand side of this equation is frequency-dependent. The frequency bands for which

$$\left|(T_{11} + T_{22})/2\right| \leqslant 1 \tag{C.8}$$

are allowed photonic bands. In these bands Q is purely real, and the light wave can propagate freely without attenuation. On the contrary, the bands for which

$$\left|(T_{11} + T_{22})/2\right| > 1 \tag{C.9}$$

are usually called stop-bands or optical gaps. In these bands Q has a non-zero imaginary part that determines the decay of propagating light waves. All this is completely analogous to conventional crystals. Eqs. (C.7)–(C.9) are also valid in the oblique incidence case, while the form of the matrix $\widehat{T}_d$ is sensitive to the angle of incidence, and band boundaries shift as one changes the incidence angle.

Reference

1. M. Born, E. Wolf, "Principles of Optics". Pergamon, Oxford, 1980.

This page intentionally left blank

Subject Index

absorption 2, 5, 6, 14, 15, 24, 33, 54, 55, 69, 76, 102, 104, 109, 118, 126, 147, 184, 229
acoustic phonons 6, 17, 22, 31, 33, 117, 121, 123, 126, 128, 199
anticrossing 2–4, 17–22, 43, 50, 57, 58, 66, 67, 76, 82, 96, 99, 101, 125

Bloch theorem 70, 73, 230
Boltzmann equation 8, 119, 124, 131, 132, 143, 148, 164, 171, 174, 184, 185, 198, 201, 206, 208, 215, 220
Born approximation 8, 126, 130, 202
Bose condensation ix, x, 5–8, 15, 24, 26, 118, 119, 132, 143, 158, 171, 183, 189, 197, 205, 207
Bose phase transition 156
bottleneck x, 6, 8, 22, 118–120, 122, 123, 135, 136, 138, 140, 141, 143, 184, 189, 198, 199, 205, 206, 218–220
Bragg mirror x, 1, 4, 6, 14, 16, 29, 36–39, 41, 42, 44, 53, 54, 66–68, 74, 75, 82, 84, 99, 104, 107
bright modes 50

CdTe 7, 43, 93, 128, 133–136, 139, 140, 143, 161–163, 195, 196, 200, 207, 213
coherence 7, 23–25, 58, 102, 117, 152, 156, 164, 174–176, 184, 185, 188, 200, 201, 204, 208–211, 220
coherent state 170, 175, 176, 204, 208, 209
cooling 128
coupled cavities 55–57
critical density 150, 186, 196
critical temperature 8, 24, 25, 184, 187, 193, 194, 196, 197, 220

dark excitons 143, 189
dark modes 50, 52
dispersion relation 7, 44, 118, 121–124, 143, 151, 152, 154, 157, 158, 167, 186, 191, 194
distribution function 20, 21, 95, 96, 99, 119, 122, 123, 125, 126, 129, 131–136, 138–143, 155, 164, 165, 185, 186, 190, 193, 194, 198–200, 206, 207, 209, 216, 220

elastic circle 106, 125
electrons 15, 123, 129, 183, 188, 208, 214
exciton formation 127, 143

finite system 132, 187, 206

GaAs 3, 4, 7, 18, 23, 31, 33, 43, 50, 53, 55–57, 59, 60, 65–67, 69, 78–82, 91, 93, 99, 100, 104–106, 109, 112, 140, 141, 143, 149–151, 155–157, 161, 162, 166, 193, 195, 196, 198–200, 206
GaN 18, 31, 43, 51, 93, 110, 111, 144, 162, 163, 195, 196, 205

inhomogeneous broadening 18, 19, 43, 53, 82, 88, 95–99, 102, 107, 108, 110–112, 118, 133–136, 138, 165, 197

Kosterlitz–Thouless 25, 185, 189, 190, 193, 196, 220

Landau levels 78
local model 30, 102, 104
longitudinal-transverse splitting 45, 59, 60, 70, 80, 89, 94, 212, 214, 217, 219

magic angle 23, 155, 158, 159
magnetic field x, 3, 5, 17, 20, 34, 47, 62, 77–79, 81, 82, 84, 112, 214, 217, 218, 225–227
Markov approximation 185, 202, 220
master equation 185, 202, 220

Maxwell equations ix, x, 2, 19, 29, 34, 42, 63, 64, 149, 225
motional narrowing ix, 4, 20, 21, 53, 95–99, 101, 110
multiple quantum wells 47

optical phonons x, 117, 121, 126–128
order parameter 175, 187, 188, 198, 204, 205, 209, 220
organic materials 15

parametric amplifier 23, 164, 183
parametric oscillator 23, 172
phase diagram 8, 184, 185, 195
phase transition 5, 7, 25, 156, 176, 178, 179, 183–190, 193, 195–197, 220
photoluminescence x, 5, 21, 22, 33, 87, 96, 101, 104, 105, 117, 120, 161, 198, 205, 212, 213, 218, 219
polariton laser x, 6–8, 15, 22, 24, 25, 58, 183, 184, 190, 198, 201, 202, 207, 220
polariton trap 118, 122, 123, 138
polariton–electron scattering x, 122, 129, 206, 207
polariton–phonon scattering 202, 206
polariton–polariton scattering x, 23, 122, 131, 135, 136, 142, 143, 154, 155, 161, 206, 207, 212
polarization 5, 34, 57, 70, 72, 77, 83, 87, 158, 227
pump-probe 8, 23, 83, 84, 87, 147, 148, 151, 164, 179

quantum dot x, 1, 19, 33, 70, 72, 88
quantum well ix, x, 1, 2, 4, 8, 15, 29, 40, 41, 47, 48, 55, 71, 77, 82, 107, 111, 151, 162, 163, 189, 206, 211, 214
quantum wire x, 1, 2, 4, 5, 19, 47, 70, 74–77

Rabi splitting 2, 3, 13, 17, 18, 20, 43, 52, 53, 66–69, 76, 78, 80, 81, 118, 128, 133, 138, 149, 151, 156, 161, 162
radiative life-time 33, 72
rate equations 218
Rayleigh scattering 5, 21, 22, 43, 53, 87, 90, 96, 101, 102, 105–107
relaxation kinetic 8, 121, 122, 124, 133, 135, 184, 185, 190, 198, 201
resonant excitation 7, 8, 25, 131, 147–149, 161, 164, 193, 200, 212, 217

scattering processes 16, 124, 133, 135, 136, 165, 178, 206
screening x, 17, 151, 195
spatial dispersion 30, 58, 60, 63, 67, 69
spin 7, 8, 19, 20, 45, 77, 83, 129, 148, 150, 158, 183, 185, 189, 200, 211–215, 217, 218, 220
stimulated scattering ix, x, 5–8, 22–24, 84, 143, 156, 157, 164, 166, 174, 178, 183, 184, 190, 200, 201, 204, 205, 208, 215, 219
Stokes shift 118
strong coupling ix, x, 8, 13, 16, 17, 19, 43–45, 51, 52, 66, 93, 134, 140, 149, 164, 195, 196, 198, 200, 201, 207
superfluidity 25, 185, 187–189, 193, 197
superlattice 30, 53
symmetry breaking 7, 25, 26, 156, 174–176, 188, 190, 203

thermal 6, 26, 122, 123, 129, 134, 136, 138, 195, 202, 205–207
transfer matrix x, xi, 4, 36, 41, 42, 48, 49, 54, 60, 62–64, 74, 93, 99, 102, 110, 214, 225–230

weak coupling x, 13, 17, 20, 113, 124, 207

ZnO 18, 31, 93, 144, 164, 195, 196, 205
ZnSe 93, 144, 162, 163, 205

Recent Volumes In This Series

Maurice H. Francombe and John L. Vossen, *Physics of Thin Films*, Volume 16, 1992.

Maurice H. Francombe and John L. Vossen, *Physics of Thin Films*, Volume 17, 1993.

Maurice H. Francombe and John L. Vossen, *Physics of Thin Films, Advances in Research and Development, Plasma Sources for Thin Film Deposition and Etching*, Volume 18, 1994.

K. Vedam (guest editor), *Physics of Thin Films, Advances in Research and Development, Optical Characterization of Real Surfaces and Films*, Volume 19, 1994.

Abraham Ulman, *Thin Films, Organic Thin Films and Surfaces: Directions for the Nineties*, Volume 20, 1995.

Maurice H. Francombe and John L. Vossen, *Homojunction and Quantum-Well Infrared Detectors*, Volume 21, 1995.

Stephen Rossnagel and Abraham Ulman, *Modeling of Film Deposition for Microelectronic Applications*, Volume 22, 1996.

Maurice H. Francombe and John L. Vossen, *Advances in Research and Development*, Volume 23, 1998.

Abraham Ulman, *Self-Assembled Monolayers of Thiols*, Volume 24, 1998.

Subject and Author Cumulative Index, Volumes 1–24, 1998.

Ronald A. Powell and Stephen Rossnagel, *PVD for Microelectronics: Sputter Deposition Applied to Semiconductor Manufacturing*, Volume 26, 1998.

Jeffrey A. Hopwood, *Ionized Physical Vapor Deposition*, Volume 27, 2000.

Maurice H. Francombe, *Frontiers of Thin Film Technology*, Volume 28, 2001.

Maurice H. Francombe, *Non-Crystalline Films for Device Structures*, Volume 29, 2002.

Maurice H. Francombe, *Advances in Plasma-Grown Hydrogenated Films*, Volume 30, 2002.

Vladimir Agranovich and Franco Bassani, *Electronic Excitations in Organic Based Nanostructures*, Volume 31, 2003.